U.S. Department
of Transportation
National Highway
Traffic Safety
Administration

NHTSA

DOT HS 813 686

July 2025

Heavy-Truck Rear-Impact-Guard Finite Element Simulation and Analysis

This page is intentionally left blank.

DISCLAIMER

This publication is distributed by the U.S. Department of Transportation, National Highway Traffic Safety Administration, in the interest of information exchange. The opinions, findings, and conclusions expressed in this publication are those of the authors and not necessarily those of the Department of Transportation or the National Highway Traffic Safety Administration. The United States Government assumes no liability for its contents or use thereof. If trade or manufacturers' names or products are mentioned, it is because they are considered essential to the object of the publication and should not be construed as an endorsement. The United States Government does not endorse products or manufacturers.

NOTE: This report is published in the interest of advancing motor vehicle safety research. While the report may provide results from research or tests using specifically identified motor vehicle models, it is not intended to make conclusions about the safety performance or safety compliance of those motor vehicles, and no such conclusions should be drawn.

Suggested APA Format Citation:

Kalmar-Gonzalo, A., Guleyupoglu, B., & Jones, D. A. (2025, July). *Heavy-truck rear-impact-guard finite element simulation and analysis* (Report No. DOT HS 813 686). National Highway Traffic Safety Administration.

This page is intentionally left blank.

Technical Report Documentation Page

1. Report No.	2. Government Accession No.	3. Recipient's Catalog No.
DOT HS 813 686		

4. Title and Subtitle	5. Report Date
Heavy-Truck Rear-Impact-Guard Finite Element Simulation and Analysis	July 2025
	6. Performing Organization Code

7. Authors	8. Performing Organization Report No.
Derek A. Jones, Principal Investigator; Alex Kalmar-Gonzalo, Berkan Guleyupoglu, all Elemance LLC	

9. Performing Organization Name and Address	10. Work Unit No. (TRAIS)
Elemance, LLC 450 N. Patterson Ave, Ste 310 Winston-Salem, NC 27101	
	11. Contract or Grant No. 693JJ921D000042

12. Sponsoring Agency Name and Address	13. Type of Report and Period Covered
National Highway Traffic Safety Administration 1200 New Jersey Avenue SE Washington, DC 20590	Final Report
	14. Sponsoring Agency Code

15. Supplementary Notes

16. Abstract

This report describes a finite element (FE) modeling exercise to develop models of rear-impact guards and simulate both FMVSS No. 223 tests as well as full motor vehicle crashes into the rear of truck-trailers. In this effort, both the THOR-50M anthropomorphic test device and the GHBMC human body model representing a 50th percentile male were used to assess occupant injury risk. The exercise developed three FE models of rear-impact guards, simulation, and analysis of FMVSS No. 223 test protocols, and simulation and analysis of full vehicle into truck-trailer rears with rear-impact guards attached at 35 mph, 40 mph, 45 mph, and 65 mph.

At speeds of 45 mph and under, the simulation results indicate that intrusion of the trailer bumper into the occupant compartment of the passenger car can be prevented in certain crash scenarios depending on the guard design and the amount of vehicle-to-bumper overlap. Simulations of 65-mph crashes indicate that such crashes are unsurvivable for all guard designs studied.

17. Key Words	18. Distribution Statement
rear-impact guards, FMVSS No. 223, FMVSS No. 224, THOR-50M, GHBMC, finite element, injury biomechanics, FE	Document is available to the public from the DOT, BTS, National Transportation Library, Repository & Open Science Access Portal, https://rosap.ntl.bts.gov.

19. Security Classif. (of this report)	20. Security Classif. (of this page)	21. No. of Pages	22. Price
Unclassified	Unclassified	218	

Form DOT F 1700.7 (8-72) Reproduction of completed page authorized

This page is intentionally left blank.

Table of Contents

Executive Summary **1**

Introduction and Scope of Work **3**
Introduction 3
Program Tasks Summary 4

Aim 1: Developing Rear-Impact Guard Finite Element Models **5**
Background: FMVSS No. 223 5
Background: Passenger Compartment Intrusion 6
Selection and Procurement 6
CAD Development 7
Material Characterization 9
Material Model Development 10
Mesh Development 15
Model Validation 17
Description of Experimental Data 17
Initial Simulation Setup 18
Modifications to Simulation Setup 19
Validation Results 24
Aim 1: Summary 33

Aim 2: Assessing the Relationship Between Quasi-Static Testing and Dynamic Crash Response **35**
Rear-Impact Guard Modification to Minimally Comply With FMVSS No. 223 35
Dynamic Impact Assessment – Honda Accord 40
Trailer Model 40
Baseline Rear-Impact Guard Dynamic Response 43
Minimally Compliant Rear-Impact Guard Dynamic Response 47
Guard Strengthening – Midsize 48
Quasi-Static Reassessment – Midsize Strengthened 50
Dynamic Impact Assessment – Toyota Yaris 54
Guard Strengthening – Compact 56
Quasi-Static Reassessment – Strengthened Compact 61
Aim 2: Summary 63

Aim 3: Occupant Response in High-Speed Collisions into Strengthened Rear-Impact Guards **65**
Design of Experiments 65
Model Setup 65
Occupant Models Positioning Settling 65
Seat Belt Restraints 67
Air Bags 67
Simulation Results 71
Passenger Compartment Intrusion – 40 and 45 mph Simulations 71
Occupant Response 73
Discussion on THOR-50M and GHBMC Usage 73

Injury Assessment References 74
Injury Risks 76
Structural Response at 65 MPH 107
Aim 3: Summary 113
References 115
Appendix A: Mechanical Characterization Data A-1
Appendix B: Dynamic Simulation Results From Baseline and Minimally Compliant Guards B-1
Appendix C: THOR-50M and GHBMC Occupant Injury Metric Response C-1
Appendix D: THOR-50M and GHBMC Occupant Data Channels from Dynamic Crash Simulations D-1

List of Figures

Figure 1. Truck rear-impact guards selected for this study. Photographs from IIHS dynamic test series. 7
Figure 2. Geometry of the Wabash guard rendered in SolidWorks....7
Figure 3. Geometry of the Great Dane guard rendered in SolidWorks 8
Figure 4. Geometry of the Manc guard rendered in SolidWorks 8
Figure 5. Experimental and Simulation stress-strain response of the Wabash dog bone specimens. (a) full data set, (b) close-up of the elastic range and yield point, (c) close-up of post-yield behavior.....12
Figure 6. Experimental and Simulation stress-strain response of the Great Dane dog bone specimens. (a) full data set, (b) close-up of the elastic range and yield point, (c) close-up of post-yield behavior.....13
Figure 7. Experimental and Simulation stress-strain response of the Manac dog bone specimens. (a) full data set, (b) close-up of the elastic range and yield point, (c) close-up of post-yield behavior.....14
Figure 8. Finite element models of the rear-impact Guards (a) Wabash, (b) Great Dane, (c) Manac. Images are not to scale. 16
Figure 9. Impact locations for quasi-static loading as specified by FMVSS No.223 (2004) 17
Figure 10. Finite element model of the square impactor 18
Figure 11. Video evidence of fixture motion during P3 impact case. Video still from test start (a) and mid-test (b) Orange outline of upper fixture added and superimposed on mid-test picture.....20
Figure 12. Diagram of fixture stiffness spring and boundary conditions used for model validation 21
Figure 13. Simulation set up for quasi-static validation simulations showing the position of P1, P2, and P3 impactors on the Wabash (a) Great Dane (b) and Manac (c) rear-impact guard models. Springs representing the fixture flexure are in green. 22
Figure 14. Picture evidence of secondary impact during Manac P3 physical testing....23
Figure 15. Simulation results of the P3 impact case with and without a backing plate compared to experimental results....24
Figure 16. Sheet metal thickness values for each part in the models compared to the original measured values for the (a) Wabash, (b) Great Dane, and (c) Manac rear-impact guards 27
Figure 17. Images of post-test deformation in the P3 impact case comparing experimental results to simulation results for the Wabash guard....28
Figure 18. Images of post-test deformation in the P3 impact case comparing experimental results to simulation results for the Great Dane guard 29
Figure 19. Images of post-test deformation in the P3 impact case comparing experimental results to simulation results for the Manac guard....30
Figure 20. Experimental and simulation force-deflection results for the Wabash, Great Dane, and Manac rear-impact guards from FMVSS No.223 (2004) protocol 31

Figure 21. Experimental and simulation energy-displacement results for the Wabash, Great Dane, and Manac rear-impact guards from FMVSS No.223 (2004) protocol 32
Figure 22. Simulation responses of the guard models in FMVSS No. 223 (2022) protocol using the baseline (blue), and minimally compliant (green) models 38
Figure 23. Sheet metal thickness values for each part in the models comparing the measured, tuned, and minimally compliant versions, (a) Wabash, (b) Great Dane, (c) Manac 39
Figure 24. Finite element trailer model with the rear-impact guard removed 40
Figure 25. Connection locations between the guard and trailer for the (a) Wabash, (b) Manac, and (c) Great Dane 42
Figure 26. Comparison of IIHS physical testing and computational modeling post-impact Wabash guard plastic deformation at 35 mph, (a) 30 percent overlap, (b) 50 percent overlap, and (c, d) full overlap 44
Figure 27. Comparison of IIHS physical testing and computational modeling post-impact Great Dane guard plastic deformation at 35 mph, (a) 30 percent overlap, (b) 50 percent overlap, and (c, d) full overlap 45
Figure 28. Comparison of IIHS physical testing and computational modeling post-impact Manac guard plastic deformation at 35 mph, (a) 30 percent overlap, (b) 50 percent overlap, and (c, d) full overlap 46
Figure 29. X acceleration profile for the Honda Accord during impacts with the Wabash (green), Manac (blue), and Great Dane (purple) in a 30 percent overlap 35 mph condition.....47
Figure 30. Comparison of Honda Accord rear sill x-velocity across guards, overlap.....48
Figure 31. Example of baseline and strengthened guard effective plastic strain at 150 ms in a 30 percent overlap 35 mph Honda Accord simulation.....49
Figure 32. Images from 175 ms into 30 percent overlap 35 mph simulations of the baseline and midsize strengthened Wabash and Great Dane guards demonstrating PCI prevention 50
Figure 33. Simulation responses of the Wabash Guard in FMVSS No. 223 (2022) protocol using the baseline (blue), minimally compliant (green), and midsize strengthened (yellow) models 51
Figure 34. Effective plastic strain and gross deformation response of the Wabash baseline and midsize strengthened guard for given timepoints in the P1 and UDL FMVSS No. 223 (2022) simulations 52
Figure 35. Simulation responses of the Great Dane Guard in FMVSS No. 223 (2022) protocol using the baseline (blue), minimally compliant (green), and midsize strengthened (yellow) models 53
Figure 36. Effective plastic strain and gross deformation response of the Wabash baseline and midsize strengthened guard for given timepoints in the P1 and UDL FMVSS No. 223 (2022) simulations 54
Figure 37. 30 percent overlap 35 mph simulations of the Toyota Yaris into the (a) Wabash, (b) Manac, (c) Great Dane guard models with thicknesses arrived at following midsize strengthening.....55
Figure 38. Sheet metal thickness values for each part in the models compared to the original measured values, (a) Wabash, (b) Great Dane, (c) Manac 57

Figure 39. Sheet metal thickness values (mm) for each part in the models compared to the original measured values, (a) Wabash, (b) Great Dane, (c) Manac 58
Figure 40. Overlays of the Honda Accord (red, solid line) and the Toyota Yaris (blue, dashed line) models. Aligned in x-direction at the bottom left tire (a), and the front of the windscreen (b). 59
Figure 41. 30 percent overlap 35 mph simulations of the Toyota Yaris into the (a) Wabash, (b) Manac, (c) Great Dane guard models with thicknesses arrived at following compact strengthening 60
Figure 42. Simulation responses of the guard models in FMVSS No. 223 (2022) protocol using the models of various strengths 62
Figure 43. Example of removing penetrations in the shoulder post-positioning.....66
Figure 44. Initial (a) and positioned (b) state of the GHBMC M50-OS in the driver posture 66
Figure 45. Initial (a) and settled (b) state of the THOR-50M M50 67
Figure 46. Belted THOR-50M M50 passenger and driver 67
Figure 47. Passenger air bag response in preliminary simulations.....68
Figure 48. Passenger air bag response before and after vent area modification.....69
Figure 49. Seated and belted GHBMC M50-OS (a) and THOR-50M (b) models in the Honda Accord vehicle.....70
Figure 50. Simplified diagram of the typical rear-impact guard 72
Figure 51. Rear-impact guard connections to trailer for (a) Manac, (b) Wabash, and (c) Great Dane.....73
Figure 52. HIC-15 values for occupants in the midsize sedan full vehicle-to-trailer impacts simulations.....77
Figure 53. AIS 2+ head injury risks for occupants in the midsize sedan full vehicle-to-trailer impacts simulations 78
Figure 54. Rear-impact guard (a) and overlap percentage (b) comparisons for head injury risk. Both THOR-50M and GHBMC M50-OS data included. Statistical analysis performed with α=0.05.....79
Figure 55. Occupant seating location (a) and model (b) comparisons for head injury risk. Both THOR-50M and GHBMC M50-OS data included. Statistical analysis performed with α=0.05 79
Figure 56. BrIC values for occupants in the midsize sedan full vehicle-to-trailer impacts simulations.....81
Figure 57. AIS 3+ brain injury risks for occupants in the midsize sedan full vehicle-to-trailer impacts simulations 82
Figure 58. Rear-impact guard (a) and overlap percentage (b) comparisons for HIC-15 levels and injury risk. Both THOR-50M and GHBMC M50-OS data included. Statistical analysis performed with α=0.05.....83
Figure 59. Occupant seating location (a) and model (b) comparisons for BrIC levels and injury risk. Both THOR-50M and GHBMC M50-OS data included. Statistical analysis performed with α=0.05.....83

Figure 60. A sample of head rotational velocity kinematics comparing THOR-50M and GHBMC M50-OS 84
Figure 61. Nij values for occupants in the midsize sedan full vehicle-to-trailer impacts simulations....86
Figure 62. AIS 2+ neck injury risks for occupants in the midsize sedan full vehicle-to-trailer impacts simulations 86
Figure 63. Rear-impact guard (a) and overlap percentage (b) comparisons for neck injury risk. Both THOR-50M and GHBMC M50-OS data included. Statistical analysis performed with α=0.05.....87
Figure 64. Occupant seating location (a) and model (b) comparisons for neck injury risk. Both THOR-50M and GHBMC M50-OS data included. Statistical analysis performed with α=0.05. 87
Figure 65. Multi-point thoracic criterion values for THOR-50M occupants and center chest deflection for the GHBMC M50-OS in the midsize sedan full vehicle-to-trailer impacts simulations 89
Figure 66. AIS 3+ chest injury risks for occupants in the midsize sedan full vehicle-to-trailer impacts simulations 90
Figure 67. Rear-impact guard (a) and overlap percentage (b) comparisons for chest injury risk. Statistical analysis performed with α=0.05. 90
Figure 68. Comparisons for chest injury risk by occupant seating location. Statistical analysis performed with α=0.05.....91
Figure 69. Approximate center chest deflection of the THOR 50M compared to the measured center chest deflection in the GHBMC M50-OS 91
Figure 70. Box and whisker plot of the distribution of approximated THOR 50M center chest deflection and the measured GHBMC M50-OS chest deflection 92
Figure 71. Peak left femur force values for occupants in the midsize sedan full vehicle-to-trailer impacts simulations 95
Figure 72. Peak right femur force values for occupants in the midsize sedan full vehicle-to-trailer impacts simulations....96
Figure 73. AIS 2+ left femur injury risks for occupants in the midsize sedan full vehicle-to-trailer impacts simulations....96
Figure 74. AIS 2+ right femur injury risks for occupants in the midsize sedan full vehicle-to-trailer impacts simulations....97
Figure 75. Revised tibia index values for occupants' left lower leg in the midsize sedan full vehicle-to-trailer impacts simulations 102
Figure 76. Revised tibia index values for occupants' left upper leg in the midsize sedan full vehicle-to-trailer impacts simulations 103
Figure 77. Revised tibia index values for occupants' right lower leg in the midsize sedan full vehicle-to-trailer impacts simulations 103
Figure 78. Revised tibia index values for occupants' right upper leg in the midsize sedan full vehicle-to-trailer impacts simulations 104

Figure 79. AIS 2+ leg injury risks for occupants' left lower leg in the midsize sedan full vehicle-to-trailer impacts simulations 104
Figure 80. AIS 2+ leg injury risks for occupants' left upper leg in the midsize sedan full vehicle-to-trailer impacts simulations 105
Figure 81. AIS 2+ leg injury risks for occupants' right lower leg in the midsize sedan full vehicle-to-trailer impacts simulations 105
Figure 82. AIS 2+ leg injury risks for occupants' right lower leg in the midsize sedan full vehicle-to-trailer impacts simulations 106
Figure 83. Progression of instrument panel intrusion and a-pillar deformation during 50 percent overlap 65 mph simulation with the strengthened Wabash guard 108
Figure 84. 65 mph full width simulation with the strengthened Wabash guard 109
Figure 85. 65 mph full width simulation data channels with the strengthened Wabash guard 109
Figure 86. 65 mph strengthened Manac simulation head strikes 110
Figure 87. Head strikes to the rear of the trailer in the 65 mph 30 percent (a) and 50 percent (b) overlap simulations with the Great Dane rear-impact guard 111
Figure 88. 65 mph full width simulation with the strengthened Great Dane guard 112
Figure 89. 65 mph full width simulation data channels with the strengthened Great Dane guard 112
Figure 90. Full overlap 35 mph impact to the Wabash baseline and minimally compliant guards B-2
Figure 91. 50 percent overlap 35 mph impact to the Wabash baseline and minimally compliant guards B-3
Figure 92. 30 percent overlap 35 mph impact to the Wabash baseline and minimally compliant guards B-4
Figure 93. Full overlap 35 mph impact to the Great Dane baseline and minimally compliant guards B-5
Figure 94. 50 percent overlap 35 mph impact to the Great Dane baseline and minimally compliant guards B-6
Figure 95. 30 percent overlap 35 mph impact to the Great Dane baseline and minimally compliant guards B-7
Figure 96. Full overlap 35 mph impact to the Manac baseline and minimally compliant guards B-8
Figure 97. 50 percent overlap 35 mph impact to the Manac baseline and minimally compliant guards B-9
Figure 98. 30 percent overlap 35 mph impact to the Manac baseline and minimally compliant guards B-10
Figure 99. HIC results for the GHBMC and THOR-50M occupants in 40 mph and 45 mph simulations C-3
Figure 100. BrIC results for the GHBMC and THOR-50M occupants in 40 mph and 45 mph simulations C-4
Figure 101. Peak neck tension force for the GHBMC and THOR-50M occupants in 40 mph and 45 mph simulations C-6

Figure 102. Peak neck flexion moment for the GHBMC and THOR-50M occupants in 40 mph and 45 mph simulations....C-7
Figure 103. Peak Nij for the GHBMC and THOR-50M occupants in 40 mph and 45 mph simulations....C-8
Figure 104. Multi-point thoracic injury criterion and peak thoracoabdominal compression for the THOR-50M and GHBMC occupants in 40 mph and 45 mph simulations....C-10
Figure 105. Peak T6 linear acceleration for the GHBMC and THOR-50M occupants in 40 mph and 45 mph simulations....C-11
Figure 106. Peak abdominal compression for the GHBMC and THOR-50M occupants in 40 mph and 45 mph simulations....C-12
Figure 107. Peak lumbar spine compression force for the GHBMC and THOR-50M occupants in 40 mph and 45 mph simulations....C-13
Figure 108. Peak lumbar spine tension force for the GHBMC and THOR-50M occupants in 40 mph and 45 mph simulations....C-14
Figure 109. Peak pelvis linear acceleration for the GHBMC and THOR-50M occupants in 40 mph and 45 mph simulations....C-16
Figure 110. Peak left femur force for the GHBMC and THOR-50M occupants in 40 mph and 45 mph simulations....C-17
Figure 111. Peak right femur force for the GHBMC and THOR-50M occupants in 40 mph and 45 mph simulations....C-18
Figure 112. Peak left upper tibia force for the GHBMC and THOR-50M occupants in 40 mph and 45 mph simulations....C-19
Figure 113. Peak right upper tibia force for the GHBMC and THOR-50M occupants in 40 mph and 45 mph simulations....C-20
Figure 114. Peak left lower tibia force for the GHBMC and THOR-50M occupants in 40 mph and 45 mph simulations....C-21
Figure 115. Peak right lower tibia force for the GHBMC and THOR-50M occupants in 40 mph and 45 mph simulations....C-22
Figure 116. Peak left tibia moment for the GHBMC and THOR-50M occupants in 40 mph and 45 mph simulations....C-23
Figure 117. Peak right tibia moment for the GHBMC and THOR-50M occupants in 40 mph and 45 mph simulations....C-24
Figure 118. Left Revised tibia index for the GHBMC and THOR-50M occupants in 40 mph and 45 mph simulations....C-25
Figure 119. Right Revised tibia index for the GHBMC and THOR-50M occupants in 40 mph and 45 mph simulations....C-26
Figure 120. Strengthened Wabash 40 mph, 30 percent overlap THOR-50M and GHBMC upper body data channels....D-2
Figure 121. Strengthened Wabash 40 mph, 30 percent overlap THOR-50M and GHBMC lower body data channels....D-3
Figure 122. Strengthened Wabash 40 mph, 30 percent overlap THOR-50M and GHBMC upper body data channels....D-4

Figure 123. Strengthened Wabash 40 mph, 30 percent overlap THOR-50M and GHBMC lower body data channels D-5
Figure 124. Strengthened Wabash 40 mph, full width overlap THOR-50M and GHBMC upper body data channels D-6
Figure 125. Strengthened Wabash 40 mph, full width overlap THOR-50M and GHBMC lower body data channels D-7
Figure 126. Strengthened Wabash 45 mph, 30 percent overlap THOR-50M and GHBMC upper body data channels D-8
Figure 127. Strengthened Wabash 45 mph, 30 percent overlap THOR-50M and GHBMC lower body data channels D-9
Figure 128. Strengthened Wabash 45 mph, 50 percent overlap THOR-50M and GHBMC upper body data channels D-10
Figure 129. Strengthened Wabash 45 mph, 50 percent overlap THOR-50M and GHBMC lower body data channels D-11
Figure 130. Strengthened Wabash 45 mph, full width overlap THOR-50M and GHBMC upper body data channels D-12
Figure 131. Strengthened Wabash 45 mph, full width overlap THOR-50M and GHBMC lower body data channels D-13
Figure 132. Strengthened Manac 40 mph, 30 percent overlap THOR-50M and GHBMC upper body data channels D-14
Figure 133. Strengthened Manac 40 mph, 30 percent overlap THOR-50M and GHBMC lower body data channels D-15
Figure 134. Strengthened Manac 40 mph, 50 percent overlap THOR-50M and GHBMC upper body data channels D-16
Figure 135. Strengthened Manac 40 mph, 50 percent overlap THOR-50M and GHBMC lower body data channels D-17
Figure 136. Strengthened Manac 40 mph, full width overlap THOR-50M and GHBMC upper body data channels D-18
Figure 137. Strengthened Manac 40 mph, full width overlap THOR-50M and GHBMC lower body data channels D-19
Figure 138. Strengthened Manac 45 mph, 30 percent overlap THOR-50M and GHBMC upper body data channels D-20
Figure 139. Strengthened Manac 45 mph, 30 percent overlap THOR-50M and GHBMC lower body data channels D-21
Figure 140. Strengthened Manac 45 mph, 50 percent overlap THOR-50M and GHBMC upper body data channels D-22
Figure 141. Strengthened Manac 45 mph, 50 percent overlap THOR-50M and GHBMC lower body data channels D-23
Figure 142. Strengthened Manac 45 mph, full width overlap THOR-50M and GHBMC upper body data channels D-24
Figure 143. Strengthened Manac 45 mph, full width overlap THOR-50M and GHBMC lower body data channels D-25

Figure 144. Strengthened Great Dane 40 mph, 30 percent overlap THOR-50M and GHBMC upper body data channels..... D-26
Figure 145. Strengthened Great Dane 40 mph, 30 percent overlap THOR-50M and GHBMC lower body data channels..... D-27
Figure 146. Strengthened Great Dane 40 mph, 50 percent overlap THOR-50M and GHBMC upper body data channels..... D-28
Figure 147. Strengthened Great Dane 40 mph, 50 percent overlap THOR-50M and GHBMC lower body data channels..... D-29
Figure 148. Strengthened Great Dane 40 mph, full width overlap THOR-50M and GHBMC upper body data channels..... D-30
Figure 149. Strengthened Great Dane 40 mph, full width overlap THOR-50M and GHBMC lower body data channels..... D-31
Figure 150. Strengthened Great Dane 45 mph, 30 percent overlap THOR-50M and GHBMC upper body data channels..... D-32
Figure 151. Strengthened Great Dane 45 mph, 30 percent overlap THOR-50M and GHBMC lower body data channels..... D-33
Figure 152. Strengthened Great Dane 45 mph, 50 percent overlap THOR-50M and GHBMC upper body data channels..... D-34
Figure 153. Strengthened Great Dane 45 mph, 50 percent overlap THOR-50M and GHBMC lower body data channels..... D-35
Figure 154. Strengthened Great Dane 45 mph, full width overlap THOR-50M and GHBMC upper body data channels..... D-36
Figure 155. Strengthened Manac 45 mph, full width overlap THOR-50M and GHBMC lower body data channels D-37

List of Tables

Table 1. Chemical composition analysis; tensile test results 10
Table 2. Material properties used for each truck-trailer rear-impact guard 11
Table 3. CORA scores for the force-displacement signals from the computational models 33
Table 4. Simulated FMVSS No. 223 (2022) results for the baseline and minimally compliant models 37
Table 5. Summary table for FMVSS No. 223 (2022) simulation results 63
Table 6. Summary table of guard designs and performance 64
Table 7. PCI observations – Strengthened guards 71
Table 8. Dimensions of rear-impact guards 72
Table 9. Abbreviated injury scale scoring system 74
Table 10. THOR-50M and GHBMC M50-OS comparative reference values 75
Table 11. Honda Accord, head injury risk 76
Table 12. Honda Accord, brain injury risk 80
Table 13. Honda Accord, neck injury risk 85
Table 14. Honda Accord, chest injury risk (THOR-50M chest deflection is multi-point thoracic criterion; GHBMC M50-OS chest deflection taken from center chest instrumentation. Bolded values represent values above IARV. Italicized values represent similar compression levels between THOR-50M and GHBMC M50-OS.) 88
Table 15. Honda Accord, left femur injury risk 93
Table 16. Honda Accord, right femur injury risk 94
Table 17. Honda Accord, lower left tibia injury risk 98
Table 18. Honda Accord, upper left tibia Injury Risk. 99
Table 19. Honda Accord, lower right Tibia injury risk 100
Table 20. Honda Accord, upper right tibia injury risk 101
Table 21. 65 mph full width – Wabash strengthened, Honda Accord simulation injury metrics 108
Table 22. 65 mph full width – Great Dane strengthened, Honda Accord 111
Table 23. Summary of head, neck, and Thorax injury metric differences in the 40 mph and 45 mph simulations C-28
Table 24. Summary of pelvis and lower extremity injury metric differences in the 40 mph and 45 mph simulations C-29

List of Acronyms/Definitions

AIS	Abbreviated Injury Scale
ATD	anthropomorphic test device
AP	anterior-posterior
BIW	body-in-white
BrIC	brain injury criteria
CAB	curtain Air Bag
CORA	CORrelation and Analysis
DAB	driver air bag
DOE	design of experiments
FE	finite element
FMVSS	Federal Motor Vehicle Safety Standard
GHBMC	Global Human Body Models Consortium
HBM	human body model
HIC	head injury criterion
IIHS	Insurance Institute for Highway Safety
IR-TRACC	infrared-telescoping rod for assessment of chest compression
M50	50th percentile male
Nij	neck injury criterion
PAB	passenger Air Bag
PCI	passenger compartment intrusion
RIG	rear-impact guard
RTI	revised tibia index
THOR-50M	Test device for Human Occupant Restraint

Executive Summary

This report presents a finite element modeling study aimed at developing models of rear-impact guards and simulating tests of Federal Motor Vehicle Safety Standard No. 223, *Rear impact guards*, as along with full motor vehicle crashes into the rear of truck-trailers. The study consisted of three primary objectives, summarized here.

Objective 1. Develop FE models of three different rear-impact guards. Three market available guards were selected for this study manufactured by Wabash National[1] model 05006821-07, Great Dane[2] model GDP11716266, and Manac[3] model 914-0901002-G. All three models were certified as compliant with FMVSS No. 223. The FE guard models were validated using data from physical tests with each guard according to the quasi-static test protocols specified in FMVSS 223. All three models exhibited excellent correlation with quasi-static load cases, as assessed through an objective rating system and qualitative comparison of gross plastic deformation.

Objective 2. Assess the relationship between quasi-static testing and dynamic crash response. A model optimization routine was conducted to reduce the strength of each guard to a minimum level required for compliance with FMVSS No. 223. This was achieved by maintaining the basic dimensions of the guards while only decreasing the wall thicknesses of the steel members. The baseline and minimally compliant guards were then used in dynamic crashes simulations, where the guards were mounted to a trailer and struck by a vehicle travelling at 35 mph. Three different points of impact were simulated.

a. Center of the guard, full vehicle overlap
b. 50 percent of vehicle overlaps the guard
c. 30 percent of the vehicle overlaps the guard

For each simulation, any instance of passenger compartment intrusion was documented. PCI occurs when there is trailer contact with the windshield, A-pillars, or roof of the striking vehicle. Two previously established and validated simulation models of striking vehicles were used in the simulations: a 2014 Honda Accord (mid-sized sedan) and a 2010 Toyota Yaris (compact sedan). Six guard designs were assessed, including three baseline and three "minimally compliant" designs. All six guard designs prevented PCI in the full and 50 percent overlap impact simulations. However, only the Manac guard design prevented PCI in the 30 percent overlap simulated crash, and only when the Honda Accord was used as the striking vehicle. None prevented PCI with the smaller Toyota Yaris in the 30 percent overlap scenario.

Optimizations were then carried out to strengthen the guards in attempts to prevent PCI in the 30 percent overlap test for both the mid-size and compact sedans at 35 mph. This strengthening was achieved by maintaining the basic dimensions of the guards and only increasing the wall thicknesses of the steel members. In general, PCI outcomes were influenced by both the striking vehicle and the spacing between the guard's vertical support members. It was more difficult to prevent PCI when the vertical supports were closer together and when the smaller Toyota Yaris was used. In the case of the Great Dane guard, which had the closest spacing between cross

[1] Wabash National Corporation, Lafayette, IN.
[2] Great Dane LLC, Chicago, IL.
[3] Manac Inc., Saint-Georges, Quebec, Canada.

members, a strengthened design that prevented PCI could not be achieved when the Toyota Yaris was used as the striking vehicle.

Objective 3. Simulate and analyze full vehicle crashes at higher speeds. Additional simulations were carried out to gain an understanding on whether an underride guard can be designed to:

a. Prevent PCI at speeds up to 65 mph; and
b. Protect passengers against severe injury at speeds up to 65 mph.

The dynamic tests described in Objective 2 were simulated at impact speeds of 40, 45, and 65 mph. In this part of the simulated tests, only the guards that were strengthened to prevent PCI with the Toyota Yaris (compact sedan) were used and only the Honda Accord was used as the striking vehicle. Separate simulations were carried out in which the driver and passenger positions of the Accord vehicle were occupied by either the THOR-50M dummy model or the M50-OS human body model available from the Global Human Body Models Consortium.[4] The observations from these simulations are summarized as follows.

- At 40 mph simulated crash, all three strengthened guards prevented PCI in the full and 50 percent overlap tests, but only the Manac prevented PCI in the 30 percent overlap test. However, in the full overlap test, the simulated injury risks were high for all guard designs including the Manac (approximately 80 percent risk of AIS 3+ thorax injury) due to the forces of vehicle deceleration exerted on occupants.
- In a 45-mph simulated crash, all three strengthened guards prevented PCI in the full, but none could prevent PCI in the 30 percent overlap test. In the full overlap test, simulated injury risks were high for all guard designs (approximately 88 percent risk of AIS 3+ thorax injury) due to the forces of vehicle deceleration exerted on occupants.
- A 65-mph crash in this simulated study was observed to be unsurvivable for all guard designs studied.
- Regarding injury risk, there were no clear "Best Design" attributes among the three strengthened guards.
- THOR-50M and MS50-OS were generally in agreement with each other in terms of the relative injury risk assessments among the three guard designs.

[4] Global Human Body Models Consortium, Rochester Hills, MI.

Introduction and Scope of Work

Introduction

Truck-trailer underride crashes are among the most severe collisions that occur on the road each year, often leading to severe injuries or fatalities. A truck-trailer underride crash is defined as a crash that occurs when a passenger vehicle impacts the side or back of a truck-trailer and slides under the body of the larger truck or trailer. A mitigation measure for these types of events are trailer impact guards, which work to absorb a portion of the striking vehicle's kinetic energy. However, these structures do not always prevent PCI. Recently, NHTSA upgraded FMVSS No. 223,[5] which specifies the strength and energy absorption requirements that rear-impact guards must meet. Previously, the relationship between the quasi-static test protocols specified in FMVSS No. 223 and the rear-impact guard performance in high-speed dynamic crashes was not well characterized. Furthermore, the occupant response in rear-impact guard crash events that far exceeded the FMVSS No. 223 requirements was unknown. To this end, this project aimed to investigate these gaps in the literature through finite element simulation and analysis.

[5] See 49 CFR Part 571, FR. 89-124, 53505, June 27, 2024. www.govinfo.gov/content/pkg/FR-2024-06-27/pdf/2024-13957.pdf

Program Tasks Summary

The objectives were to develop finite element models of heavy truck rear-impact guards, simulate quasi-static FMVSS No. 223 test protocols, simulate dynamic testing of midsize and compact passenger vehicle frontal impacts into a trailer fitted with the previously developed rear-impact guard models, evaluate passenger compartment intrusion in these simulations, and evaluate THOR-50M and GHBMC response (injury risk prediction) in 40 mph, 45 mph, and 65 mph simulations.

This report summarizes the work performed under contract 693JJ921D000042 that includes the following:

- Aim 1: Developing Rear-Impact Guards Finite Element Models
- Aim 2: Assessing the Relationship Between Quasi-Static Testing and Dynamic Crash Response
- Aim 3: Evaluating Occupant Response (injury risk prediction) in High-Speed Collisions into Strengthened Rear-Impact Guards

Aim 1: Developing Rear-Impact Guard Finite Element Models

Background: FMVSS No. 223

In 1996 the Department of Transportation issued a final rule that established two new FMVSS, which operating together were intended to reduce the number of injuries and fatalities resulting from the collision of passenger vehicles into the rear end of heavy trailers and semi-trailers. The first standard, FMVSS No. 223, *Rear impact guards*, specifies the performance requirements that rear-impact guards must meet to be installed on new trailers and semi-trailers. The second standard, FMVSS No. 224, *Rear impact protection*, specifies which vehicles must be equipped with a rear-impact guard. The two rules address the problem of a rear underride crash where a passenger vehicle collides with the rear end of a trailer and the front end of the passenger vehicle slides under the rear end of the trailer. In the most severe cases, the passenger vehicle underrides so far that the rear end of the trailer strikes and enters the passenger compartment, which is referred to as "passenger compartment intrusion."

When issued for the first time in 1996, FMVSS No. 223 specified the guard would be tested either mounted to a rigid test fixture or a secured trailer (61 FR 2004, Jan 24, 1996). Additionally, it specified how to identify three test locations across the width of the guard. These locations are denoted "P1", "P2", and "P3". Test location P1 is located at a distance 3/8 the guard width from the vertical longitudinal plane passing through the center of the guard. Test location P2 lies at the center of the guard's horizontal member. P3 is any point on the rearmost surface of the horizontal member that is not less than 355 mm and not more than 635 mm from the vertical longitudinal plane passing through the center of the guard. At each test location, a square force application device is pushed into the guard slowly (1.0-1.5 mm/sec) until 125 mm deflection is met. To achieve compliance, by the time 125 mm of deflection is reached, the guard must resist a force of at least 50 kN at P1 and P2. At P3, the guard must resist 100 kN of force before 125mm of deflection is reached as well as absorb at least 5,650 J of energy through plastic deformation. Additionally, the maximum ground clearance of the rear-impact guard was set to 560 mm.

In 1998, FMVSS No. 223 was amended (63 FR 3662, Jan 26, 1998). The amendment clarified minimum dimensions specified in 1996 as well as modified the force application device displacement rate. The new application rate was specified to be between 2.0 to 9.0 cm/min (previously 6.0-9.0 cm/min). At this time, FMVSS No. 224 was amended, adjusting which types of vehicles were subject to the Standard.

In 2004, FMVSS No. 223 was amended (69 FR 67662, Nov 19, 2004), adjusting where the compliance label should be placed on the rear-impact guard, but no technical modifications were made to the standard.

Also in 2004, Canada published a similar standard to FMVSS No. 223. Entitled Canadian Motor Safety Standard (CMVSS) No. 223, *Rear impact guards* (9 Canada Gazette Part II, Vol. 138, No. 20, 2004-10-06), a second North American standard was developed and went into effect in 2007. In many ways CMVSS No. 223 and FMVSS No. 223 at this time were similar. Each allowed for a rear-impact guard to be tested on either a rigid fixture, or a fixed trailer. Both specified a force application device with a 203 mm x 203 mm square face. Both included P1 and P2 impact locations as previously defined by FMVSS No. 223 in 1996. For these locations, the guard must resist 50 kN of force with no more than 125 mm of deflection. However, CMVSS No. 223 has

no requirements for resistance at the P3 location. Instead, a uniform distributed load (UDL) application device is described. The face of this device must have a height of 203 mm, and a width that exceeds the distance between the outside edges of the outermost upright supports. The UDL application device is pushed into the guard 125 mm, and then returned to its original location. The guard must resist at least 350 kN of load in this test and absorb at least 20 kJ of energy through plastic deformation.

On July 15, 2022, NHTSA issued a final rule upgrading FMVSS No. 223 (87 FR 42366, July 15, 2022). This change was the largest since FMVSS No. 223 was established in 1996 and, in many ways, harmonized FMVSS No. 223 and CMVSS No. 223. P1 and P2 location definitions, force applicators, and resistance requirements (50 kN) remained the same. The P3 force application previously specified by FMVSS No. 223 was replaced with the UDL as described by CMVSS No. 223. The UDL force resistance requirements were set to the same level as CMVSS No. 223 (350 kN); the plastic deformation energy absorption requirements were set at the same level as well (20 kJ). The rule also requires that the guard maintain a maximum ground clearance of 560 mm following the UDL test.

Background: Passenger Compartment Intrusion

Passenger compartment intrusion has conflicting definitions depending on the source. In 2016, the Insurance Institute for Highway Safety issued a test protocol for dynamic tests of passenger vehicles striking the rear-impact guard attached to truck-trailers. In that protocol, PCI was defined by the IIHS as any portion of the trailer intruding beyond the precrash position of the rear surface of either A-pillar (Semi-Trailer Underride Evaluation Crash Test Protocol Version I, 2016). In the following years, the IIHS updated this protocol. Semi-Trailer Underride Evaluation Crash Test Protocol (Version II, 2021) redefined PCI as any portion of the trailer contacting the windshield, A-pillars, or roof of the striking vehicle. This updated, more stringent, definition of PCI was used in this project.

Selection and Procurement

Three unique truck-trailer rear-impact guards were specified by NHTSA for FE model development. The three guards were manufactured by Wabash National, Great Dane, and Manac. Specifically, the Wabash 05006821-07, Great Dane GDP11716266, and the Manac 914-0901002-G rear-impact guards were ordered (Figure 1). These guards were certified as meeting FMVSS No. 223 and CMVSS No. 223 as specified at the time of manufacture (pre-2022 update). NHTSA had previously sponsored quasi-static research testing based on the 2004 edition of FMVSS No. 223 to be conducted on these three guards at the MGA Research Corporation (Troy, Michigan). The data were provided to be used to validate the FE models for this project. A single guard of each type was purchased from certified dealers for each company and delivered to the Elemance, LLC headquarters in Winston-Salem, NC. The guards were new from the manufacturer. It should be noted that the Wabash “S-Tubes” visible on the outboard edges in Figure 1 are not included in the base Wabash guard. As NHTSA had tested the Wabash guard for compliance without these add-ons, and this data was to serve as the validation data for the guard model, this structure was not included in this project.

Great Dane GDP11716266 Manac 914-0901002-G Wabash 05006821-07

Figure 1. Truck rear-impact guards selected for this study. Photographs from IIHS dynamic test series.

CAD Development

Upon receipt of the rear-impact guards, traditional measuring techniques were used including digital calipers (Mitutoyo 500-196-30), a digital outside micrometer (Mitutoyo 293-832-30), and measuring tape to record dimensions of each guard. Sheet metal and metal plates were measured at multiple locations to account for machining variations. The average of the measurements were then calculated to develop the guards' baseline dimensions. Using SolidWorks[6] CAD models of each guard were created. These were then exported in Initial Graphics Exchange Specification (IGES) format. Figure 2, Figure 3, and Figure 4 depict the rendered CAD drawings of the Wabash, Great Dane, and Manac guard, respectively. The reader is referred to the open-source FE models of the guards for exact dimensions.

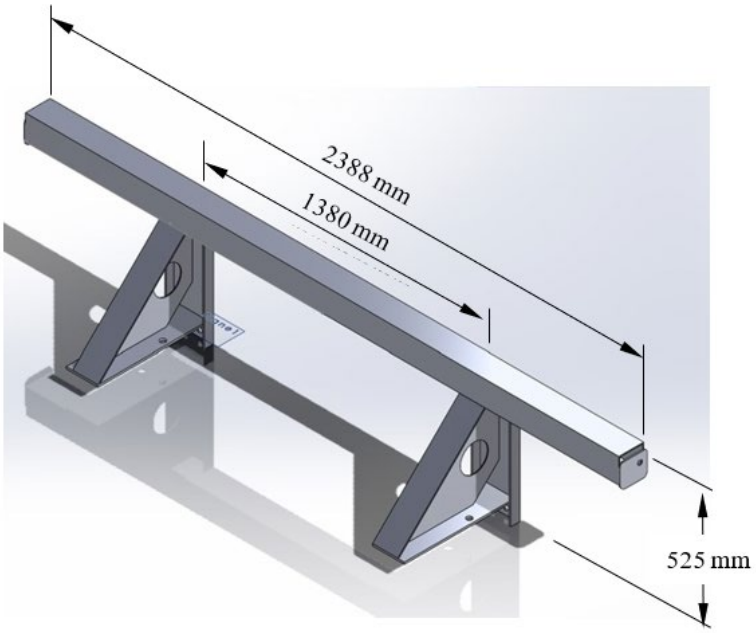

Figure 2. Geometry of the Wabash guard rendered in SolidWorks

[6] Dassault Systemes, Velizy-Villacoublay, France.

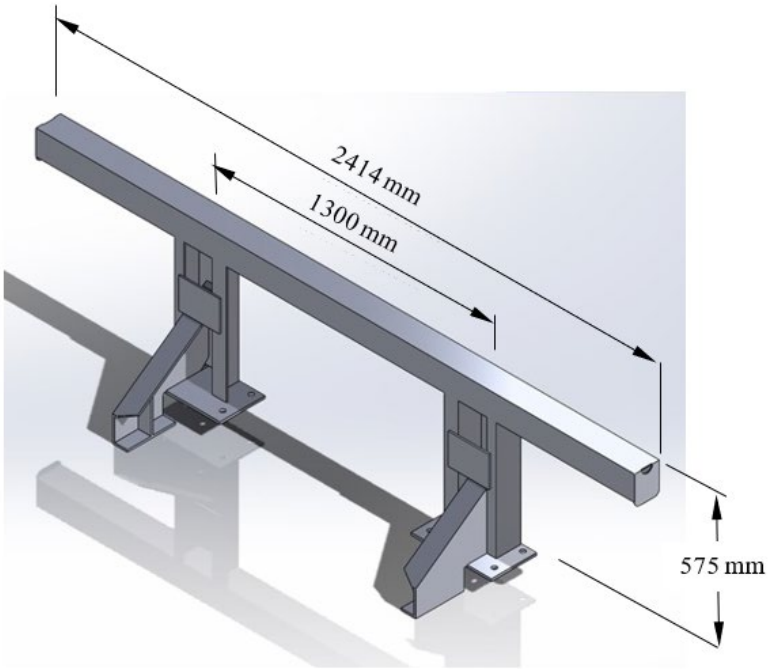

Figure 3. Geometry of the Great Dane guard rendered in SolidWorks

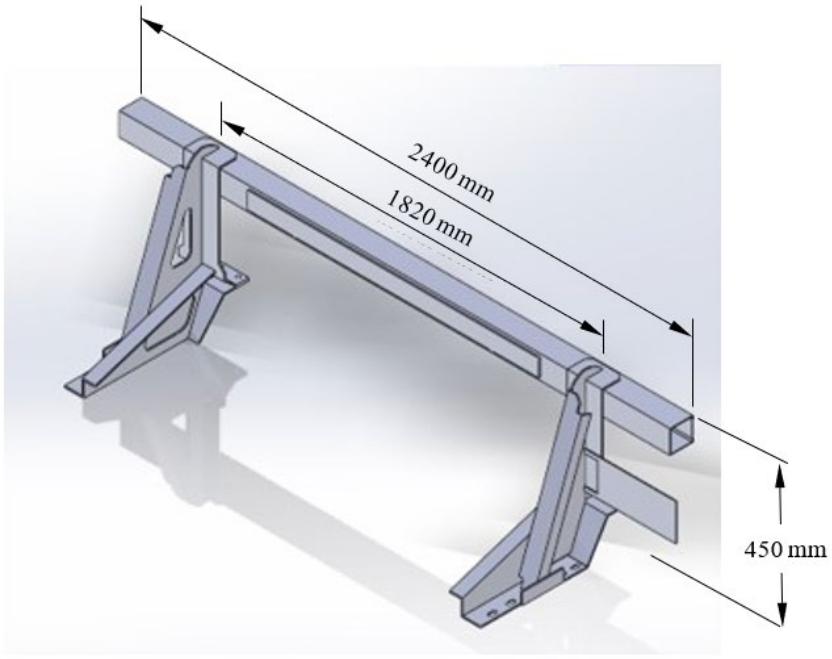

Figure 4. Geometry of the Manc guard rendered in SolidWorks

Material Characterization

Following geometry capture, the physical guards were then cut in half vertically. One half remained onsite for future reference during the project, and the second half was used for material characterization. Metallurgical Technologies, Inc.[7] was contracted to conduct metallurgical analysis on the three guards including chemical composition analysis and tensile testing. Composition analysis was performed using an optical emission spectrometer in accordance with ASTM E415. For chemical composition analysis, one sample was obtained from the horizontal member and one sample was obtained from the upright support for each guard. Results indicated that they met the chemical composition product analysis requirements for ASTM A572 Grade 65 Type 1 high strength, low alloy steel. Two samples were tested for each guard. The sample labeled Wabash B exhibited slightly elevated manganese, above permissible product variations. The chemical composition analysis demonstrated the vertical supports, and the horizontal member were composed of the same type of steel for each guard. Therefore, tensile testing specimens were machined from the horizontal member of each guard. Tensile testing of the samples was performed in accordance with ASTM A370 and E8. Results of the chemical composition analysis and tensile testing are provided in Table 1. Raw stress-strain curves from the tensile testing are provided in Appendix A: Mechanical Characterization Data.

[7] Metallurgical Technologies, Inc., Mooresville, NC.

Table 1. Chemical composition analysis; tensile test results

Element	Wabash Sample A	Wabash Sample B	Great Dane Sample A	Great Dane Sample B	Manac Sample A	Manac Sample B	ASTM A572 Grade 65 TYPE 1 Requirements
Carbon	0.09	0.10	0.10	0.10	0.11	0.10	0.26 max
Manganese	0.69	1.46	1.04	0.56	0.66	0.59	1.35 max
Silicon	0.08	0.12	0.05	0.24	0.05	0.19	0.40 max
Columbium	0.02	0.03	0.04	0.02	0.03	0.02	0.005-0.05
Phosphorous	0.01	0.01	0.02	0.02	0.02	0.01	0.04 max
Sulfur	0.01	0.01	0.01	0.01	0.01	0.01	0.05 max
Property	**Wabash Test 1**	**Wabash Test 2**	**Great Dane Test 1**	**Great Dane Test 2**	**Manac Test 1**	**Manac Test 2**	**ASTM A572 Grade 65**
Yield Strength (MPa)	619.1	599.2	611.6	630.9	599.8	639.1	448.2
Ultimate Strength (MPa)	702.6	701.2	687.4	703.3	670.2	695.0	551.6
% Elongation at Fracture	18.0	18.0	21.0	20.2	23.5	21.0	17 min

Material Model Development

For each guard, the stress and strain data were averaged to create a characteristic engineering stress – engineering strain curve. This was done by averaging the engineering stress measured in each sample for a given strain value. The *MAT_SIMPLIFIED_JOHNSON_COOK material model in LS-DYNA was selected for modeling the steels for each guard. This material model was selected due to its relatively low mesh-sensitivity and for its ability to capture the elasto-plastic behavior of steel. *MAT_SIMPLIFIED_JOHNSON_COOK can capture strain-rate sensitivity, but for this project, that capability was not included as the experimental characterization was only conducted at quasi-static rates. The material model is governed by several equations as described below. First, the user must specify a modulus of elasticity and then the yield stress is governed by the following equation:

$$\sigma_y = (A + B\bar{\varepsilon}^{p^N})(1 + C \ln \dot{\varepsilon}^*)$$

Here, σ_y is the stress post-yield, A, and B are input constants with units of stress, $\bar{\varepsilon}^p$ is effective plastic strain, N is a unitless constant governing the shape of the post-yield response and C is a strain-rate sensitivity constant. As mentioned above, since strain rate sensitivity is not considered for this project C was kept at 0 which also eliminates the use of $SIGSAT$ which is the maximum effective stress after rate effects are added. Furthermore, the maximum stress is limited by user-specified maximum stress, *SIGMAX*, which modifies σ_y through the following equation:

$$\sigma_y = min\left[A + B\bar{\varepsilon}^{p^N}, SIGMAX\right]$$

Finally, a tensile failure criterion can be incorporated into the model by setting $PSFAIL$ (effective plastic strain at failure) to a nonzero value. Thus, six total parameters govern the model behavior: E, A, B, N, $SIGMAX$, and $PSFAIL$.

In this study, LS-OPT was employed to fit the *MAT_SIMPLIFIED_JOHNSON_COOK parameters through inverse FE analysis. Models of tensile test specimens, or dog bones, were developed using 2D shells with identical dimensions as the ASTM E8 physical specimens and were pulled in tension while monitoring engineering stress and strain. While varying the six material parameters previously described the absolute error between model response and the average experimental stress-strain was minimized. A direct optimization through a genetic algorithm was used in LS-OPT and a limit of 100 generations of 30 designs was set (i.e., 3000 simulations). After the LS-OPT program finished, the final optimal parameters were extracted, and the engineering stress – engineering strain from the optimal simulation was overlayed on the experimental data (Figure 5, Figure 6, Figure 7). The material parameters are provided in Table 2. It should be noted that in the later simulations, element erosion was not included, and thus $PSFAIL$ was not used.

Table 2. Material properties used for each truck-trailer rear-impact guard (All values are in GPa, except for "N" and "PSFAIL," which are unitless.)

Guard	E	A	B	N	SIGMAX	PSFAIL
Wabash	189.93	.6274	.7788	.8780	.7057	.187
Great Dane	196.84	.6177	.7432	.8963	.7565	.189
Manac	209.91	.6007	.7271	.8944	.7402	.197

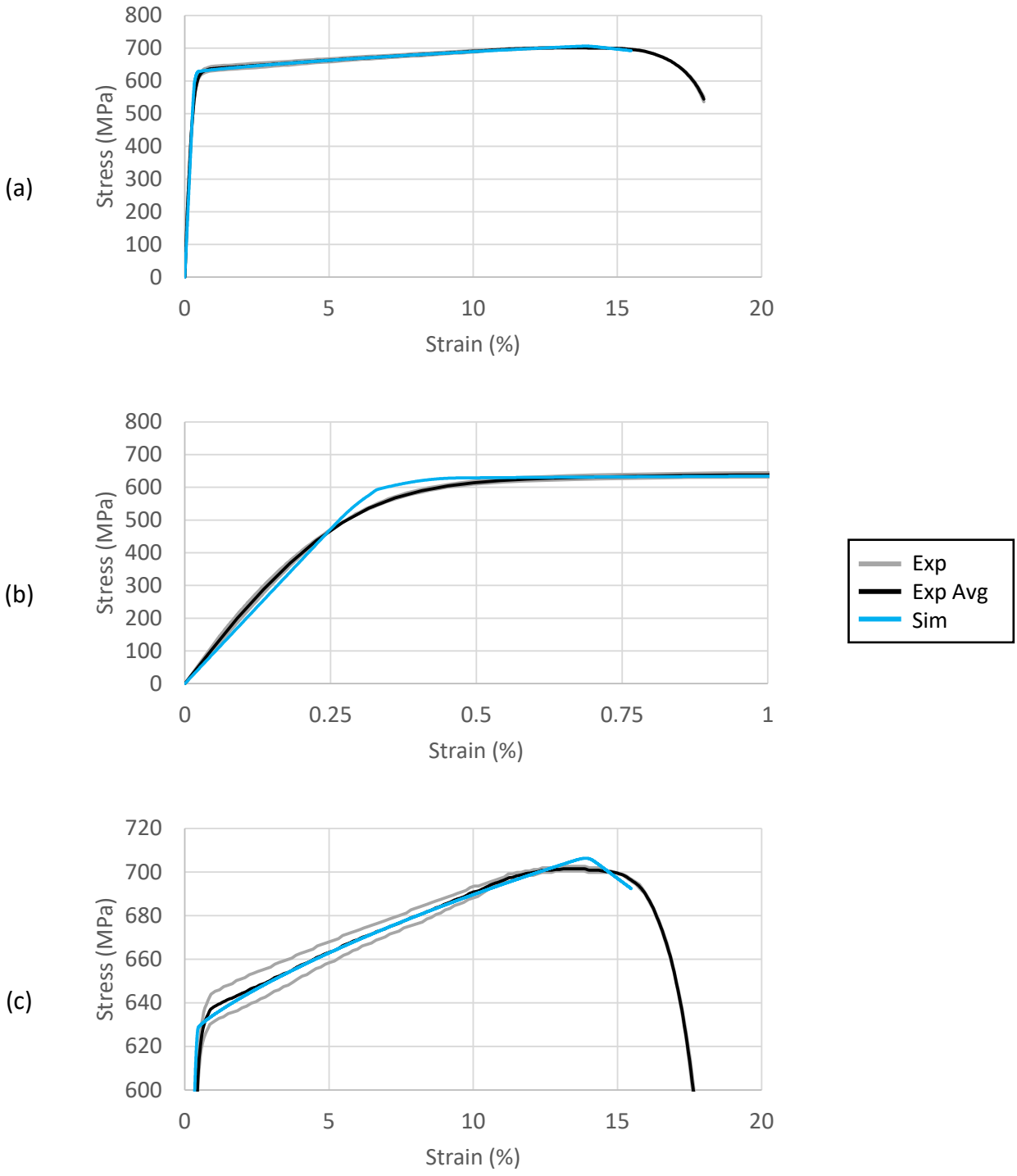

Figure 5. Experimental and Simulation stress-strain response of the Wabash dog bone specimens. (a) full data set, (b) close-up of the elastic range and yield point, (c) close-up of post-yield behavior.

(a)

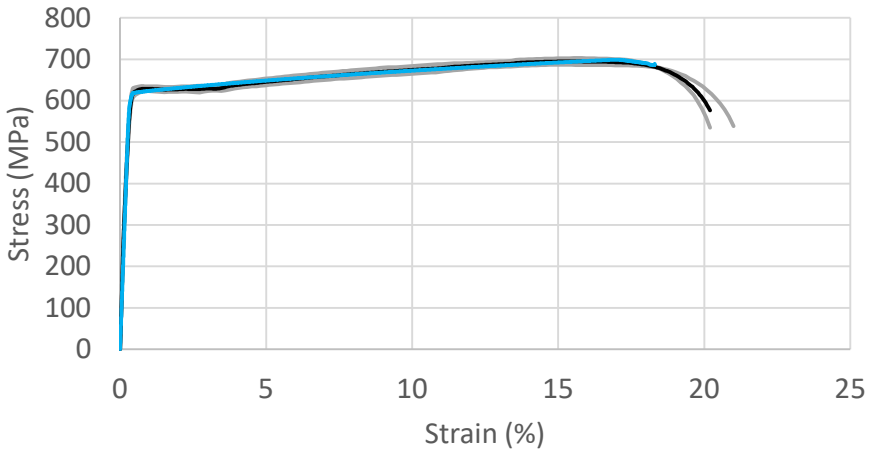

(b)

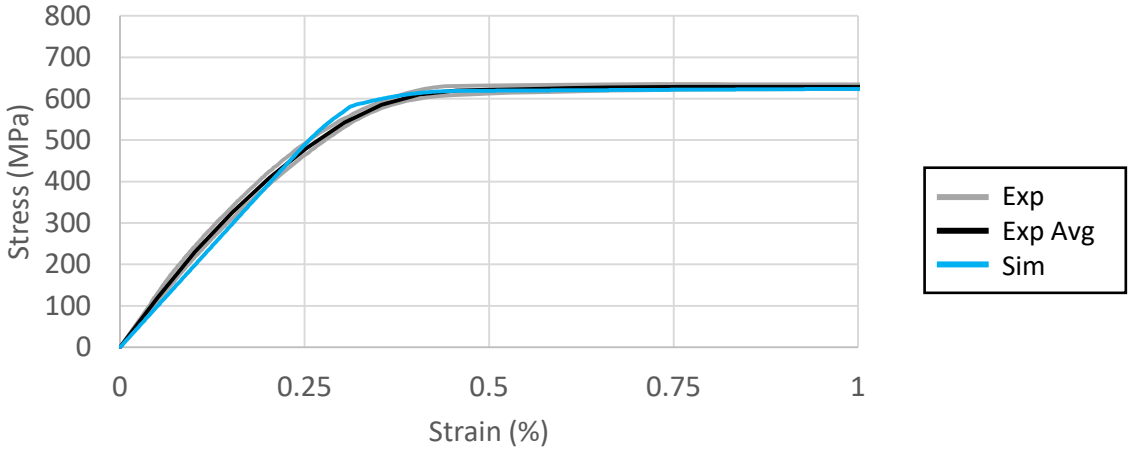

(c)

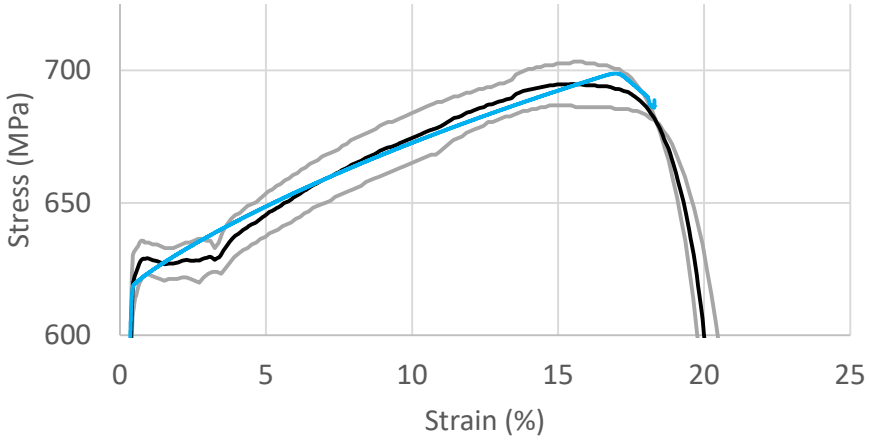

Figure 6. Experimental and Simulation stress-strain response of the Great Dane dog bone specimens. (a) full data set, (b) close-up of the elastic range and yield point, (c) close-up of post-yield behavior.

(a)

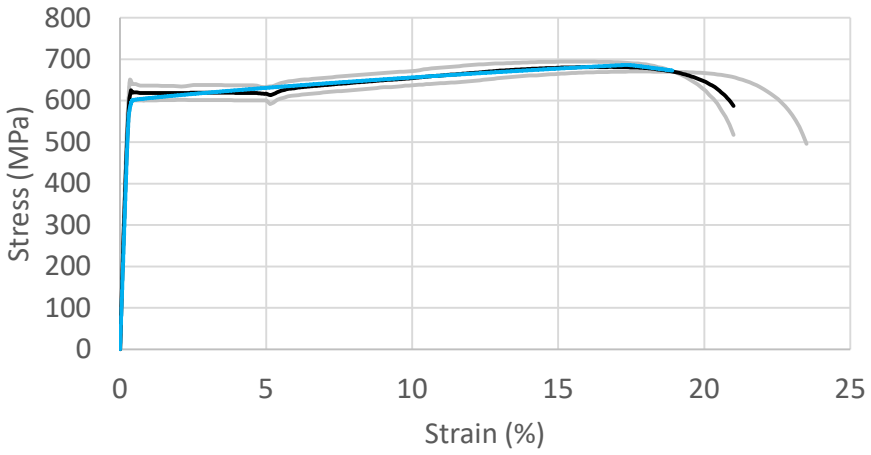

(b)

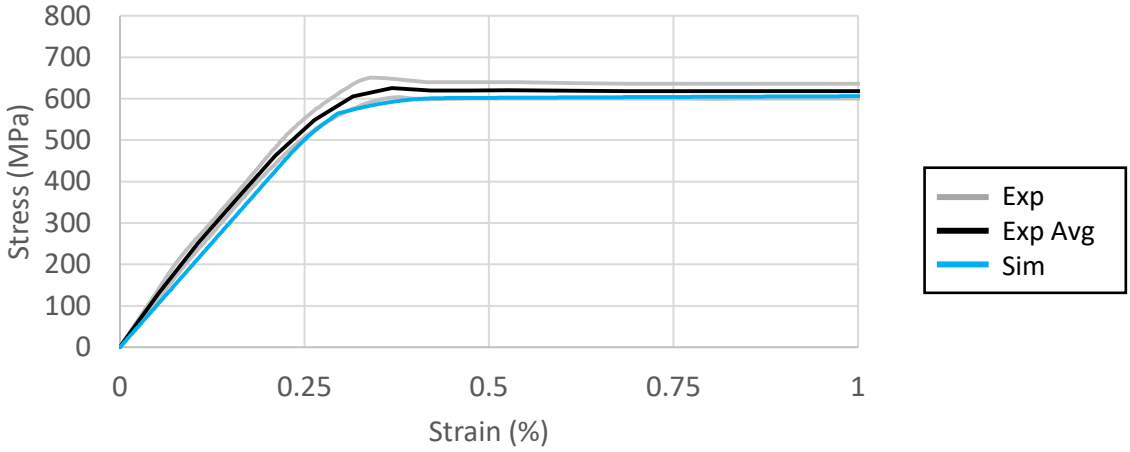

(c)

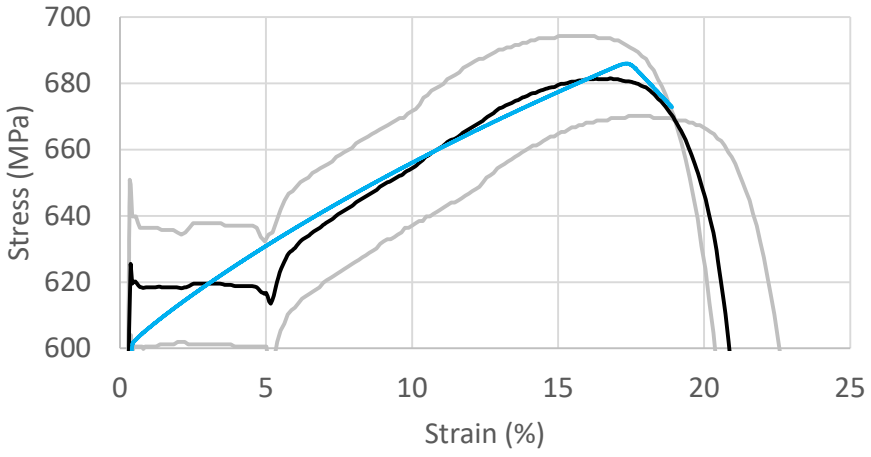

Figure 7. Experimental and Simulation stress-strain response of the Manac dog bone specimens. (a) full data set, (b) close-up of the elastic range and yield point, (c) close-up of post-yield behavior.

Mesh Development

The generated CAD was exported as an IGES file and then imported into Beta ANSA[8] (for meshing. As the guards were all constructed of bent and welded sheet and plate steel, shell elements were selected for development of the LS-DYNA models. Where possible, welded portions of the guard were represented by node-to-node mesh techniques. *CONTACT_TIED_NODES_TO_SURFACE was used to represent the welded portions of the guard where node-to-node connections were not possible. A heat effected zone from welding of the physical guards was not considered. Ultimately, sheet metal thickness was represented by shell element projection (NLOC) within the *SECTION_SHELL card for each part. Therefore, in some cases the outer face of the CAD was meshed, in some cases the inner face of the CAD was meshed, and in some cases, a mid-surface was generated before meshing. The NLOC directions were set such that thickness projections matched the physical guard, and shell element thicknesses were then assigned based on physical measurements. Quadrilateral shell elements accounted for more than 99 percent of the final meshed models, with triangular shell elements used where required. Target element edge length was set to 10 mm as this length was anticipated to yield both reasonable run times and accuracy. The total element count for each truck-trailer rear-impact guard was 15,688 (Wabash), 18,414 (Great Dane), and 21,338 (Manac). Both the Wabash and Great Dane models were developed to be symmetric about the mid-plane. The Manac guard was symmetric about the mid-plane except for the license-plate sheet metal attached to the left vertical support. Element formulation (ELFORM) 2 (Belytschko-Tsay; under integrated shell elements) were used throughout the guards with a stiffness formulation *HOURGLASS card (type 5). Images of the guards with the mesh turned off are provided in Figure 8.

[8] Beta CAE, Thessalonika, Greece.

(a)

(b)

(c)

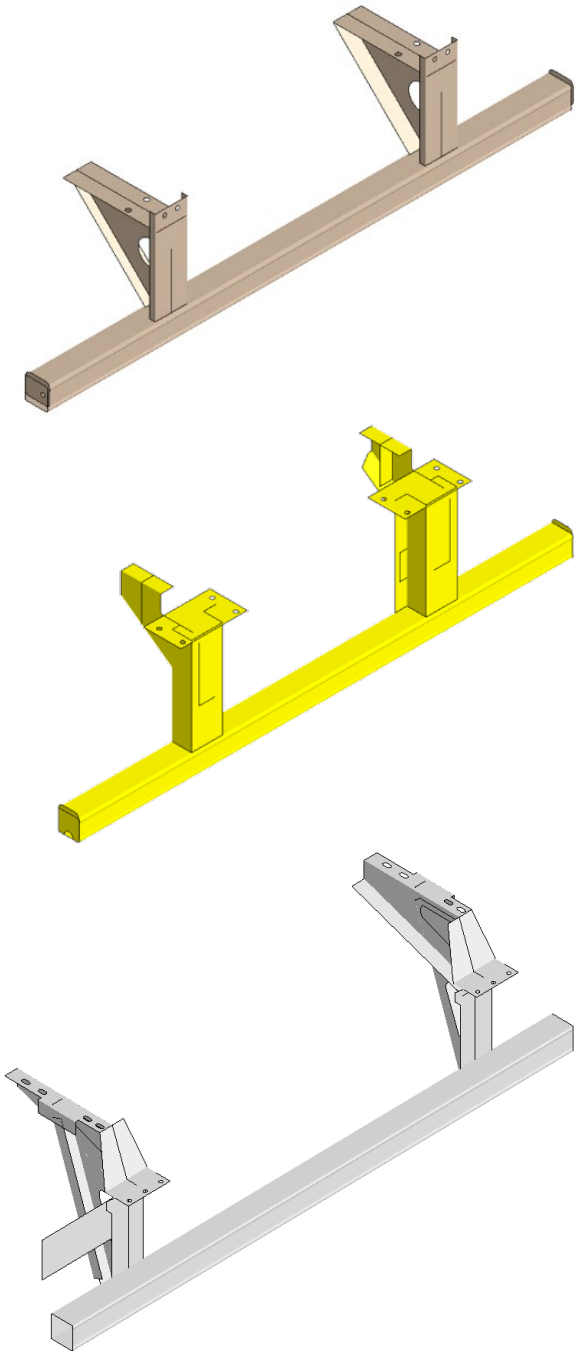

Figure 8. Finite element models of the rear-impact Guards
(a) Wabash, (b) Great Dane, (c) Manac. Images are not to scale.

Model Validation

Description of Experimental Data

At the time of manufacture of each guard, FMVSS No. 223 specified quasi-static loading of the rear-impact guards at three different locations (P1, P2, P3) (Figure 9). Each point load location was loaded by a steel impacting face with dimensions 203mm x 203mm, and an edge radius of 5mm. Test location P1 is located at 3/8th of the width of the horizontal member on either side of the centerline of the horizontal member. Test location P2 is located at the centerline of the horizontal member. Test location P3 is located between 355 mm and 635 mm from the horizontal member centerline. At the P1 and P2 test locations, a force of 50 kN is applied. At P3, a force of 100 kN is applied. For P1 and P2, the force is applied until the force requirement is met, or the guard deflects 125 mm. For P3, in addition to the force requirements, the guard must absorb 5.65 kJ of energy through plastic deformation. The applied loading rate must be between 1 mm/s and 1.5 mm/s. During testing, the guard may be either attached to a rigid fixture, or a trailer.

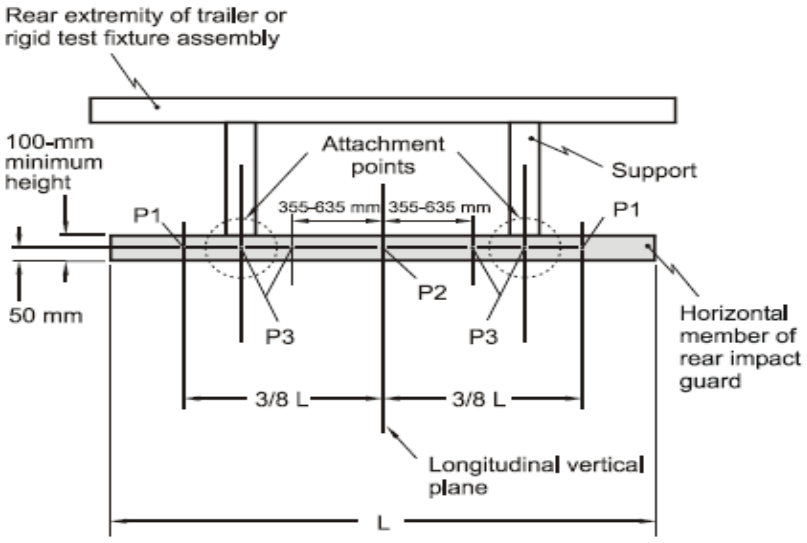

Figure 9. Impact locations for quasi-static loading as specified by FMVSS No.223 (2004)

Prior to the project start, as part of its compliance test program, NHTSA had contracted with MGA Research Corporation to conduct the previously described tests on each of the guards used in this project. The accompanying reports are available in the NHTSA compliance database.[9] Both force-deflection data and images of the guards before and after testing were included. The data represented a sample size of one for each impact location. Videos of the tests were not included. The Great Dane and the Manac guard were tested on a rigid fixture, while the Wabash guard was tested on a trailer.

[9] Wabash: https://static.nhtsa.gov/odi/ctr/9999/TRTR-646016-2018-001.pdf;
Manac: https://static.nhtsa.gov/odi/ctr/9999/TRTR-646006-2018-001.pdf;
Great Dane: https://static.nhtsa.gov/odi/ctr/9999/TRTR-646004-2018-001.pdf

Initial Simulation Setup

The first step in validating the rear-impact guard models involved creating the impactor used in the physical tests. This impactor is described in FMVSS No. 223 and above. SolidWorks was used to develop a CAD version of the impactor and then it was imported to Beta Ansa for meshing. As the impactor is constructed of solid steel, it was modeled as a rigid body in LS-DYNA. Figure 10 depicts the impactor model, which included approximately 1,000 elements. The face of the impactor model was meshed with a similar element size as the guards (~10 mm) to ensure proper contact interaction during simulation. This precluded a true 5 mm edge radius from being formed, and instead a chamfered design was incorporated.

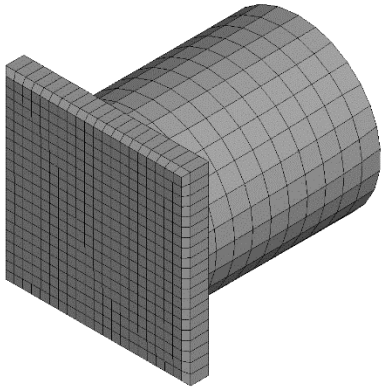

Figure 10. Finite element model of the square impactor

Using measurements reported by MGA Research Corporation in the experimental reports, the model impactor was positioned in the same locations as the physical tests. Additionally, the side of the guard tested physically was tested in the simulation. This was most important for the Manac guard, which was not left/right symmetrical due to the inclusion of a license plate holder. This decision also allowed for easier qualitative comparison of the post-test and post-simulation plastic deformation. Using images from the experimental test reports as guidance, simple models of the fixture at the attachment points were created and modeled as rigid steel. The nodes surrounding the bolt holes in the rear-impact guards were then constrained to these fixtures using *CONSTRAINED_EXTRA_NODES_SET. A secondary purpose of the simplified fixture models was to provide a surface for the top of the guard to interact with to resist deformation, while not rigidifying the rear-impact guard.

As the guard models were intended to be used in LS-DYNA Explicit simulation software later in the project, a decision was made to test the guards in the Explicit solver for validation. This precluded a 1-1.5 mm/s displacement rate in the simulation as the termination time would have needed to be set at least 8300 ms for P1 and P2, and higher for P3. Instead, the simulations were conducted at 1 mm/ms displacement rate. A one-off simulation at a slower rate demonstrated the increased speed did not significantly affect the force-displacement response of the impact condition and did not introduce inertial effects.

The rigid fixtures that supported the rear-impact guards during the FMVSS No. 223 simulations were originally constrained in space, though this proved later to be an incorrect modeling assumption. The impactor was constrained to move only in the X-direction, precluding

movement in Y or Z as well as restricting any rotational motion. The force recorded from the contact between the impactor face and the rear-impact guard was exported from each simulation along with the impactor motion. A *CONTACT_SINGLE_SURFACE was implemented which included all rear-impact guard parts so that during deformation the guard could predict reaction forces from guard self-contact.

Having implemented material models from inverse FE analysis, and modeling the guard with appropriate thicknesses and geometries, initial FMVSS No. 223 validation simulation results were dissimilar to the experimental tests. The most prominent difference came from the stiffness response of the guards in the P1 and P2 impact conditions, with the model exhibiting significantly stiffer response than the physical counterparts. Within the first two millimeters of displacement, the simulations were showing double to triple the resistance force as the experimental results. This triggered a re-examination of all model assumptions.

Modifications to Simulation Setup

Having seen demonstrably different results between model and experimental results in the P1 and P2 validation cases across each of the three models, the boundary conditions of the simulation and test were re-examined. While videos of the experimental tests were not included in the provided validation data from NHTSA, videos of similar tests are available online.[10] Examining these videos revealed a potential for the fixtures to move slightly during the loading of the rear-impact guards. Figure 11 is an example of this evidence from a stationary camera from another test series for a Wabash guard. Figure 11a is a freeze-frame of a P3 load case at the point of initial loading. Orange lines have been added around the boundary of the upper support in the top right corner of the image. A second freeze frame from a time in the middle of the test is provided in Figure 11b, with the original orange lines unmoved. The upper fixture is translated upward and rearward during loading, and that the assumption of a fixed boundary condition for the simulation was not accurate.

[10] www.youtube.com/watch?v=dRr1Y-l-IeI. Reiz Auto Parts Truck Bumper Tube test procedure for FMVSS 223 & CMVSS 223, *Rear impact guards*.

(a) (b)

Figure 11. Video evidence of fixture motion during P3 impact case. Video still from test start (a) and mid-test (b) Orange outline of upper fixture added and superimposed on mid-test picture.

While the displacement of the test fixture was small, the P1 and P2 test conditions also imposed small displacements (7 to 15 mm). It was hypothesized that this motion was a driving factor of the discrepancies between the model results and the experimental results. As the characterization of the motion of the fixtures was outside of the scope of this work, a model assumption was necessary. To incorporate the potential flexure of the physical fixture in the simulation, a stiff 1D spring was added to each of the support locations for the model. These were allowed to deform independently, but the motion of the fixture was only allowed to translate in the X-direction. A diagram of this addition and new boundary conditions is provided in Figure 12.

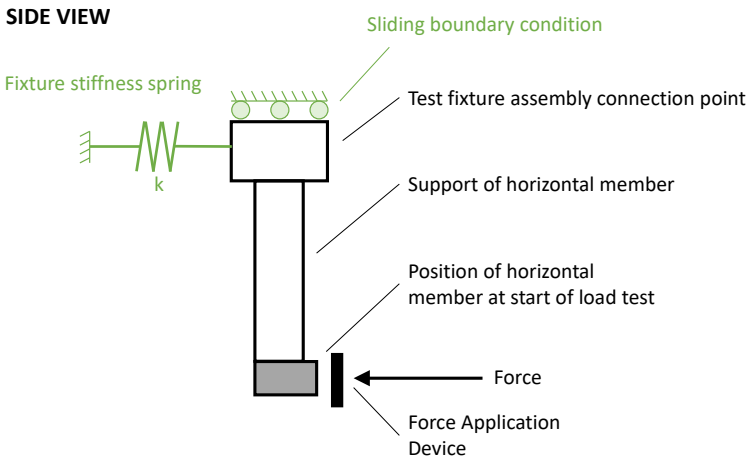

Figure 12. Diagram of fixture stiffness spring and boundary conditions used for model validation

The appropriate stiffness constant for the spring was unknown and thus a series of one-off simulations were conducted to test the hypothesis of a moving fixture. By incorporating the spring and setting a high stiffness constant (~20 kN/mm) for the Manac and Great Dane guard, which were tested on a rigid fixture, and a stiffness constant of 10 kN/mm for the Wabash guard, which was tested on a trailer, the initial stiffness of the simulation response dropped significantly.

However, small simulation discrepancies persisted. A decision to tune the thickness of the sheet metal models in conjunction with the stiff spring was made. Using LS-OPT, a small design of experiments (DOE) was developed to perturb the assigned sheet metal thicknesses of the models as well as the spring constant for each fixture model. P1, P2, and P3 impact cases were conducted and the absolute error between the simulation results and the experimental data were minimized through a genetic algorithm approach. A total of 270 combinations of sheet metal thicknesses and spring constants were simulated, and the optimal result was then incorporated into the rear-impact guard models. The P3 impact response was given a weighting factor of 1, while the P1 and P2 impact responses were given a weighting factor of 0.5 as the plastic deformation of a large impact was determined to be the most important. The impactor locations for these simulations can be seen in Figure 13.

(a)

(b)

(c)

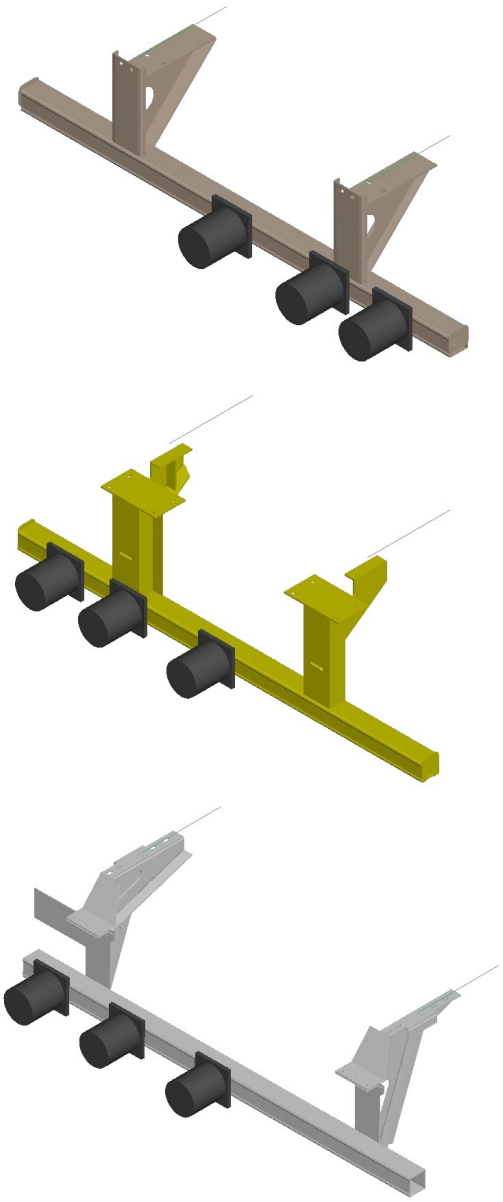

Figure 13. Simulation set up for quasi-static validation simulations showing the position of P1, P2, and P3 impactors on the Wabash (a) Great Dane (b) and Manac (c) rear-impact guard models. Springs representing the fixture flexure are in green.

The results of the model tuning returned exceptional results, except for the Manac P3 impact case. In the experimental data, a sharp inflection in force is recorded at approximately 100 mm of displacement. This inflection was absent in all the 270 simulations. Again, the boundary conditions were re-examined to ensure a proper simulation setup for this case. A careful examination of the post-test images included in the MGA test report revealed a red mark on a plate rearward of the impactor (Figure 14a, b) that was not present in the pre-test images. Additionally, a close-up image of the left edge of the Manac guard showed small deformation as well as the presence of red reflective marking tape. It was hypothesized that during the displacement of the quasi-static loader, the rear-impact guard deformed such that the offset of the

impactor face from the driver side of the quasi-static loader was not large enough to preclude contact and that the rectangular backing caused a secondary loading point after 100 mm of displacement as indicated in the arrow in Figure 14c.

(a)

Post-Test Photograph No. 14 of Test R18183 (P3)

(b)

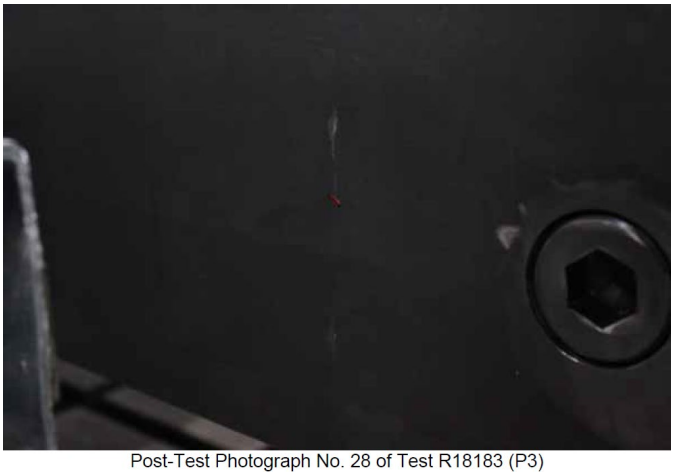

Post-Test Photograph No. 28 of Test R18183 (P3)

(c)

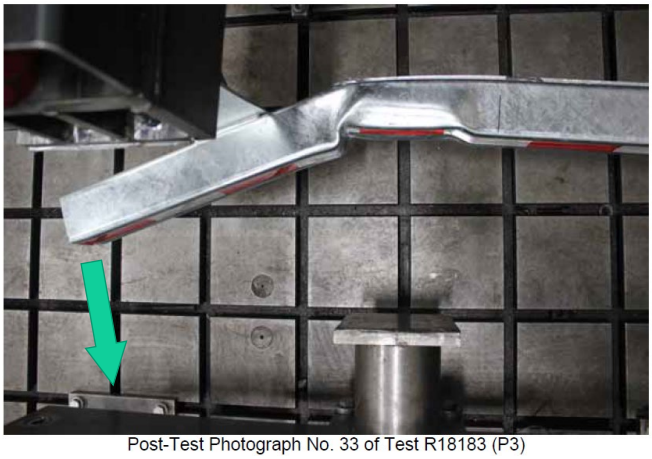

Post-Test Photograph No. 33 of Test R18183 (P3)

Figure 14. Picture evidence of secondary impact during Manac P3 physical testing

To test this hypothesis, a backing plate was modeled and offset from the impactor face using dimensions from known parts in the setup. This backing plate was then simulated to move with the impactor face in a one-off simulation. In this simulation, the horizontal member of the Manac guard model deformed enough to contact the backing plate, and this produced the inflection of the force response like the experimental results (Figure 15). Having arrived at boundary conditions that matched the experimental conditions, the simulation results were processed.

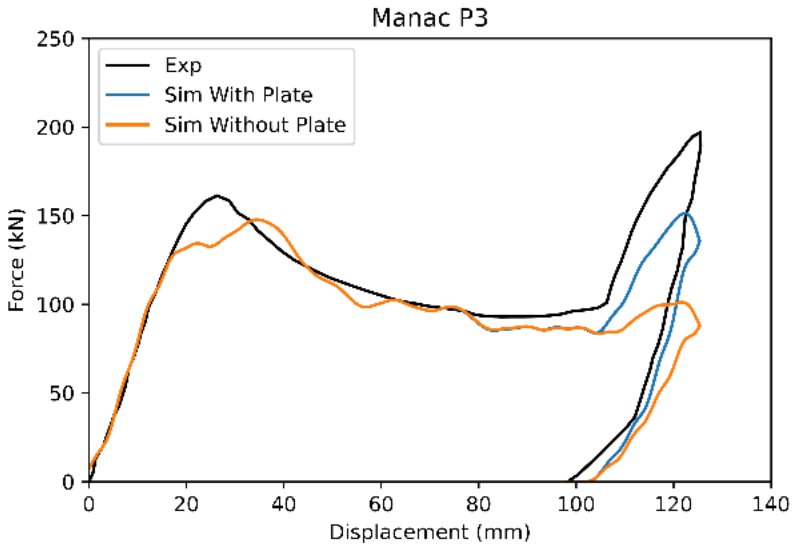

Figure 15. Simulation results of the P3 impact case with and without a backing plate compared to experimental results

Validation Results

The results of the validation of the rear-impact guards are detailed below. The LS-OPT fixture spring stiffness and sheet metal tuning resulted in very small differences between the average measured value of a given part and the final thickness assigned to that part in each model. The average absolute difference in thickness changes from measured to assigned was 0.14 ± 0.10 mm for the Wabash guard, 0.35 ± 0.37 mm for the Great Dane, and 0.33 ± 0.28 mm for the Manac guard. Figure 16 graphically depicts the deviations from the measured values for each part in each guard. The optimal fixture stiffness values were 9 kN/mm for the Wabash guard, 16 kN/mm for the Great Dane guard, and 20 kN/mm for the Manac guard. These values reflect a difference in testing a guard mounted to a large steel fixture (Great Dane and Manac) and mounting the guard to a trailer (Wabash).

First, the simulation results were compared qualitatively (visually). No discernable plastic deformation was noticed in either the computational or experimental results for the P1 and P2 impact cases. This was expected as the displacements in the tests were quite small, less than 15 mm. P3, however, displaced the impactor to 125 mm before returning the start position. Furthermore, the P3 impact is designed to plasticly deform the rear-impact guards to ensure energy absorption. Therefore, these tests lent themselves more easily to visual comparison. Figure 17, Figure 18, and Figure 19 contain images taken from several angles of the post-test deformation observed in both the physical tests and simulations.

The Wabash guard was impacted just inside of the right vertical support. The right vertical upright plasticly deformed backwards, with the flat rear facing sheet metal bending just below the front bolt connection point (Figure 17a). The horizontal member bent along the vertical axis with a slight upright deformation (Figure 17b). The section of the horizontal member that aligned with the impactor deformed plasticly on the inboard side of the impactor face (Figure 17c). The triangular piece of sheet metal buckled at the circular cutout (Figure 17d). The left upright support was not discernably deformed. Each of these deformations were captured by the computational model.

The Great Dane guard was impacted nearly square with the left vertical support. The left vertical upright deformed at the junction of the flat rear facing piece of sheet metal and the triangular offshoot of the design (Figure 18a). The horizontal member rotated slightly along its long axis. The flat steel plate that is parallel to the ground at the top of the vertical support deformed in a downward U-shape, with the areas that were bolted to the fixture retaining their original shape (Figure 18b). The right upright did not discernably deform (Figure 18c). Each of these phenomena were captured by the computational model of the guard.

The Manac guard demonstrated the largest deformations of the three rear-impact guards. The P3 impactor was positioned several inches inboard of the left vertical support. Specifically, the lateral distance between the inner most edge of the vertical support and the outermost edge of the impact face was 125mm. The left upright twisted inboard, and the left side of the horizontal member moved away from the fixture (Figure 19a). The right vertical support also demonstrated inboard rotation, but to a lesser degree than the left vertical support (Figure 19b). The portion of horizontal member directly in contact with the impact face underwent significant deformation, with buckling on both sides of the impactor. The outboard side of the horizontal member exhibited a nearly 90° kink following the test, with the upper face of the horizontal member bulging upward (Figure 19c). Both the gross and local deformations were replicated by the computational model of the guard.

P1, P2, and P3 force-deflection plots along with P3 energy-deflection plots are shown in Figure 20 and Figure 21. The simulations generally replicated the experimental data traces well. The P2 cases on average were the closest between experimental and simulations in magnitude and shape, followed by P1, and then P3. A small deviation in the force-displacement response in the Wabash P1 case was noted after 10 mm of displacement. At this point in the test, the Wabash computational model load began to flatline, whereas the physical model continued to show increased load to 15 mm. Great Dane and Manac P1 impact cases were more like experimental data.

The P3 impact simulations were the most dissimilar between the simulations and the experiments, though the general shapes of the curves were the same. The Wabash guard load curve continues to increase monotonically until approximately 40 mm of displacement, upon which a sharp drop in the force occurs. At approximately 75 mm of displacement, the load begins to increase again. The computational model exhibited this two-peak response as well, albeit with slightly higher force values. The Great Dane guard P3 force-displacement response demonstrated a monotonically increasing load all the way until 125 mm of displacement, which was also seen in the simulation. The simulation guard predicted a slightly higher peak force than the experiment. The Manac guard P3 impact case had the steepest initial force-displacement curve, reaching a peak of approximately 160 kN at 25 mm of displacement before a gradual decrease in force before rising again at 100 mm. The simulation response followed this initial

rise in force but did not achieve the same peak force. The gradual decrease in force was also captured by the computational model. As previously described, the edge of the horizontal member contacted the backing plate on the impacting device at 100 mm of displacement, which caused a sharp rise in the force values until 125 mm. The computational model for this impact also included this backing plate, and so the secondary impact was also seen computationally.

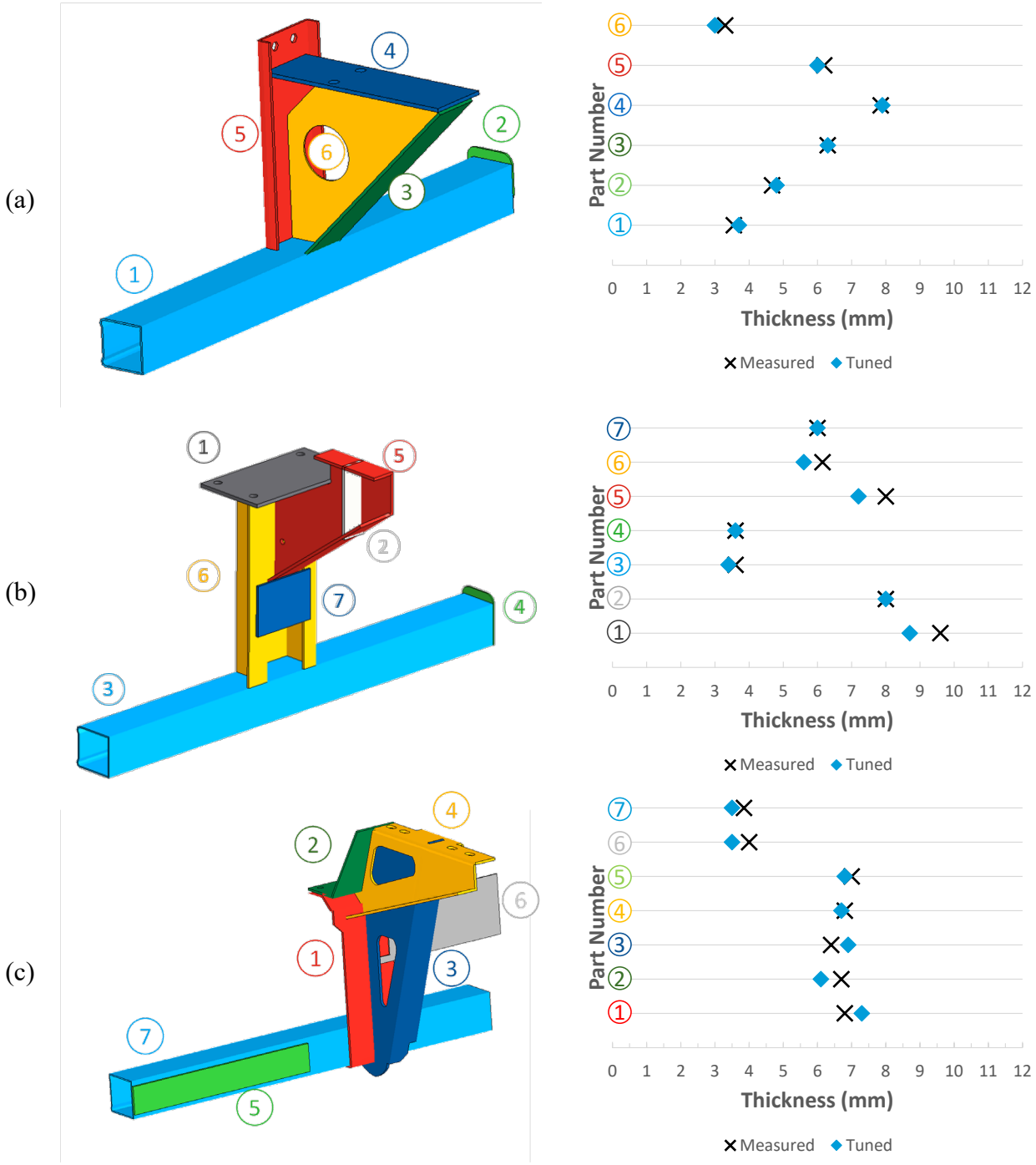

Figure 16. Sheet metal thickness values for each part in the models compared to the original measured values for the (a) Wabash, (b) Great Dane, and (c) Manac rear-impact guards

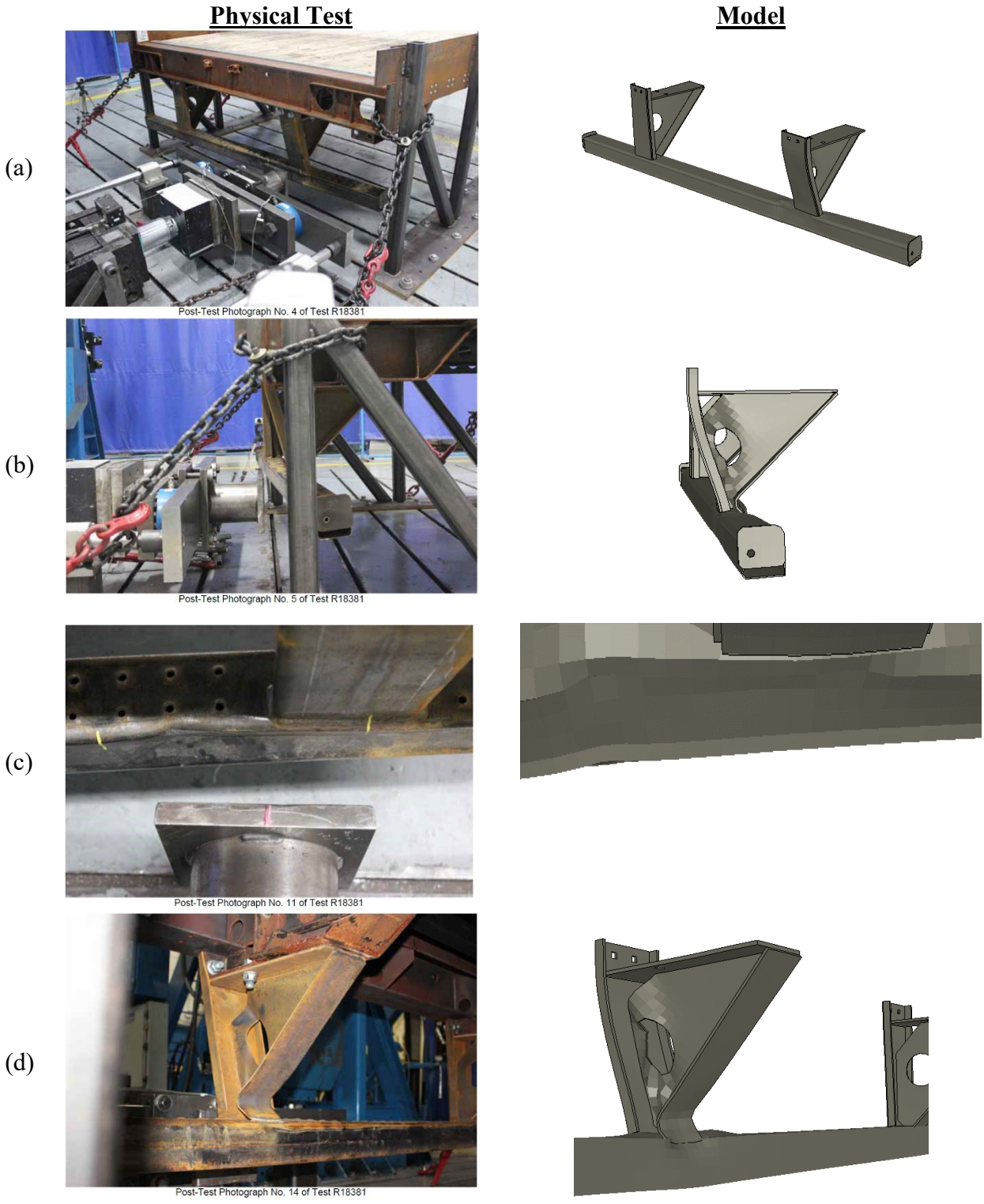

Figure 17. Images of post-test deformation in the P3 impact case comparing experimental results to simulation results for the Wabash guard

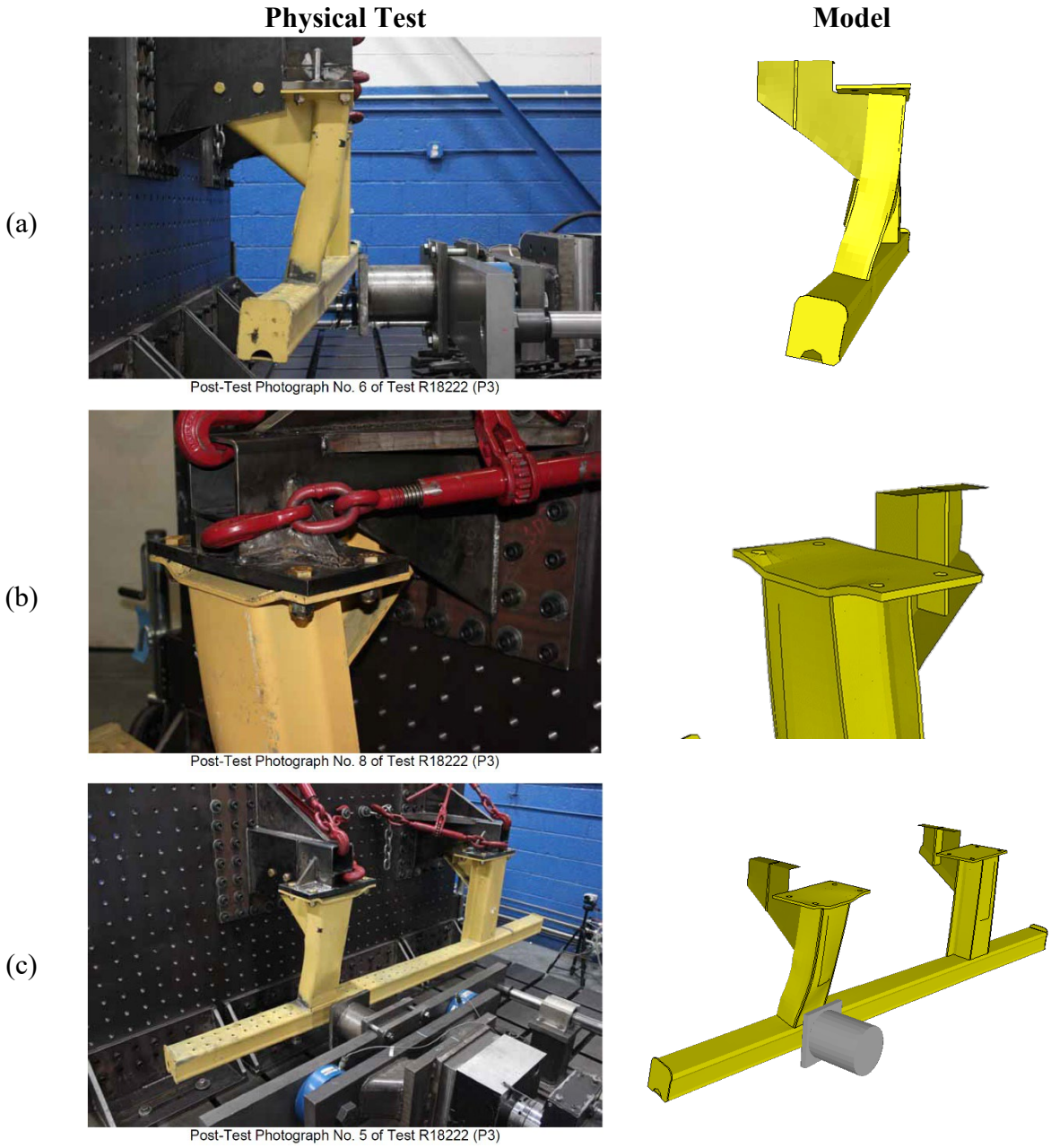

Figure 18. Images of post-test deformation in the P3 impact case comparing experimental results to simulation results for the Great Dane guard

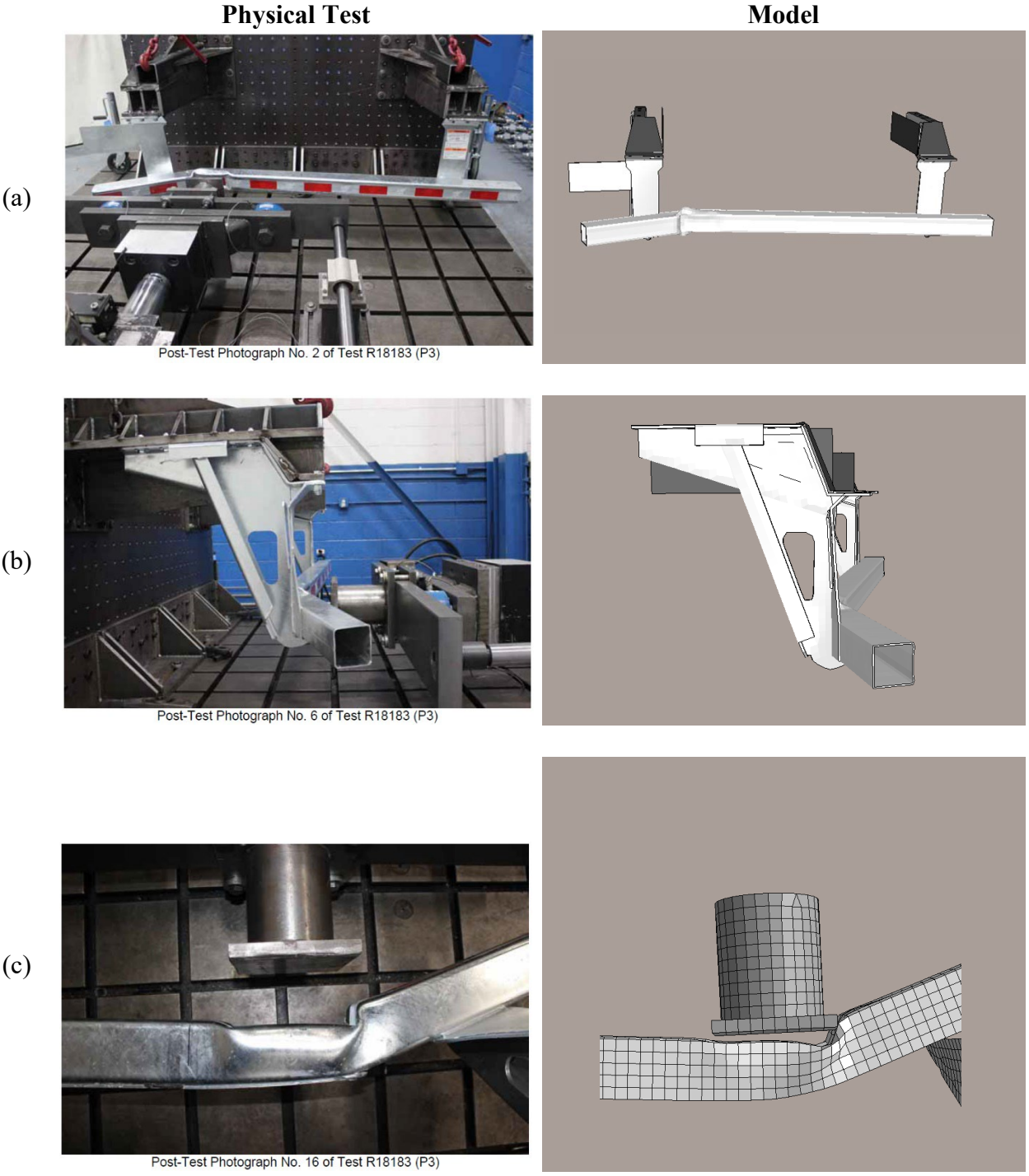

Figure 19. Images of post-test deformation in the P3 impact case comparing experimental results to simulation results for the Manac guard

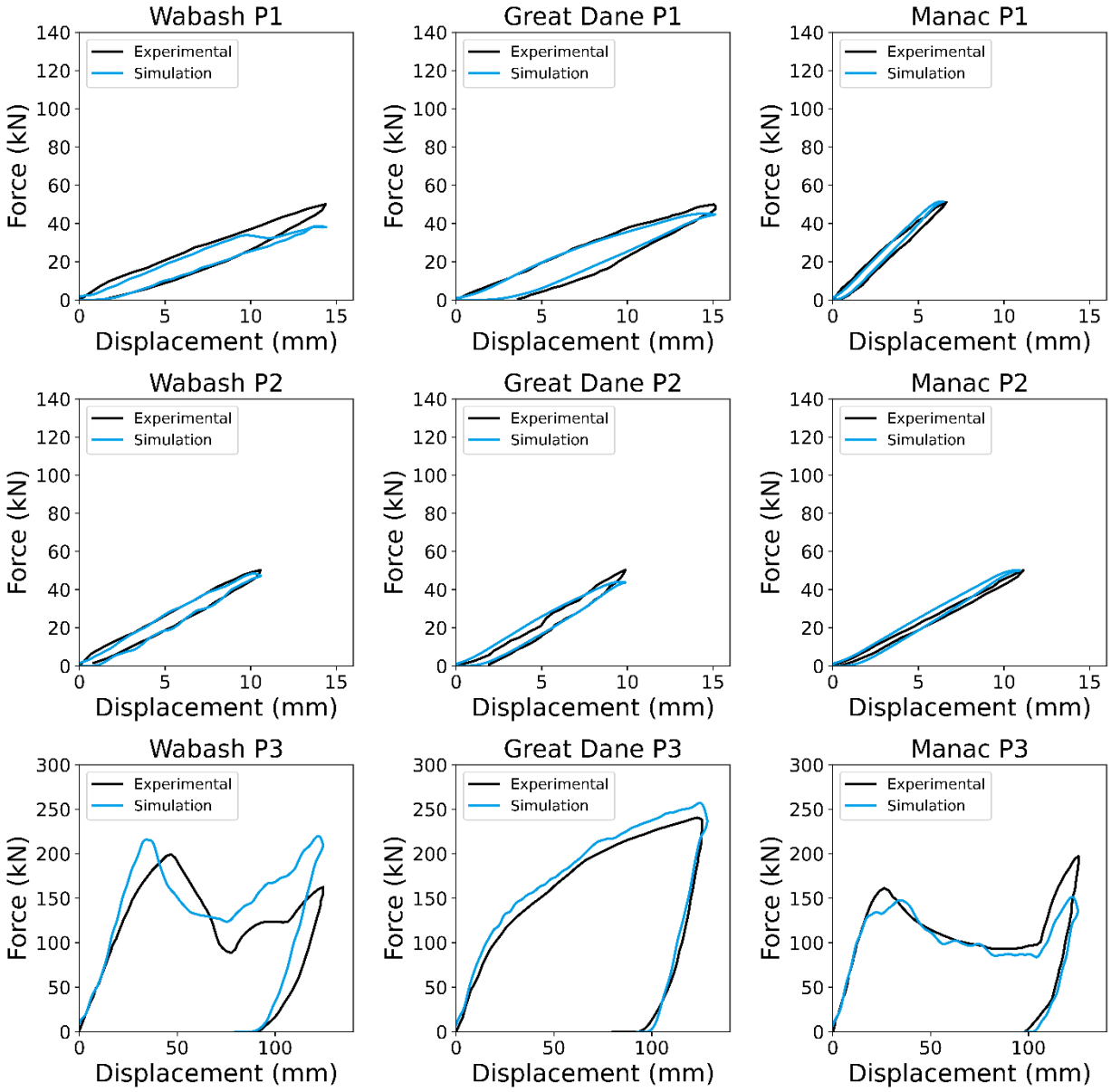

Figure 20. Experimental and simulation force-deflection results for the Wabash, Great Dane, and Manac rear-impact guards from FMVSS No.223 (2004) protocol

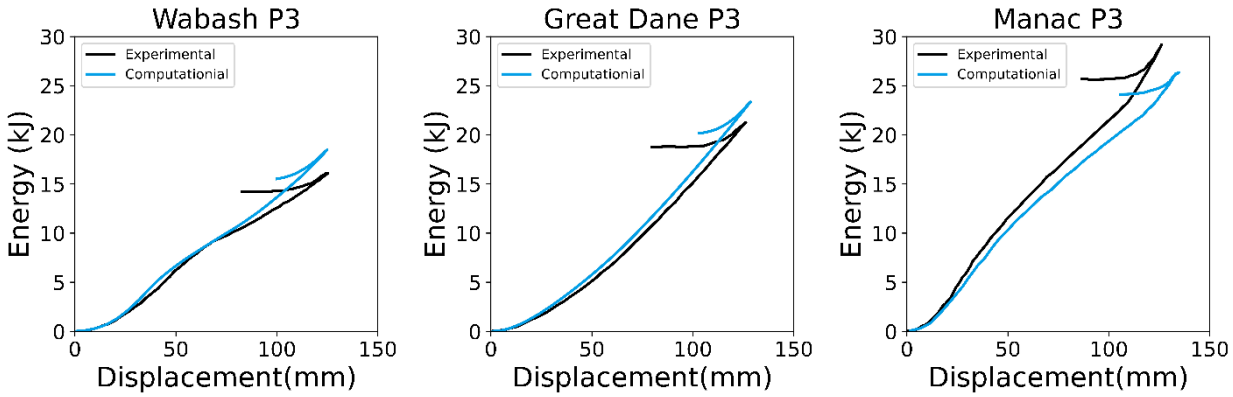

Figure 21. Experimental and simulation energy-displacement results for the Wabash, Great Dane, and Manac rear-impact guards from FMVSS No.223 (2004) protocol

CORrelation and Analysis (CORA) was used to compare the signals quantitatively. As the experiments and simulations were driven through displacement control, the signals were able to be converted to Force-time history signals before computing CORA. The default CORA settings were used, and the interval of evaluation was set at the beginning and end of the test series, effectively removing the ability for the curve to shift during calculation. As the experimental tests were conducted without repeats, the corridor portion of CORA was not used. Table 3 provides tabulated CORA scores for the simulations. As indicated visually, the P2 response was the most similar between simulation and experiment, with an average CORA score of 0.962 ± 0.047. This was followed by an average CORA score of 0.958 ± 0.048 for P2 across all models, and 0.906 ± 0.095 for P3. Of the guards, The Manac demonstrated the most similarity between simulation and experiment, achieving an average CORA score 0.954 ± 0.035. This was followed by the Great Dane (0.951 ± 0.019) and then the Wabash (0.921 ± 0.053). However, it should be noted that the lowest score achieved in any given test was 0.867 in the Wabash P3 impact, which is still considered “excellent” by ISO/TR 9790 categorization. The average CORA score across all simulations was 0.942 ± 0.041, demonstrating excellent correlation between simulations and experiments.

Table 3. CORA scores for the force-displacement signals from the computational models

Guard and force application point		Phase	Size	Shape	Total	Average
Wabash	P1	1.000	0.734	0.976	0.903	0.921
	P2	1.000	0.985	0.995	0.993	
	P3	1.000	0.712	0.890	0.867	
Great Dane	P1	1.000	0.946	0.989	0.978	0.951
	P2	1.000	0.810	0.989	0.933	
	P3	1.000	0.836	0.989	0.942	
Manac	P1	1.000	1.0000	0.981	0.994	0.954
	P2	1.000	0.889	0.994	0.961	
	P3	1.000	0.780	0.943	0.908	

Aim 1: Summary

Three guards were selected for this study. They were manufactured by Wabash National (model 05006821-07), Great Dane (model GDP11716266), and Manac (model 914-0901002-G). All three were certified as meeting FMVSS No. 223. The FE guard models were validated against data on each guard from physical tests that followed FMVSS No. 223's quasi-static test protocols. The three models demonstrated excellent correlation with quasi-static load cases as assessed by an objective rating system and qualitative comparison of gross plastic deformation.

A model optimization routine was then performed to reduce the strength of each guard to be minimally compliant with FMVSS No. 223. For all three guards, the UDL requirement was the limiting requirement. That is, for the baseline guards, the Manac has the lowest compliance margin for the UDL requirement, which arguably is the most important one since it reflects most crashes.

This page is intentionally left blank.

Aim 2: Assessing the Relationship Between Quasi-Static Testing and Dynamic Crash Response

The second main aim of this project was to assess the relationship between quasi-static testing of isolated rear-impact guards and dynamic crash response of those guards when mounted to truck-trailers and subjected to impacts by midsize and compact passenger vehicles. This was conducted in several iterative stages. First, the rear-impact guard models were subjected to the updated FMVSS No. 223 (2022) testing protocol to assess their baseline performance. Then, a series of simulations were conducted to modify the guards until they were minimally compliant with FMVSS No. 223, effectively removing their built-in factors of safety. Then, both the baseline and the minimally compliant guard models were attached to a previously developed and validated truck-trailer model and impacted with a midsize sedan model at 35 mph in various levels of overlap. The rear-impact guard models were strengthened until they prevented PCI and then re-tested in the FMVSS No. 223 protocol. The guards were then strengthened again to protect against PCI when impacted by a compact sedan. Finally, the guard models were again subjected to the quasi-static test protocol. The differences in strength as quantified by FMVSS No. 223 and the dynamic outcome were analyzed.

PCI has conflicting definitions depending on the source. In 2016, the IIHS issued a test protocol for dynamic tests of passenger vehicles striking the rear-impact guard attached to truck-trailers. In that protocol, PCI was defined by the IIHS as any portion of the trailer intruding beyond the precrash position of the rear surface of either A-pillar (Semi-Trailer Underride Evaluation Crash Test Protocol Version I, 2016). In the following years, the IIHS updated this protocol. Semi-Trailer Underride Evaluation Crash Test Protocol (Version II, 2021) redefined PCI as any portion of the trailer contacting the windshield, A-pillars, or roof of the striking vehicle. This updated, more stringent, definition of PCI was used in this project.

Rear-Impact Guard Modification to Minimally Comply With FMVSS No. 223

Each of the three guards used in this project were certified as meeting FMVSS No. 223 requirements in effect at the time of their manufacture by their fabricating manufacturers. At the start of this project, the requirements in FMVSS No. 223 had last been updated by NHTSA in 2004. NHTSA procured these guards as part of its compliance test program and contracted with MGA Research to perform the testing for NHTSA. These test series were used as validation cases during development of the models. In each condition specified by that protocol, the physical and computational guards exceeded the minimum force-deflection and energy absorption thresholds. As is standard in the engineering industry, a factor of safety was built into those designs. The baseline RIGs have been previously tested in dynamic impacts by the IIHS; however, the specifications and behavior of a minimally compliant design has not been previously published. The aim of this subsection of the project is to determine what a minimally compliant design would be for each of the three RIGs.

Recently, NHTSA issued a final rule upgrading FMVSS No. 223 (87 FR 42339, July 15, 2022). The updated FMVSS No. 223 (2022) protocol replaces the P3 load case with a uniform distributed load. This UDL application device is to be unyielding, have a height of 203 mm, and have a width that exceeds the distance between the outside edges of the outermost supports to which the test portion of the horizontal member is attached. A single model of the UDL was created that met these criteria for all three rear-impact guards, which resulted in a geometry of 203 mm x 2000 mm. To develop minimally compliant RIGs, the updated FMVSS No. 223

standard was used. The P1 and P2 protocols remain unchanged from the previous standard: each location must resist 50 kN of load before deflecting 125 mm. A RIG must resist 350 kN of load during the UDL test before deflecting 125 mm while also absorbing at least 20 kJ of energy through plastic deformation.

With the aim of modifying the RIG models to be minimally compliant with the FMVSS No. 223 (2022) standard, development of an objective function was required. The objective function is provided below, and is set to minimize the amount of force and absorbed energy above the set thresholds, while also placing a small weight on reducing the mass of the guard:

$$y = \frac{P_{UDL} - 350\ kN}{350\ kN} + \frac{P_{P2} - 50\ kN}{50\ kN} + \frac{P_{P1} - 50\ kN}{50\ kN} + \frac{U_{UDL} - 20\ kJ}{20\ kJ} + 0.25\frac{M_{Sim}}{M_0}$$

Where:

- P_{UDL}, P_{P2}, and P_{P1} are the peak force from the UDL, P2, and P1 test locations
- U_{UDL} is the plastic energy absorbed during the UDL test
- M_{Sim} and M_0 are the current guard mass and the baseline guard mass, respectively

Constraints:

- $P_{UDL} \geq 350$ kN
- $U_{UDL} \geq 20$ kJ
- P_{P2} , $P_{P1} \geq 50$ kN
- Ground Clearance ≤ 22 in

For each guard model an LS-OPT analysis was set up. The guards were attached to the stiff springs previously described, but a single value for the stiffness constant was used across all three guards. 18 kN/mm was selected as it was the average of the two guards mounted to the rigid test fixtures. In the LS-OPT, each part of the guards was allowed to change thicknesses independently but was never allowed to increase thickness above the start value. A genetic algorithm was employed to minimize the previously defined objective function. For each set of thickness values, the P1, P2, and UDL cases were simulated. A total of 900 trials were conducted per guard and only guard model designs that met the previously described constraints were analyzed.

The minimally compliant designs resulted in a decrease of 13.8 ± 3.4 kg. Table 4 provides the results of the FMVSS No. 223 test series with the minimally compliant guards. In each case, the UDL force was the closest to the FMVSS No. 223 minimum force requirement limit of 350 kN. The Wabash, Great Dane, and Manac minimally compliant guard models produced 350.4, 350.4, and 351.9 kN of force in the simulated UDL test case. A corresponding 25.6, 29.4 and 33.3 kJ of absorbed energy through plastic deformation was also measured during the simulations, all above the 20 kJ minimum requirements. The P1 and P2 cases had a larger margin between FMVSS No. 223 minimum requirements and the simulated guard response, indicating the UDL case was the limiting case. The results of the original and minimally compliant guard response is also provided visually in Figure 22. Finally, the thicknesses of each part are provided in Figure 23.

Table 4. Simulated FMVSS No. 223 (2022) results for the baseline and minimally compliant models

Guard	Condition	P1 (3/4 offset)	P2 (center of guard)	Uniformly Distributed Load		Mass (kg)
		Max Force @<125mm (kN)	Max Force @<125mm (kN)	Max Force @<125mm (kN)	Energy @<125mm (kJ)	
Wabash	Baseline	135.8	125.4	394.7	32.1	54.4
	Minimally Compliant	79.6	68.5	350.4	25.6	38.9
Great Dane	Baseline	120.5	149.4	441.7	36.6	69.4
	Minimally Compliant	67.2	77.0	350.4	29.4	52.5
Manac	Baseline	172.5	83.3	356.2	36.8	84.8
	Minimally Compliant	157.1	52.5	351.9	33.3	75.7
FMVSS No. 223 Req.		≥50	≥50	≥350	≥20	N/A

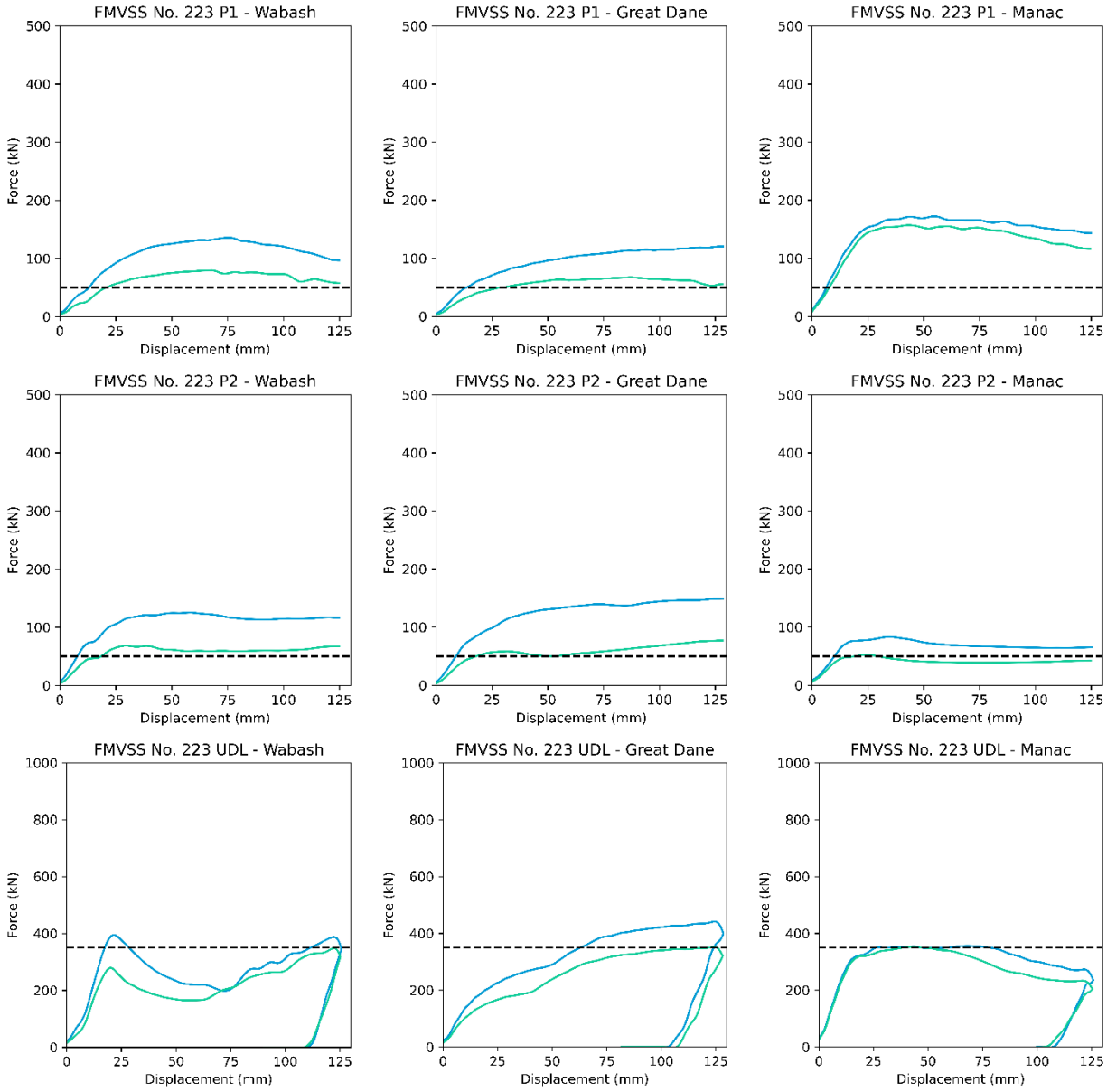

Figure 22. Simulation responses of the guard models in FMVSS No. 223 (2022) protocol using the baseline (blue), and minimally compliant (green) models

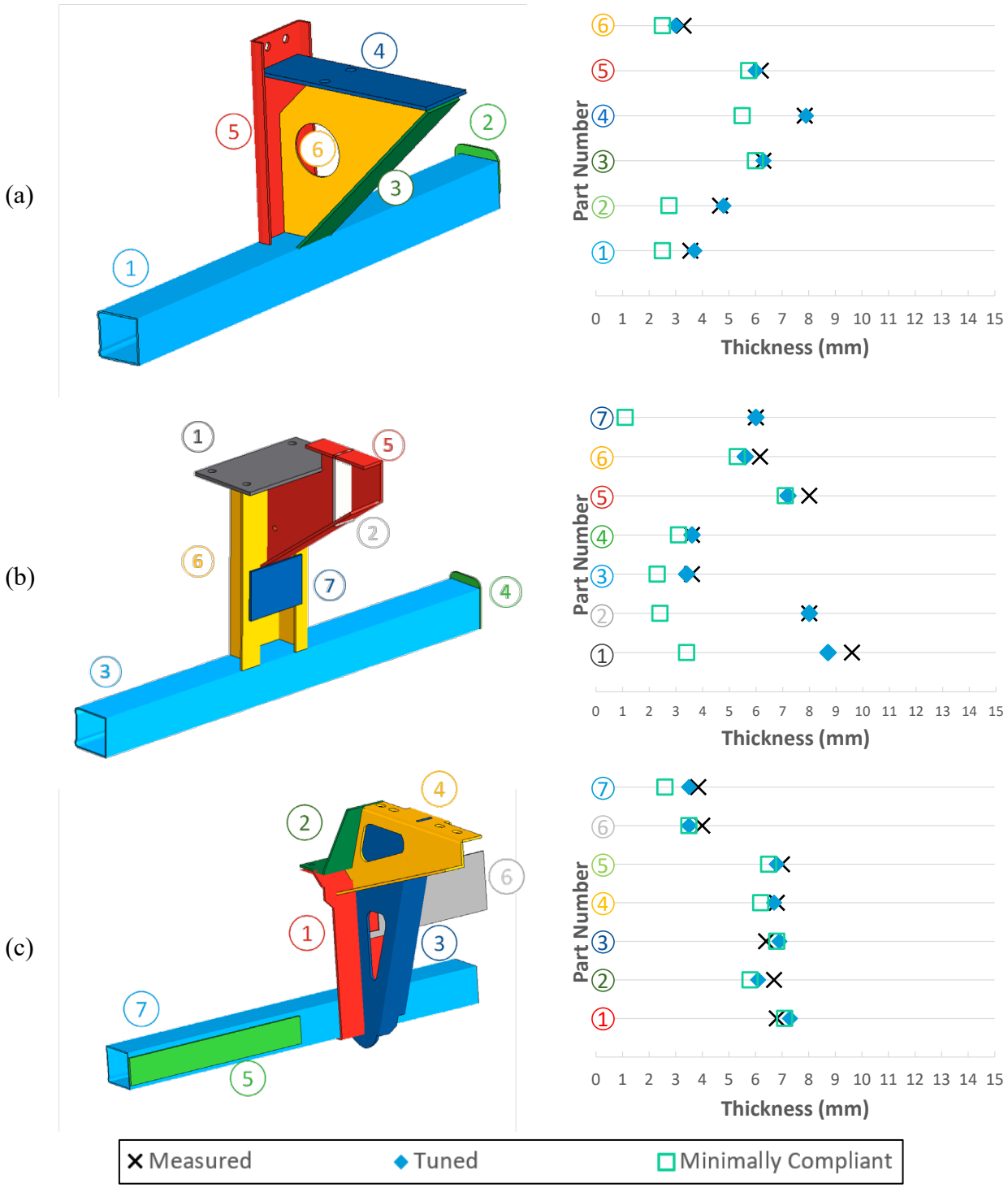

Figure 23. Sheet metal thickness values for each part in the models comparing the measured, tuned, and minimally compliant versions, (a) Wabash, (b) Great Dane, (c) Manac

Dynamic Impact Assessment – Honda Accord

Trailer Model

The next phase of the project involved simulating impacts to a truck trailer equipped with the various versions (i.e., baseline, minimally compliant, strengthened) rear-impact guard models. A previously developed generic trailer model was used for this project. Specifically, the National Transportation Research Center (NTRC) 48' trailer model was employed (Miele et al., 2010). This model was developed by the NTRC University Transportation Center under a grant from the U.S. Department of Transportation Research and Innovative Technology Administration (#DTRT06G-0043) and Federal Highway Administration under Purchase Order #DTFH61-07-P-00235. Briefly, this trailer model was constructed using material properties from several key structural elements of a 1990 Stoughton box trailer, was 48 feet long, was validated against several crash events, and was freely available (Figure 24). The reader is directed to the original documentation for further information.

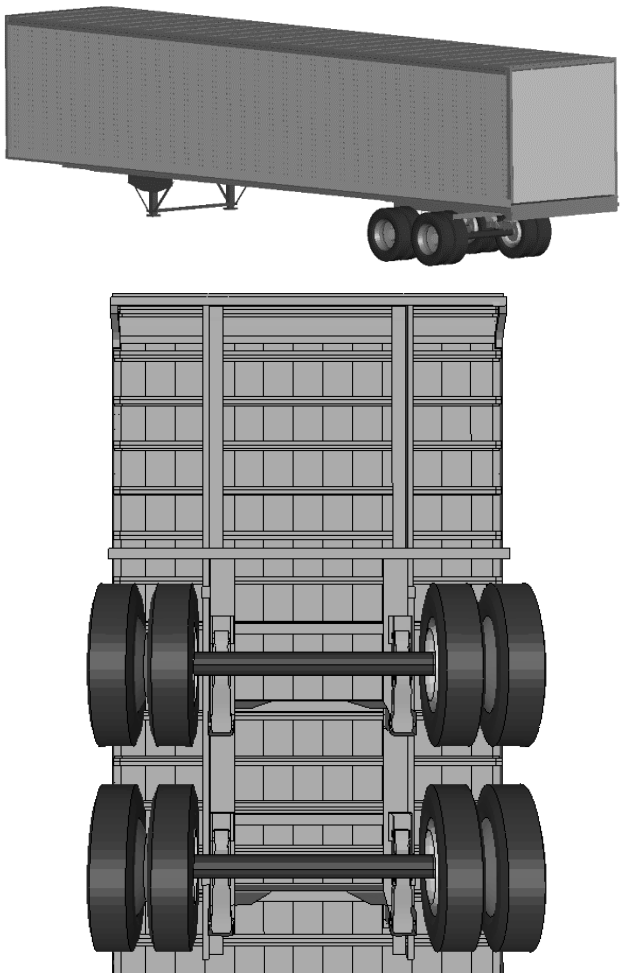

Figure 24. Finite element trailer model with the rear-impact guard removed

In physical tests at IIHS, guard-specific trailers were used. In other words, the Wabash guard was tested on a Wabash trailer, and so forth. Thus, each guard had its own unique guard-to-trailer attachment hardware and mounting system. A full description may be found in the IIHS test reports. For reference, brief descriptions are given here.

Wabash, IIHS Report No. CF10026: The guard's two main vertical support members were attached to the trailer's chassis with four bolts on each side and positioned such that the top steel plate on the support members overlapped reinforced sections on the trailer chassis.

Manac, IIHS Report No. CF12001: The guard's two main vertical support members were attached to the trailer's chassis with seven bolts on each side, three bolts on the rear sill and four bolts fastened to flanges on the trailer floor structure.

Great Dane, IIHS Report No. CF13002: The guard's two main vertical support members were attached to the trailer's chassis with six bolts on each side, four bolts on the bottom of the rear sill and two bolts fastened to the trailer's wheel assembly slide rails.

Using this information, along with information on ground clearance height of each guard as reported in physical testing at IIHS, the guard models were positioned in space at the rear of the trailer model. The various attachment point geometries for each trailer needed to be approximated. To do so, using images from previous trailer and rear-impact guard testing as well as examining local trailers, extra structural components were modeled and constrained to the longitudinal and lateral rails at the rear of the trailer model.

*CONSTRAINED_EXTRA_NODES_SET cards were used to connect the trailer at the bolt holes (Figure 25). This method assumes the space between the top of the rear-impact guard models and the bottom of the trailer are rigid assemblies that translate the forces between the impact guard and the bottom of the trailer. One limitation that comes from this approach is that the failure of the bolts was not modeled.

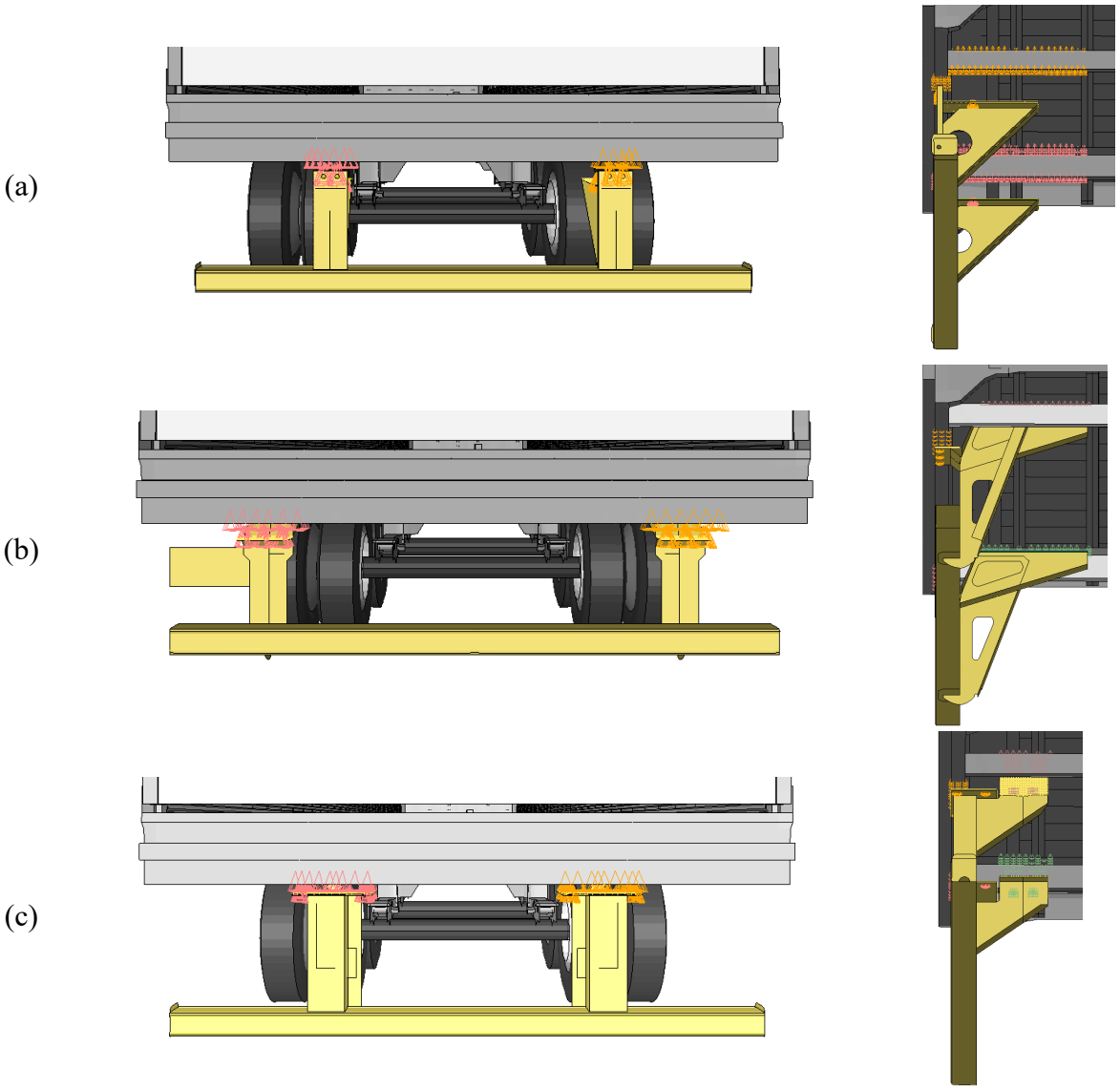

Figure 25. Connection locations between the guard and trailer for the (a) Wabash, (b) Manac, and (c) Great Dane

Baseline Rear-Impact Guard Dynamic Response

Each trailer-rear-impact guard model was then subjected to preliminary validation to ensure reasonable full model response. Each of the rear-impact guards modeled in this project have previously been tested in full vehicle crash tests by the IIHS using a 2010 Chevrolet Malibu. These tests consisted of rear impacts with overlaps of full width (FW), 50 percent overlaps, and 30 percent overlaps, all conducted at 35 mph. While not a perfect match to the Honda Accord model simulations, these cases were used for qualitative assessment of the impact guard model response as there did not exist physical testing data with the Honda Accord nor is there a finite element model of the Chevy Malibu used in the RIG impacts. Therefore, after attaching the guard models to the trailer, a series of nine simulations were conducted, and rear-impact guard plastic deformations were compared to the physical response. The simulations were conducted with the 2014 Honda Accord model developed by NHTSA. The combined trailer-guard models performed well in a qualitative comparison, and were deemed adequate for further use (Figure 26, Figure 27, Figure 28).

The Wabash physical guard prevented PCI in both the full width and 50 percent overlap cases but was unable to prevent PCI for the 30 percent overlap case. In the 30 percent overlap case, the right edge of the horizontal member bent at a 90° angle, and the right upright support twisted outboard. In the 50 percent overlap case, the right outboard portion of the horizontal member bent towards the front of the trailer as well as upwards from the horizontal. The computational model behaved similarly, but the vertical support twisted slightly more in the simulation than the physical guard. It is possible that this discrepancy could be caused by the lack of outboard "S-tubes" in the model. The choice to not include them is described in detail in the model development section of this report. In the full overlap case, the horizontal member did not move with respect to the ground a significant amount, but the portion of the guard inboard of the vertical supports was crumpled following the test.

The differences in upright support placement on each of the guards played a role in the acceleration profiles observed by the Honda Accord during the 30 percent overlap cases (Figure 29). While there were differences in how the upright supports were reinforced for the Wabash and Great Dane guards, the distance between the two upright supports were similar. As a result, the overall acceleration profiles of the two guards were similar with minor differences potentially attributable to the structural differences. The Manac guard had the upright supports spaced the furthest apart of all three guards simulated for this investigation. The acceleration profile for the Manac guard significantly deviated from that of the Wabash and Great Dane guards indicating that the spacing of the upright supports may play a large role in the shape of the acceleration profile. Having a larger gap between upright supports allows for the front end of the Honda Accord to engage one of the upright supports during the impact. Conversely, the upright support is not engaged by the vehicle in the simulations using the Great Dane and Wabash guards where the gap between the horizontal members is smaller. The rapid increase in acceleration observed at around 150 msec in the Great Dane and Wabash guard impact simulations correlates with the time point where the vehicle engages the tire of the trailer.

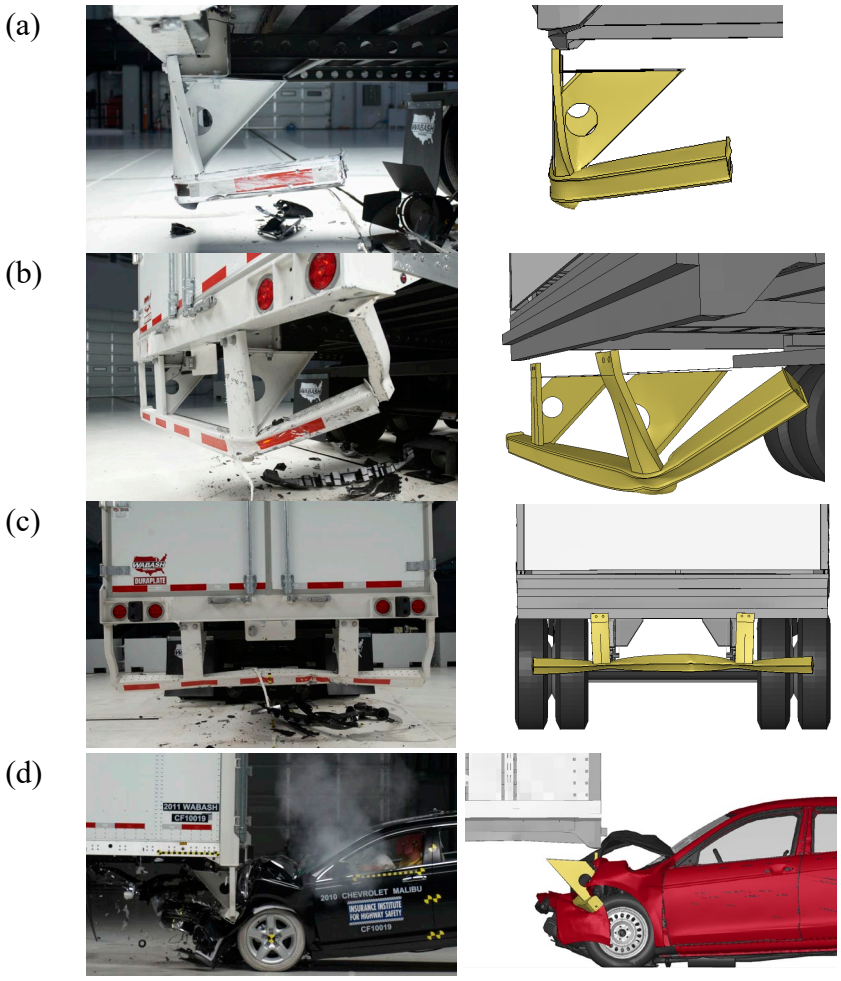

Figure 26. Comparison of IIHS physical testing and computational modeling post-impact Wabash guard plastic deformation at 35 mph, (a) 30 percent overlap, (b) 50 percent overlap, and (c, d) full overlap

The Great Dane physical guard prevented PCI in both the full width and 50 percent overlap cases but was unable to prevent PCI for the 30 percent overlap case. In the 30 percent overlap case, the right edge of the physical horizontal member bent at a 90° angle. While the computational model accurately predicted PCI, the final deformation of the horizontal member was less than the angle seen physically. In the 50 percent overlap case, the right outboard portion of the horizontal member bent towards the front of the trailer as well as upwards from the horizontal. The right upright support bent at approximately 45°. The computational model showed a similar deformation pattern, but more upright deformation of the horizontal member and less bending of the upright support. In the full overlap case, both vertical uprights were pushed towards the front of the trailer evenly, which the simulation also showed, albeit with smaller total deformation.

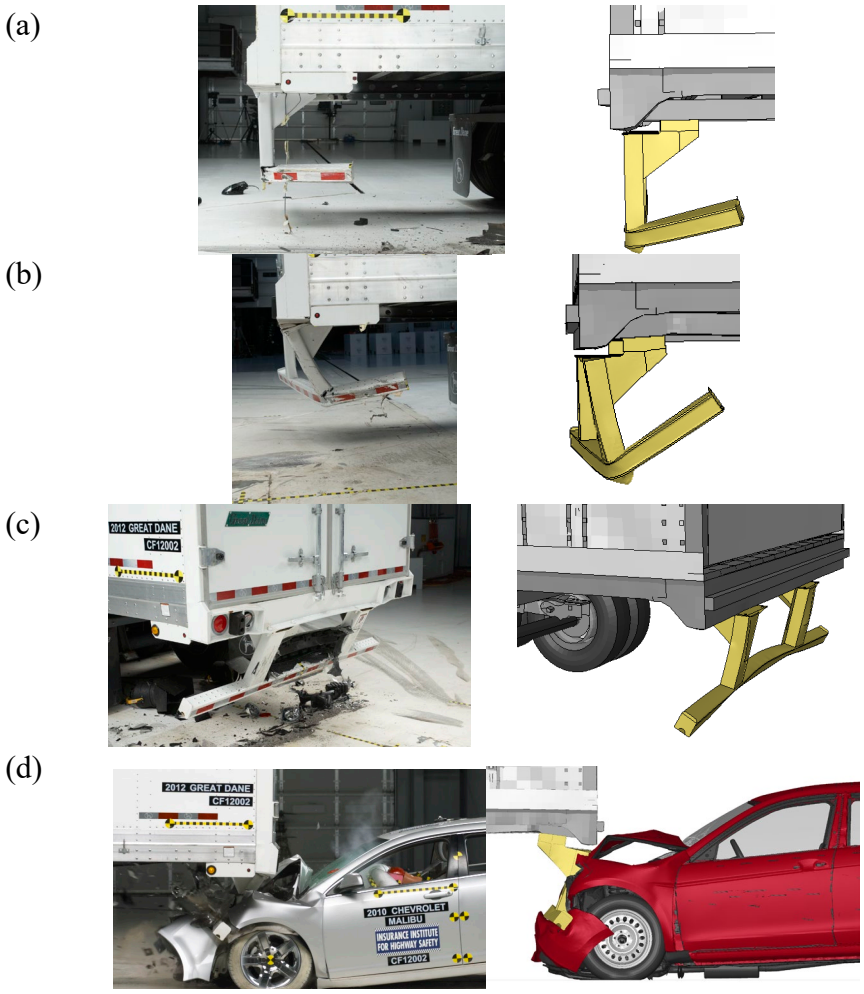

Figure 27. Comparison of IIHS physical testing and computational modeling post-impact Great Dane guard plastic deformation at 35 mph, (a) 30 percent overlap, (b) 50 percent overlap, and (c, d) full overlap

The Manac physical guard prevented PCI in both the full width and 50 percent overlap cases but was unable to prevent PCI for the 30 percent overlap case.[11] It should be noted that the trailer did not intrude into the occupant compartment past the original pre-test positions of the A-pillars in the physical test. In the 30 percent overlap case, the right edge of the horizontal member bent at the vertical support towards the front of the trailer and slight twisting of the vertical upright was observed. The connection bolts failed in the physical test at the top of the right vertical upright. In the model, the forward bend of the horizontal member was observed as well as the twisting of the vertical support, though more twisting was seen in the simulation. Further, as the bolts were not modeled explicitly with failure, any occurrence of bolt failure in the physical tests were not captured. In the simulation, PCI was prevented. In the 50 percent overlap case, the right vertical support underwent dramatic plastic deformation, bending nearly 90° towards the front of the

[11] IIHS had reported that PCI was prevented in the 30% overlap case (Crash Test Report 2010 Chevrolet Malibu Front into 2012 Manac Trailer Rear 56 km/h; 30 percent overlap CF11020), but that was based on their older, less stringent definition of PCI explained on p.17.

trailer. The simulated response matched. The full overlap case resulted in a distinctly different response between the Manac and the other two guards. The horizontal member underwent plastic deformation, bending at two distinct points inboard of the vertical supports. Both vertical supports twisted inboard during the event. The computational model matched this pattern. Some of the physical bolts failed in this physical crash test.

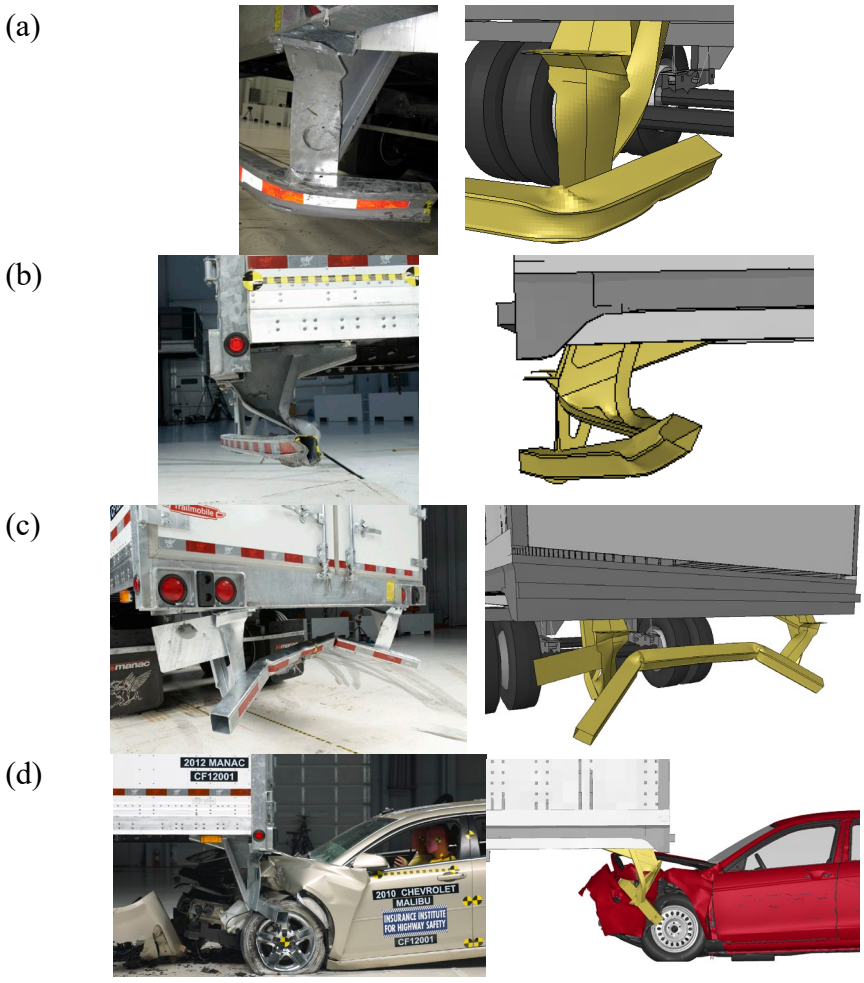

Figure 28. Comparison of IIHS physical testing and computational modeling post-impact Manac guard plastic deformation at 35 mph, (a) 30 percent overlap, (b) 50 percent overlap, and (c, d) full overlap

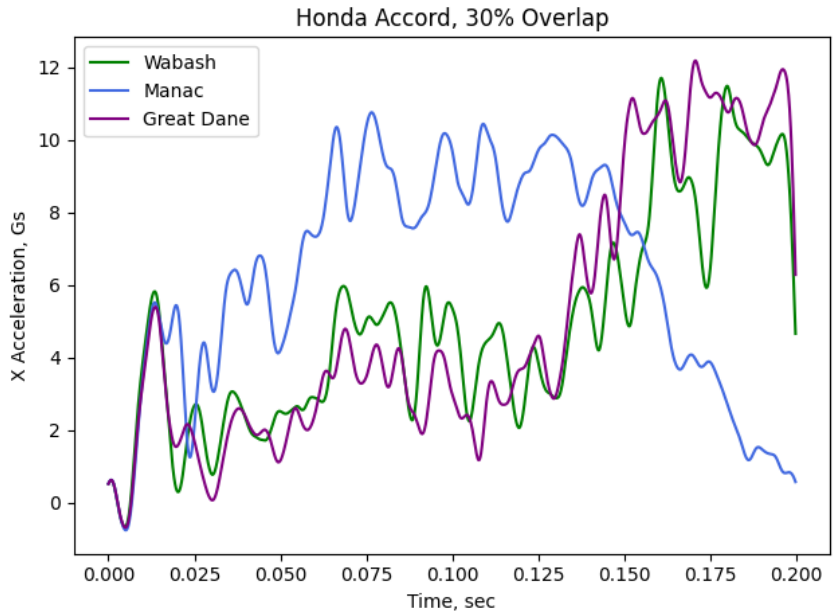

Figure 29. X acceleration profile for the Honda Accord during impacts with the Wabash (green), Manac (blue), and Great Dane (purple) in a 30 percent overlap 35 mph condition

The baseline guard models attached to the generic trailer model performed reasonably well compared to the physical tests, with some discrepancies caused by the simplifications. First, the difference in passenger vehicle internal structural design was expected to produce slightly different results between the physical Chevrolet Malibu and the computational Honda Accord. Secondly, the bolt failures in some physical tests produced differences in the responses. This was particularly notable in the Manac 30 percent overlap case. This limits the subsequent findings of this study as the modeling technique used does not include bolt failure at the connection points. The modeling of specific trailer geometries and structures was outside of the scope of this study but could influence the results. Another difference between the physical Chevrolet Malibu test and the simulated Honda Accord test was the height difference of the wheels and tires. The Chevrolet Malibu was equipped with P215/55R17 tires (height = 26.3”) compared to the Honda Accord model with tire height of 25.9” tires. This modified the interaction time in some cases where the top of the tire struck the horizontal member of the guard at different times.

In summary, the simulated baseline guards prevented PCI for the full overlap and 50 percent overlap cases. The simulated Manac guard model prevented PCI for the 30 percent overlap case, while the simulated Wabash and simulated Great Dane baseline guards did not.

Minimally Compliant Rear-Impact Guard Dynamic Response

Following the LS-OPT to modify the guard models until they minimally complied with FMVSS No. 223 requirements, the guard and truck model were updated with the new metal thickness values and again subjected to a series of 35 mph impacts with the Honda Accord vehicle model. No changes in PCI prevention were seen. In other words, where PCI was prevented with the baseline guard, it was also prevented with the minimally compliant guards. However, x-velocity delta-v timing was shifted compared to baseline (Figure 30). When the guards were minimally compliant, the time between impact and zero velocity (rebound) was greater than baseline.

Further, in many cases, the rebound velocity was lessened. Images from a lateral view of the simulations are provided in Appendix B: Dynamic Simulation Results from baseline and minimally compliant guards.

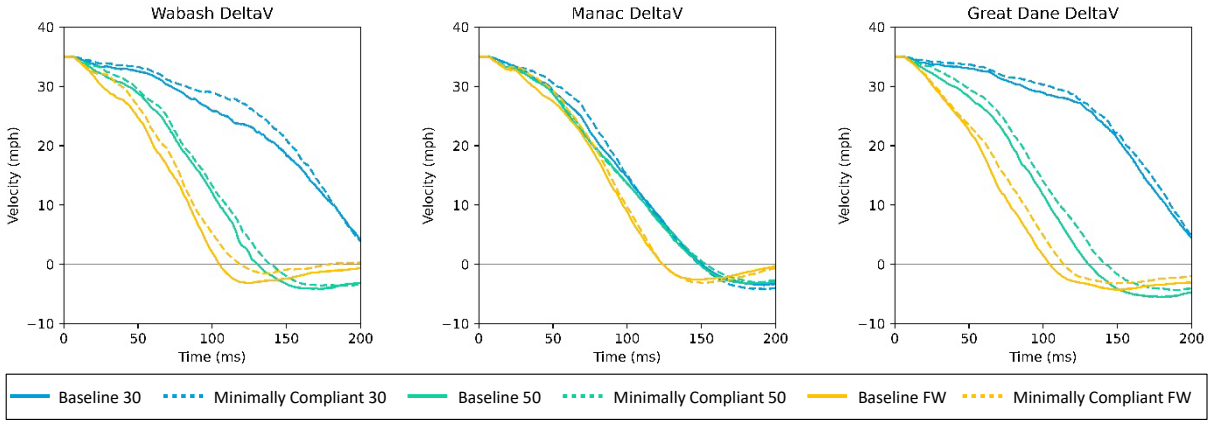

Figure 30. Comparison of Honda Accord rear sill x-velocity across guards, overlap

Guard Strengthening – Midsize

An investigation into the required sheet metal thickness and guard weight needed to prevent PCI for all modes of 35 mph impact testing (30%, 50%, FW) with a midsize passenger vehicle was then conducted. The choice to limit the designs to those that could be manufactured with readily available tubing stock was made by the researchers and NHTSA. As the 30 percent overlap case was the only case that did not prevent PCI for the Wabash and the Great Dane guard models, this scenario was the focus of this investigation. The Manac guard model was not modified further as the minimally compliant guard model effectively prevented PCI. The simulation time and hardware requirement to run full vehicle and full trailer simulations was large, precluding an LS-OPT at this step. Instead, engineering analysis of each simulation was performed iteratively. First, the absorbed energy for each part of a given guard was calculated from the simulation outputs. Secondly, the observed onset and location of plastic deformation was checked (Figure 31). Then, modifications to the contributing guard parts were thickened slightly and a simulation was run. If the guard model still did not prevent PCI, the same process was followed, and a subsequent simulation conducted. For each iteration, the mass of the guard and the sheet metal thicknesses were recorded. Once a modified guard model achieved PCI prevention, the opposite process was followed, identifying areas that did not contribute to the total energy absorption, and decreasing the thickness in these areas. Thus, a feedback loop was used to narrow in on the minimum thickness and mass modifications needed to prevent PCI for the Wabash and the Great Dane guard models.

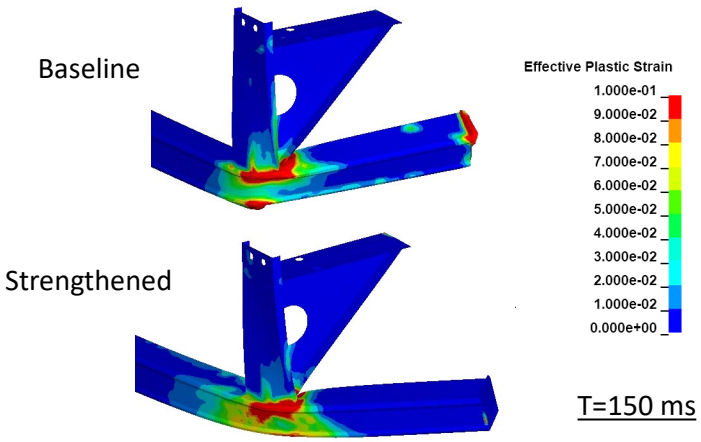

Figure 31. Example of baseline and strengthened guard effective plastic strain at 150 ms in a 30 percent overlap 35 mph Honda Accord simulation

The Manac guard needed no modifications to prevent PCI with the midsize sedan. The Wabash guard required thicknesses that increased the mass to 75.8 kg, up from 38.9 (minimally compliant) and 54.4 kg (baseline). The Great Dane guard required thicknesses that increased the mass to 101.1 kg, up from 52.5 kg (minimally compliant) and 69.4 kg (baseline). The final thicknesses and weights are provided in Figure 38 and Figure 39. Images from the simulations of the strengthened and baseline guard models are provided in Figure 32.

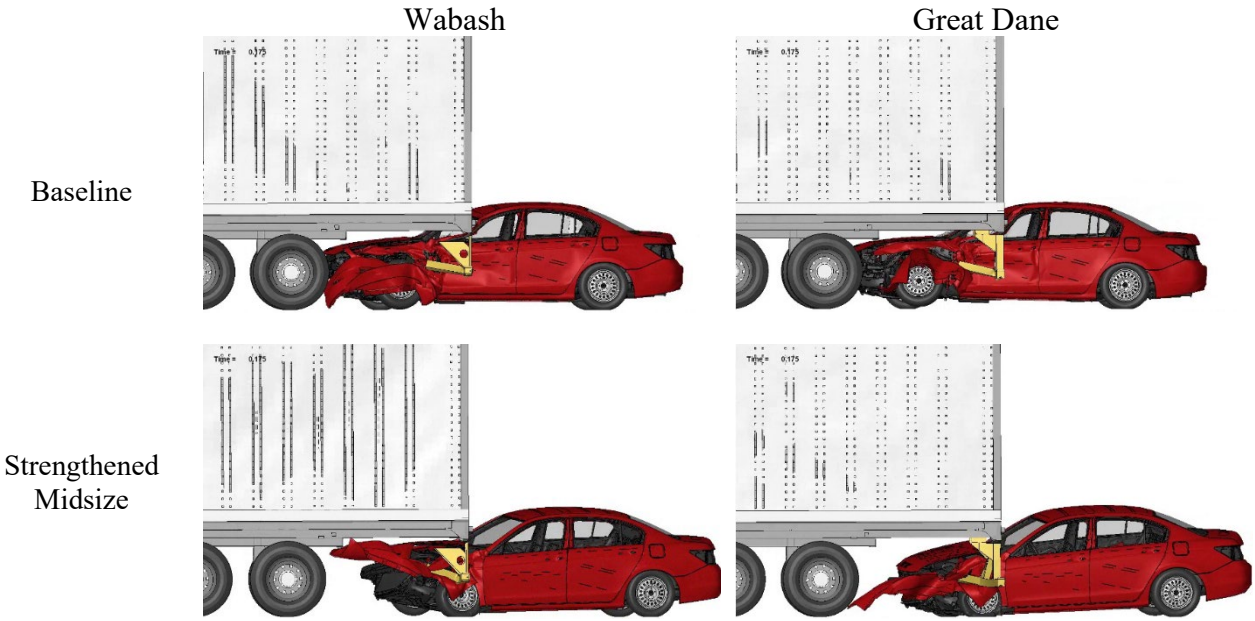

Figure 32. Images from 175 ms into 30 percent overlap 35 mph simulations of the baseline and midsize strengthened Wabash and Great Dane guards demonstrating PCI prevention

To prevent PCI for a midsize sedan impact, the Wabash guard needed to be modified in two areas: the horizontal member, and the triangular plate in the vertical support. The first is loaded in a cantilever manner, and the second resists rearward deformation of the vertical support. The horizontal member thickness needed to be increased from 3.7 mm (baseline) to 6.5 mm (midsize strengthened), a 76 percent increase. The triangular plate thickness needed to be increased from 3 mm (baseline) to 6 mm (midsize strengthened), a 100 percent increase. The Great Dane guard also required two parts to be bolstered. First, the horizontal member required a 106 percent increase in thickness from 3.4 mm (baseline) to 8.7 mm (midsize strengthened). The second part that required modification was the connection plate that bolts to the rear of the trailer. This plate was modified from 5.6 mm (baseline) to 7.0 mm (midsize strengthened), a 25 percent increase.

Quasi-Static Reassessment – Midsize Strengthened

The strengthened Wabash and Great Dane guards were then simulated through the FMVSS No. 223 (2022) protocol again (Figure 33, Figure 35). In both guards, the peak forces observed during the P1, P2, and UDL scenarios increased. Additionally, the displacement at which the FMVSS No. 223 force requirement was met decreased (i.e., the guard provided more resistive force for a given displacement).

For P1, the Wabash guard met the required 50 kN of resistive force at 20.72 mm, 13.01 mm, and 7.91 mm of displacement in the minimally compliant, baseline, and midsize strengthened configurations, respectively. Additionally, the peak forces were 79.6 kN, 135.8 kN, and 295.7 kN in the minimally compliant, baseline, and midsize strengthened configurations, respectively.

For P2, the Wabash guard met the required 50 kN of resistive force at 18.31 mm, 7.81 mm, and 5.0 mm of displacement in the minimally compliant, baseline, and midsize strengthened configurations, respectively. Additionally, the peak forces were 68.5 kN, 125.4 kN, and 243.8 kN in the minimally compliant, baseline, and midsize strengthened configurations, respectively.

For UDL, the Wabash guard met the required 350 kN of resistive force at 122.18 mm, 17.41 mm, and 15.4 mm of displacement in the minimally compliant, baseline, and midsize strengthened configurations, respectively. Additionally, the peak forces were 350.4 kN, 394.7 kN, and 928.1 kN in the minimally compliant, baseline, and midsize strengthened configurations, respectively.

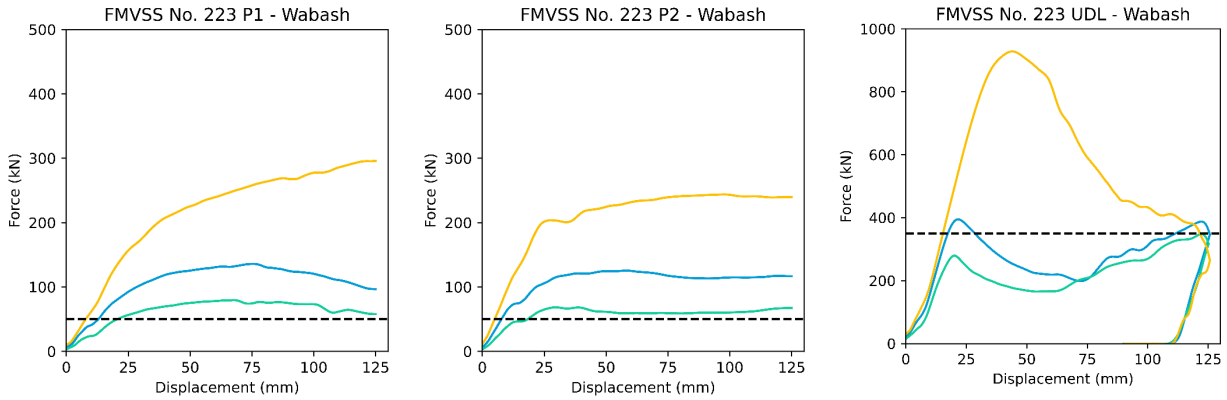

Figure 33. Simulation responses of the Wabash Guard in FMVSS No. 223 (2022) protocol using the baseline (blue), minimally compliant (green), and midsize strengthened (yellow) models

The observable differences in the guard response between baseline and midsize strengthened are predominantly in the coupling between the vertical support and the horizontal member. By simultaneously strengthening the horizontal member as well as the triangular plate steel, the structure moves backward together before plastically deforming. Thus, more load is carried in the beginning and intermediate portions of the test (Figure 35).

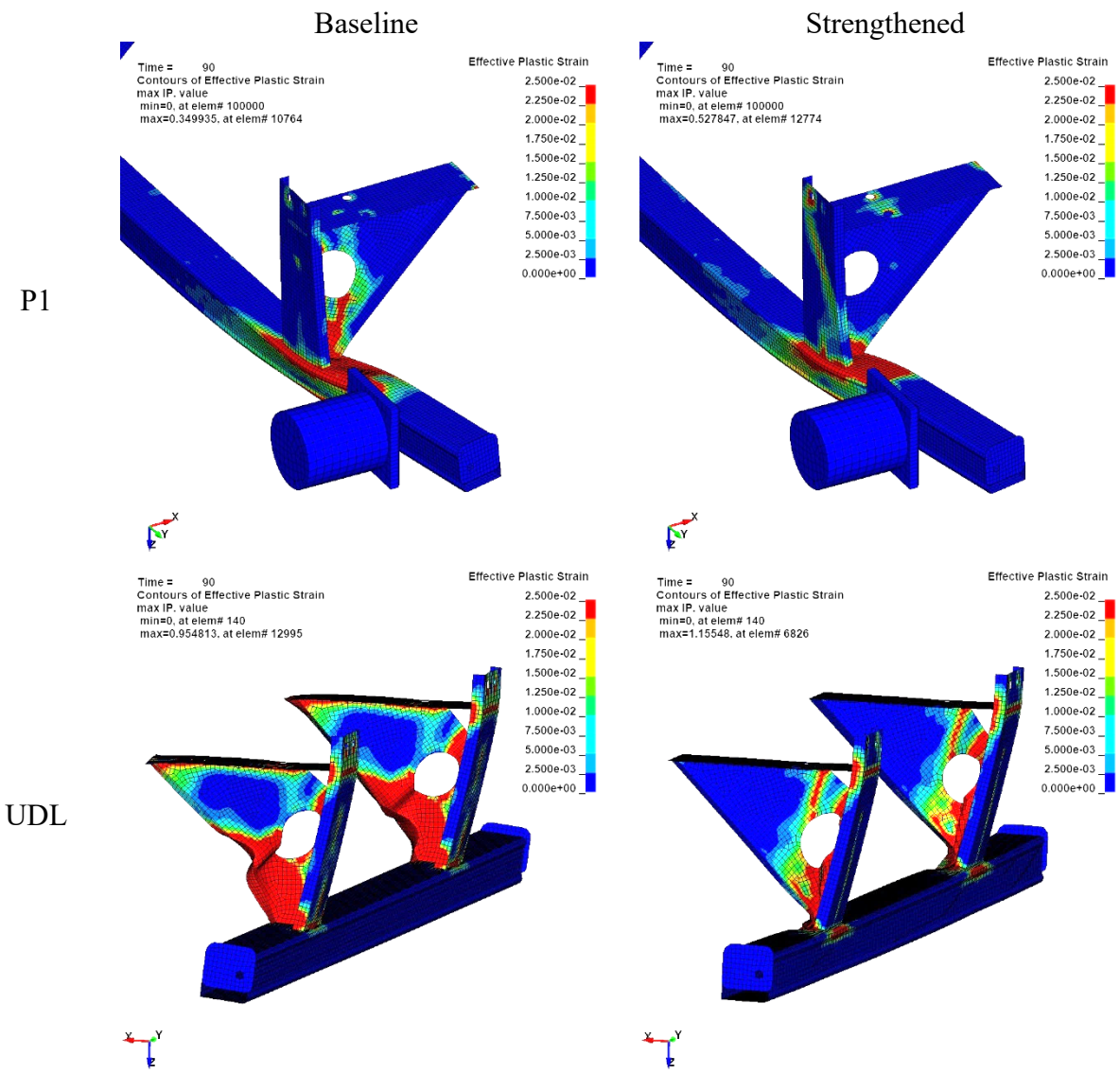

Figure 34. Effective plastic strain and gross deformation response of the Wabash baseline and midsize strengthened guard for given timepoints in the P1 and UDL FMVSS No. 223 (2022) simulations

For P1, the Great Dane guard met the required 50 kN of resistive force at 29.62 mm, 13.68 mm, and 8.33 mm of displacement in the minimally compliant, baseline, and midsize strengthened configurations, respectively. Additionally, the peak forces were 67.2 kN, 120.5 kN, and 192.1 kN in the minimally compliant, baseline, and midsize strengthened configurations, respectively.

For P2, the Great Dane guard met the required 50 kN of resistive force at 18.1 mm, 8.95 mm, and 5.25 mm of displacement in the minimally compliant, baseline, and midsize strengthened configurations, respectively. Additionally, the peak forces were 68.5 kN, 125.4 kN, and 243.8 kN in the minimally compliant, baseline, and midsize strengthened configurations, respectively.

For UDL, the Great Dane guard met the required 350 kN of resistive force at 122.41 mm, 62.95 mm, and 39.81 mm of displacement in the minimally compliant, baseline, and midsize strengthened configurations, respectively. Additionally, the peak forces were 350.4 kN, 441.7 kN, and 495.4 kN in the minimally compliant, baseline, and midsize strengthened configurations, respectively.

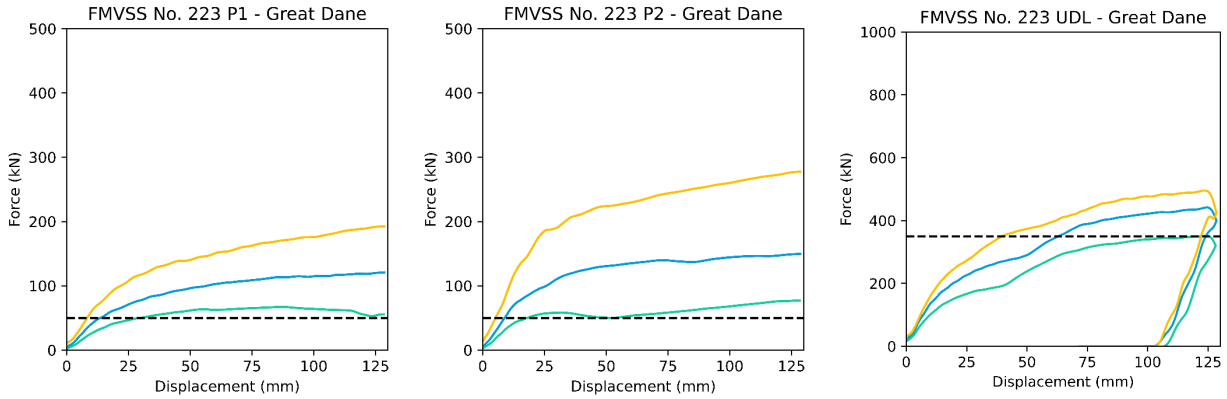

Figure 35. Simulation responses of the Great Dane Guard in FMVSS No. 223 (2022) protocol using the baseline (blue), minimally compliant (green), and midsize strengthened (yellow) models

The observable differences in the guard response between baseline and midsize strengthened are predominantly in the buckling of the horizontal member and the horizontal connection plate. By strengthening the horizontal member, the load is transferred to the vertical upright support and the connection plate. In P1, the baseline guard deforms around the impactor face, while in the midsize, strengthened guard does not. In P2, the horizontal member undergoes significant deformation with minimal backward translation of the connection plate. This phenomenon reverses once strengthened (Figure 36).

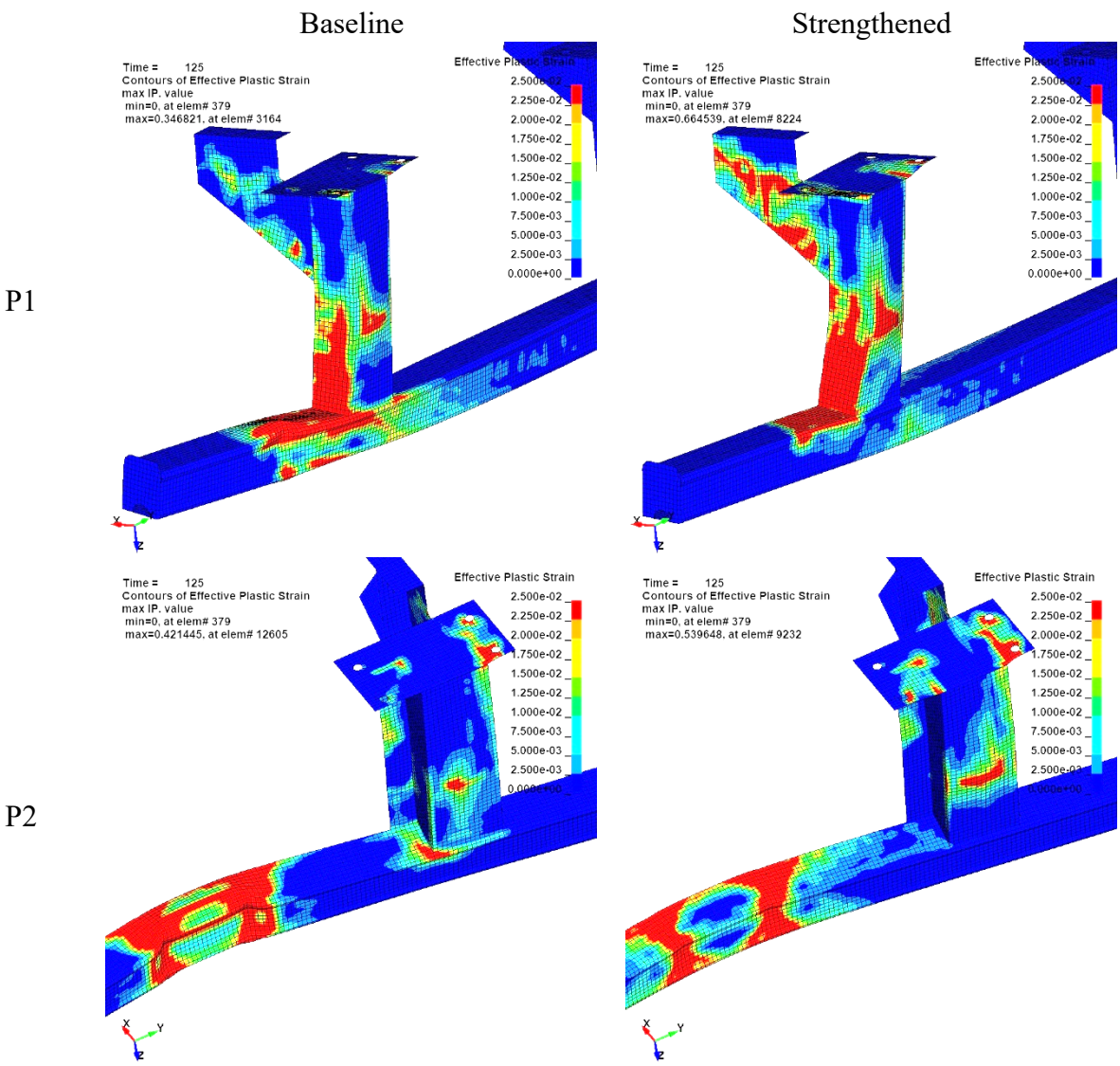

Figure 36. Effective plastic strain and gross deformation response of the Wabash baseline and midsize strengthened guard for given timepoints in the P1 and UDL FMVSS No. 223 (2022) simulations

Dynamic Impact Assessment – Toyota Yaris

The Toyota Yaris vehicle model, developed by NHTSA, was then positioned for 30 percent overlap simulations into the rear of the trailer equipped with the strengthened guard models. A 35-mph simulation was performed for each of the three guard-trailer combinations, each resulting in PCI for the Toyota Yaris (Figure 37).

(a)

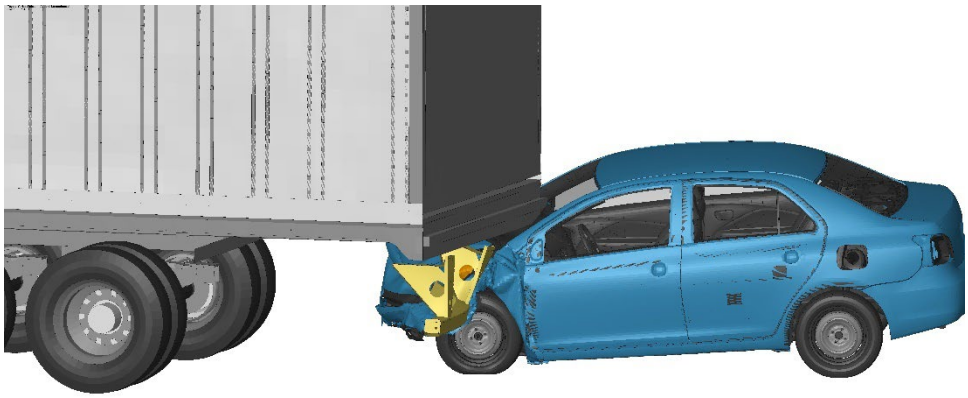

(b)

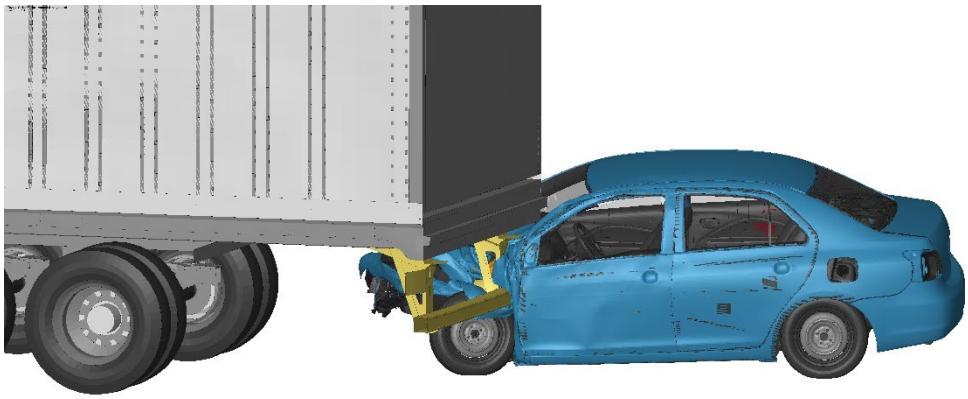

(c)

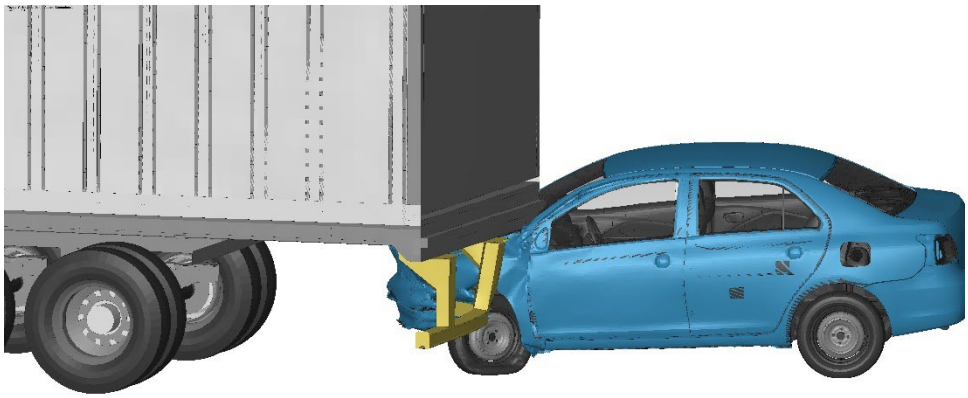

Figure 37. 30 percent overlap 35 mph simulations of the Toyota Yaris into the (a) Wabash, (b) Manac, (c) Great Dane guard models with thicknesses arrived at following midsize strengthening

Guard Strengthening – Compact

Using the methodology employed for strengthening the Great Dane and Wabash guards to prevent PCI for the Honda Accord, the three guards were strengthened to prevent PCI for the Toyota Yaris. The resulting thickness values are provided in Figure 38 and Figure 39. The Wabash and Manac rear-impact guard were able to be strengthened enough to prevent PCI for the full range of overlaps tested at 35 mph. However, the Great Dane was not able to be strengthened enough to prevent PCI for the 30 percent overlap case with the Toyota Yaris at 35 mph within manufacturable ranges of sheet metal. The limiting part was the horizontal member. Four-inch rectangular tubing can only be procured with metal thicknesses of up to 0.5 in (12.7 mm) and this value was used as the final value. Thus, the Great Dane compact strengthened rear-impact guard was only able to prevent PCI for the Toyota Yaris at full overlap and 50 percent overlap at 35 mph.

Increasing the strength of the guards to prevent PCI for the Toyota Yaris proved more difficult than the Honda Accord. This was due to several factors. First, the height of the bumper of the Yaris is approximately 1 inch lower than the Honda Accord, which limits bumper to rear-impact guard engagement. This delays the reduction in speed of the vehicle until the rear-impact guard begins loading the tire and engine block. In the Honda Accord simulations, the tire to rear-impact guard engagement was a large contributing factor in slowing the vehicle. However, the height of the tire was smaller in the Toyota Yaris compared the Honda Accord (23.8 in versus 25.9 in), which reduced the interaction between it and the horizontal member of each rear-impact guard. This delayed the timing of significant structural engagement between the vehicle and the rear-impact guard until the engine block contacted the rear-impact guard. As the length of the vehicle hood is smaller in a compact vehicle compared to a midsize vehicle, this delay reduced the overall available time for the vehicle to slow. A second factor was the angle of the windscreen between the Accord and Yaris. The Yaris windscreen is angled more than the Accord with respect to the ground, which creates the potential for a trailer-windscreen impact earlier (Figure 40).

Combining these two differences (smaller tire//delayed engagement) and a more upright windscreen required the rear-impact guards to be bolstered significantly to prevent PCI for the Yaris. Beginning with the Wabash guard, three of the six distinct parts of the guard needed to be strengthened again. The horizontal member thickness was increased an additional 2.5 mm (38%) compared to the midsize strengthened. The rear flat plate underwent an increase of 1.7 mm (27%). Finally, the front plate on the vertical upright was increased 2 mm (33%) compared to the midsize strengthened. These combined for an additional 22.7 kg. In summary, the minimally compliant, baseline, midsize strengthened, and compact strengthened Wabash guard models were 38.9 kg, 54.4 kg, 75.8 kg, and 98.5 kg, respectively. The Manac guard, which prevented PCI for the Honda Accord when minimally compliant required several modifications to prevent PCI for the Toyota Yaris. All but one part resulted in an increased thickness value. The three largest increases were required at the horizontal member (+2.15 mm, +83%) followed by the rear triangular portion of the vertical support (+1.2 mm, +18%), and then the front portion of the vertical support (+0.9 mm, +13%). In summary, the minimally compliant, baseline, and compact strengthened Manac guard models were 75.7 kg, 84.8 kg, and 98.5 kg, respectively. Finally, the Great Dane guard was strengthened to prevent PCI for the Toyota Yaris. Ultimately, this was not achievable with physically manufacturable thicknesses of sheet metal.

(a)

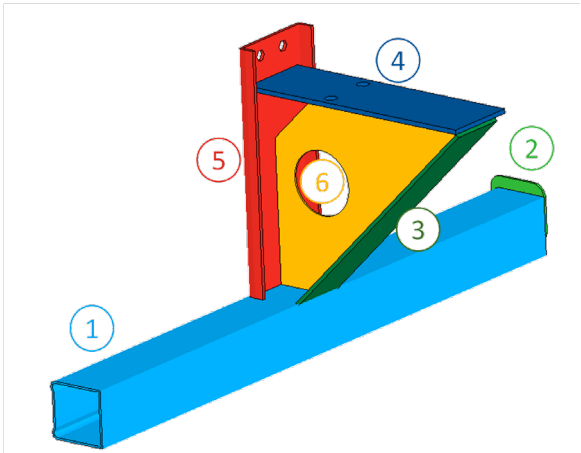

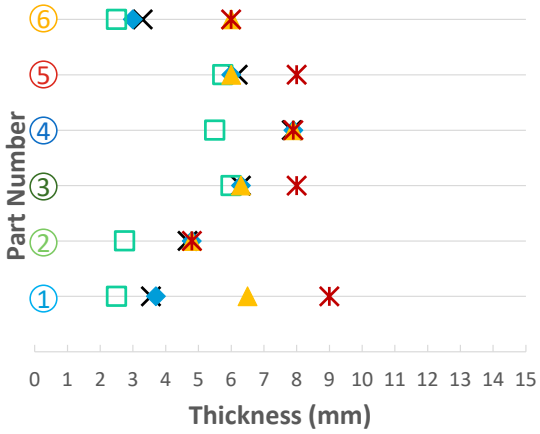

(b)

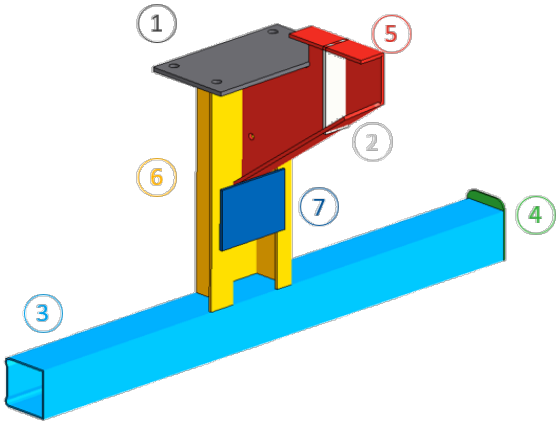

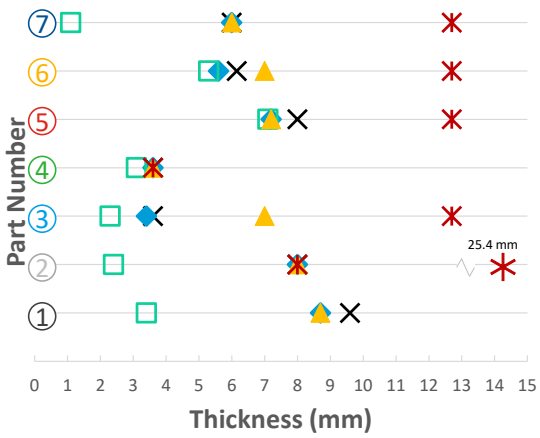

(c)

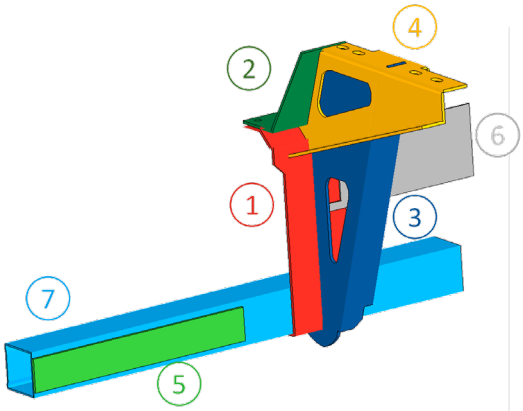

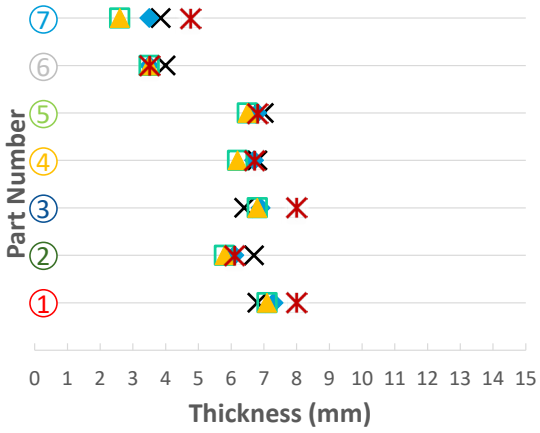

Figure 38. Sheet metal thickness values for each part in the models compared to the original measured values, (a) Wabash, (b) Great Dane, (c) Manac

(a)

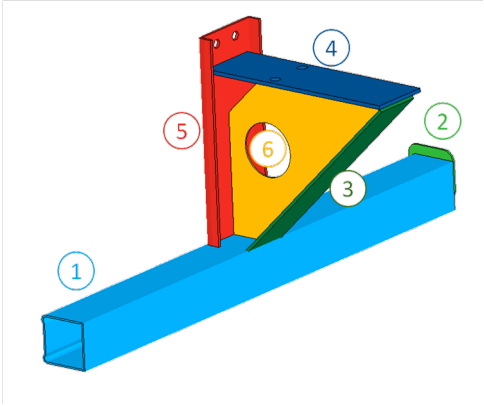

Part #	Measured	Tuned	Minimally Compliant	Midsize Strengthened	Compact Strengthened
1	3.55	3.70	2.50	6.50	9.00
2	4.67	4.80	2.75	4.80	4.80
3	6.30	6.30	6.00	6.30	8.00
4	7.85	7.90	5.50	7.90	7.90
5	6.20	6.00	5.75	6.00	8.00
6	3.30	3.00	2.50	6.00	6.00

(b)

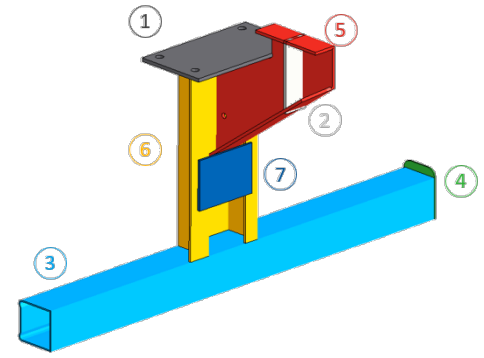

Part #	Measured	Tuned	Minimally Compliant	Midsize Strengthened	Compact Strengthened
1	9.60	8.70	3.40	8.70	25.40
2	8.00	8.00	2.40	8.00	8.00
3	3.60	3.40	2.30	7.00	12.70
4	3.60	3.60	3.10	3.60	3.60
5	8.00	7.20	7.10	7.20	12.70
6	6.15	5.60	5.30	7.00	12.70
7	6.00	6.00	1.10	6.00	12.70

(c)

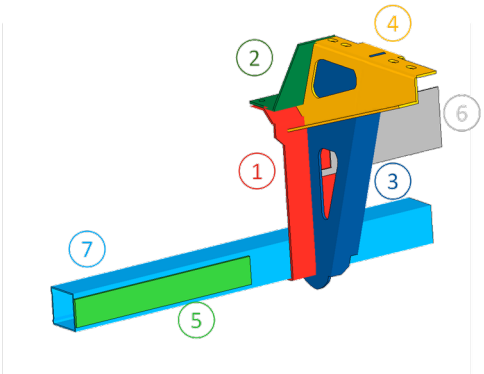

Part #	Measured	Tuned	Minimally Compliant	Midsize Strengthened	Compact Strengthened
1	6.80	7.30	7.10	7.10	8.00
2	6.70	6.10	5.80	5.80	6.10
3	6.40	6.90	6.80	6.80	8.00
4	6.80	6.70	6.20	6.20	6.70
5	7.00	6.80	6.50	6.50	6.80
6	4.00	3.50	3.50	3.50	3.50
7	3.85	3.50	2.60	2.60	4.75

Figure 39. Sheet metal thickness values (mm) for each part in the models compared to the original measured values, (a) Wabash, (b) Great Dane, (c) Manac

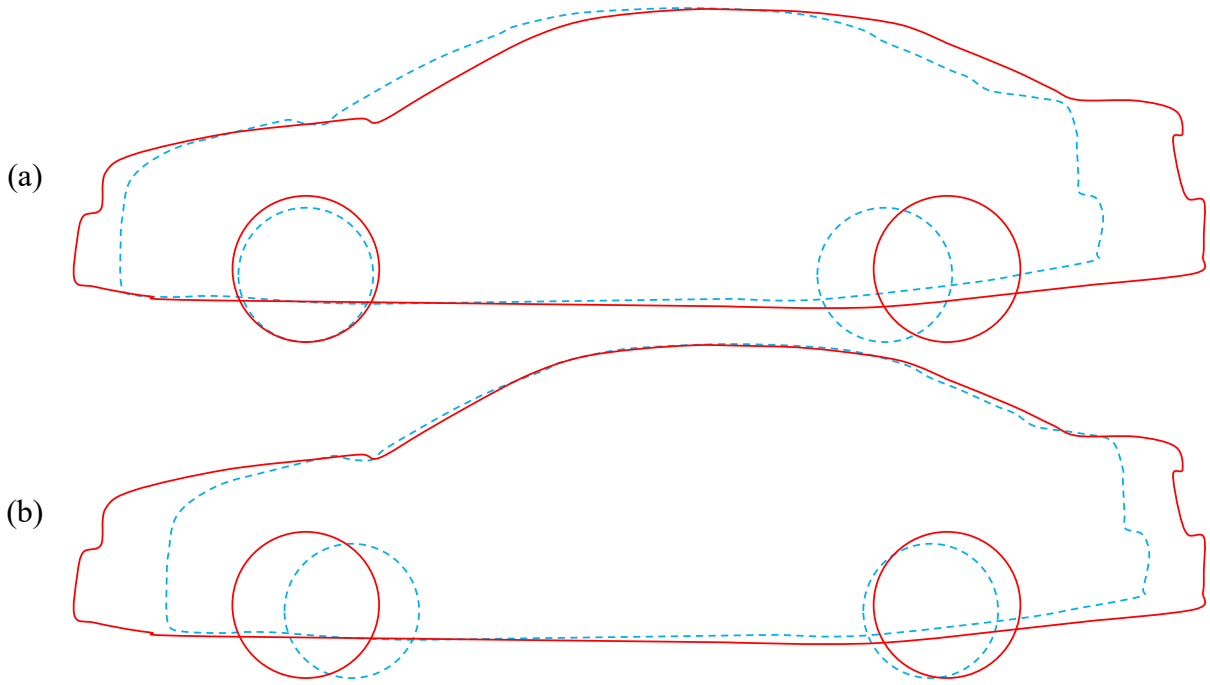

Figure 40. Overlays of the Honda Accord (red, solid line) and the Toyota Yaris (blue, dashed line) models. Aligned in x-direction at the bottom left tire (a), and the front of the windscreen (b).

(a)

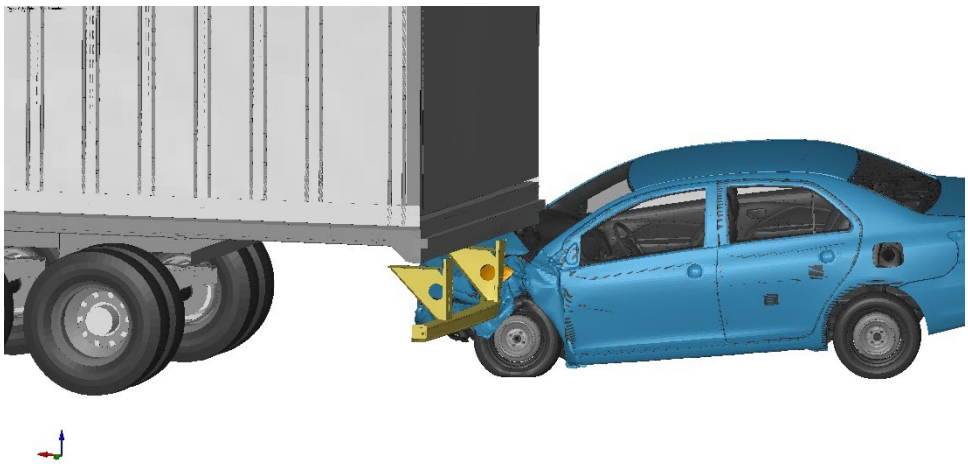

(b)

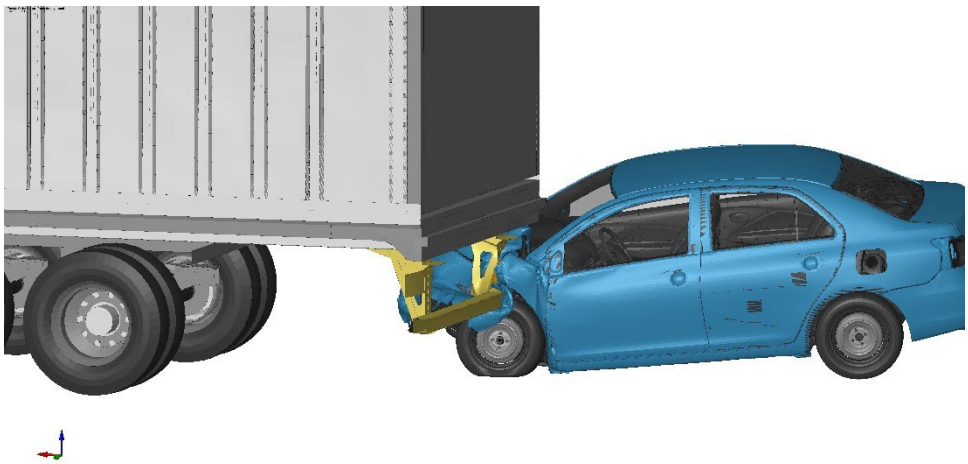

(c)

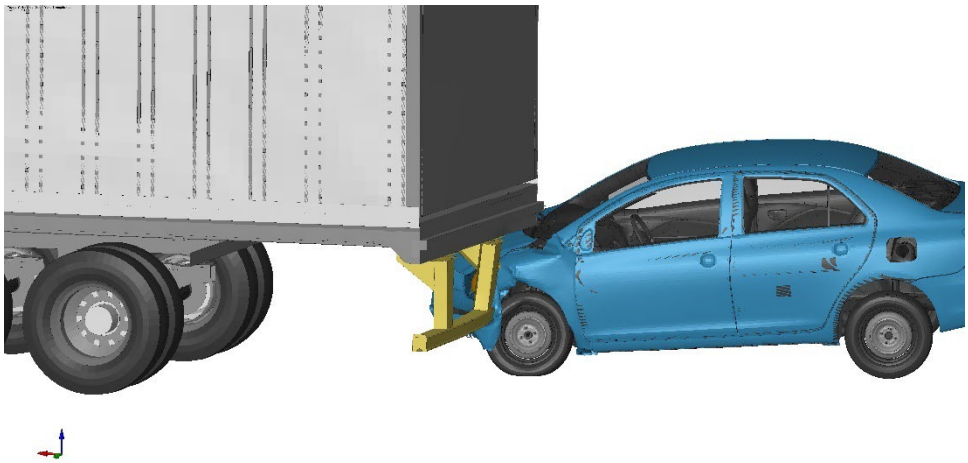

Figure 41. 30 percent overlap 35 mph simulations of the Toyota Yaris into the (a) Wabash, (b) Manac, (c) Great Dane guard models with thicknesses arrived at following compact strengthening

Quasi-Static Reassessment – Strengthened Compact

The strengthened Wabash, Manac, and Great Dane guards were then simulated through the FMVSS No. 223 (2022) protocol again (Figure 42). In all three guards, the peak forces observed during the P1, P2, and UDL scenarios increased. Additionally, the displacement at which the FMVSS No. 223 force requirement was met decreased (i.e., the guard provided more resistive force for a given displacement). Tabulated results are provided in Table 5.

For P1, the compact strengthened Wabash guard met the required 50 kN of resistive force at 7.31 mm of displacement. Additionally, the peak force was 393.1 kN. For P2, the Wabash guard met the required 50 kN of resistive force at 4.0 mm of displacement. The peak force was 353.8 kN. For UDL, the Wabash guard met the required 350 kN of resistive force at 14.9 mm of displacement. The peak force was 1,210.3 kN.

For P1, the compact strengthened Manac guard met the required 50 kN of resistive force at 5.52 mm of displacement. Additionally, the peak force was 208.0 kN. For P2, the Manac guard met the required 50 kN of resistive force at 8.03 mm of displacement. The peak force was 124.5 kN. For UDL, the Wabash guard met the required 350 kN of resistive force at 15.14 mm of displacement. The peak force was 451.7 kN.

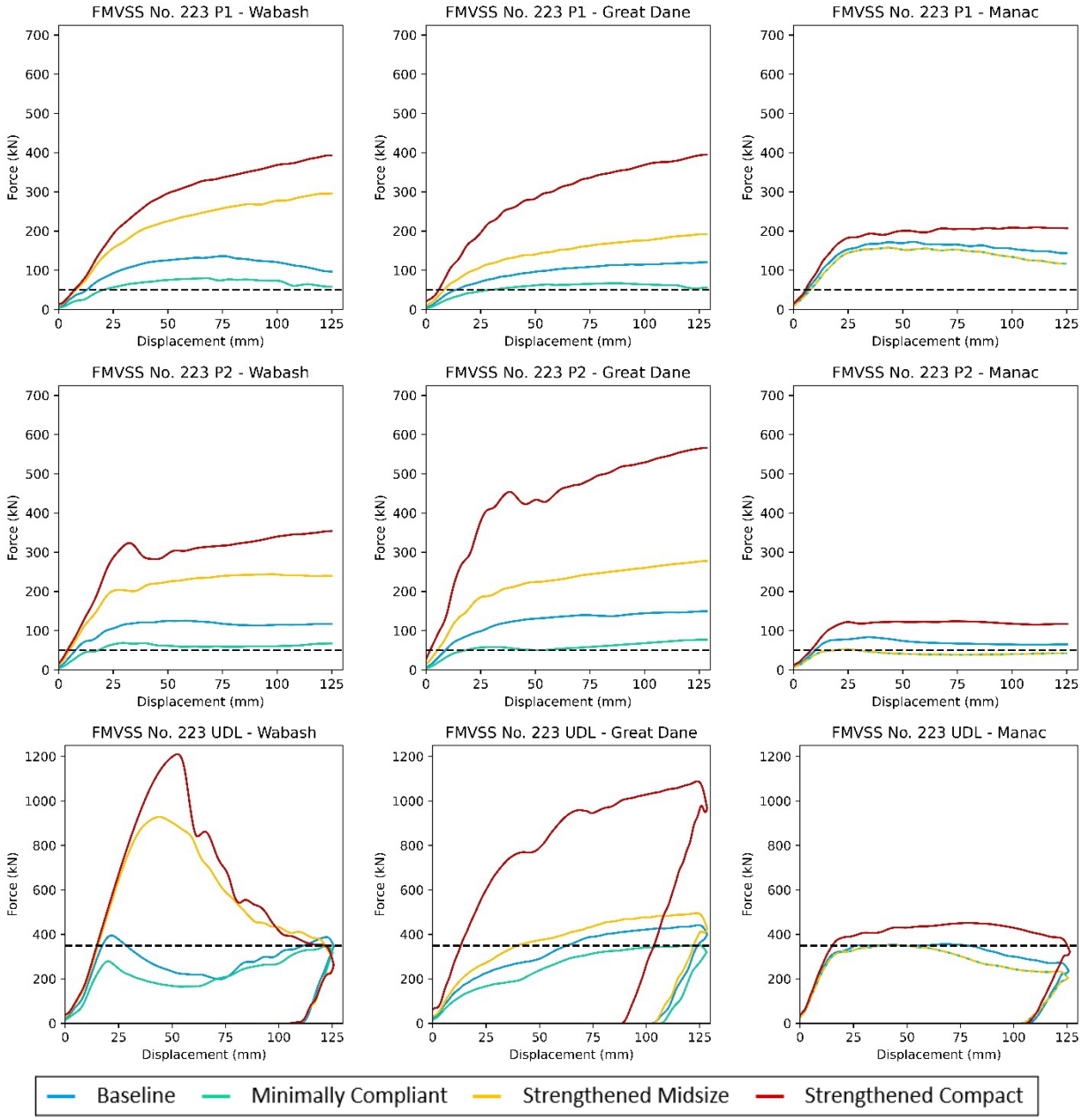

Figure 42. Simulation responses of the guard models in FMVSS No. 223 (2022) protocol using the models of various strengths

Table 5. Summary table for FMVSS No. 223 (2022) simulation results

Rear-Impact Guard		P1 (offset from center)		P2 (center of guard)		Uniformly Distributed Load			Mass (kg)
		Defl @50kN (mm)	Max Force @<125mm (kN)	Defl @50kN (mm)	Max Force @<125mm (kN)	Defl @350kN (mm)	Max Force @<125mm (kN)	Energy @125mm (kJ)	
FMVSS No. 223(2022)		*<125mm*	*>50 kN*	*<125mm*	*>50 kN*	*<125mm*	*>350 kN*	*>20 kJ*	--
Wabash	Baseline	13.01	135.8	7.81	125.4	17.41	394.7	32.1	54.4
	Minimally Compliant	20.72	79.6	18.31	68.5	122.18	350.4	25.6	38.9
	Strengthened Midsize	7.91	295.7	5.0	243.8	15.4	928.1	68.0	75.8
	Strengthened Compact	7.31	393.1	4.0	353.8	14.9	1210.3	76.4	98.5
Manac	Baseline	6.4	172.5	10.04	83.3	26.15	356.2	36.8	84.8
	Minimally Compliant	7.78	157.1	19.58	52.5	38.61	351.9	33.3	75.7
	Strengthened Midsize	n/a	n/a	n/a	n/a	n/a	n/a	n/a	n/a
	Strengthened Compact	5.52	208	8.03	124.5	15.14	451.7	46.5	98.5
Great Dane	Baseline	13.68	120.5	8.95	149.4	62.95	441.7	36.6	69.4
	Minimally Compliant	29.62	67.2	18.1	77	122.41	350.4	29.4	52.5
	Strengthened Midsize	8.33	192.1	5.25	277.3	39.81	495.4	42.8	101.1
	Strengthened Compact	5.86	394.6	1.95	566.1	13.27	1088.2	84.7	190.4

Aim 2: Summary

A model optimization routine was performed to reduce the strength of each baseline guard to be minimally compliant with FMVSS No. 223. For all three guards, the UDL force requirement of 350 kN was the limiting requirement. That is, the member wall thicknesses were reduced until one of the requirements were just met, and in all cases that requirement was the UDL force requirement. All other requirements had some margin of compliance. For the baseline guards, the Manac had the lowest compliance margin for the UDL force requirement, and thus had the least amount of weight reduction.

The baseline and minimally compliant guards were then used in simulations of dynamic crashes. In these simulations, the guards were mounted to a trailer and were stuck by a vehicle travelling at 35 mph. Three different points of impact were simulated.

a. Center of the guard, full vehicle overlap

b. 50 percent of vehicle overlaps the guard
c. 30 percent of the vehicle overlaps the guard

For each simulation, any instance of PCI was noted. (PCI occurs when three is trailer contact with the windshield, A-pillars, or roof of the striking vehicle.) Two striking vehicles were used in the simulations: a 2014 Honda Accord (mid-sized sedan) and a 2010 Toyota Yaris (compact sedan). All guard designs were assessed: three baseline and three "minimally compliant" for a total of six designs. All guard designs prevented PCI in the full and 50 percent overlap impacts. However, only the Manac guard design prevented PCI in the 30 percent overlap, and only when the Honda Accord was used as the striking vehicle. None prevented PCI with the smaller Toyota Yaris.

Optimizations were then performed to strengthen the guards to prevent PCI in the 30 percent overlap test for both the mid-size and compact sedans at 35 mph. Strengthening was performed by retaining the basic dimensions of the guards and only increasing the wall thicknesses of the steel members. In general, PCI outcomes depended on the striking vehicle and the distance between a guard's vertical support members. It was more difficult to prevent PCI when the vertical supports were closer together and when the smaller Toyota Yaris was used. In the case of the Great Dane guard (supports were closest together), a strengthened design that prevent PCI could not be attained when the Toyota Yaris was used as the striking vehicle.

Finally, compliance of the strengthened guards with FMVSS No. 223 (2022) was re-assessed. Compliance margins for the UDL force requirement are summarized below, where it is seen that the margin increases by as much as 3.46 and as little as no increase at all depending on the striking vehicle and the baseline guard design.

Table 6. Summary table of guard designs and performance

Rear-Impact Guard	Condition	FMVSS No. 223 UDL Force Requirement		Guard Mass		PCI in 35 mph, 30% overlap
		Max force (kN)	Compliance margin (x times)	Mass (kg)	Increase/decrease (x times)	
FMVSS No. 223		350				
Wabash	Baseline	395	1.13	54	1.00	Y
	Minimally Compliant	350	1.00	39	0.72	Y
	Strengthened Accord (midsize)	928	2.65	76	1.41	N
	Strengthened Yaris (compact)	1210	3.46	99	1.83	N
Manac	Baseline	356	1.02	85	1.00	N
	Minimally Compliant	352	1.01	76	0.89	N
	Strengthened Accord (midsize)	*no strengthening needed*				
	Strengthened Yaris (compact)	452	1.29	99	1.16	N
Great Dane	Baseline	442	1.26	69	1.00	Y
	Minimally Compliant	350	1.00	53	0.77	Y
	Strengthened Accord (midsize)	495	1.42	101	1.46	N
	Strengthened Yaris (compact)	1088	3.11	190	2.75	Y

Aim 3: Occupant Response in High-Speed Collisions into Strengthened Rear-Impact Guards

Following the strengthening of the rear-impact guard models to prevent PCI for the compact Toyota Yaris, a series of simulations to assess occupant response were performed. Speeds of interest were 40 mph, 45 mph, and 65 mph. The response of matched pair THOR-50M and GHBMC was of interest. Injury metrics from all areas of the body were calculated and statistical analysis was performed on the 40-mph and 45-mph cases. The structural integrity of the vehicle was assessed in the 65-mph cases, and in those that the body-in-white was not catastrophically compromised, a subsection of injury metrics were calculated.

Design of Experiments

A design of experiments was developed to assess the occupant response to impacts into the strengthened rear-impact guards that were able to prevent PCI for the Toyota Yaris. Both the THOR-50M and GHBMC M50-OS were used in this analysis, in part to identify any differences in response between an ATD and a HBM. Simulations were conducted with the Honda Accord model with either a THOR-50M in both the passenger and driver seat, or a GHBMC M50-OS in the passenger and driver seat. Speeds selected were 40 mph, 45 mph, and 65 mph. The three overlap percentages previously used were carried forward (e.g., 30%, 50%, and full width). Each guard was used. A full factorial DOE was selected, resulting in 54 simulations (3 guards x 3 speeds x 3 overlaps x 2 occupant types). Analysis was planned to compare occupant response in a four matched-pair analyses (THOR-50M Driver vs THOR-50M Passenger, THOR-50M Driver versus GHBMC Driver, GHBMC Driver versus GHBMC Passenger, THOR-50M Passenger versus GHBMC Passenger).

Model Setup

Occupant Models Positioning Settling

The computational THOR-50M ATD selected was the THOR-50M-M50 v2.7, developed by the University of Virginia and NHTSA (Center for Applied Biomechanics, 2020). This model is open-source and validated for frontal and oblique crash simulations against physical ATD response. The model needed to be positioned in both a driver and passenger position. NHTSA hosts a series of files that include an outdated THOR-50M FE model in the driver and passenger seat of the 2014 Honda Accord model. The positioning used in that model download was used as a reference. First, the LS-PrePost positioning tree was used to move the arms and legs into the appropriate location. Then, the model was rotated and translated in space such that the h-point matched the target location of the old models. Following positioning with the LS-PrePost positioning tree, some small contact penetrations existed. Simulations using *BOUNDARY_PRESCRIBED_FINAL_GEOMETRY were used to “push” small portions of parts out of the way. An example of this was in the shoulder (Figure 43).

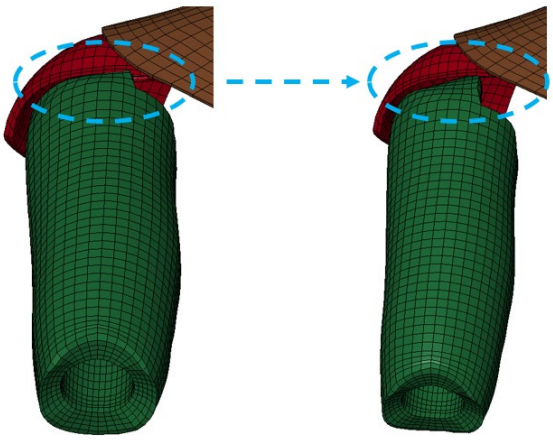

Figure 43. Example of removing penetrations in the shoulder post-positioning

The GHBMC M50-OS models target position was the same as the THOR-50M models. Instead of using the built-in LS-PrePost positioning tree, the Oasys Primer "marionette" positioning tool was used. This tool allows for the position to be achieved through a single simulation, which generally decreases the likelihood of intersections of the mesh at the final position (Figure 44).

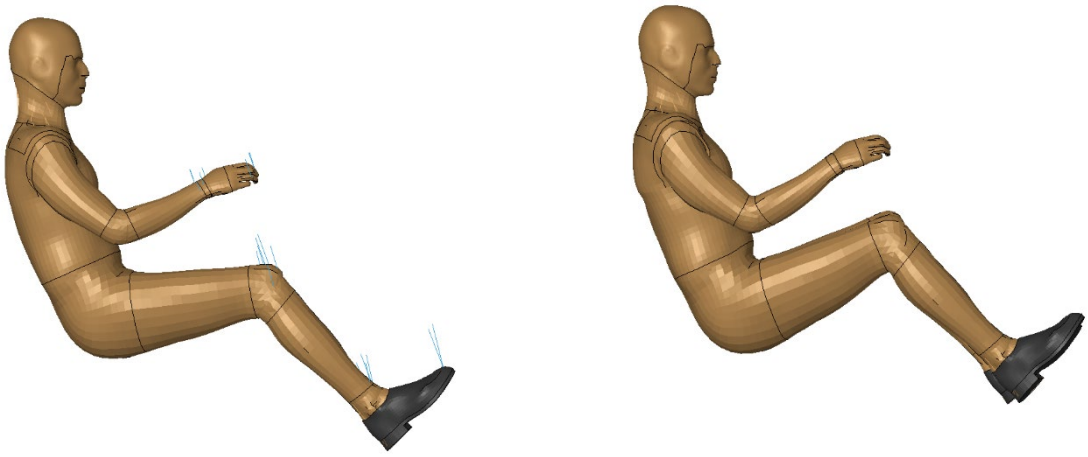

(a) (b)

Figure 44. Initial (a) and positioned (b) state of the GHBMC M50-OS in the driver posture

The occupant models were settled into the seats of the Honda Accord using *LOAD_BODY_Z after locking the joints. This allowed for the back and lower extremity rubber flesh to conform to the seat (Figure 45).

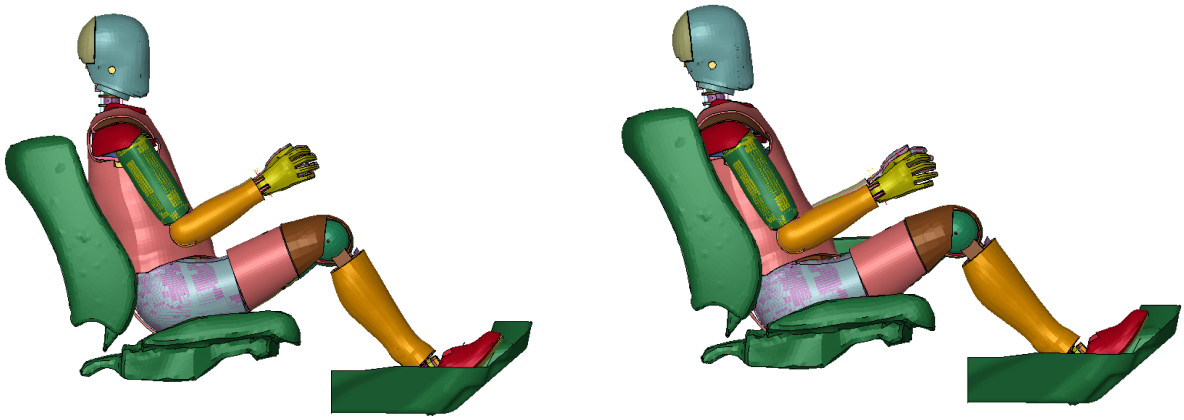

(a) (b)

Figure 45. Initial (a) and settled (b) state of the THOR-50M M50

Seat Belt Restraints

Once seated, the models were restrained with seat belts using a combination of 2D and 1D elements in Oasys Primer. Sliprings were included at the inboard buckle location as well as the d-ring. A seat belt load limiter was employed and was set to a limiting value of 2.5 kN for both the driver and passenger. The seat belts were pretensioned to 3.5 kN during the precrash phase of each simulation. A dynamic and static friction coefficient of 0.3 was used for both the driver and passenger chest to seat belt contact.

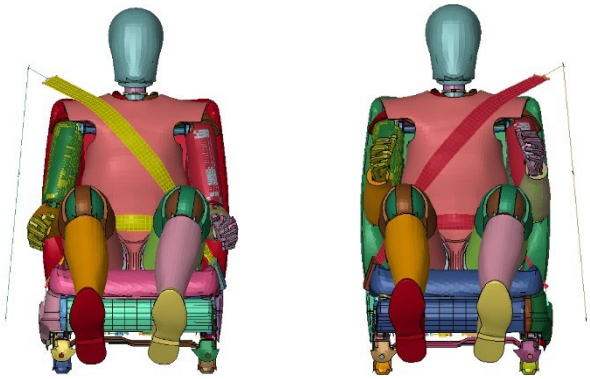

Figure 46. Belted THOR-50M M50 passenger and driver

Air Bags

The Honda Accord model is equipped with a driver air bag, passenger air bag, and a curtain air bag. The deployment times are set for a frontal impact into a rigid barrier, and the DAB, PAB, and CAB deployment times are 14 ms, 16 ms, and 42 ms, respectively. During this project, NHTSA sponsored another group to update the PAB model for the Honda Accord. This updated PAB model was incorporated into the Honda Accord model for occupant simulations. Preliminary simulations were conducted to ensure the proper functioning of the seat belt, occupants, and air bags before simulating the full DOE. It was discovered that the air bags were

deployed earlier than similar physical tests based on IIHS trailer impact crash test videos. Querying data from IIHS truck-trailer rear-impact guard tests, driver side small overlap tests, and passenger side small overlap tests, the average deployment times of the air bags were recorded and averaged. In these tests, the DAB, PAB, and CAB deployment times were 35.4 ± 4.3 ms, 30.1 ± 10.6 ms, and 40.0 ± 5 ms, respectively. Updates to the deployment timing of the simulation air bags were made; DAB and PAB were set to fire at 35 ms, and the CAB was deployed at 42 ms. In 35 mph test cases with these modified deployment times, the THOR-50M occupants' faces loaded the air bags at approximately 85 ms, which was within 1 standard deviation of experimental results.

A secondary finding from the preliminary simulations was a discrepancy in expected PAB response. In the simulations, the PAB deflated quickly, and did not provide much resistance to the head and torso of the passenger. Both an on-board and side view of a frontal crash demonstrates this (Figure 47). In the passenger side view, it is evident that in a physical crash, the head of the passenger should be just forward of the head of the driver. However, in the simulation, the passenger head struck the instrument panel while the driver head was stopped by the DAB.

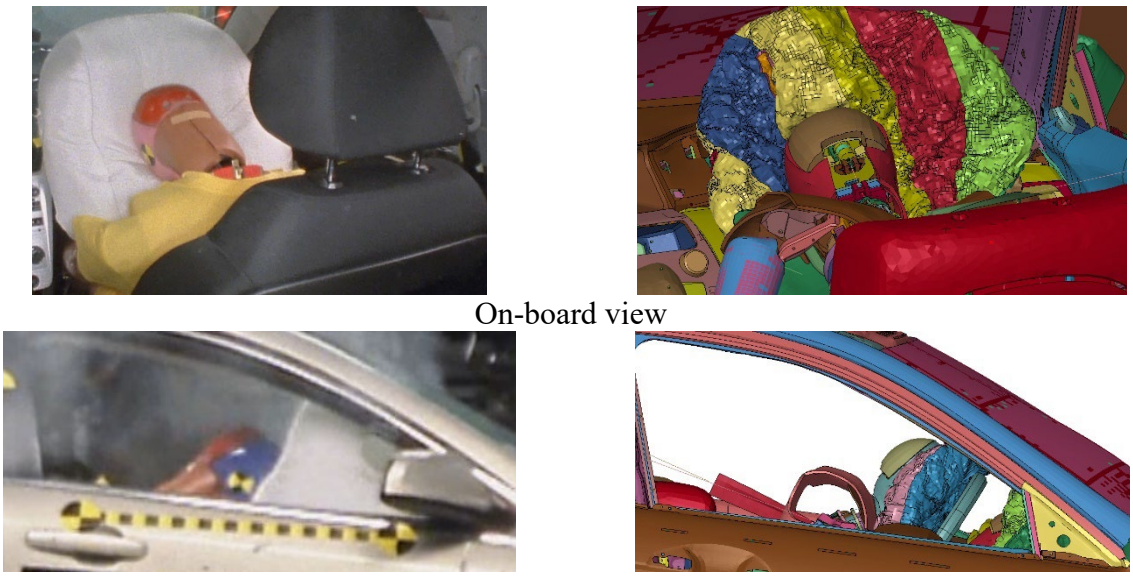

Figure 47. Passenger air bag response in preliminary simulations

A modification to the vent area was made for the passenger air bag, reducing the value from 5200 mm^2 to 4000 mm^2, which matched that of the DAB. Using a reduced simulation, containing just the air bag, instrument panel, and the windscreen, it is clear this modification results in the PAB remaining inflated throughout the crash phase, whereas the base model deflates prematurely on its own (Figure 48).

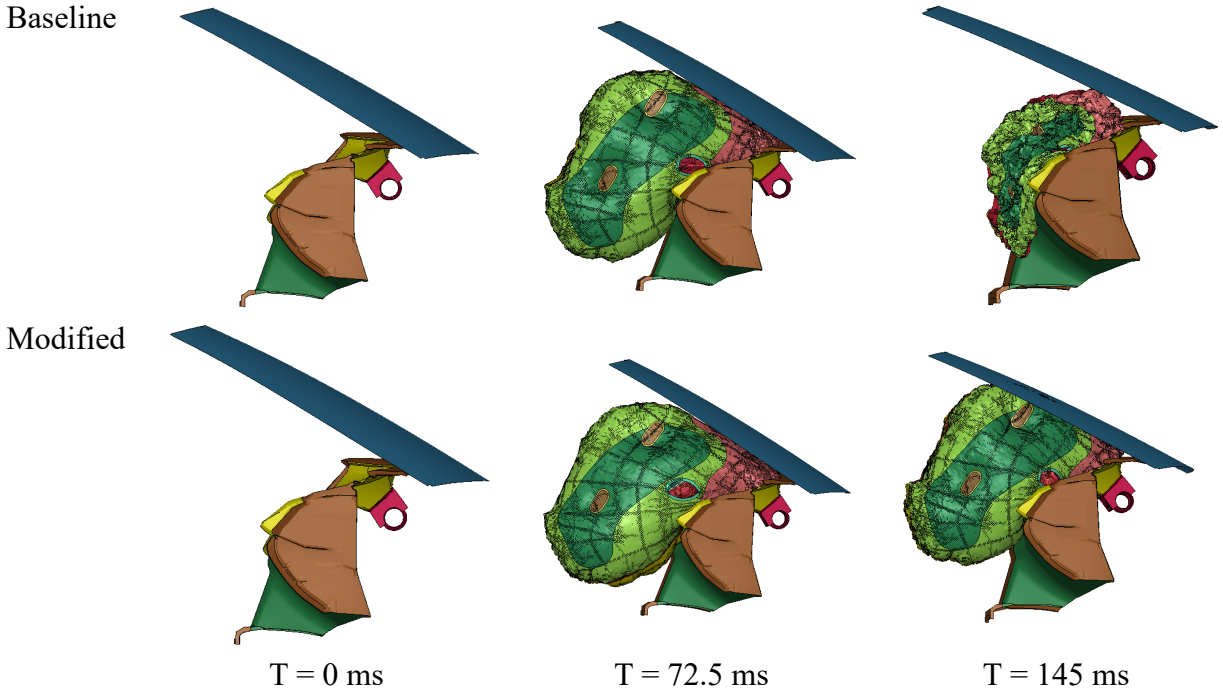

Figure 48. Passenger air bag response before and after vent area modification

The final belted and positioned GHBMC M50-OS and THOR-50M M50 models can be viewed in Figure 49.

(a)

(b)

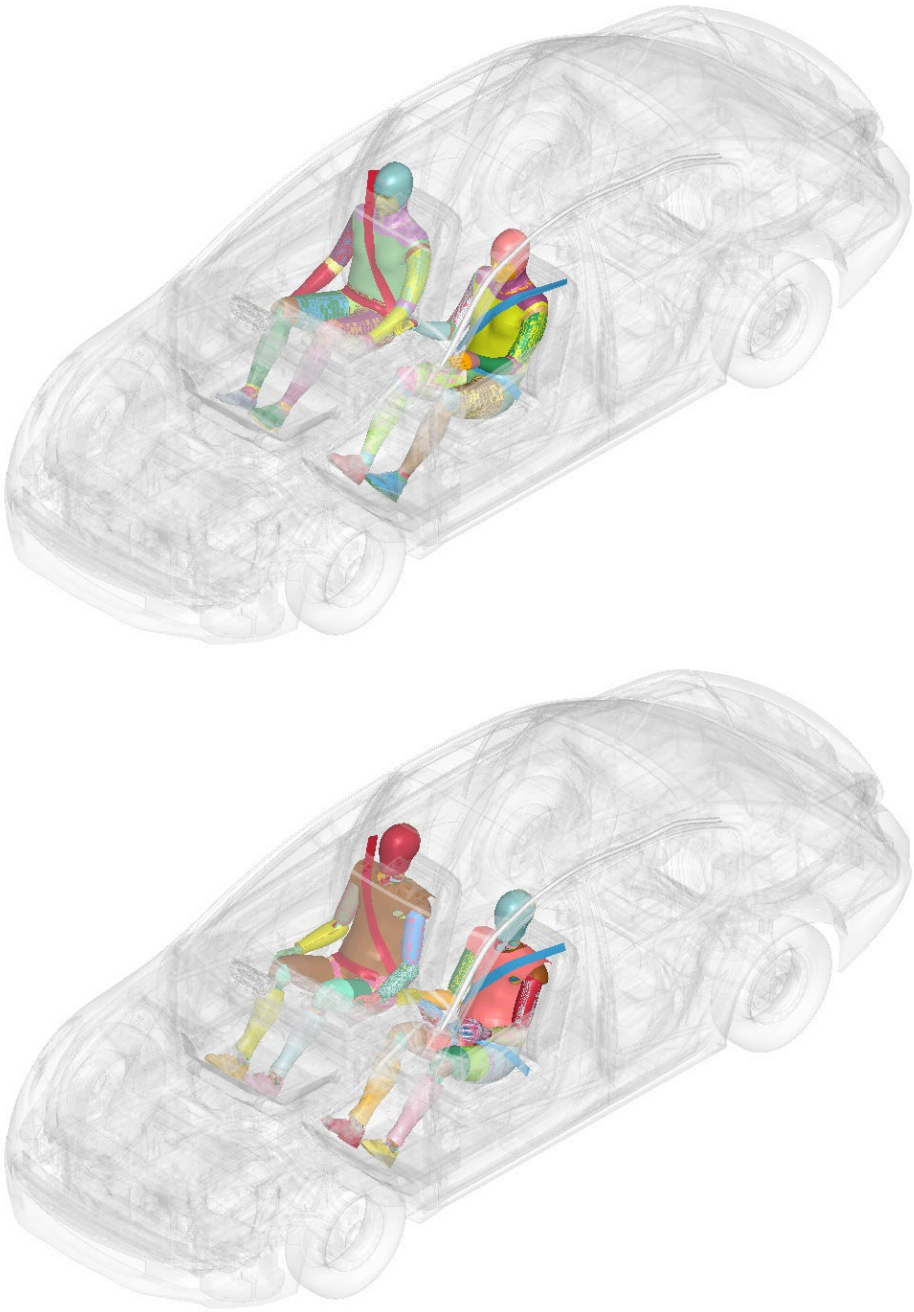

Figure 49. Seated and belted GHBMC M50-OS (a) and THOR-50M (b) models in the Honda Accord vehicle

Simulation Results

All of the simulations conducted at 40 mph and 45 mph were usable for injury metric calculation. Three simulations error terminated after 125 ms, but the peak injury metric response had already been captured. Visually, no areas of concern were identified within the period of injury metric calculation. Energy distributions were checked to ensure that no non-physical energy trends occurred in the simulations that normal terminated. Mass additions due to timestep were primarily located at the spotwelds of the trailer model and are not expected to have contributed to the results of the occupant responses. The majority of the 65 mph cases error terminated due to catastrophic deformation of the passenger vehicle parts. In some cases, the 65 mph simulations error terminated before the vehicle reached a zero forward velocity, while in some cases rebound had begun to occur. The results of the 40 and 45 mph cases were analyzed separately from the 65 mph cases.

Passenger Compartment Intrusion – 40 and 45 mph Simulations

As defined previously, passenger compartment intrusion was determined to occur in the simulation if the rear of the trailer contacted the passenger vehicle anywhere above the base of the a-pillar. The strengthened guards were impacted at 30 percent, 50 percent and full-width overlap using the midsize sedan model. Each of the strengthened guard models could prevent PCI at 40 mph in the 50 percent overlap and the full width overlap simulations. Only the strengthened Manac guard could prevent PCI in the 40-mph 30 percent overlap case. When increasing the closing speed to 45 mph, all three strengthened guards prevented PCI in the full-width configuration. Both the strengthened Wabash and Manac guard prevented PCI in the 45 mph 50 percent overlap simulations, while PCI occurred with the strengthened Great Dane guard model. None of the strengthened guards prevented PCI in the 45 mph 30 percent overlap simulations. A summary table of these results is presented in Table 7.

Table 7. PCI observations – Strengthened guards

Overlap	**Strengthened Guard**	**40 mph**	**45 mph**
		PCI//No-PCI	**PCI//No-PCI**
30 Percent Overlap	Wabash	PCI	PCI
	Manac	No PCI	PCI
	Great Dane	PCI	PCI
50 Percent Overlap	Wabash	No PCI	No PCI
	Manac	No PCI	No PCI
	Great Dane	No PCI	PCI
Full Width	Wabash	No PCI	No PCI
	Manac	No PCI	No PCI
	Great Dane	No PCI	No PCI

The major trend observed was that the strengthened Manac guard was most capable of preventing PCI. The strengthened Great Dane guard was the least capable of preventing PCI at the higher speeds. The strengthened Wabash guard's capability to prevent PCI was between the other two guards. Examining the design features of the three guards leads to some insight into why the different guards may produce different results. Simplifying the typical rear-impact guard into principal design components yields the diagram in Figure 50.

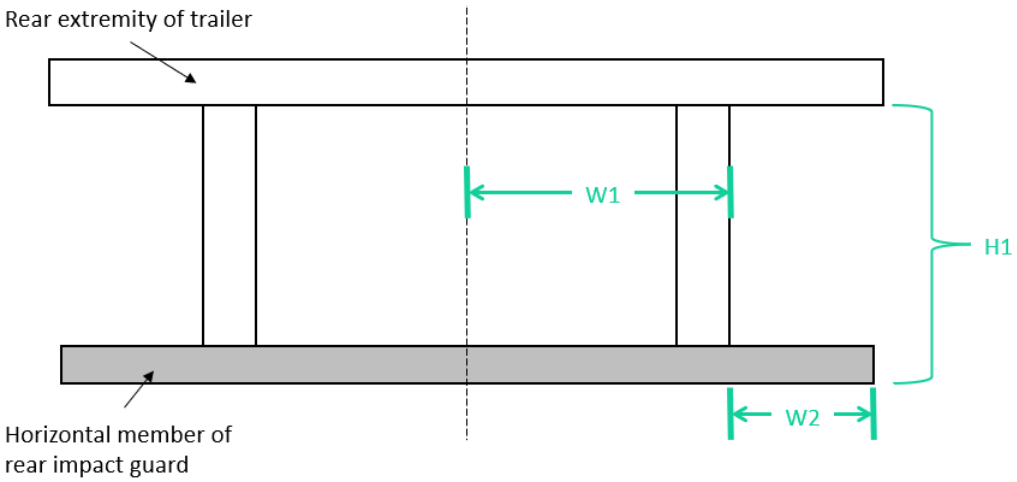

Figure 50. Simplified diagram of the typical rear-impact guard

The rear-impact guard is typically symmetrical with two vertical supports connecting to the rear extremity of the trailer and a horizontal member. The distance between the center line and the outer edge of a vertical support is denoted "W1." The height of the guard as measured from the bottom of the trailer to the bottom of the horizontal member is denoted "H1." Finally, the length from the outer edge of a vertical support to the edge of the horizontal member on the same side of the guard is denoted "W2." These are reported in Table 8 for the three guards modeled here.

Table 8. Dimensions of rear-impact guards

Dimensional References	**Manac**	**Wabash**	**Great Dane**
Upright Width From Center (W1)	910 mm	690 mm	650 mm
Distance From Upright to Edge (W2)	290 mm	504.2 mm	556.5 mm
Height of Upright (H1)	450 mm	525 mm	575 mm

As the percentage of overlap between the rear-impact guard and the passenger vehicle decreases, the section of the horizontal member denoted W2 becomes more like a cantilevered beam. Furthermore, the horizontal member is supported by a vertical cantilevered beam from the upright support. Thus, as both lengths increase, it would be expected that the guard would be less capable of supporting higher loads. In fact, the trend in PCI prevention previously seen in the simulations mirrors the trend in these two measurements. As W1 decreases, W2 increases, and H1 increases, the guard is less able to prevent PCI, even when strengthened. This is seen in the 30 percent overlap simulations with the Wabash and Great Dane guards, where the vertical posts remain largely intact and untouched. The vehicle bends the horizontal member about the vertical post and intrudes all the way to the truck tires (see Figs. 93 and 95 in Appendix B). This effect is worse for smaller (narrower) vehicles, such as the Toyota Yaris, because the edge of the vehicle is further away from the vertical post in a 30 percent overlap, creating an even greater moment arm to bend the horizontal member more easily.

Another key feature of the rear-impact guards that is not described in this simple diagram is their connection points to the trailer. Each of the three guards in this study used very different designs in this area as depicted in Figure 51. The Manac guard connection spans the longest length forward underneath the trailer, followed by the Wabash, and then finally the Great Dane. This support increases the guard's ability to resist bending underneath of the trailer.

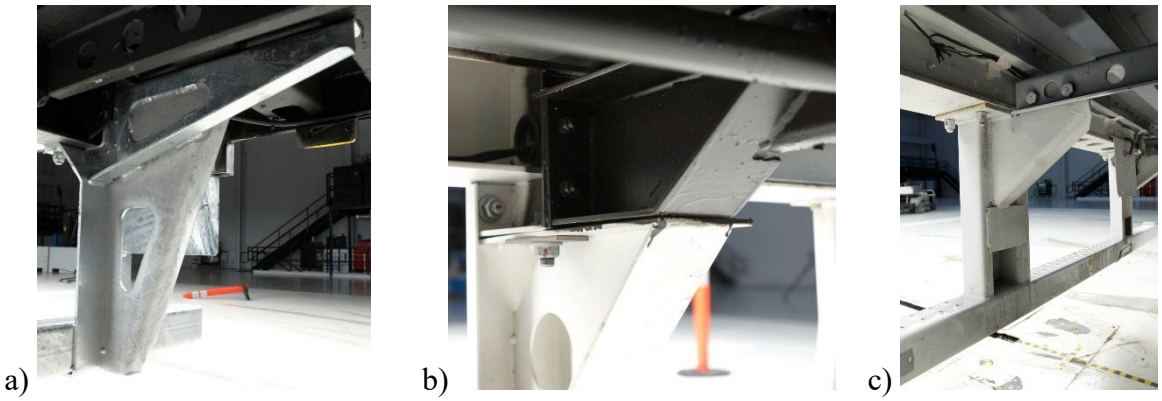

Figure 51. Rear-impact guard connections to trailer for (a) Manac, (b) Wabash, and (c) Great Dane

Occupant Response

The signal data from the THOR-50M and GHBMC occupants were extracted from the LS-DYNA binout files using a custom Python code and Metriks[12] ly. Signals were filtered to remove noise before calculating injury metric values or extracting peak values. For the head, HIC and brain injury criteria were calculated. For the neck, peak upper neck tension, peak upper neck flexion moment, and Nij were calculated. For the thorax, the multi-point thoracic injury criterion, the abdomen compression, and peak T6 acceleration were calculated for the THOR-50M. For the GHBMC, the peak compression value from the thorax and abdomen instrumentation was calculated and compared to the multi-point thoracic injury criterion in the THOR-50M. Additionally, the peak abdomen compression and T6 peak linear acceleration were calculated for the GHBMC. The peak lumbar tension and compression force values were calculated for the THOR-50M and GHBMC. Peak pelvis center of gravity linear acceleration was computed for both occupant models. Peak axial femur loads, upper tibia bending moment, upper tibia axial force, and upper tibia index were calculated for both the left and right legs of the GHBMC and THOR-50M. Results of the injury metric analysis are provided below as well as in Appendix C, and the individual channel traces from simulations are provided in Appendix D.

Discussion on THOR-50M and GHBMC Usage

Each combination of speed and overlap percentage were simulated twice, once with a THOR-50M in both the driver and passenger seat, and once with the GHBMC M50-OS in the driver and passenger seat. Each of these surrogates are developed to represent a human response in a frontal and/or oblique automotive impact and their response has been well established in the literature. Both are capable of predicting occupant injury; however, their intended purposes are slightly different. The GHBMC, as a human body model, is intended to behave like a human occupant or

[12] Elemance LLC, Clemmons, NC.

postmortem human subject. Thus, the model is designed to have highly deformable elements that capture soft tissue response, as well as the highly complex skeletal system. The THOR-50M model, on the other hand, is intended to predict the response a physical ATD would exhibit in a real-world experiment. While developed with the intention of replicating human response in crash tests, design considerations for robustness and re-usability of the physical ATD produce some differences between true-human response and THOR-50M response. As PMHS experiments are often significantly more complex than ATD experiments, and are hard to repeat, the THOR-50M is the go-to human surrogate for crash testing. It is expected that the injury metrics measured by each surrogate (GHBMC, THOR-50M) will be different. However, each surrogate has corresponding injury risk curves that are developed to translate the measured kinematics/kinetics to the injury risk expected to an occupant. Should the predicted injury risk be similar between the GHBMC and THOR, it would demonstrate greater confidence in the predicted result. Where predicted injury risks differ, more analysis should be conducted to investigate which prediction is more accurate.

Injury Assessment References

As mentioned previously, while injury metrics are calculable for each model (THOR-50M and GHBMC M50-OS), the meaningfulness of those metrics only comes when comparing them to corresponding injury risk curves. The most widely used injury scoring system in the injury biomechanics literature is the Abbreviated Injury Scale, which is published by the Association for the Advancement of Automotive Medicine (2016). AIS classifies injury on a 6-point scale based on relative severity (Table 9). This study primarily focuses on AIS 2+ and 3+ injury severity, which correspond to “moderate” and “serious” injury levels, respectively.

Table 9. Abbreviated injury scale scoring system

AIS Score	Injury
1	Minor
2	Moderate
3	Serious
4	Severe
5	Critical
6	Unsurvivable

In conjunction with injury risk curves and injury metrics, Injury Assessment Reference Values (IARVs) are often used for quick comparison points and regulatory purposes. Saunders et al. (2023) recently published the IARVs for common THOR-50M injury metrics. A portion of this is recreated in Table 10 alongside GHBMC M50-OS IARV values.

The injury risk curves that were used to determine risk of injury for the THOR-50M ATD model were adapted from those published by Craig et al. (2009). For the M50-OS model, the same risk curves were used with two exceptions. The first exception was for the prediction of femur injury risk which used the curves published by Rupp et al. (2020) as the Craig et al. risk curve does not consider the difference between the applied force at the knee of the PMHS and the peak axial compression force measured at the femur load cell of the ATD.

The second exception is in the prediction of chest injury risk. While chest deflections are reported, chest injury risk was not calculated for the M50-OS. Differences in instrumentation hinder fair comparison of performance between the two models. Accurate prediction of chest injury risk with a human body model would require the extraction and processing of element level rib strain data in combination with other measures. The generation of new sensors and analysis of element level strain data was out of scope for this investigation.

Table 10. THOR-50M and GHBMC M50-OS comparative reference values

Body Region	Measurement or Criterion	Units	THOR-50M Baseline Comparative	GHBMC-50M Baseline Comparative	Injury Severity, Risk Level
Head	HIC15	none	700	700	AIS 2+, 11%
	BriC	none	0.96	0.96	AIS 3+, 50%
Neck	Nij	none	0.88	0.88	AIS 2+, 30%
Chest	Deflection	mm	51.4		AIS 3+, 50%
Femur	Peak Compression	N	9450	9450	AIS 2+, 30%
Lower Leg	Revised Tibia Index	none	1.23	1.23	AIS 2+, 50%

Injury Risks

Head Injury Risk

Table 11. Honda Accord, head injury risk
(Bolded values represent values above IARV. Italicized values represent similar risk between THOR-50M and GHBMC M50-OS.)

		Strengthened Underride Guard	**Driver**				**Passenger**				PCI/No PCI
			THOR-50M		GHMBC		THOR-50M		GHMBC		
			HIC	AIS 2+ Risk (%)	HIC	AIS 2+ Risk (%)	HIC	AIS 2+ Risk (%)	HIC	AIS 2+ Risk (%)	
40 mph	30% overlap	Wabash	*135*	*0.75*	*125*	*0.59*	114	0.43	41	0.01	PCI
		Manac	**2379**	**83.09**	220	3.17	115	0.44	71	0.07	No PCI
		GrDane	*99*	*0.26*	*113*	*0.42*	87	0.16	51	0.02	PCI
	50% overlap	Wabash	399	12.46	317	7.73	*143*	*0.91*	*123*	*0.55*	No PCI
		Manac	**1238**	**57.47**	100	0.27	77	0.10	53	0.02	No PCI
		GrDane	251	4.49	202	2.53	*100*	*0.26*	*83*	*0.14*	No PCI
	Full width	Wabash	***801***	***37.13***	***773***	***35.58***	***755***	***34.56***	*643*	*27.82*	No PCI
		Manac	*295*	*6.59*	*289*	*6.26*	*152*	*1.10*	*174*	*1.67*	No PCI
		GrDane	*613*	*26.00*	*517*	*19.92*	417	13.57	426	14.13	No PCI
		Strengthened Underride Guard	**Driver**				**Passenger**				PCI/No PCI
			THOR-50M		GHMBC		THOR-50M		GHMBC		
			HIC	AIS 2+ Risk (%)	HIC	AIS 2+ Risk (%)	HIC	AIS 2+ Risk (%)	HIC	AIS 2+ Risk (%)	
45 mph	30% overlap	Wabash	*144*	*0.93*	*158*	*1.25*	85	0.15	42	0.01	PCI
		Manac	*150*	*1.05*	*154*	*1.15*	100	0.27	68	0.06	PCI
		GrDane	*112*	*0.41*	*127*	*0.61*	76	0.09	49	0.02	PCI
	50% overlap	Wabash	537	21.16	404	12.81	*164*	*1.40*	*178*	*1.78*	No PCI
		Manac	*249*	*4.38*	*252*	*4.50*	*83*	*0.14*	*78*	*0.10*	No PCI
		GrDane	298	6.73	238	3.93	*110*	*0.37*	*122*	*0.53*	PCI
	Full width	Wabash	***956***	***45.28***	***1162***	***54.45***	***1413***	***63.40***	***1217***	***56.61***	No PCI
		Manac	477	17.37	383	11.50	*220*	*3.19*	*250*	*4.41*	No PCI
		GrDane	*663*	*29.05*	*652*	*28.38*	**991**	**46.96**	620	26.42	No PCI

Head Injury Risk Discussion

Head injury risk was assessed using the head injury criterion (HIC-15) metric. While previously reported tabularly, both the injury metric value and AIS 2+ injury risks for each occupant in each simulation are proved in Figure 52 and Figure 53, respectively. Most simulations produced HIC values below the IARV of 700, with some exceptions.

Beginning with the Manac guard, the THOR-50M driver head struck the steering wheel in both the 40-mph 30 percent and 40-mph 50 percent overlap simulations. The GHBMC M50-OS driver head struck the steering wheel in the Manac 40 mph 30 percent overlap case, and narrowly avoided contact in the 40-mph 50 percent overlap case. In the simulation configuration where both the THOR-50M and GHBMC M50-OS heads struck the steering wheel, the raw and filtered acceleration peak for the THOR-50M was significantly higher than the GHBMC M50-OS, which produced a much higher HIC value. Surprisingly, increasing the closing speed in the same overlap and guard configuration protected the occupant from striking the steering wheel. This observation is counterintuitive, and the authors believe it may be attributable to the air bag model hard-coded timing. The driver air bag model has a time-based change in the ventilation area, which helps with ensuring the air bag inflates fully, and then absorbs energy consistent with a real-world air bag for a rigid wall impact simulation. In the Manac 40 mph 30 percent and 50 percent overlap simulations the vehicle deceleration is the lowest of the simulations, which delays the head-air bag contact time into the increased ventilation period. Therefore, the authors would suggest caution in interpreting this result.

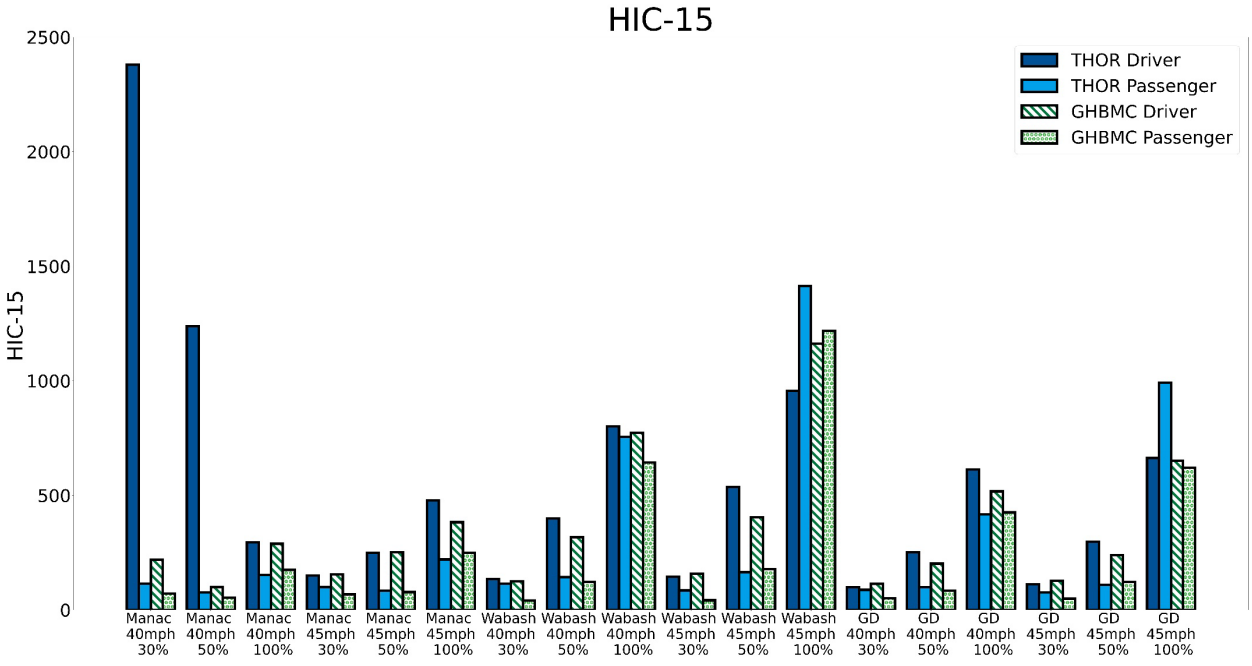

Figure 52. HIC-15 values for occupants in the midsize sedan full vehicle-to-trailer impacts simulations

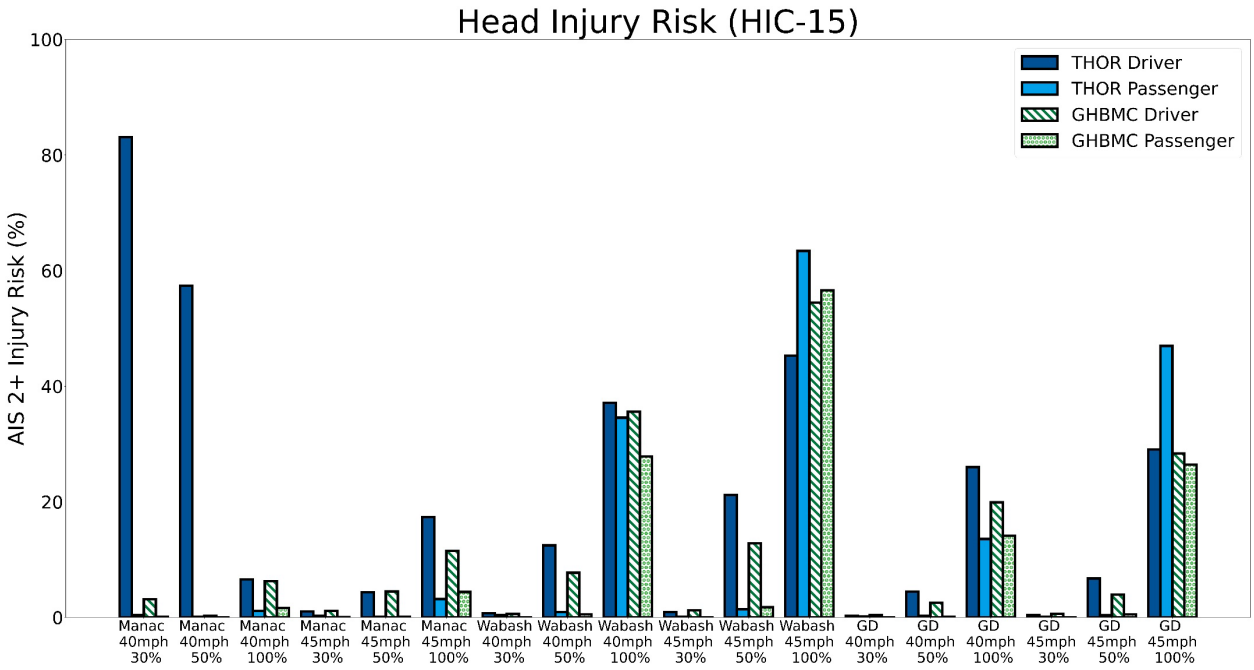

Figure 53. AIS 2+ head injury risks for occupants in the midsize sedan full vehicle-to-trailer impacts simulations

When comparing all occupant head injury risks across the rear-impact guard models, there was no statistically significant difference attributable to the rear-impact guard (Figure 54a). While not statistically significant, the Wabash guard indicated a higher prevalence for increased HIC values compared to the other rear-impact guard models. A statistically significant trend was noted between the overlap percentage and the occupant head injury risk (Figure 54b); as the overlap percentage increased an increase in injury risk was observed. This is likely attributable to the greater deceleration of the vehicle as overlap percentage increased, thus imparting forces onto the driver more quickly. Additionally, a comparison between occupant and driver HIC-15 response was completed (Figure 55). While the driver median and max HIC-15 value was higher than the passenger median and max, there was no statistically significant difference between the two seating positions. Additionally, there was no statistically significant difference between the THOR-50M and GHBMC M50-OS when combining both driver and passenger data together. A more in-depth comparison between individual cases of THOR-50M and GHBMC M50-OS is in Appendix C.

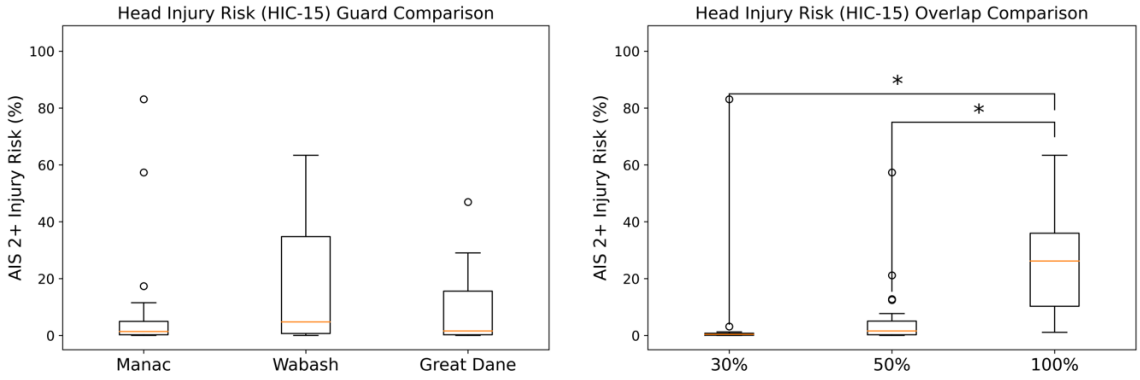

a.) b.)

Figure 54. Rear-impact guard (a) and overlap percentage (b) comparisons for head injury risk. Both THOR-50M and GHBMC M50-OS data included. Statistical analysis performed with α=0.05

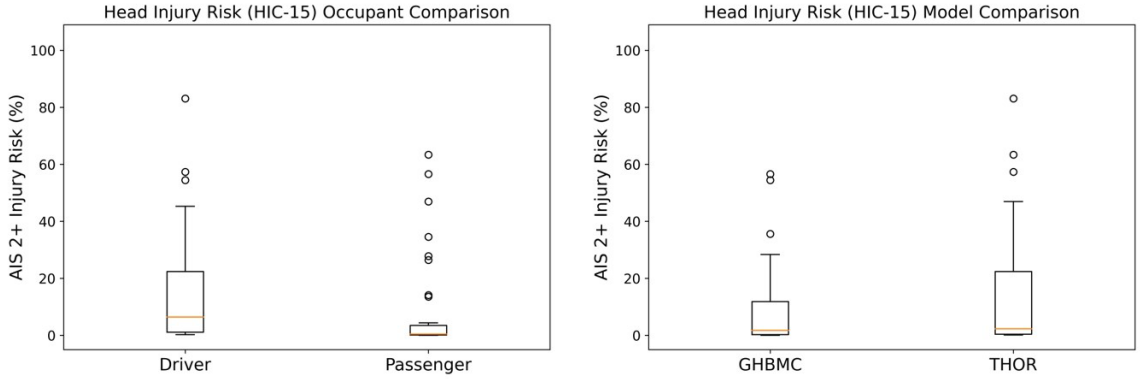

a.) b.)

Figure 55. Occupant seating location (a) and model (b) comparisons for head injury risk. Both THOR-50M and GHBMC M50-OS data included. Statistical analysis performed with α=0.05

Brain Injury Risk

Table 12. Honda Accord, brain injury risk
(Bolded values represent values above IARV. Italicized values represent similar risk between THOR-50M and GHBMC M50-OS.)

		Strengthened Underride Guard	**Driver**				**Passenger**				PCI/No PCI
			THOR-50M		GHMBC		THOR-50M		GHMBC		
			BrIC	AIS 3+ Risk (%)	BrIC	AIS 3+ Risk (%)	BrIC	AIS 3+ Risk (%)	BrIC	AIS 3+ Risk (%)	
40 mph	30% overlap	Wabash	*0.63*	*5.09*	*0.64*	*6.69*	*0.54*	*0.13*	*0.63*	*5.06*	PCI
		Manac	*0.70*	*12.41*	*0.65*	*7.14*	*0.61*	*4.08*	*0.53*	*0.02*	No PCI
		GrDane	*0.61*	*3.42*	*0.63*	*5.32*	*0.52*	*0.00*	*0.49*	*0.00*	PCI
	50% overlap	Wabash	*0.84*	*32.86*	*0.75*	*19.14*	0.76	20.87	0.57	1.17	No PCI
		Manac	*0.70*	*13.54*	*0.64*	*6.02*	*0.58*	*1.80*	*0.58*	*1.83*	No PCI
		GrDane	*0.74*	*18.38*	*0.73*	*16.63*	*0.79*	*25.61*	*0.67*	*9.18*	No PCI
	Full width	Wabash	**1.06**	**63.33**	0.77	22.28	*0.75*	*19.68*	*0.73*	*17.00*	No PCI
		Manac	*0.82*	*29.58*	*0.72*	*15.64*	*0.78*	*23.91*	*0.64*	*6.48*	No PCI
		GrDane	**0.95**	**49.78**	0.70	13.02	*0.80*	*26.30*	*0.70*	*12.74*	No PCI
		Strengthened Underride Guard	**Driver**				**Passenger**				PCI/No PCI
			THOR-50M		GHMBC		THOR-50M		GHMBC		
			BrIC	AIS 3+ Risk (%)	BrIC	AIS 3+ Risk (%)	BrIC	AIS 3+ Risk (%)	BrIC	AIS 3+ Risk (%)	
45 mph	30% overlap	Wabash	*0.63*	*5.82*	*0.68*	*10.95*	*0.59*	*2.18*	*0.58*	*1.53*	PCI
		Manac	*0.69*	*11.62*	*0.64*	*6.36*	*0.54*	*0.16*	*0.52*	*0.00*	PCI
		GrDane	*0.63*	*5.51*	*0.63*	*5.14*	*0.51*	*0.00*	*0.46*	*0.00*	PCI
	50% overlap	Wabash	0.84	32.95	0.68	10.40	*0.72*	*15.09*	*0.62*	*4.21*	No PCI
		Manac	*0.79*	*24.63*	*0.67*	*9.37*	*0.61*	*3.77*	*0.57*	*1.37*	No PCI
		GrDane	*0.75*	*19.67*	*0.77*	*22.85*	0.77	22.01	0.58	1.90	PCI
	Full width	Wabash	***1.09***	***67.08***	*0.91*	*42.52*	**1.35**	**89.24**	0.80	26.92	No PCI
		Manac	**1.05**	**63.25**	0.64	6.73	0.84	33.24	0.61	3.59	No PCI
		GrDane	**1.16**	**75.45**	0.81	28.25	**0.96**	**50.04**	0.75	19.80	No PCI

Brain Injury Risk Discussion

Brain injury risk was assessed using the BrIC metric, which is based on head peak rotational velocities. While previously reported tabularly, both the injury metric value and AIS 3+ injury risks for each occupant in each simulation are proved in Figure 56 and Figure 57, respectively. Most simulations produced BrIC values below the IARV of 0.96, but most of the 100 percent overlap cases produced either occupant or driver response exceeding the IARV. While HIC-15 (previously discussed) and BrIC are injury metrics for the same region of the body, the relative risk of injury as predicted by BrIC exceeded that predicted by HIC substantially. Neither occupant or driver BrIC values exceeded the IARV for 30 percent or 50 percent overlap for any rear-impact guard or occupant model configuration. Indeed, the GHBMC M50-OS models never experienced BrIC values above 0.96; instead, the simulations that recorded higher BrIC values than the IARV were completely exclusive to the THOR-50M. In most of the simulations, the driver was more susceptible to higher BrIC values than the passenger.

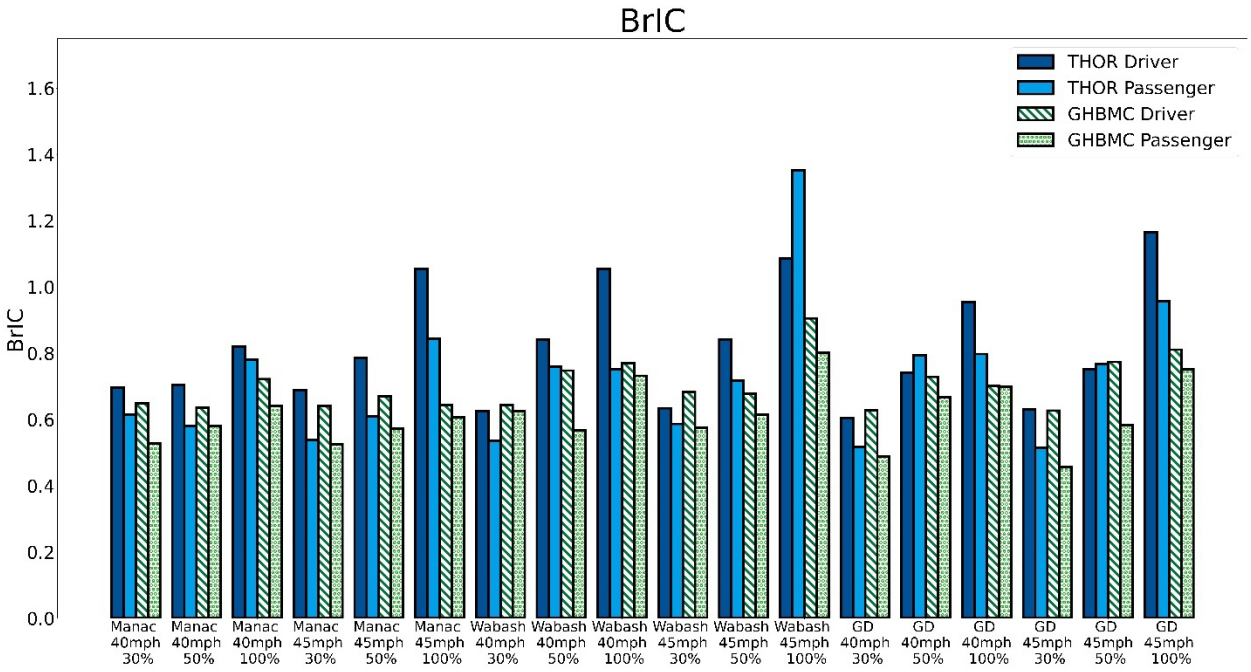

Figure 56. BrIC values for occupants in the midsize sedan full vehicle-to-trailer impacts simulations

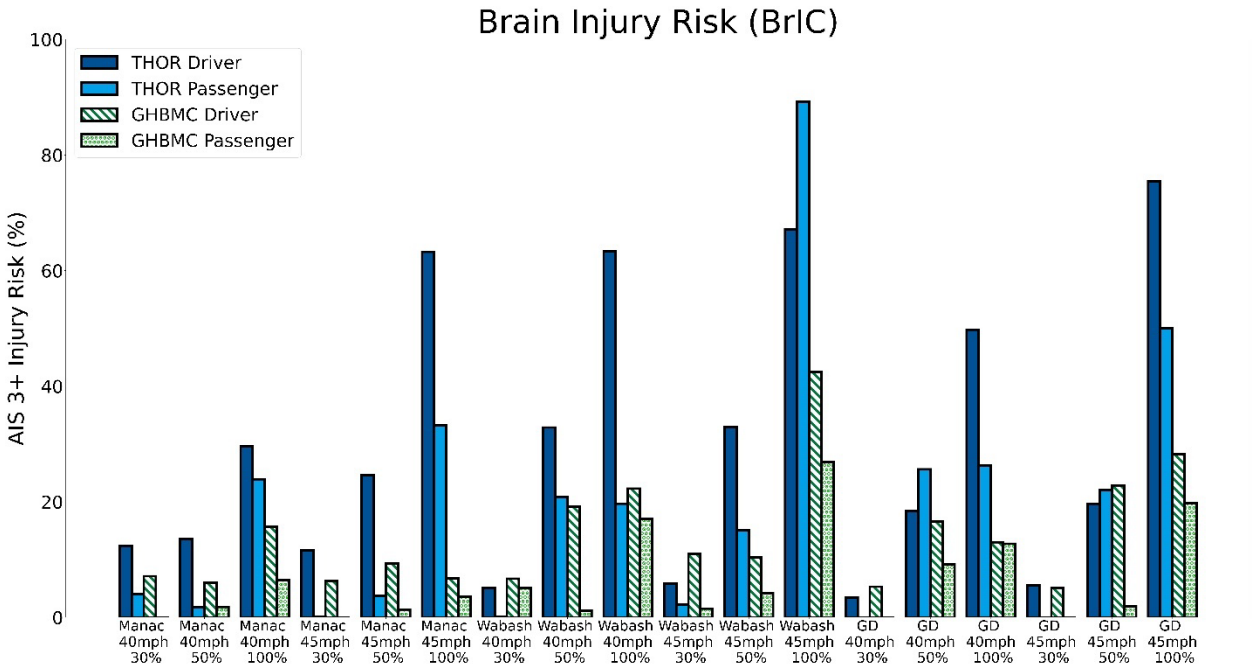

Figure 57. AIS 3+ brain injury risks for occupants in the midsize sedan full vehicle-to-trailer impacts simulations

When comparing all occupant brain injury risks across the rear-impact guard models, there was no statistically significant difference attributable to the rear-impact guard (Figure 58a). As with HIC-15, while not statistically significant, the Wabash guard produced the highest median and max BrIC values across the simulations. A significant trend was observed across overlap percentages. As the percent overlap between the Honda Accord and the rear-impact guard increased, the BrIC values and injury risks experienced by the occupants also increased (Figure 58b).

According to the BrIC, the driver was statistically significantly more predisposed to brain injury than the passenger (Figure 59a). The mean and standard deviation of BrIC for the driver across the simulations was 0.759 ± 0.143 compared to 0.668 ± 0.163 for the passenger.

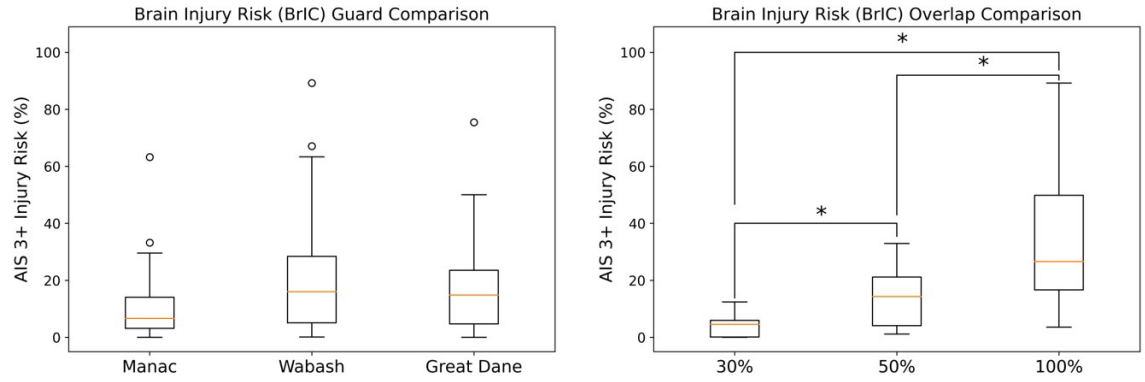

Figure 58. Rear-impact guard (a) and overlap percentage (b) comparisons for HIC-15 levels and injury risk. Both THOR-50M and GHBMC M50-OS data included. Statistical analysis performed with α=0.05.

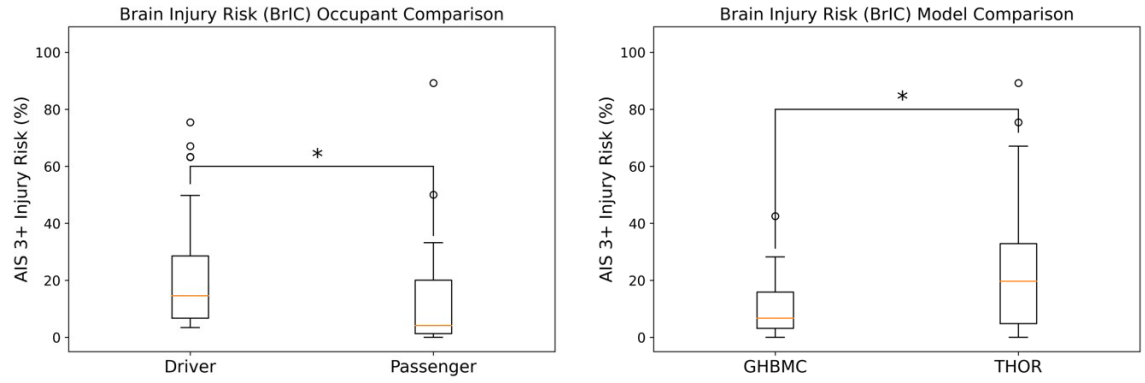

Figure 59. Occupant seating location (a) and model (b) comparisons for BrIC levels and injury risk. Both THOR-50M and GHBMC M50-OS data included. Statistical analysis performed with α=0.05.

BrIC and the corresponding brain injury risk was elevated for the THOR-50M compared to the GHBMC M50-OS (Figure 59b). The average risk of AIS 3+ brain injury predicted by the GHBMC M50-OS was on average 14 percent lower than the THOR-50M. This difference is meaningful and spurred further examination. Appendix D: includes each simulation's kinematic time-history traces and a sub-sample of head rotational velocity plots are provided in Figure 60. It is notable that the THOR-50M y-rotational velocity is consistently higher than the GHBMC M50-OS y-rotational velocity. Albert et al. (2018) noted differences in head y-rotational velocities between THOR-50M and PMHS for frontal experimental sled pulses, but the trends were not consistent across restraint systems. Parent et al. (2017) found that the head angle and neck flexion angle for the THOR-50M exceeded the PMHS targets. It is unclear which of the two occupant models is more representative of the expected real-world occupant.

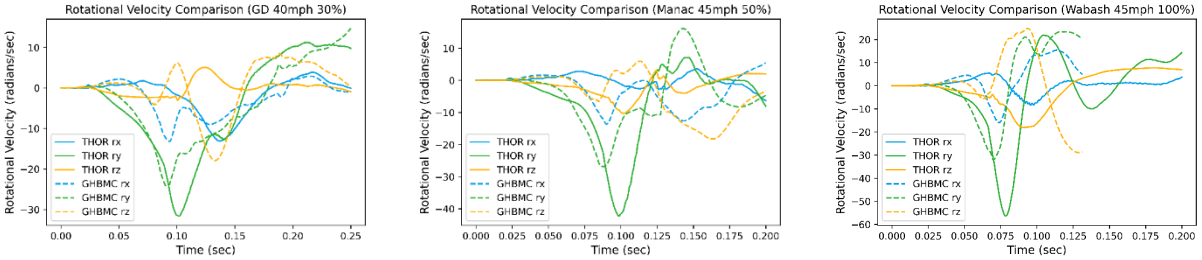

(a) (b) (c)

Figure 60. A sample of head rotational velocity kinematics comparing THOR-50M and GHBMC M50-OS

Neck Injury Risk

Table 13. Honda Accord, neck injury risk
(Bolded values represent values above IARV. Italicized values represent similar risk between THOR-50M and GHBMC M50-OS.)

		Strengthened Underride Guard	**Driver**				**Passenger**				PCI/No PCI
			THOR-50M		GHMBC		THOR-50M		GHMBC		
			Nij	AIS 2+ Risk (%)	Nij	AIS 2+ Risk (%)	Nij	AIS 2+ Risk (%)	Nij	AIS 2+ Risk (%)	
40 mph	30% overlap	Wabash	0.50	4.95	0.82	23.69	0.50	4.83	0.71	14.38	PCI
		Manac	0.60	8.33	0.83	24.66	0.51	5.11	0.79	20.45	No PCI
		GrDane	0.50	4.84	0.70	13.42	0.55	6.36	0.77	18.99	PCI
	50% overlap	Wabash	0.73	16.11	**1.02**	**49.25**	0.69	12.80	0.84	26.03	No PCI
		Manac	*0.71*	*14.46*	*0.73*	*15.67*	0.43	3.37	0.68	12.50	No PCI
		GrDane	0.64	10.31	0.83	25.36	*0.68*	*12.39*	*0.73*	*15.85*	No PCI
	Full width	Wabash	**0.89**	**31.55**	**1.16**	**68.02**	0.84	26.32	**1.07**	**56.78**	No PCI
		Manac	*0.85*	*27.00*	***0.98***	***43.29***	0.71	14.09	**0.97**	**41.90**	No PCI
		GrDane	*0.83*	*24.84*	***0.92***	***34.99***	*0.83*	*24.85*	***0.90***	***33.40***	No PCI
		Strengthened Underride Guard	**Driver**				**Passenger**				PCI/No PCI
			THOR-50M		GHMBC		THOR-50M		GHMBC		
			Nij	AIS 2+ Risk (%)	Nij	AIS 2+ Risk (%)	Nij	AIS 2+ Risk (%)	Nij	AIS 2+ Risk (%)	
45 mph	30% overlap	Wabash	0.51	5.01	**0.89**	**31.82**	0.45	3.66	0.82	24.10	PCI
		Manac	0.58	7.40	0.86	28.19	0.53	5.65	0.66	11.40	PCI
		GrDane	0.44	3.51	0.78	20.14	0.50	4.81	0.78	19.70	PCI
	50% overlap	Wabash	0.86	28.62	**1.07**	**55.83**	0.54	5.96	0.92	35.22	No PCI
		Manac	***0.94***	***38.02***	*0.80*	*21.65*	0.44	3.41	0.76	18.29	No PCI
		GrDane	0.72	15.33	0.92	36.25	0.65	10.82	0.81	22.99	PCI
	Full width	Wabash	**1.05**	**53.21**	**1.31**	**83.86**	***1.06***	***54.62***	***1.22***	***75.25***	No PCI
		Manac	***0.88***	***30.75***	***1.04***	***52.49***	0.79	21.16	**1.03**	**50.84**	No PCI
		GrDane	***0.95***	***40.09***	***1.02***	***49.64***	***1.08***	***58.14***	***1.03***	***50.13***	No PCI

Neck Injury Risk Discussion

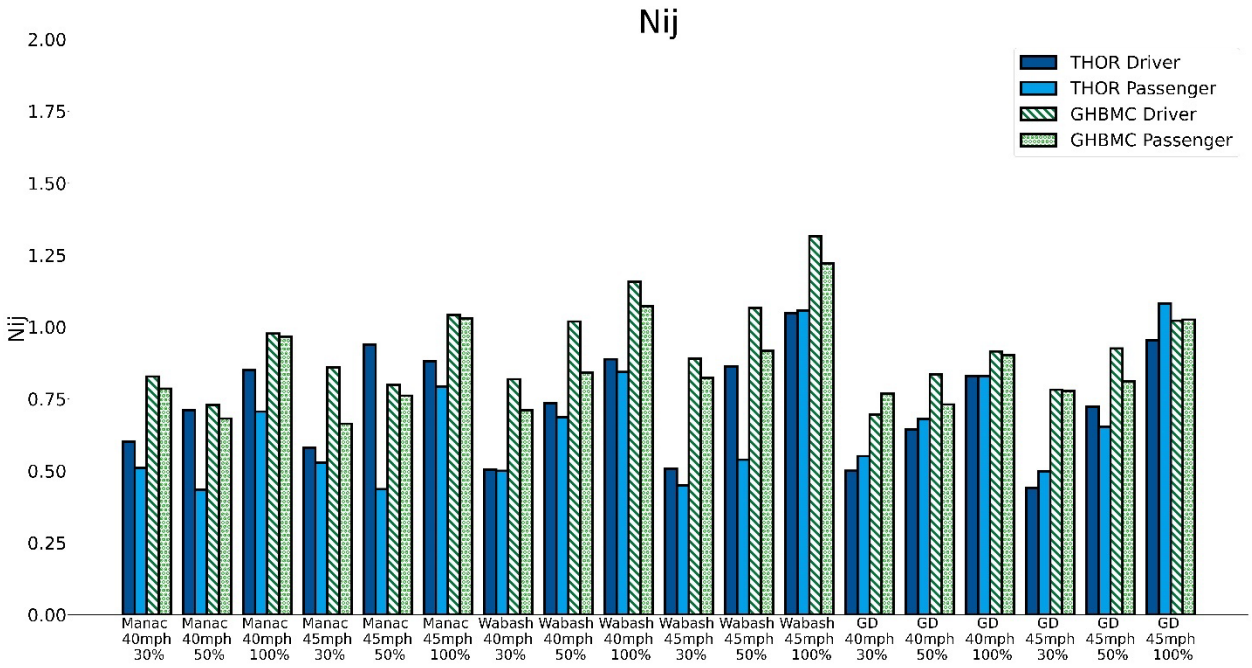

Figure 61. Nij values for occupants in the midsize sedan full vehicle-to-trailer impacts simulations

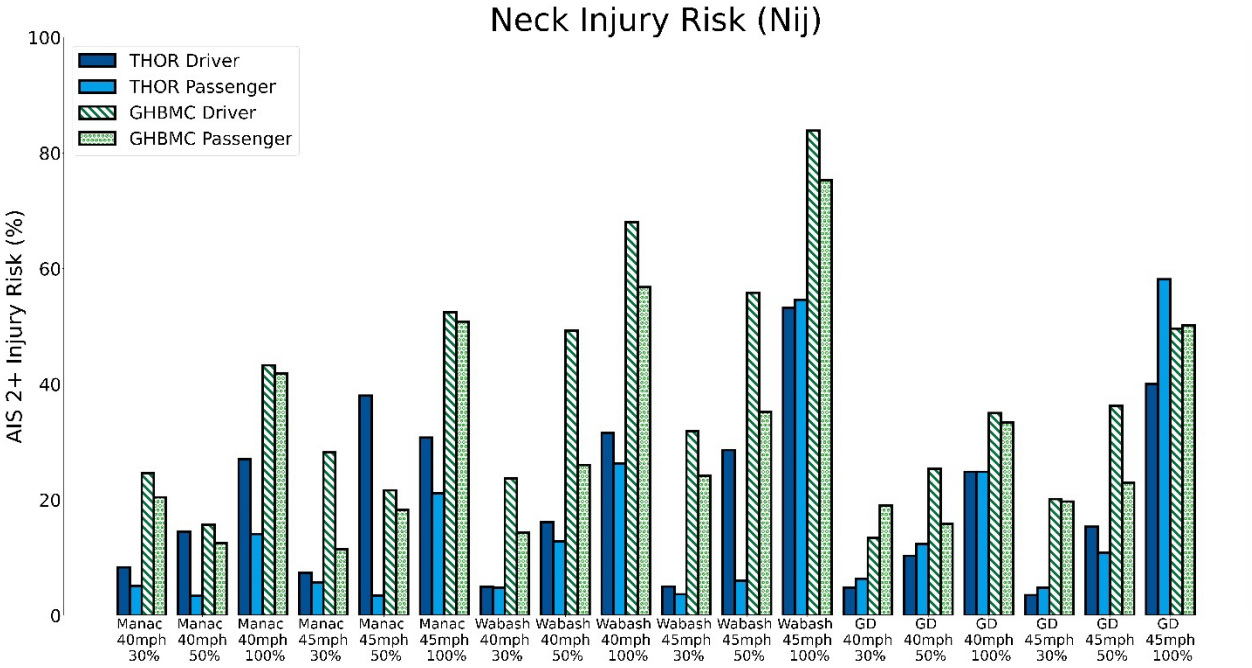

Figure 62. AIS 2+ neck injury risks for occupants in the midsize sedan full vehicle-to-trailer impacts simulations

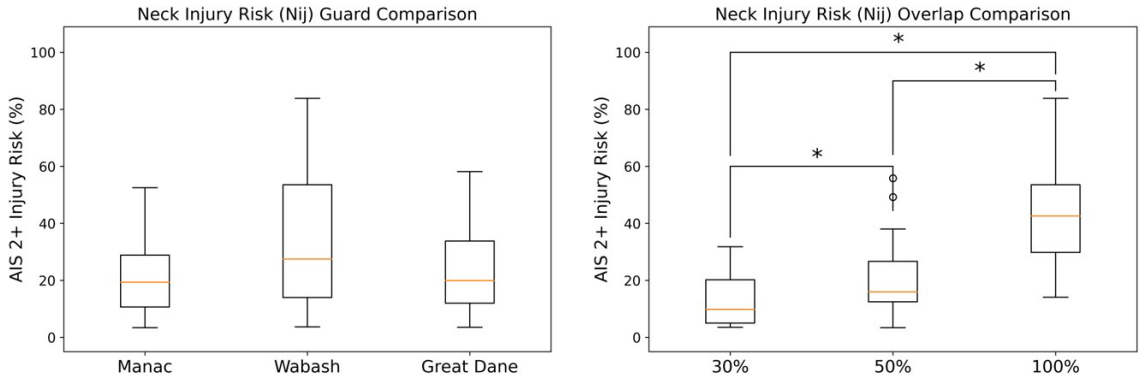

a.) b.)

Figure 63. Rear-impact guard (a) and overlap percentage (b) comparisons for neck injury risk. Both THOR-50M and GHBMC M50-OS data included. Statistical analysis performed with α=0.05.

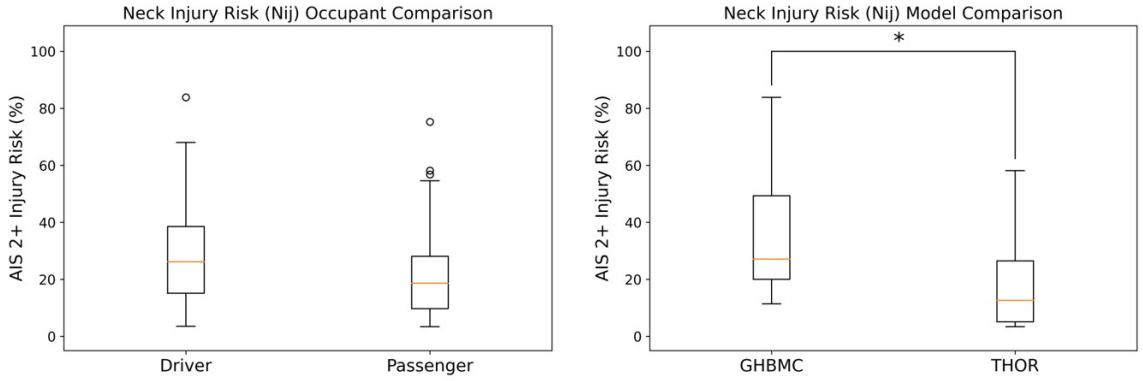

a.) b.)

Figure 64. Occupant seating location (a) and model (b) comparisons for neck injury risk. Both THOR-50M and GHBMC M50-OS data included. Statistical analysis performed with α=0.05.

Chest Injury Risk

Table 14. Honda Accord, chest injury risk
(THOR-50M chest deflection is multi-point thoracic criterion; GHBMC M50-OS chest deflection taken from center chest instrumentation. Bolded values represent values above IARV. Italicized values represent similar compression levels between THOR-50M and GHBMC M50-OS.)

			Driver				Passenger				PCI/No PCI
		Strengthened Underride Guard	THOR-50M		GHMBC		THOR-50M		GHMBC		
			Chest Deflection (mm)	AIS 3+ Risk (%)	Chest Deflection (mm)	AIS 3+ Risk (%)	Chest Deflection (mm)	AIS 3+ Risk (%)	Chest Deflection (mm)	AIS 3+ Risk (%)	
40 mph	30% overlap	Wabash	***51.7***	***50.6***	*45.0*		*49.8*	*46.6*	*46.1*		PCI
		Manac	**61.1**	**68.6**	44.3		**61.0**	**68.4**	48.0		No PCI
		GrDane	*46.8*	*40.7*	*42.2*		***54.9***	***56.8***	*48.5*		PCI
	50% overlap	Wabash	**63.1**	**72.0**	44.1		**63.4**	**72.6**	51.0		No PCI
		Manac	**52.2**	**51.4**	40.7		**60.3**	**67.0**	46.8		No PCI
		GrDane	**57.3**	**61.5**	42.7		***54.8***	***56.8***	*50.6*		No PCI
	Full width	Wabash	**75.3**	**88.4**	47.5		**79.3**	**91.9**	58.6		No PCI
		Manac	**65.5**	**75.9**	44.7		***65.7***	***76.3***	*54.5*		No PCI
		GrDane	**66.5**	**77.5**	44.7		**73.2**	**86.2**	53.8		No PCI
			Driver				Passenger				PCI/No PCI
		Strengthened Underride Guard	THOR-50M		GHMBC		THOR-50M		GHMBC		
			Chest Deflection (mm)	AIS 3+ Risk (%)	Chest Deflection (mm)	AIS 3+ Risk (%)	Chest Deflection (mm)	AIS 3+ Risk (%)	Chest Deflection (mm)	AIS 3+ Risk (%)	
45 mph	30% overlap	Wabash	**55.4**	**57.9**	43.9		*51.4*	*49.9*	*43.4*		PCI
		Manac	**60.1**	**66.8**	41.4		*51.4*	*49.8*	*45.1*		PCI
		GrDane	*48.9*	*44.9*	*42.9*		***52.7***	***52.6***	*45.6*		PCI
	50% overlap	Wabash	**71.6**	**84.4**	47.0		**71.4**	**84.1**	52.2		No PCI
		Manac	**54.6**	**56.2**	43.2		***56.0***	***59.1***	*46.6*		No PCI
		GrDane	**63.5**	**72.7**	43.5		**66.1**	**76.8**	49.3		PCI
	Full width	Wabash	**82.2**	**93.9**	48.3		**87.6**	**96.6**	**61.8**		No PCI
		Manac	**70.2**	**82.5**	46.3		**69.6**	**81.8**	55.9		No PCI
		GrDane	**74.7**	**87.8**	46.3		**75.4**	**88.5**	58.9		No PCI

Chest Injury Risk Discussion

Chest injury risk was assessed using the multi-point thoracic criterion for the THOR 50M, while center chest deflection was used for the GHBMC M50-OS. The multi-point thoracic criterion assesses the deflection of each of the four IR-TRACCs within the THOR 50M chest and identifies the maximum deflection of any of the points during the event. Thus, the maximum deflection may be in the upper left, upper right, lower left, and lower right. Conversely, the GHBMC M50-OS chest compression measurement is only taken at a single point, which is not as data rich and does not capture the full thoracic compression profile. The IARV limit for 50 percent AIS 3+ injury for the THOR 50M is 51.4 mm of deflection. In all but four cases, the THOR 50M model predicted a chest deflection that exceeded the IARV (Figure 65). The driver and passenger THOR-50M model chest deflections were more similar than the driver and passenger GHBMC M50-OS models. Across both surrogates the passenger typically experienced higher chest deflections than the driver, but the difference was greater for the HBM.

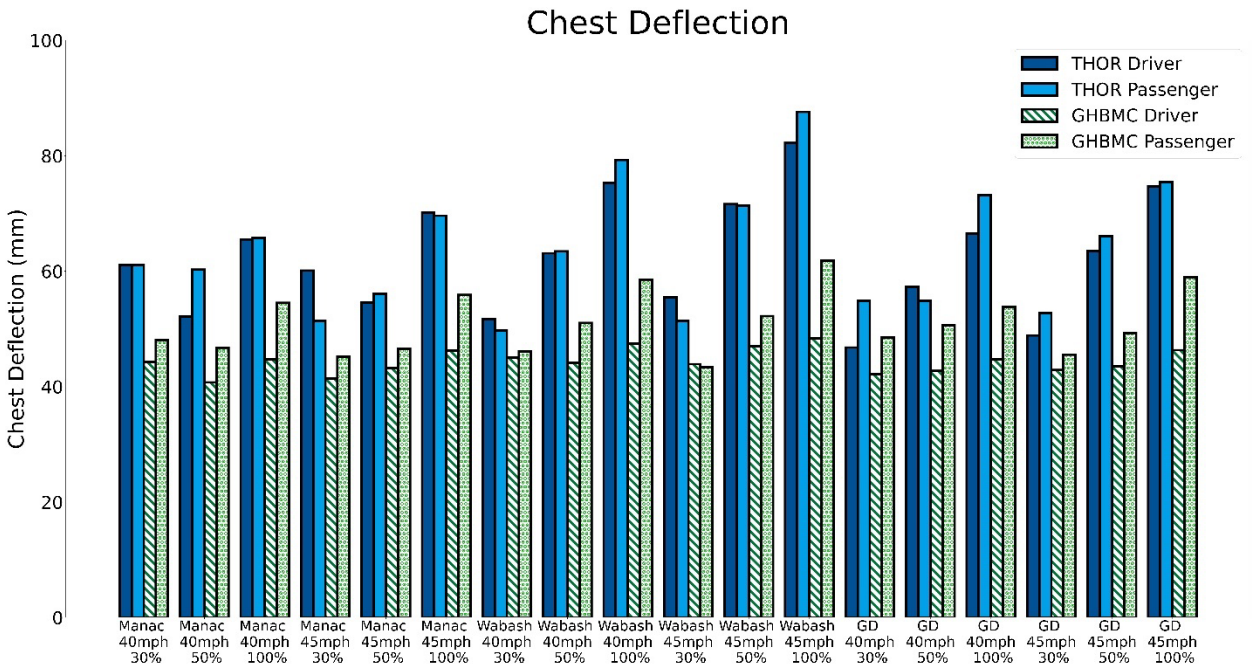

Figure 65. Multi-point thoracic criterion values for THOR-50M occupants and center chest deflection for the GHBMC M50-OS in the midsize sedan full vehicle-to-trailer impacts simulations

As previously mentioned, there are major differences in the chest deflection calculations between the THOR 50M and the GHBMC M50-OS. The THOR 50M curve was published by Craig et al. (2020).

Combining the thoracic injury risk predicted across all occupants and stratifying by impact guard did not produce a statistically significant difference (Figure 67), but as overlap increased, the risk trended upwards. A significant difference in average injury risk was observed between the 30 percent overlap cases and the 100 percent overlap cases, but no other combinations were statistically significantly different. No statistically significant differences in thoracic injury risk were found between driver and passenger (Figure 68).

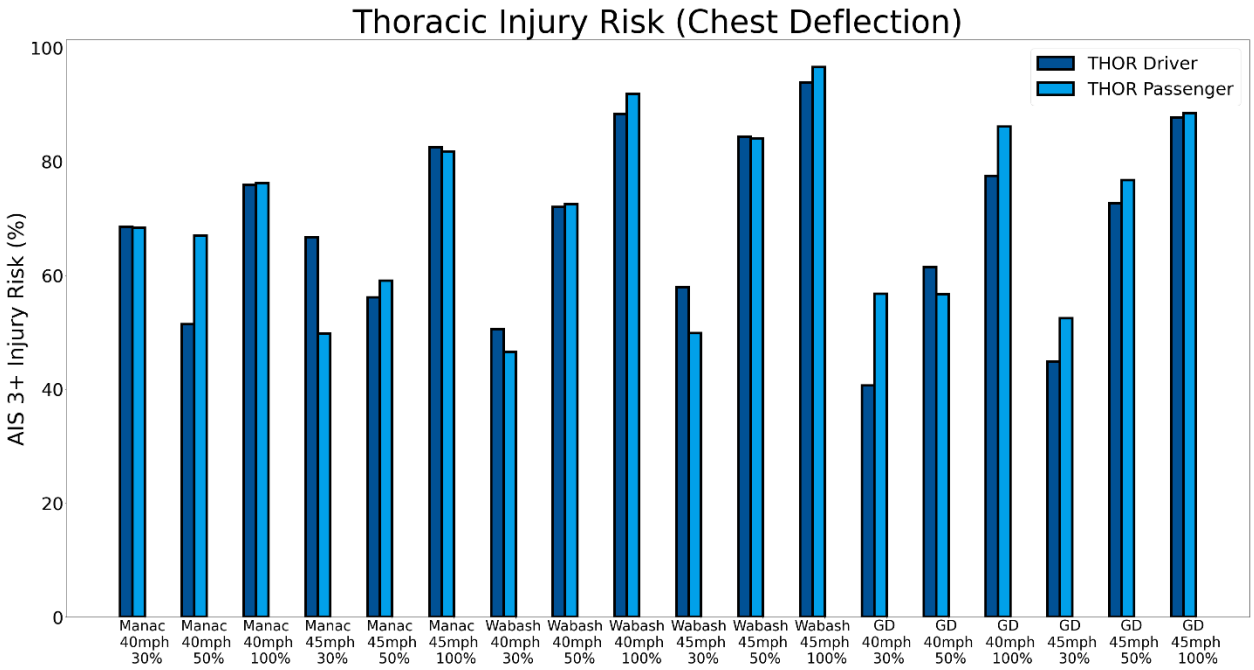

Figure 66. AIS 3+ chest injury risks for occupants in the midsize sedan full vehicle-to-trailer impacts simulations

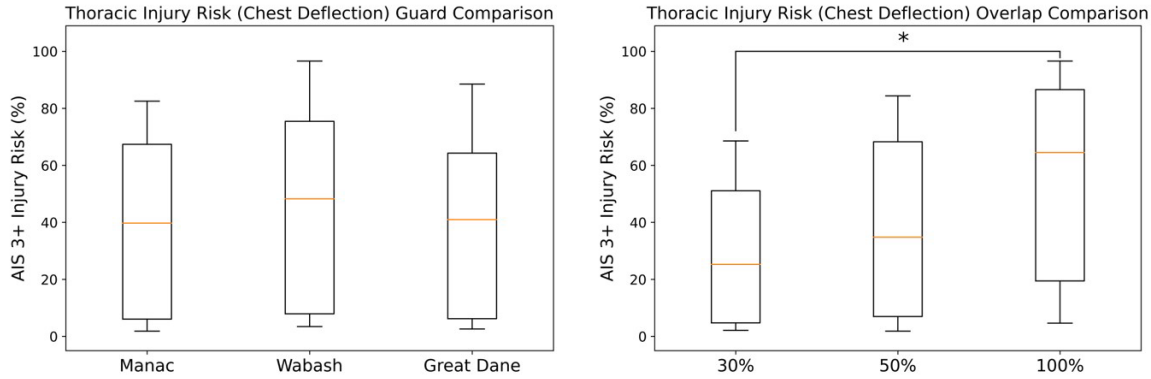

Figure 67. Rear-impact guard (a) and overlap percentage (b) comparisons for chest injury risk. Statistical analysis performed with α=0.05.

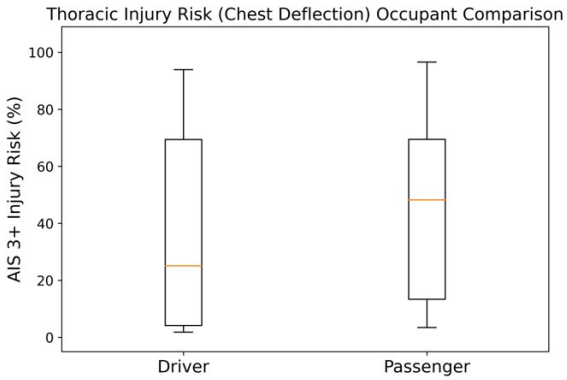

Figure 68. Comparisons for chest injury risk by occupant seating location. Statistical analysis performed with α=0.05.

The large difference in predicted chest deflection between the two human surrogate models was surprising, given the relative similarity in chest compliance between the two found by Parent et al (2017). Visual inspection of the simulations indicated a similar qualitative response between both occupant types, and so a brief investigation was completed. While the THOR 50M does not have a center-mounted chest deflection instrumentation package, the peak deflections in the upper right and upper left IR-TRACC were averaged for each simulation and compared to the center chest deflection measurement from GHBMC M50-OS. The results of this analysis are presented in Figure 69 and Figure 70. The large difference between the two occupant types is significantly decreased when analyzed with this method and is in fact reduced to no significant difference.

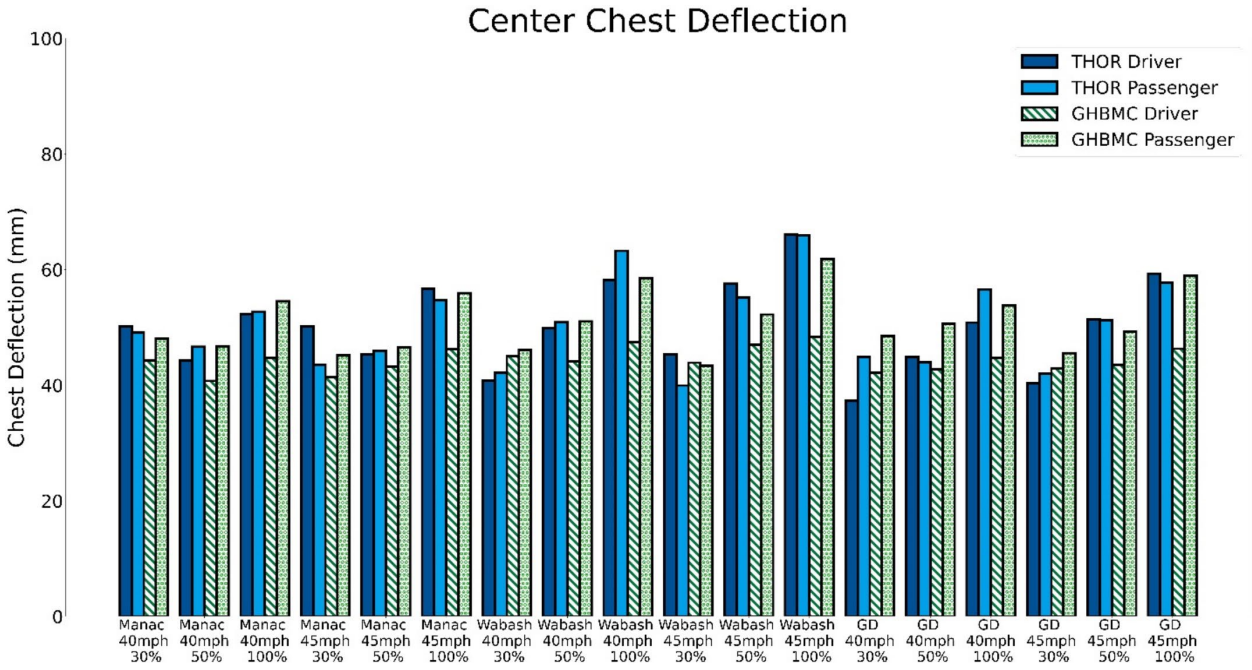

Figure 69. Approximate center chest deflection of the THOR 50M compared to the measured center chest deflection in the GHBMC M50-OS

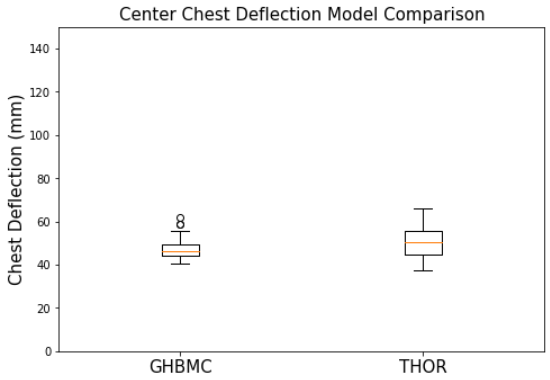

Figure 70. Box and whisker plot of the distribution of approximated THOR 50M center chest deflection and the measured GHBMC M50-OS chest deflection

Femur Injury Risk

Table 15. Honda Accord, left femur injury risk
(Bolded values represent values above IARV. Italicized values represent similar risk between THOR-50M and GHBMC M50-OS.)

		Strengthened Underride Guard	**Driver**				**Passenger**				PCI/No PCI
			THOR-50M		GHMBC		THOR-50M		GHMBC		
			Femur Fz (kN)	AIS 2+ Risk (%)	Femur Fz (kN)	AIS 2+ Risk (%)	Femur Fz (kN)	AIS 2+ Risk (%)	Femur Fz (kN)	AIS 2+ Risk (%)	
40 mph	30% overlap	Wabash	*1.8*	*0.0*	*2.0*	*0.1*	2.8	0.0	1.5	0.0	PCI
		Manac	*3.5*	*0.0*	*3.0*	*0.4*	4.1	0.1	1.8	0.1	No PCI
		GrDane	1.4	0.0	2.6	0.3	2.5	0.0	1.4	0.0	PCI
	50% overlap	Wabash	4.6	0.3	2.8	0.4	3.6	0.0	2.1	0.1	No PCI
		Manac	*2.3*	*0.0*	*2.6*	*0.3*	3.4	0.0	1.4	0.0	No PCI
		GrDane	2.9	0.0	2.4	0.2	3.4	0.0	1.7	0.1	No PCI
	Full width	Wabash	*3.5*	*0.0*	*3.0*	*0.5*	3.7	0.0	2.1	0.1	No PCI
		Manac	*2.9*	*0.0*	*2.5*	*0.2*	4.4	0.2	1.9	0.1	No PCI
		GrDane	*2.6*	*0.0*	*3.1*	*0.5*	3.3	0.0	1.5	0.0	No PCI
		Strengthened Underride Guard	**Driver**				**Passenger**				PCI/No PCI
			THOR-50M		GHMBC		THOR-50M		GHMBC		
			Femur Fz (kN)	AIS 2+ Risk (%)	Femur Fz (kN)	AIS 2+ Risk (%)	Femur Fz (kN)	AIS 2+ Risk (%)	Femur Fz (kN)	AIS 2+ Risk (%)	
45 mph	30% overlap	Wabash	2.2	0.0	2.7	0.3	2.9	0.0	1.1	0.0	PCI
		Manac	*6.5*	*5.1*	*5.4*	*4.0*	3.7	0.0	1.6	0.0	PCI
		GrDane	1.9	0.0	2.5	0.2	2.9	0.0	1.7	0.1	PCI
	50% overlap	Wabash	4.8	0.4	3.5	0.8	3.9	0.1	2.3	0.2	No PCI
		Manac	*5.5*	*1.6*	*5.1*	*3.3*	5.3	1.2	1.8	0.1	No PCI
		GrDane	*3.5*	*0.0*	*3.1*	*0.5*	3.8	0.0	1.9	0.1	PCI
	Full width	Wabash	4.1	0.1	3.0	0.4	3.8	0.0	2.3	0.2	No PCI
		Manac	3.9	0.0	2.5	0.2	4.9	0.5	2.5	0.2	No PCI
		GrDane	*3.4*	*0.0*	*3.3*	*0.6*	4.2	0.1	1.9	0.1	No PCI

Table 16. Honda Accord, right femur injury risk
(Bolded values represent values above IARV. Italicized values represent similar risk between THOR-50M and GHBMC M50-OS.)

		Strengthened Underride Guard	**Driver**				**Passenger**				PCI/No PCI
			THOR-50M		GHMBC		THOR-50M		GHMBC		
			Femur Fz (kN)	AIS 2+ Risk (%)	Femur Fz (kN)	AIS 2+ Risk (%)	Femur Fz (kN)	AIS 2+ Risk (%)	Femur Fz (kN)	AIS 2+ Risk (%)	
40 mph	30% overlap	Wabash	2.0	0.0	1.4	0.0	0.7	0.0	0.1	0.0	PCI
		Manac	3.1	0.0	2.2	0.1	0.8	0.0	0. 6	0.0	No PCI
		GrDane	1.8	0.0	1.3	0.0	0.6	0.0	0.0	0.0	PCI
	50% overlap	Wabash	3.6	0.0	2.6	0.2	1.0	0.0	0.8	0.0	No PCI
		Manac	3.4	0.0	2.1	0.1	*1.1*	*0.0*	*0.9*	*0.0*	No PCI
		GrDane	2.8	0.0	1.9	0.1	1.0	0.0	0.7	0.0	No PCI
	Full width	Wabash	*3.0*	*0.0*	*3.4*	*0.7*	2.3	0.0	1.1	0.0	No PCI
		Manac	4.2	0.1	2.4	0.2	1.9	0.0	1.5	0.0	No PCI
		GrDane	2.6	0.0	2.0	0.1	2.0	0.0	1.0	0.0	No PCI
		Strengthened Underride Guard	**Driver**				**Passenger**				PCI/No PCI
			THOR-50M		GHMBC		THOR-50M		GHMBC		
			Femur Fz (kN)	AIS 2+ Risk (%)	Femur Fz (kN)	AIS 2+ Risk (%)	Femur Fz (kN)	AIS 2+ Risk (%)	Femur Fz (kN)	AIS 2+ Risk (%)	
45 mph	30% overlap	Wabash	2.4	0.0	1.5	0.0	1.0	0.0	0.0	0.0	PCI
		Manac	*3.6*	*0.0*	*3.2*	*0.6*	0.9	0.0	0.7	0.0	PCI
		GrDane	2.0	0.0	1.2	0.0	0.8	0.0	0.1	0.0	PCI
	50% overlap	Wabash	4.1	0.1	2.1	0.1	1.1	0.0	0.7	0.0	No PCI
		Manac	5.2	0.9	3.4	0.7	*1.3*	*0.0*	*1.3*	*0.0*	No PCI
		GrDane	3.0	0.0	2.0	0.1	1.1	0. 0	0.7	0.0	PCI
	Full width	Wabash	*4.1*	*0. 1*	*4.1*	*1.5*	2.7	0.0	1.6	0.0	No PCI
		Manac	5.1	0.8	2.7	0.3	2.9	0.0	1.8	0.1	No PCI
		GrDane	*2.9*	*0.0*	*3.1*	*0.5*	1.9	0.0	1.3	0.0	No PCI

Femur Injury Risk Discussion

The peak femur forces observed by the GHBMC M50-OS and THOR 50M occupant models were all well below the 30 percent Risk of AIS 2+ injury risk IARV of 9450 N. In fact, the highest peak femur force observed in the simulations was 6.46 kN, which corresponds to a 6.5 percent risk of injury. Due to injury risk being so low across all simulations and occupants, specific comparative analysis was not performed.

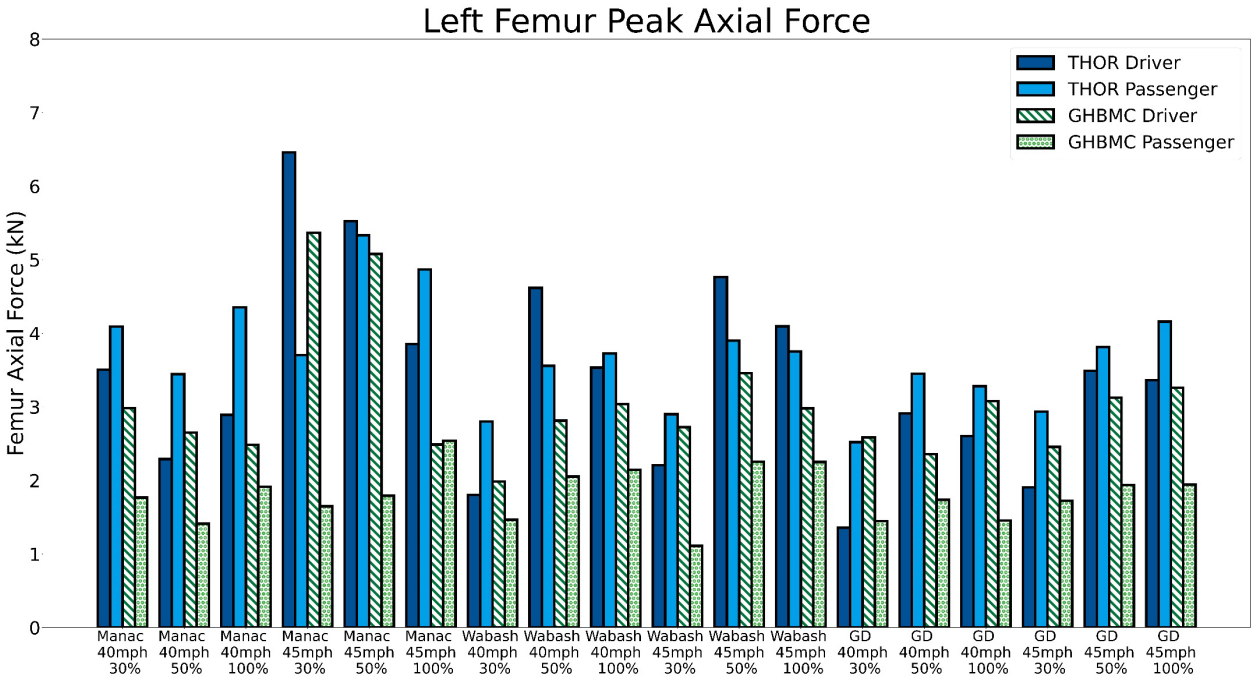

Figure 71. Peak left femur force values for occupants in the midsize sedan full vehicle-to-trailer impacts simulations

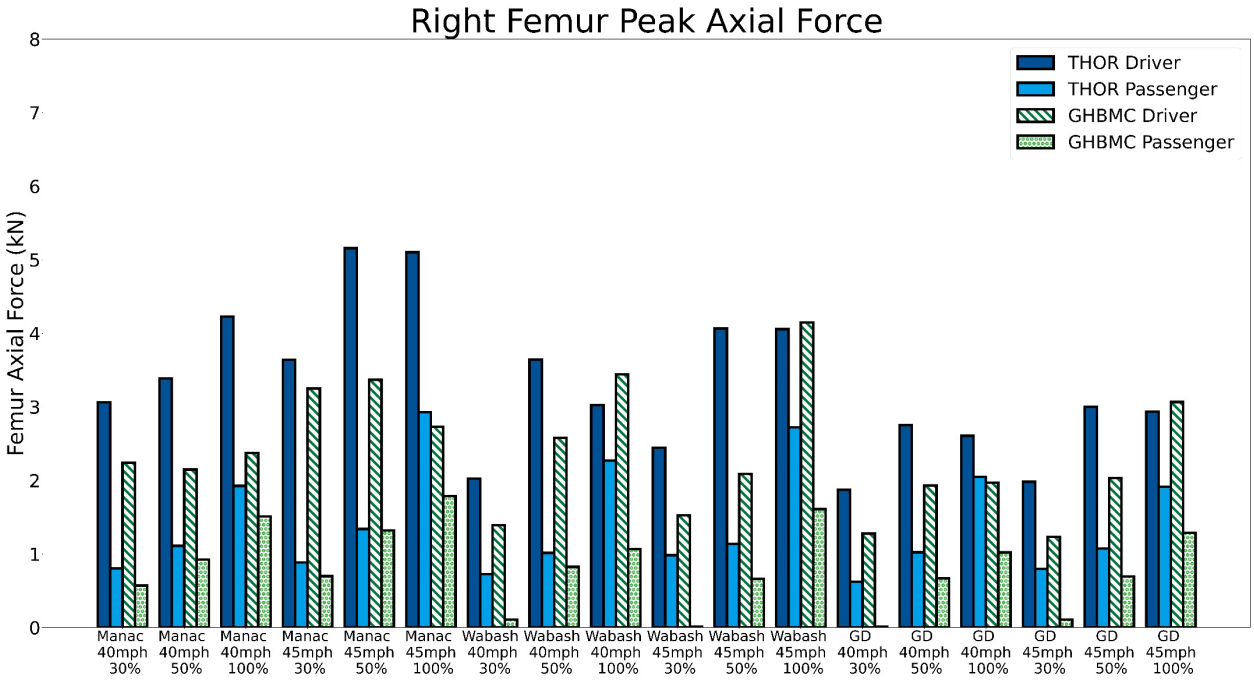

Figure 72. Peak right femur force values for occupants in the midsize sedan full vehicle-to-trailer impacts simulations

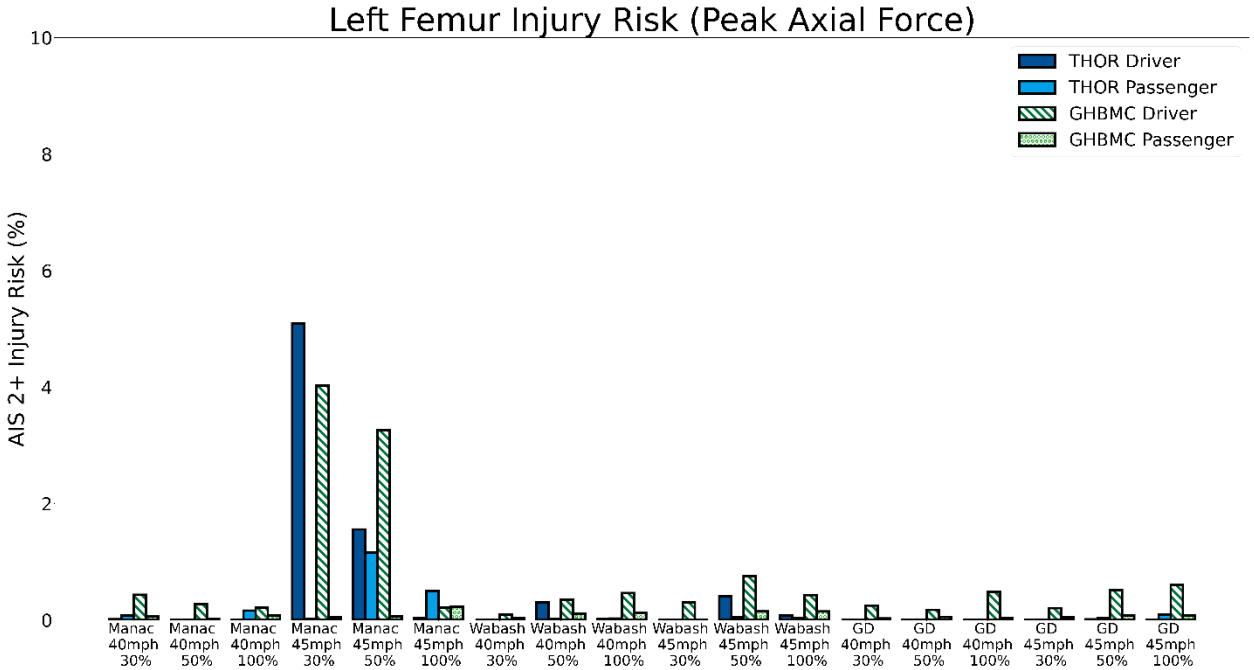

Figure 73. AIS 2+ left femur injury risks for occupants in the midsize sedan full vehicle-to-trailer impacts simulations

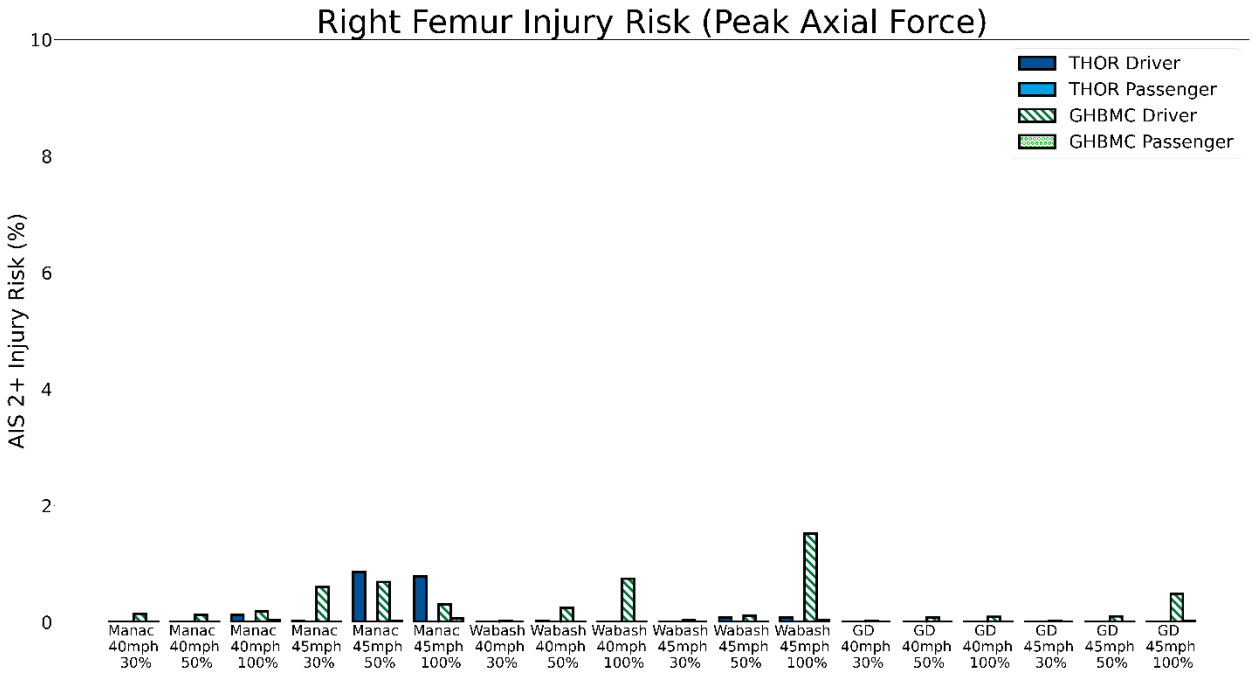

Figure 74. AIS 2+ right femur injury risks for occupants in the midsize sedan full vehicle-to-trailer impacts simulations

Tibia Injury Risk

Table 17. Honda Accord, lower left tibia injury risk
(Bolded values represent values above IARV. Italicized values represent similar risk between THOR-50M and GHBMC M50-OS.)

		Strengthened Underride Guard	**Driver**				**Passenger**				PCI/No PCI
			THOR-50M		GHMBC		THOR-50M		GHMBC		
			Tibia Index	AIS 2+ Risk (%)	Tibia Index	AIS 2+ Risk (%)	Tibia Index	AIS 2+ Risk (%)	Tibia Index	AIS 2+ Risk (%)	
40 mph	30% overlap	Wabash	0.2	0.0	0.1	0.0	*0.1*	0.0	*0.1*	0.0	PCI
		Manac	0.3	0.0	0.3	0.0	*0.2*	0.0	*0.2*	0.0	No PCI
		GrDane	0.3	0.0	0.1	0.0	*0.1*	0.0	*0.1*	0.0	PCI
	50% overlap	Wabash	0.5	0.1	0.3	0.0	0.2	0.0	0.2	0.0	No PCI
		Manac	0.5	0.8	0.2	0.0	0.2	0.0	0.1	0.0	No PCI
		GrDane	0.4	0.0	0.2	0.0	0.2	0.0	0.1	0.0	No PCI
	Full width	Wabash	*0.4*	*0.0*	*0.4*	0.0	*0.4*	0.0	*0.3*	0.0	No PCI
		Manac	0.4	0.0	0.3	0.0	*0.2*	0.0	*0.3*	0.0	No PCI
		GrDane	0.4	0.0	0.3	0.0	*0.3*	0.0	*0.4*	0.0	No PCI
		Strengthened Underride Guard	**Driver**				**Passenger**				PCI/No PCI
			THOR-50M		GHMBC		THOR-50M		GHMBC		
			Tibia Index	AIS 2+ Risk (%)	Tibia Index	AIS 2+ Risk (%)	Tibia Index	AIS 2+ Risk (%)	Tibia Index	AIS 2+ Risk (%)	
45 mph	30% overlap	Wabash	0.2	0.0	0.1	0.0	0.1	0.0	0.1	0.0	PCI
		Manac	0.4	0.0	0.2	0.0	0.3	0.0	0.2	0.0	PCI
		GrDane	0.2	0.0	0.1	0.0	*0.1*	0.0	*0.1*	0.0	PCI
	50% overlap	Wabash	*0.4*	0.0	*0.3*	0.0	*0.2*	0.0	*0.2*	0.0	No PCI
		Manac	0.4	0.1	0.3	0.0	*0.2*	0.0	*0.2*	0.0	No PCI
		GrDane	0.4	0.1	0.3	0.0	*0.2*	0.0	*0.2*	0.0	PCI
	Full width	Wabash	*0.5*	*0.3*	*0.5*	*0.5*	0.6	2.4	0.4	0.0	No PCI
		Manac	0.6	1.4	0.3	0.0	0.3	0.0	0.2	0.0	No PCI
		GrDane	*0.3*	*0.0*	*0.3*	*0.0*	*0.3*	*0.0*	*0.4*	0.0	No PCI

Table 18. Honda Accord, upper left tibia Injury Risk.
(Bolded values represent values above IARV. Italicized values represent similar risk between THOR-50M and GHBMC M50-OS.)

		Strengthened Underride Guard	**Driver**				**Passenger**				PCI/No PCI
			THOR-50M		GHMBC		THOR-50M		GHMBC		
			Tibia Index	AIS 2+ Risk (%)	Tibia Index	AIS 2+ Risk (%)	Tibia Index	AIS 2+ Risk (%)	Tibia Index	AIS 2+ Risk (%)	
40 mph	30% overlap	Wabash	0.2	0.0	0.1	0.0	0.2	0.0	0.1	0.0	PCI
		Manac	0.2	0.0	0.2	0.0	0.2	0.0	0.1	0.0	No PCI
		GrDane	0.2	0.0	0.1	0.0	0.2	0.0	0.1	0.0	PCI
	50% overlap	Wabash	0.3	0.0	0.2	0.0	0.3	0.0	0.1	0.0	No PCI
		Manac	0.3	0.0	0.1	0.0	0.2	0.0	0.1	0.0	No PCI
		GrDane	0.3	0.0	0.1	0.0	0.1	0.0	0.1	0.0	No PCI
	Full width	Wabash	0.3	0.0	0.2	0.0	0.3	0.0	0.2	0.0	No PCI
		Manac	0.3	0.0	0.1	0.0	0.2	0.0	0.1	0.0	No PCI
		GrDane	0.3	0.0	0.2	0.0	0.3	0.0	0.2	0.0	No PCI
		Strengthened Underride Guard	**Driver**				**Passenger**				PCI/No PCI
			THOR-50M		GHMBC		THOR-50M		GHMBC		
			Tibia Index	AIS 2+ Risk (%)	Tibia Index	AIS 2+ Risk (%)	Tibia Index	AIS 2+ Risk (%)	Tibia Index	AIS 2+ Risk (%)	
45 mph	30% overlap	Wabash	0.2	0.0	0.1	0.0	0.2	0.0	0.1	0.0	PCI
		Manac	0.4	0.0	0.2	0.0	0.3	0.0	0.1	0.0	PCI
		GrDane	0.2	0.0	0.1	0.0	0.2	0.0	0.1	0.0	PCI
	50% overlap	Wabash	0.3	0.0	0.2	0.0	0.2	0.0	0.1	0.0	No PCI
		Manac	0.4	0.1	0.2	0.0	0.3	0.0	0.2	0.0	No PCI
		GrDane	0.3	0.0	0.2	0.0	0.2	0.0	0.1	0.0	PCI
	Full width	Wabash	*0.3*	*0.0*	*0.3*	*0.0*	1.0	26.8	0.2	0.0	No PCI
		Manac	0.3	0.0	0.2	0.0	0.3	0.0	0.1	0.0	No PCI
		GrDane	*0.2*	*0.0*	*0.2*	*0.0*	0.3	0.0	0.2	0.0	No PCI

Table 19. Honda Accord, lower right Tibia injury risk
(Bolded values represent values above IARV. Italicized values represent similar risk between THOR-50M and GHBMC M50-OS.)

		Strengthened Underride Guard	**Driver**				**Passenger**				PCI/No PCI
			THOR-50M		GHMBC		THOR-50M		GHMBC		
			Tibia Index	AIS 2+ Risk (%)	Tibia Index	AIS 2+ Risk (%)	Tibia Index	AIS 2+ Risk (%)	Tibia Index	AIS 2+ Risk (%)	
40 mph	30% overlap	Wabash	0.3	0.0	0.2	0.0	0.2	0.0	0.1	0.0	PCI
		Manac	*0.3*	*0.0*	*0.3*	*0.0*	0.2	0.0	0.1	0.0	No PCI
		GrDane	0.4	0.1	0.2	0.0	0.2	0.0	0.1	0.0	PCI
	50% overlap	Wabash	*0.3*	*0.0*	*0.3*	*0.0*	0.2	0.0	0.1	0.0	No PCI
		Manac	0.3	0.0	0.3	0.0	0.2	0.0	0.1	0.0	No PCI
		GrDane	*0.3*	*0.0*	*0.3*	*0.0*	0.2	0.0	0.1	0.0	No PCI
	Full width	Wabash	*0.5*	*0.4*	*0.5*	*0.1*	*0.3*	*0.0*	*0.3*	*0.0*	No PCI
		Manac	0.7	3.9	0.3	0.0	0.4	0.0	0.3	0.0	No PCI
		GrDane	0.8	7.2	0.3	0.0	0.4	0.0	0.3	0.0	No PCI
		Strengthened Underride Guard	**Driver**				**Passenger**				PCI/No PCI
			THOR-50M		GHMBC		THOR-50M		GHMBC		
			Tibia Index	AIS 2+ Risk (%)	Tibia Index	AIS 2+ Risk (%)	Tibia Index	AIS 2+ Risk (%)	Tibia Index	AIS 2+ Risk (%)	
45 mph	30% overlap	Wabash	0.3	0.0	0.2	0.0	0.2	0.0	0.1	0.0	PCI
		Manac	*0.3*	*0.0*	*0.2*	*0.0*	0.2	0.0	0.1	0.0	PCI
		GrDane	0.3	0.0	0.2	0.0	0.2	0.0	0.1	0.0	PCI
	50% overlap	Wabash	*0.3*	*0.0*	*0.3*	*0.0*	0.3	0.0	0.2	0.0	No PCI
		Manac	0.3	0.0	0.5	0.2	0.2	0.0	0.2	0.0	No PCI
		GrDane	0.7	4.9	0.3	0.0	0.2	0.0	0.2	0.0	PCI
	Full width	Wabash	0.8	7.2	0.3	0.0	*0.5*	*0.2*	*0.4*	*0.0*	No PCI
		Manac	0.5	0.4	0.3	0.0	0.3	0.0	0.2	0.0	No PCI
		GrDane	0.6	1.3	0.3	0.0	0.4	0.0	0.3	0.0	No PCI

Table 20. Honda Accord, upper right tibia injury risk
(Bolded values represent values above IARV. Italicized values represent similar risk between THOR-50M and GHBMC M50-OS.)

		Strengthened Underride Guard	**Driver**				**Passenger**				PCI/No PCI
			THOR-50M		GHMBC		THOR-50M		GHMBC		
			Tibia Index	AIS 2+ Risk (%)	Tibia Index	AIS 2+ Risk (%)	Tibia Index	AIS 2+ Risk (%)	Tibia Index	AIS 2+ Risk (%)	
40 mph	30% overlap	Wabash	0.2	0.0	0.1	0.0	0.2	0.0	0.0	0.0	PCI
		Manac	0.2	0.0	0.2	0.0	0.2	0.0	0.1	0.0	No PCI
		GrDane	0.2	0.0	0.1	0.0	0.2	0.0	0.0	0.0	PCI
	50% overlap	Wabash	0.3	0.0	0.2	0.0	0.2	0.0	0.1	0.0	No PCI
		Manac	*0.2*	*0.0*	*0.2*	*0.0*	0.2	0.0	0.1	0.0	No PCI
		GrDane	*0.2*	*0.0*	*0.2*	*0.0*	0.2	0.0	0.1	0.0	No PCI
	Full width	Wabash	0.3	0.0	0.4	0.1	0.3	0.0	0.2	0.0	No PCI
		Manac	*0.3*	*0.0*	*0.2*	*0.0*	0.3	0.0	0.1	0.0	No PCI
		GrDane	0.5	0.3	0.3	0.0	0.4	0.0	0.2	0.0	No PCI
		Strengthened Underride Guard	**Driver**				**Passenger**				PCI/No PCI
			THOR-50M		GHMBC		THOR-50M		GHMBC		
			Tibia Index	AIS 2+ Risk (%)	Tibia Index	AIS 2+ Risk (%)	Tibia Index	AIS 2+ Risk (%)	Tibia Index	AIS 2+ Risk (%)	
45 mph	30% overlap	Wabash	0.2	0.0	0.1	0.0	0.2	0.0	0.1	0.0	PCI
		Manac	0.3	0.0	0.2	0.0	0.2	0.0	0.1	0.0	PCI
		GrDane	0.2	0.0	0.1	0.0	0.2	0.0	0.1	0.0	PCI
	50% overlap	Wabash	*0.2*	*0.0*	*0.2*	*0.0*	0.2	0.0	0.1	0.0	No PCI
		Manac	*0.3*	*0.0*	*0.3*	*0.0*	0.2	0.0	0.1	0.0	No PCI
		GrDane	0.4	0.0	0.2	0.0	0.2	0.0	0.1	0.0	PCI
	Full width	Wabash	*0.4*	*0.0*	*0.4*	*0.0*	0.4	0.0	0.2	0.0	No PCI
		Manac	*0.2*	*0.0*	*0.2*	*0.0*	0.3	0.0	0.1	0.0	No PCI
		GrDane	*0.3*	*0.0*	*0.3*	*0.0*	0.4	0.0	0.2	0.0	No PCI

Tibia Injury Risk Discussion

As with the femur injury metrics, the revised tibia index values across each simulation and occupant leg were small compared to the IARV of 1.23, which corresponds to a 50 percent risk of AIS 2+ leg injury. Across all simulations, the highest revised tibia index for the left lower tibia, left upper tibia, right lower tibia, and right upper tibia were 0.64, 1.03, 0.77, and 0.50, respectively. These correspond to a 2.4 percent, 26.8 percent, 7.2 percent, and 0.3 percent risk of AIS 2+ leg injury. As the risk of injury to this region was very low, a full comparative analysis was not conducted. The only simulation that produced a risk of injury above 8 percent was the Wabash 45mph 100 percent overlap simulation, in which the THOR 50M passenger's left upper revised tibia index was 1.03. In this simulation, the right toe pan is pushed further into the occupant compartment than other simulations.

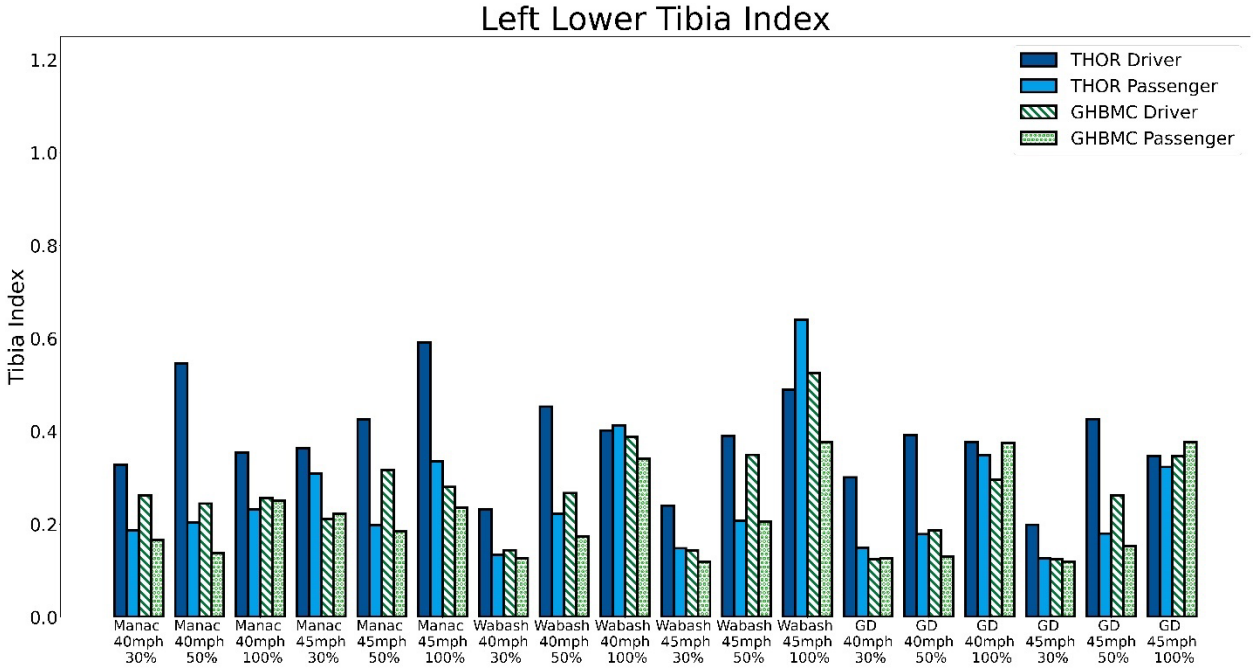

Figure 75. Revised tibia index values for occupants' left lower leg in the midsize sedan full vehicle-to-trailer impacts simulations

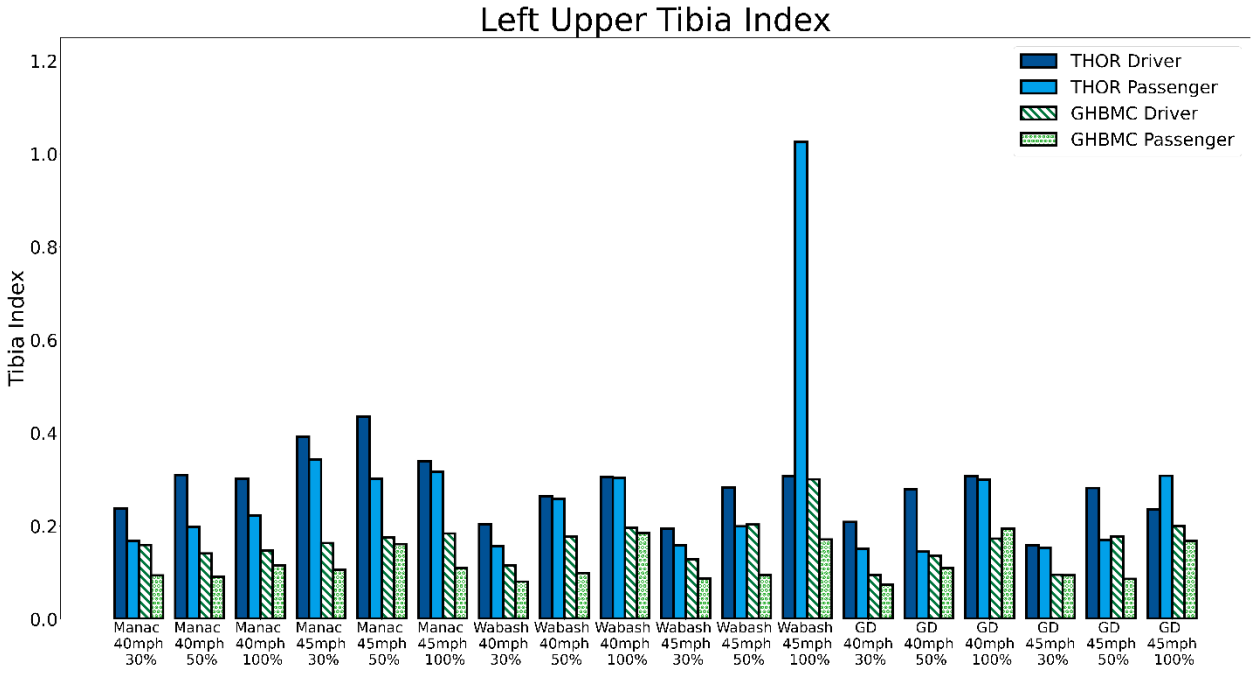

Figure 76. Revised tibia index values for occupants' left upper leg in the midsize sedan full vehicle-to-trailer impacts simulations

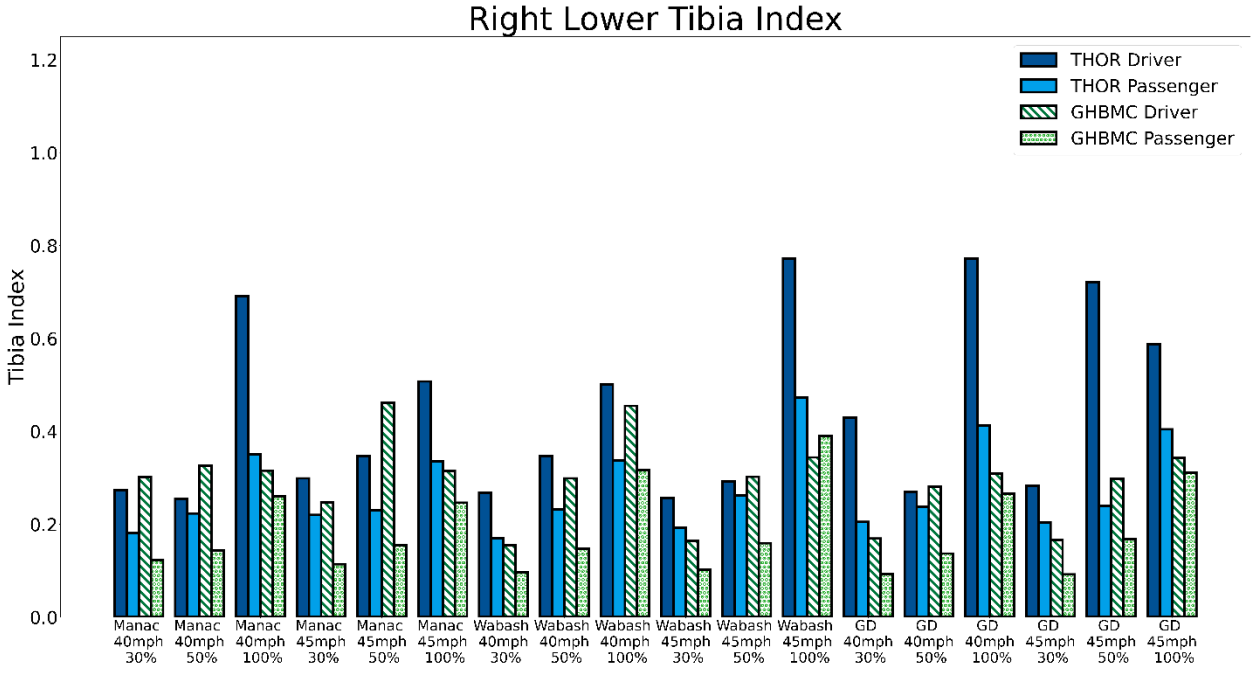

Figure 77. Revised tibia index values for occupants' right lower leg in the midsize sedan full vehicle-to-trailer impacts simulations

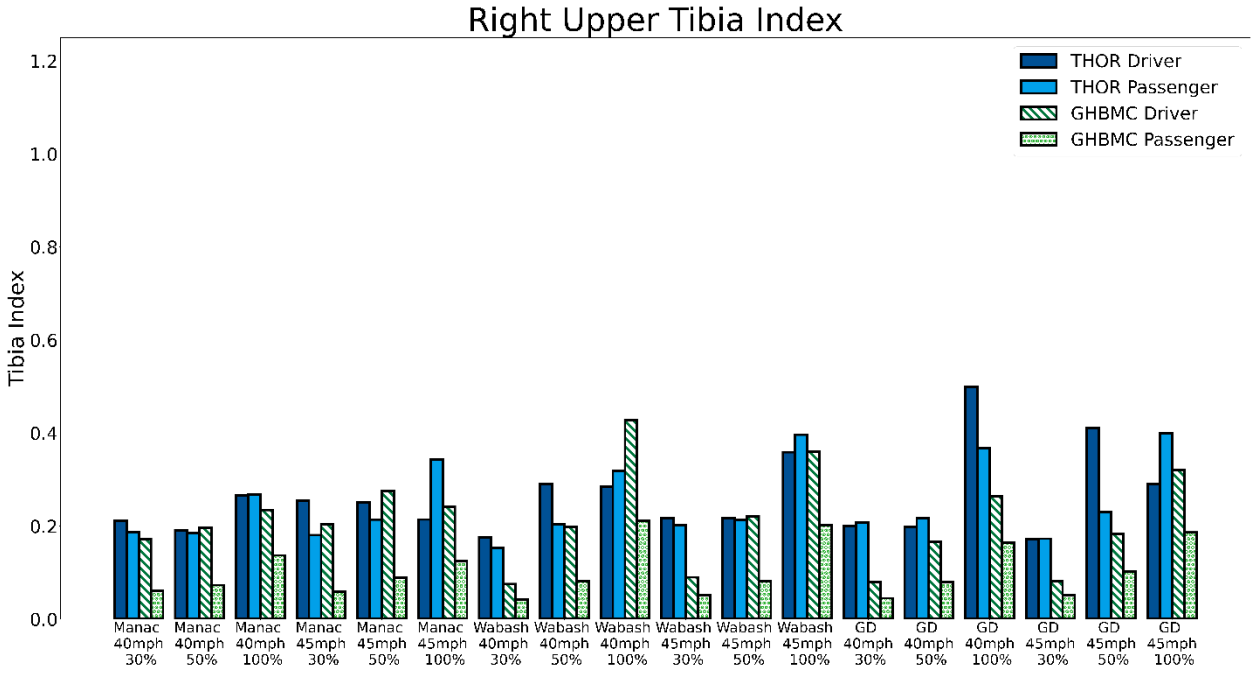

Figure 78. Revised tibia index values for occupants' right upper leg in the midsize sedan full vehicle-to-trailer impacts simulations

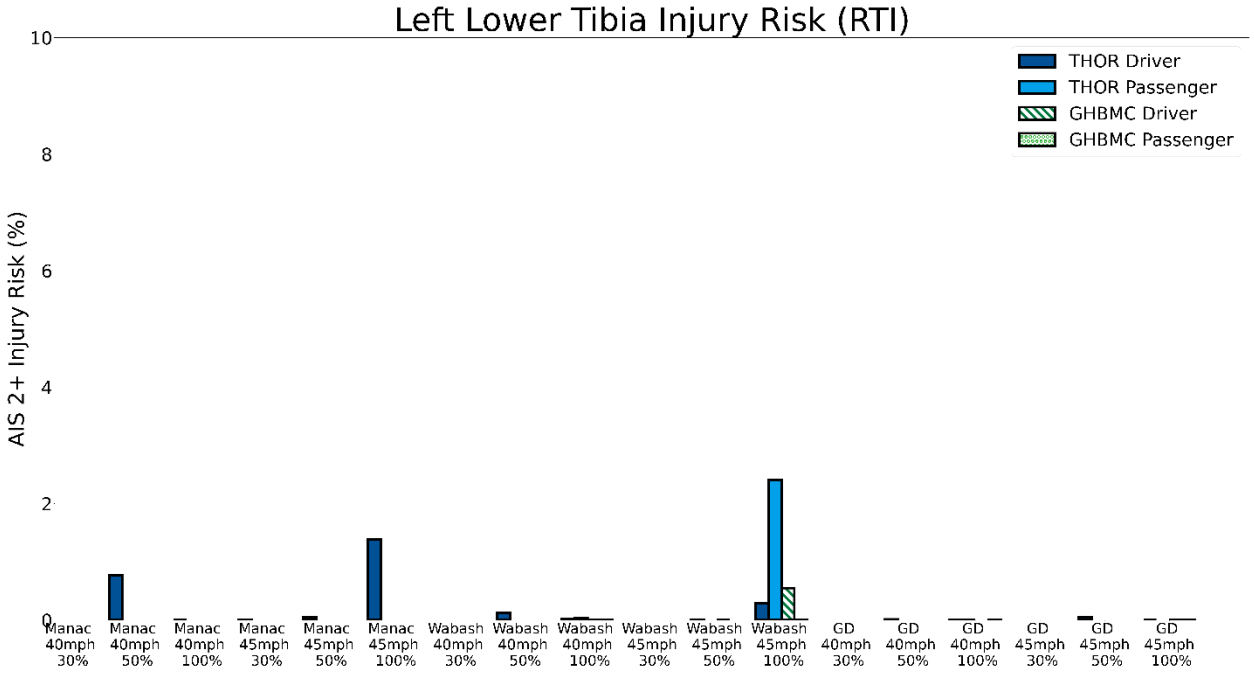

Figure 79. AIS 2+ leg injury risks for occupants' left lower leg in the midsize sedan full vehicle-to-trailer impacts simulations

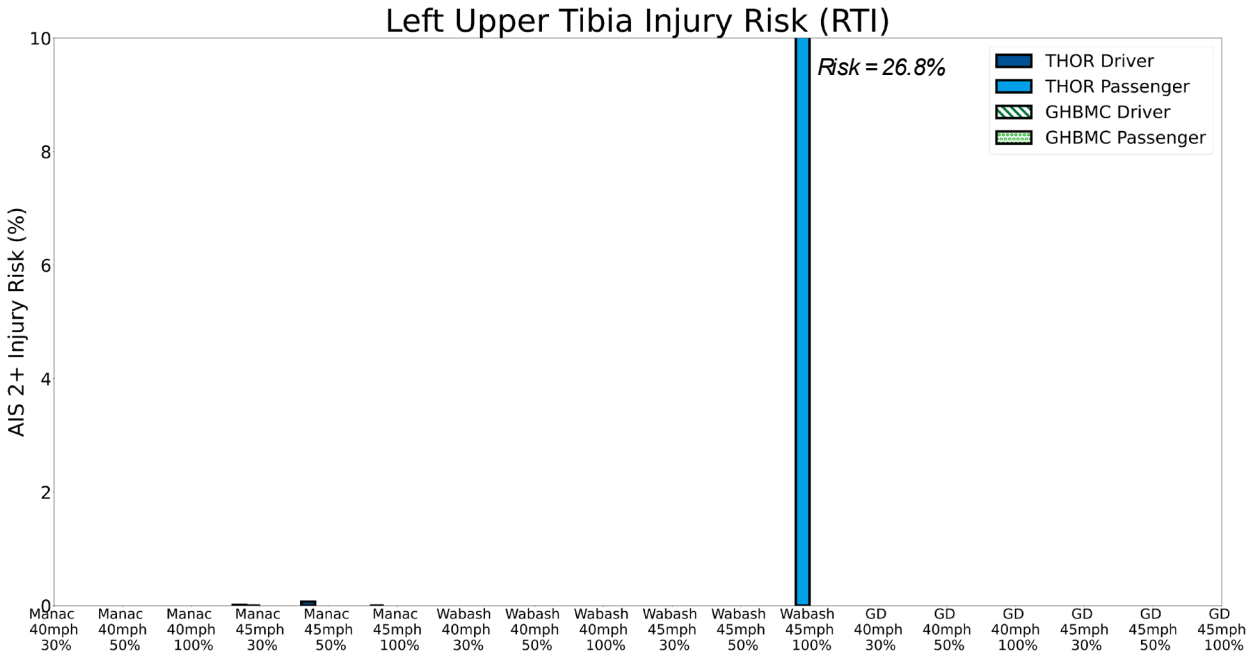

Figure 80. AIS 2+ leg injury risks for occupants' left upper leg in the midsize sedan full vehicle-to-trailer impacts simulations

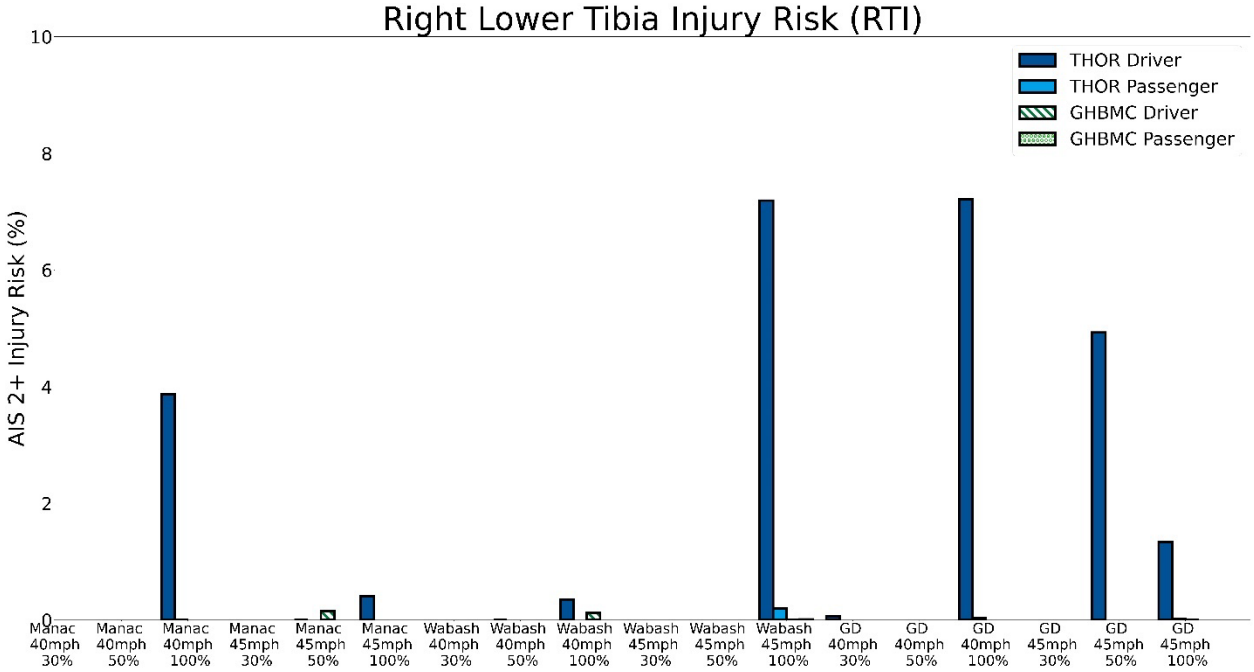

Figure 81. AIS 2+ leg injury risks for occupants' right lower leg in the midsize sedan full vehicle-to-trailer impacts simulations

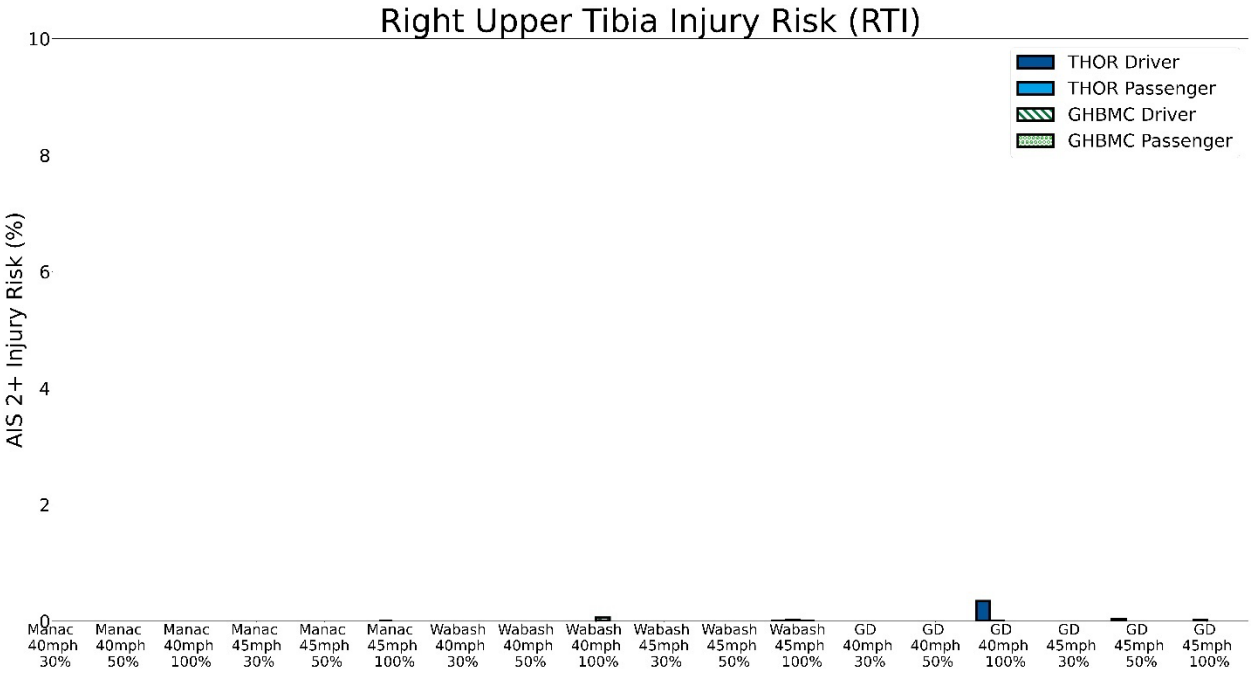

Figure 82. AIS 2+ leg injury risks for occupants' right lower leg in the midsize sedan full vehicle-to-trailer impacts simulations

Injury Risk Versus Guard Design

As noted previously, the Manac guard, which has its vertical uprights spaced further apart, produces a high vehicle acceleration in the 30 percent overlap test relative to the other two guards (see Figure 29). This appears to influence the Manac's higher HIC, BrIC, Nij scores and chest compression seen in the 40 and 45-mph simulations. On the other hand, the Manac guard prevents PCI in the 30 percent overlap 40-mph condition, unlike the Wabash and Great Dane guards. When PCI occurs, other unquantified risk factors (beyond the injury metrics reported herein) may be more influential on overall occupant risk.

Conversely, in the 40 and 45 mph full overlap simulations, the strengthened Manac's injury indicators are lower than the other two guards. This is consistent with a less severe crash pulse as seen in Figure 30, where in the full overlap condition the vehicle speed takes longer to drop from 35 to 0 mph for the Manac. And while all three strengthened guards prevent PCI in full overlap, the Manac appears to have the lowest margin of PCI prevention. This is seen by comparing Figures 26-28 for the full overlap simulations for the baseline guards. The Manac guard comes much closer to experiencing PCI. It is also seen in Table 5 which shows the FMVSS No. 223 static loadings. For the P2 (center) and fully distributed loadings, the strengthened Manac guard is seen to produce the lowest forces, absorb the least amount of energy, and allow the greatest amount of deflection as compared to the other two strengthened guards.

While this study is helpful in assessing the overall safety of various guard designs, determining the optimal design and placement of the vertical posts would require a study dependent on many factors, including the mass of the oncoming vehicle, its front-end shape, and the size of the vehicle occupant. Such an exercise is beyond the scope of this research.

Structural Response at 65 MPH

Following the 40-mph and 45-mph simulations, a series of 65-mph simulations were conducted with the THOR 50M and GHBMC M50-OS occupant models within the Honda Accord vehicle. Kinetic energy scales with the square of velocity. Increasing the speed of the passenger vehicle from 35 mph to 65 mph increases the kinetic energy 3.45x the original energy. It was hypothesized that even if passenger compartment integrity was able to be maintained for 35-mph crashes, the likelihood of the vehicle withstanding the crash at 65 mph was low. Indeed, in 14 of the 18 simulations conducted at 65 mph, catastrophic failure of the vehicle integrity occurred. Only one of the simulations reached 200 ms without simulation error. Of the simulations that error terminated, negative volume and nonrealistic energy was observed throughout vehicle parts and occupant surrogates. Major modifications to the models would likely be needed for this simulation boundary condition to achieve normal terminations including reducing the mesh size across many of the vehicle and occupant parts. Modifications to softer material cards within the occupant models in which damage initiation and propagation could occur might increase stability as well. Nonetheless, in the Great Dane full width 65 mph cases as well as the Wabash full width 65 mph cases, the vehicle reached rebound before an error termination occurred. The occupant responses from these cases will be discussed in moderate detail. The other simulation responses are summarized.

Wabash 65 mph

The 30 percent overlap 65 mph simulation with the strengthened Wabash guard resulted in catastrophic failure of the vehicle and rear-impact guard structure. Prior to the simulation error terminating, the vehicle experienced underride. The simulation error terminated before a head strike to the bumper of the trailer. However, the driver head was 8 inches from the trailer bumper and the vehicle was still traveling forward at 53 mph. At this speed, the head would likely strike the rear of the trailer within 10 ms with a very high head-to-bumper contact velocity. This is consistent with an impact having a high risk of an unsurvivable head injury, such as the head impact observed earlier in the Manac 40 mph 30 percent overlap case in which the HIC value exceeded 2000.

The 50 percent overlap 65 mph simulation with the strengthened Wabash guard error terminated due to negative volume and mass addition. However, prior to error termination the instrument panel was pushed toward the occupant abdomen, the toe pan intruded, and the left a-pillar was deformed due to underride with the trailer (Figure 83).

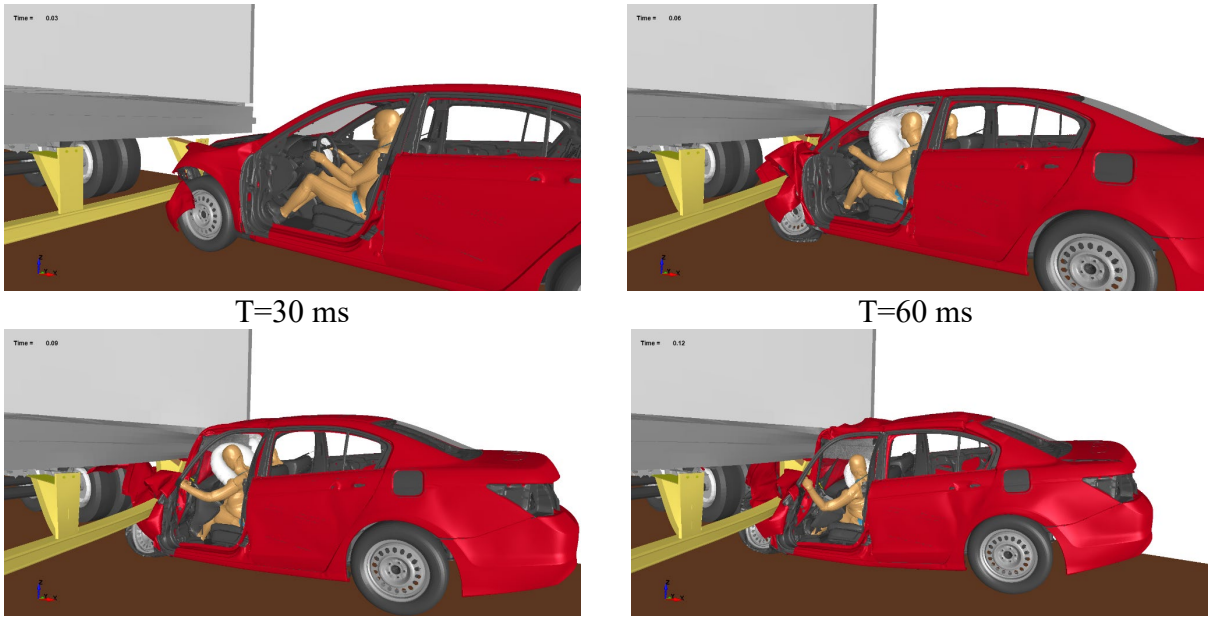

Figure 83. Progression of instrument panel intrusion and a-pillar deformation during 50 percent overlap 65 mph simulation with the strengthened Wabash guard

The full width 65 mph simulation with the strengthened Wabash guard extended far enough to calculate injury metrics. The forward progress of the THOR-50M and GHBMC occupants was arrested, and the vehicle reached rebound (Figure 84). Figure 85 provides a selection of data channels from the occupants. Table 21 tabulates the injury metrics from the full width crash simulations. Both the driver models predicted high risk of AIS 2+ head injury, and AIS 2+ neck injury. The THOR 50M driver predicted 98 percent risk of AIS 2+ chest injury. Both passenger models showed high risk of AIS 2+ head injury. The THOR-50M passenger had over 50 percent chance of neck injury, and a 98 percent chance of AIS 2+ chest injury. As discussed previously, the base GHBMC M50-OS chest instrumentation may be lacking detail to predict the chest deflections in the upper left chest, which showed the most deflection in the THOR-50M.

Table 21. 65 mph full width – Wabash strengthened, Honda Accord simulation injury metrics

	Driver				**Passenger**			
	THOR-50M		GHBMC		THOR-50M		GHBMC	
	Ref	Risk%	Ref	Risk%	Ref	Risk%	Ref	Risk%
HIC, Risk AIS 2+	5307	97.2	6192	98.2	6401	98.3	3018	89.2
BrIC, Risk AIS 2+	1.24	82.0	1.12	69.6	1.94	99.7	0.23	0
Nij, Risk AIS 2+	1.13	64.6	1.25	78.3	1.028	50.5	0.70	13.5
Chest Defl, Risk AIS 2+	95.3	98.7	57.4		93.5	98.4	58.8	

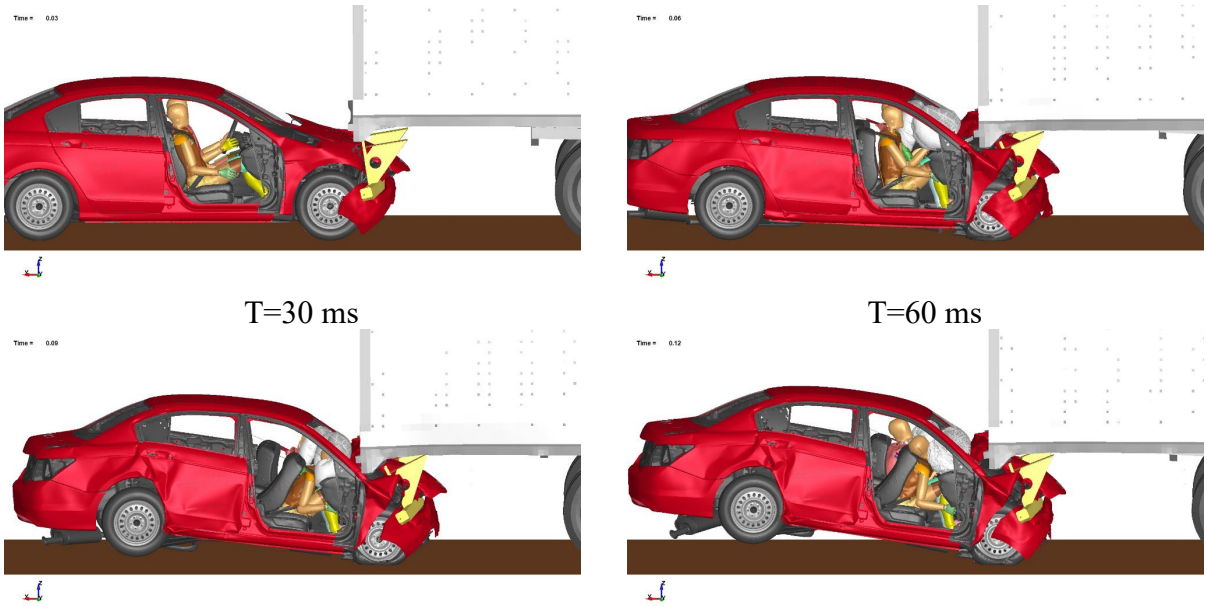

Figure 84. 65 mph full width simulation with the strengthened Wabash guard

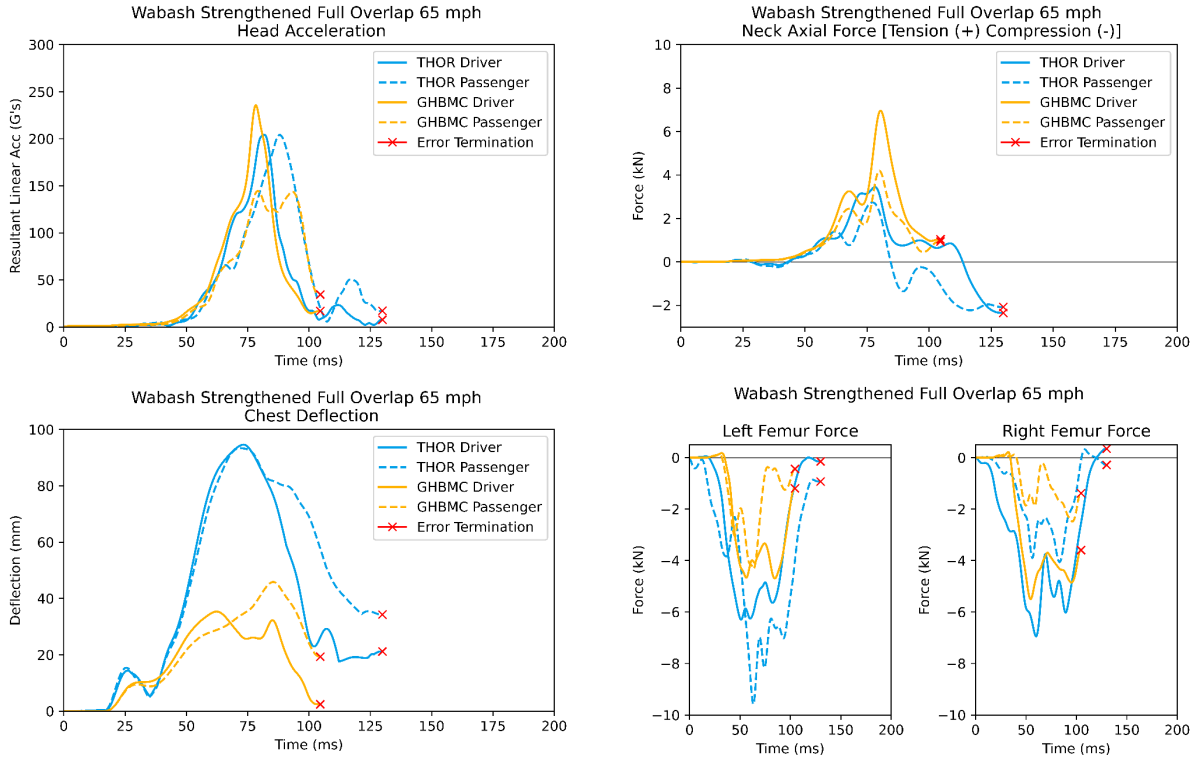

Figure 85. 65 mph full width simulation data channels with the strengthened Wabash guard

Manac 65 mph

In each of the Manac 65 mph simulations the head of the driver struck the rear bumper of the trailer. In the full width simulation, both the driver and passenger heads struck the rear bumper (Figure 86). In the 50 percent overlap, the occupant compartment collapsed. In all instances, early termination occurred, and injury metrics were incomplete. Nonetheless, in all three cases the momentum of intruding structures when contacting the driver prior to termination appears consistent with an unsurvivable contact.

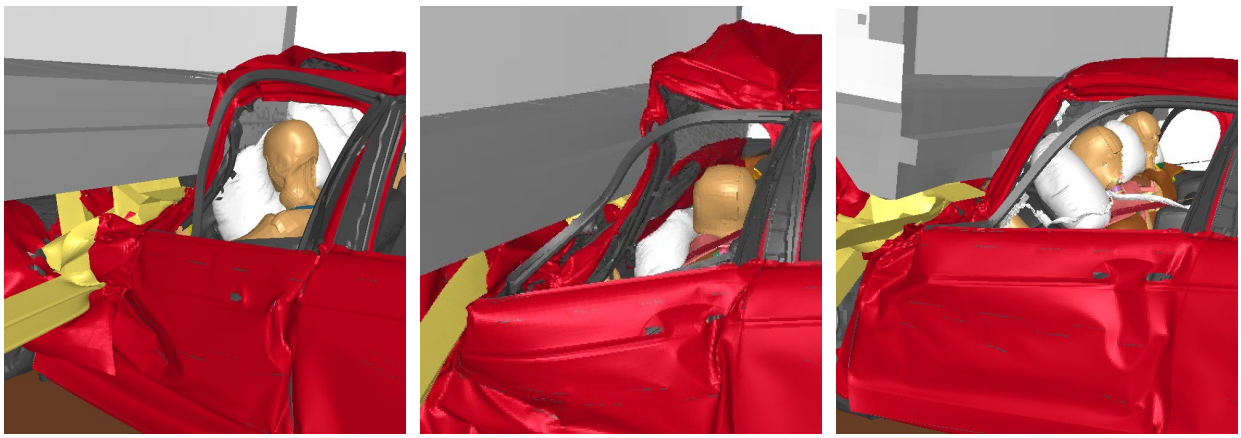

30 percent 50 percent Full Width

Figure 86. 65 mph strengthened Manac simulation head strikes

Great Dane 65 mph

The 65 mph simulations with the strengthened Great Dane guard resulted in catastrophic failure of the vehicle and rear-impact guard structure for both the 30 percent overlap (Figure 87a) and the 50 percent overlap (Figure 87b). In both cases, the vehicle experienced underride and the head of the driver struck the rear bumper of the trailer prior to the simulation error terminating. Like the Manac guard, the momentum of intruding structures contacting the driver appears consistent with an unsurvivable contact.

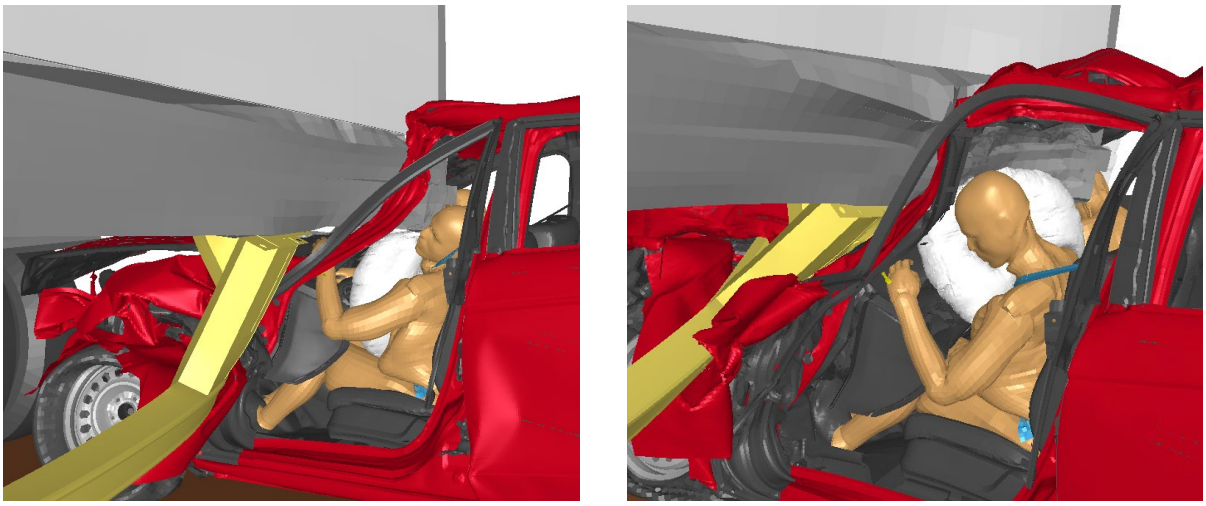

(a) (b)

Figure 87. Head strikes to the rear of the trailer in the 65 mph 30 percent (a) and 50 percent (b) overlap simulations with the Great Dane rear-impact guard

The full width 65 mph simulation with the strengthened Great Dane guard extended far enough to calculate injury metrics for the GHBMC and normally terminated with the THOR-50Ms. The forward progress of the THOR-50M and GHBMC occupants was arrested, and the vehicle reached rebound (Figure 88). Figure 89 provides a selection of data channels from the occupants. Table 22 tabulates the injury metrics from the full width crash simulations. Both the driver models predicted high risk of AIS 2+ head injury, and AIS 2+ neck injury. The THOR 50M driver predicted 97 percent risk of AIS 2+ chest injury. Both passenger models showed high risk of AIS 2+ head injury (>90%). The THOR 50M passenger had over 88 percent chance of neck injury, and a 97 percent chance of AIS 2+ chest injury. These metrics are consistent with an unsurvivable crash. As discussed previously, the base GHBMC M50-OS chest instrumentation may be lacking detail to predict the chest deflections in the upper left chest, which showed the most deflection in the THOR 50M.

Table 22. 65 mph full width – Great Dane strengthened, Honda Accord simulation injury metrics

	Driver				Passenger			
	THOR-50M		GHBMC		THOR-50M		GHBMC	
	Ref	Risk%	Ref	Risk%	Ref	Risk%	Ref	Risk%
HIC, Risk AIS 2+	2191	80.5	2269	81.6	3233	90.6	3587	92.5
BrIC, Risk AIS 2+	1.26	83.5	0.999	56.0	1.77	99.0	1.16	75.0
Nij, Risk AIS 2+	1.46	92.1	0.47	4.15	1.388	88.8	0.37	2.35
Chest Defl, Risk AIS 2+	89.1	97.1	54.1		89.8	97.4	62.2	

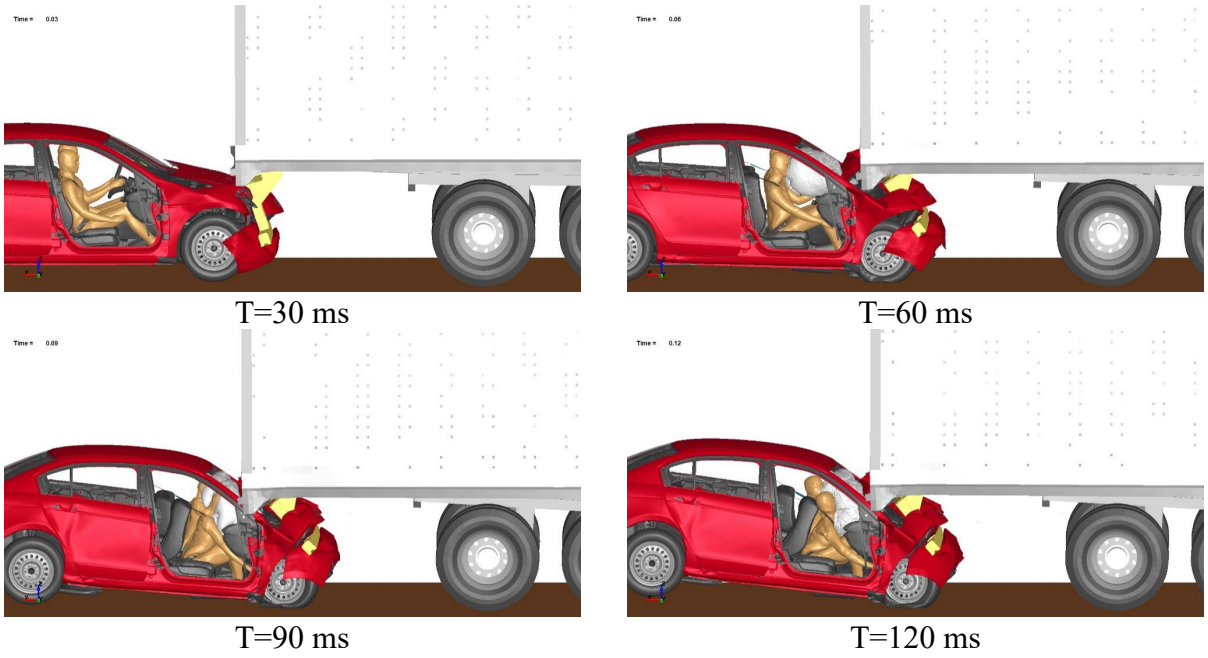

Figure 88. 65 mph full width simulation with the strengthened Great Dane guard

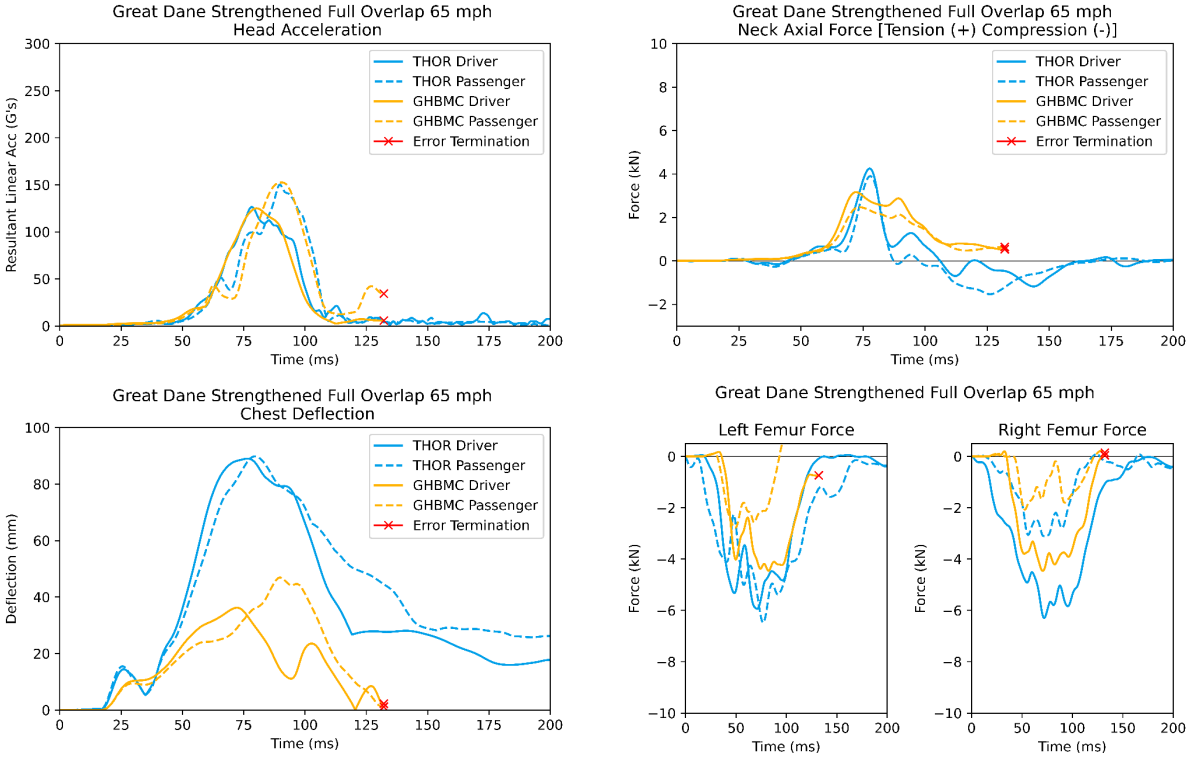

Figure 89. 65 mph full width simulation data channels with the strengthened Great Dane guard

Aim 3: Summary

Additional simulations were carried out to gain an understanding on whether an underride guard can be designed to:

- Prevent PCI at speeds up to 65 mph; and
- Protect passengers against severe injury at speeds up to 65 mph.

The dynamic tests described in Aim 2 were simulated at impact speeds of 40, 45, and 65 mph. In this exercise, only the guards that were strengthened to prevent PCI with the Toyota Yaris (compact sedan) were used and only the Honda Accord was used as the striking vehicle. Separate simulations were carried out in which the driver and passenger positions of the Accord vehicle were occupied by either the THOR-50M dummy or the M50-OS human body model available from the Global Human Body Models Consortium. Both are representative of a 50th percentile male. The results of the simulations are summarized as follows:

- At 40 mph, all three strengthened guards prevented PCI in the full and 50 percent overlap tests, but only the Manac prevented PCI in the 30 percent overlap test. However, in the full overlap test simulated injury risks were high for all guard designs including the Manac (approximately 80 percent risk of AIS 3+ thorax injury) due to the forces of vehicle deceleration exerted on occupants.
- At 45 mph, all three strengthened guards prevented PCI in the full overlap test, but none could prevent PCI in the 30 percent overlap test. In the full overlap test, simulated injury risks were high for all guard designs (approximately 88 percent risk of AIS 3+ thorax injury) due to the forces of vehicle deceleration exerted on occupants.
- A 65-mph crash in this simulated study was observed to be unsurvivable for all guard designs studied.
- Regarding injury risk, there were no clear “Best Design” attributes among the three strengthened guards.
- THOR-50M and MS50-OS were generally in agreement with each other in terms of the relative injury risk assessments among the three guard designs.

This page is intentionally left blank.

References

Albert, D. L., Beeman, S. M., & Kemper, A. R. (2018, February). Occupant kinematics of the Hybrid III, THOR-M, and postmortem human surrogates under various restraint conditions in full-scale frontal sled tests. Traffic Injury Prevention, 28;19(sup1). doi: 10.1080/15389588.2017.1405390

Association for the Advancement of Automotive Medicine. (2016). *The Abbreviated Injury Scale: 2015 Revision*.

Center for Applied Biomechanics. (2020, June 17). *THOR 50th male finite element model*. [Web page]. University of Virginia School of Engineering and Applied Science. www.engineering.virginia.edu/centers-institutes/center-applied-biomechanics/blogs/thor-50th-male-finite-element-model

Craig, M., Parent, D., Lee, E., Rudd, R., Takhounts, E., & Hasija, V. (2020). *Injury criteria for the THOR 50th male ATD* (Unnumbered report). National Highway Traffic Safety Administration. https://lindseyresearch.com/wp-content/uploads/2021/10/NHTSA-2020-0032-0003-Injury-Criteria-for-the-THOR-50th-Male-ATD-for-peer-review.pdf

Miele, C. R., Stephens, D., Plaxico, C., & Simunovic, S. (2010, September 1). U 26: *Enhanced finite element analysis crash model of tractor-trailers (Phase C)*. National Transportation Research Center. https://rosap.ntl.bts.gov/view/dot/18333

Parent, D., Craig, M., & Moorhouse, K. (2017). *Biofidelity evaluation of the THOR and Hybrid III 50th percentile male frontal impact anthropomorphic test devices* (Paper No. No. 2017-22-0009). SAE International.

Rupp, J., Flannagan, C. A., & Kuppa, S. M. (2009). *Development of new injury risk curves for the knee/distal femur and the hip for use in frontal impact testing*. University of Michigan Transportation Research Institute.

Saunders, J., Parent, D., & Martin, P. (2023, April 3-6). *THOR-50M fitness assessment in FMVSS No. 208 unbelted crash tests* (Report No. 23-0339. 2023). 27th International Technical Conference on the Enhanced Safety of Vehicles, Yokohama, Japan.

This page is intentionally left blank.

Appendix A: Mechanical Characterization Data

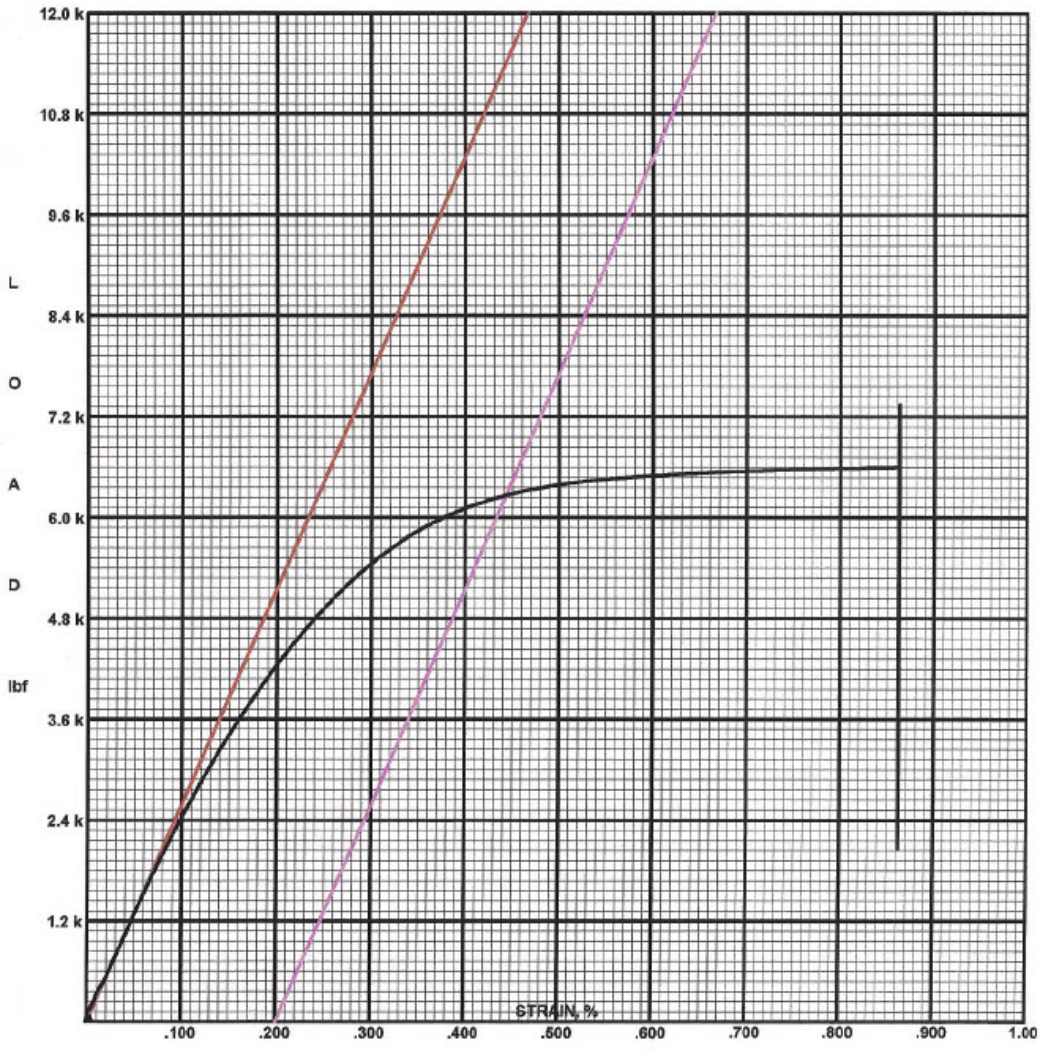

Metallurgical Technologies, Inc.
160 Bevan Drive, Mooresville, NC 28115
Tel: 704-663-5108 ; Fax: 704-662-0898

FLAT TENSILE
Program #198,524-R0

Material:	Steel
Customer:	ELEMANCE
Report Set:	Flat Tensile
Test Set:	Flat Tensile
Description:	Bumper
Matter Number:	100191138
Job Number:	2022425
Load Range:	12000 lbf
X-Axis Ranges:	1 %/<Removed>
Print Date:	November 9,2022
Inst GL/Max:	2 in/10 %
Test Set:	Flat Tensile

Sample Number:	**Wabash B (2)**
Width, in:	**0.505**
Thk, in:	**0.143**
CS Area, in²:	**0.0722**
OFS @ 0.2, ksi:	**86.8**
Ultimate, ksi:	**101.7**
TE (Man), %:	**18**

Specimen Break
Nov 9, 2022 4:13:55 PM

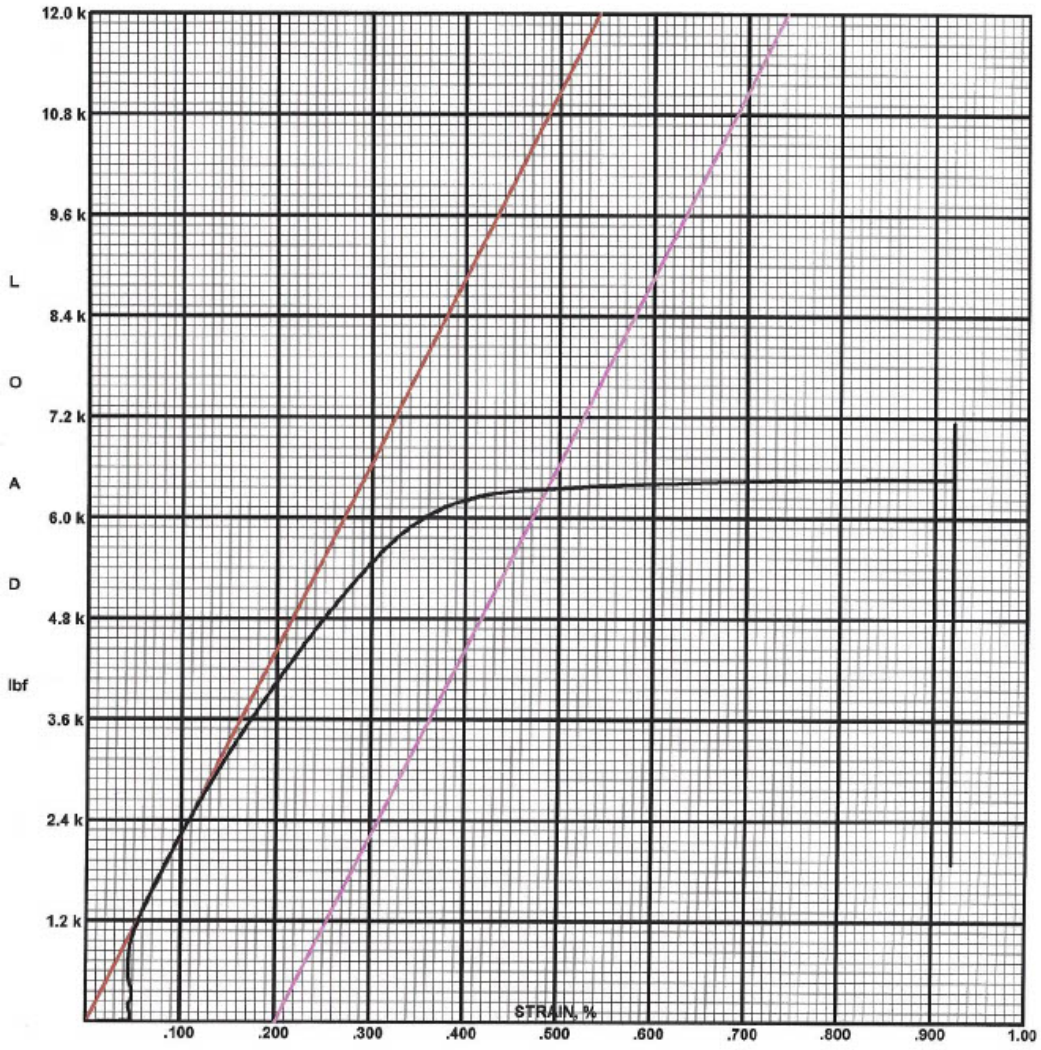

Metallurgical Technologies, Inc.
160 Bevan Drive, Mooresville, NC 28115
Tel: 704-663-5108 ; Fax: 704-662-0898

FLAT TENSILE
Program #198,524-R0

Material:	Steel
Customer:	ELEMANCE
Report Set:	Flat Tensile
Test Set:	Flat Tensile
Description:	Bumper
Matter Number:	100191138
Job Number:	2022425
Load Range:	12000 lbf
X-Axis Ranges:	1 %/<Removed>
Print Date:	November 9,2022
Inst GL/Max:	2 in/10 %
Test Set:	Flat Tensile

Sample Number:	**G. Dane B (1)**
Width, in:	**0.504**
Thk, in:	**0.142**
CS Area, in²:	**0.0716**
OFS @ 0.2, ksi:	**88.7**
Ultimate, ksi:	**99.7**
TE (Man), %:	**21**

Specimen Break
Nov 9, 2022 4:21:46 PM

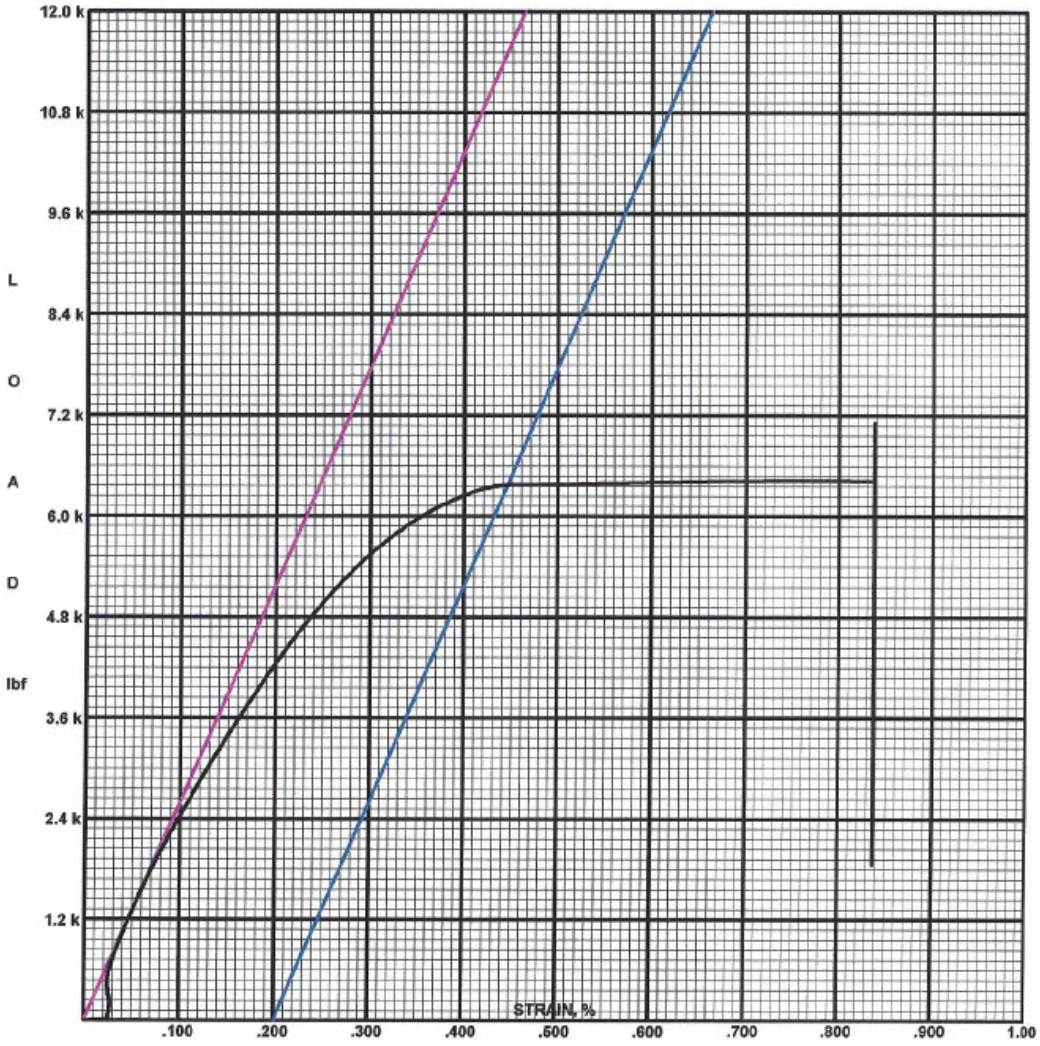

Metallurgical Technologies, Inc.
160 Bevan Drive, Mooresville, NC 28115
Tel: 704-663-5108 ; Fax: 704-662-0898

FLAT TENSILE
Program #198,524-R0

Material:	Steel
Customer:	Elemance
Report Set:	Flat Tensile
Test Set:	Flat Tensile
Description:	Bumper
Matter Number:	100191138
Job Number:	2022425
Load Range:	12000 lbf
X-Axis Ranges:	1 %/<Removed>
Print Date:	November 15,2022
Inst GL/Max:	2 in/10 %
Test Set:	Flat Tensile

Sample Number:	**Great Dane 2**
Width, in:	**0.505**
Thk, in:	**0.138**
CS Area, in²:	**0.0697**
OFS @ 0.2, ksi:	**91.5**
Ultimate, ksi:	**102**
TE (Man), %:	**20.2**

Specimen Break
Nov 15, 2022 11:08:51 AM

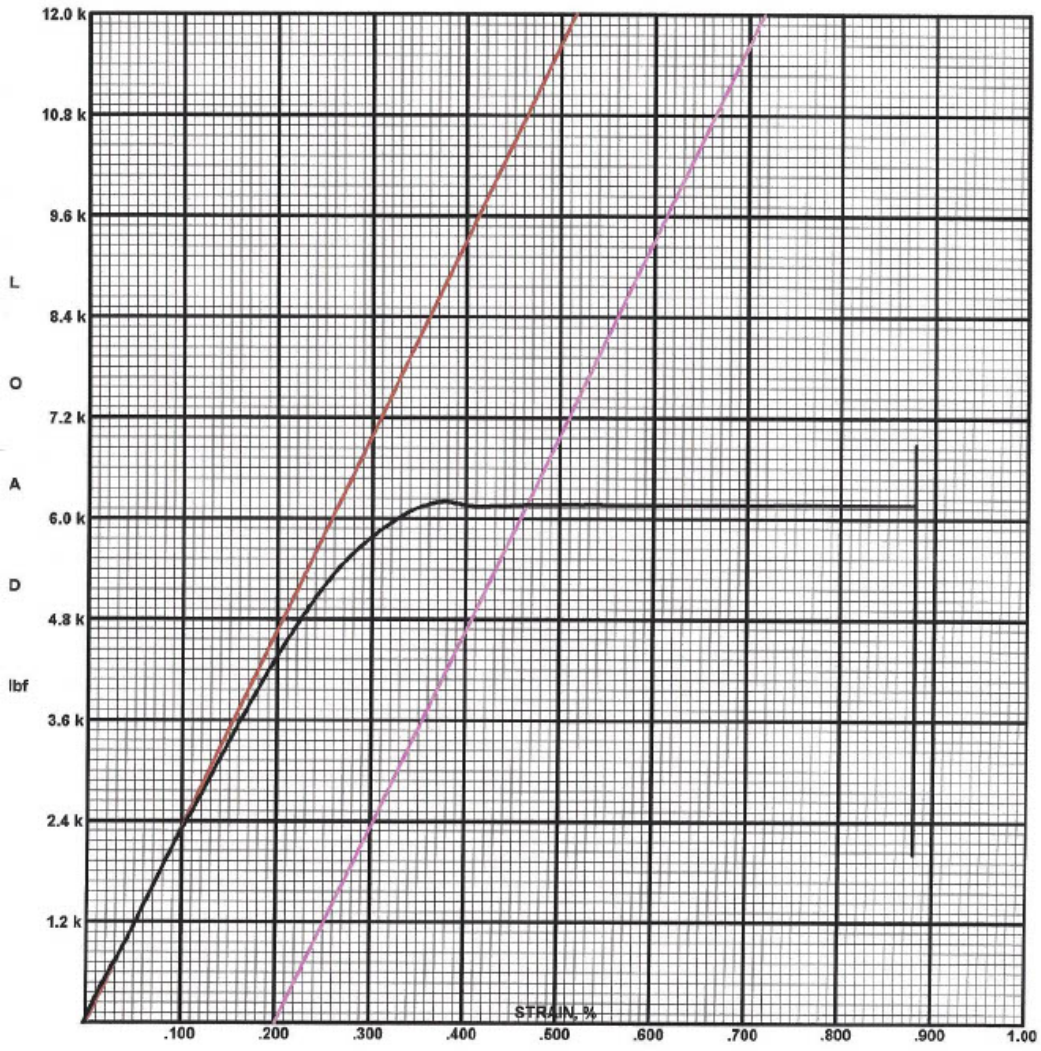

Metallurgical Technologies, Inc.
160 Bevan Drive, Mooresville, NC 28115
Tel: 704-663-5108 ; Fax: 704-662-0898

FLAT TENSILE
Program #198,524-R0

Material:	Steel
Customer:	ELEMANCE
Report Set:	Flat Tensile
Test Set:	Flat Tensile
Description:	Bumper
Matter Number:	100191138
Job Number:	2022425
Load Range:	12000 lbf
X-Axis Ranges:	1 %/<Removed>
Print Date:	November 9,2022
Inst GL/Max:	2 in/10 %
Test Set:	Flat Tensile

Sample Number:	**Manac B (1)**
Width, in:	**0.506**
Thk, in:	**0.14**
CS Area, in²:	**0.0708**
OFS @ 0.2, ksi:	**87**
Ultimate, ksi:	**97.2**
TE (Man), %:	**23.5**

Specimen Break
Nov 9, 2022 4:35:12 PM

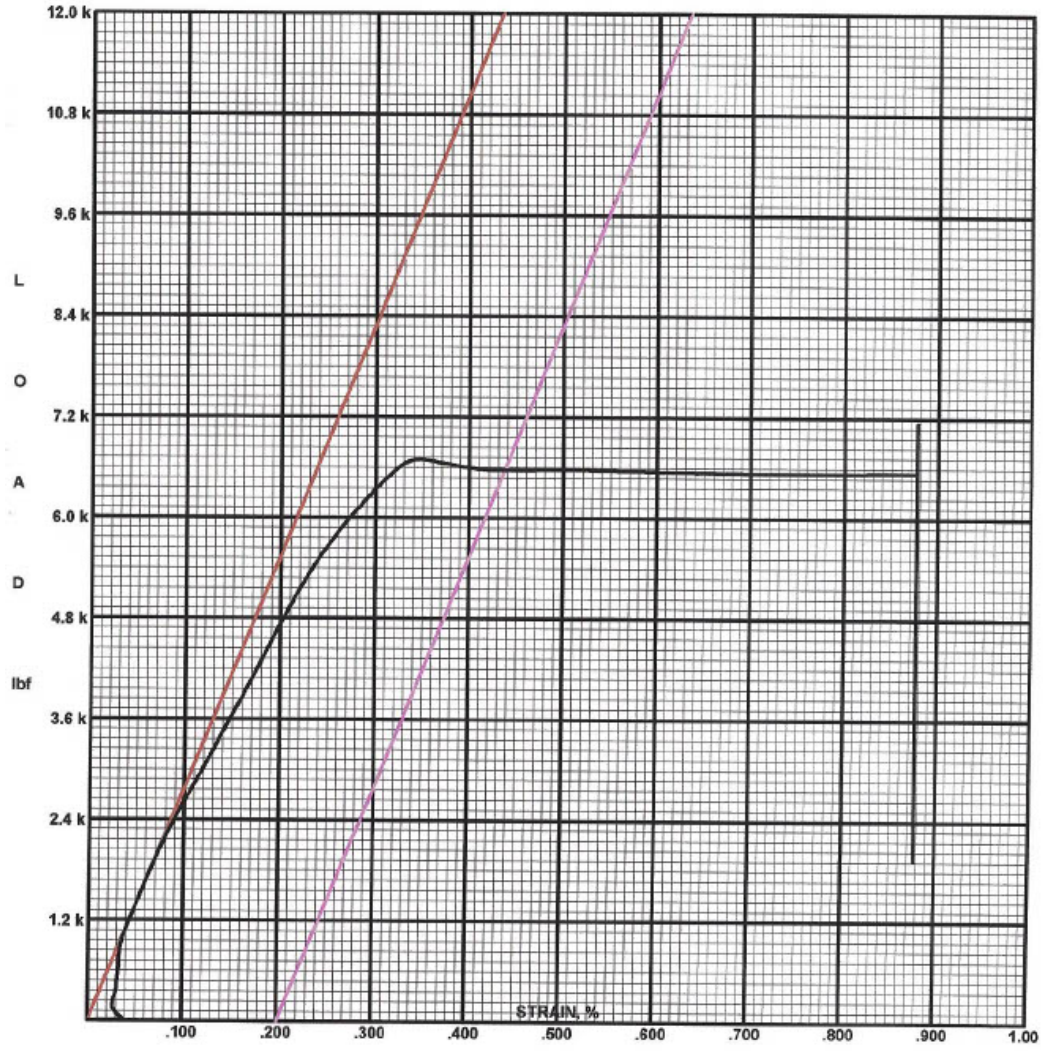

Metallurgical Technologies, Inc.
160 Bevan Drive, Mooresville, NC 28115
Tel: 704-663-5108 ; Fax: 704-662-0898

FLAT TENSILE
Program #198,524-R0

Material:	Steel
Customer:	ELEMANCE
Report Set:	Flat Tensile
Test Set:	Flat Tensile
Description:	Bumper
Matter Number:	100191138
Job Number:	2022425
Load Range:	12000 lbf
X-Axis Ranges:	1 %/<Removed>
Print Date:	November 9,2022
Inst GL/Max:	2 in/10 %
Test Set:	Flat Tensile

Sample Number:	**Manac B (2)**
Width, in:	**0.506**
Thk, in:	**0.14**
CS Area, in²:	**0.0708**
OFS @ 0.2, ksi:	**92.7**
Ultimate, ksi:	**100.8**
TE (Man), %:	**21**

Specimen Break
Nov 9, 2022 4:39:25 PM

Appendix B: Dynamic Simulation Results From Baseline and Minimally Compliant Guards

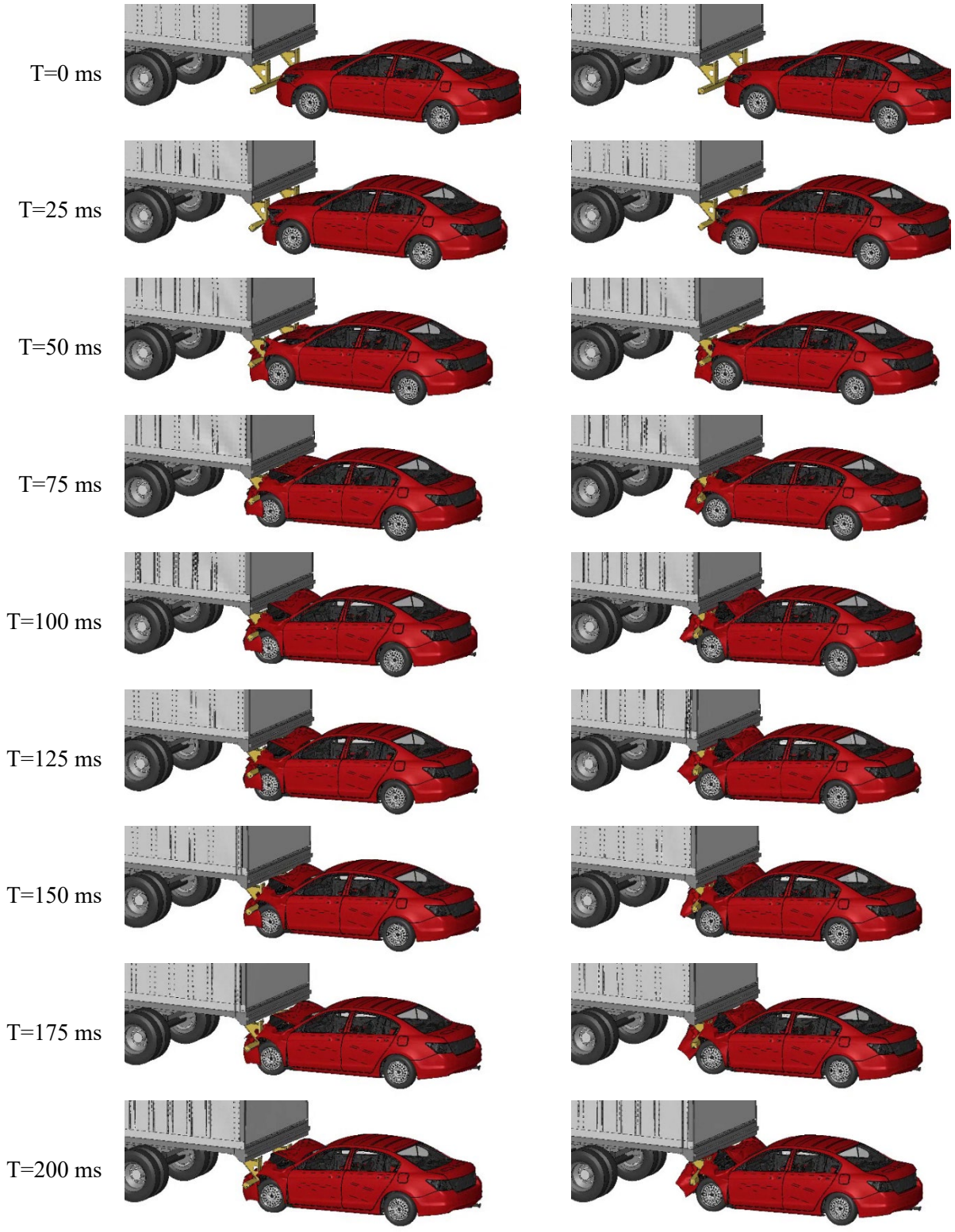

Figure 90. Full overlap 35 mph impact to the Wabash baseline and minimally compliant guards

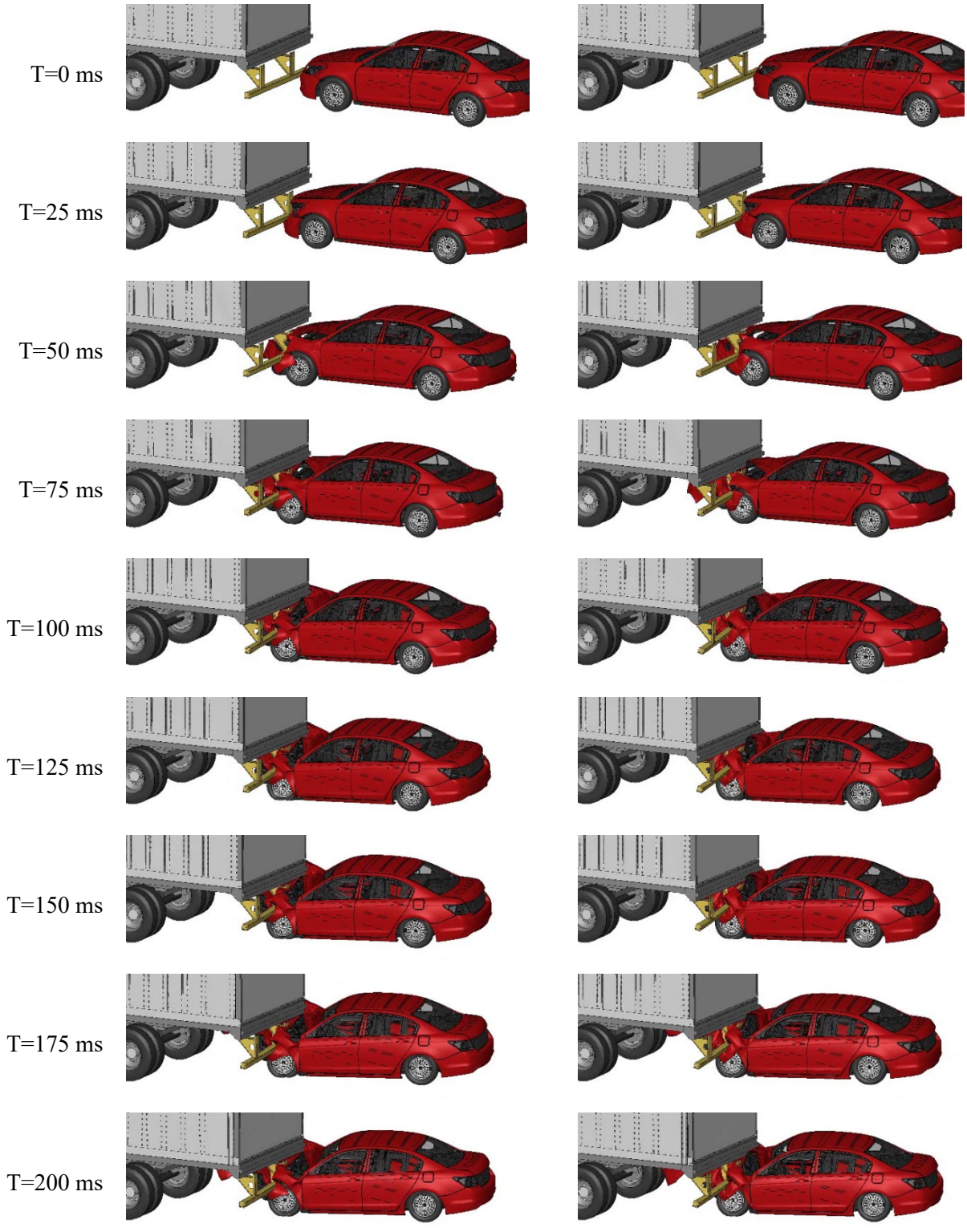

Figure 91. 50 percent overlap 35 mph impact to the Wabash baseline and minimally compliant guards

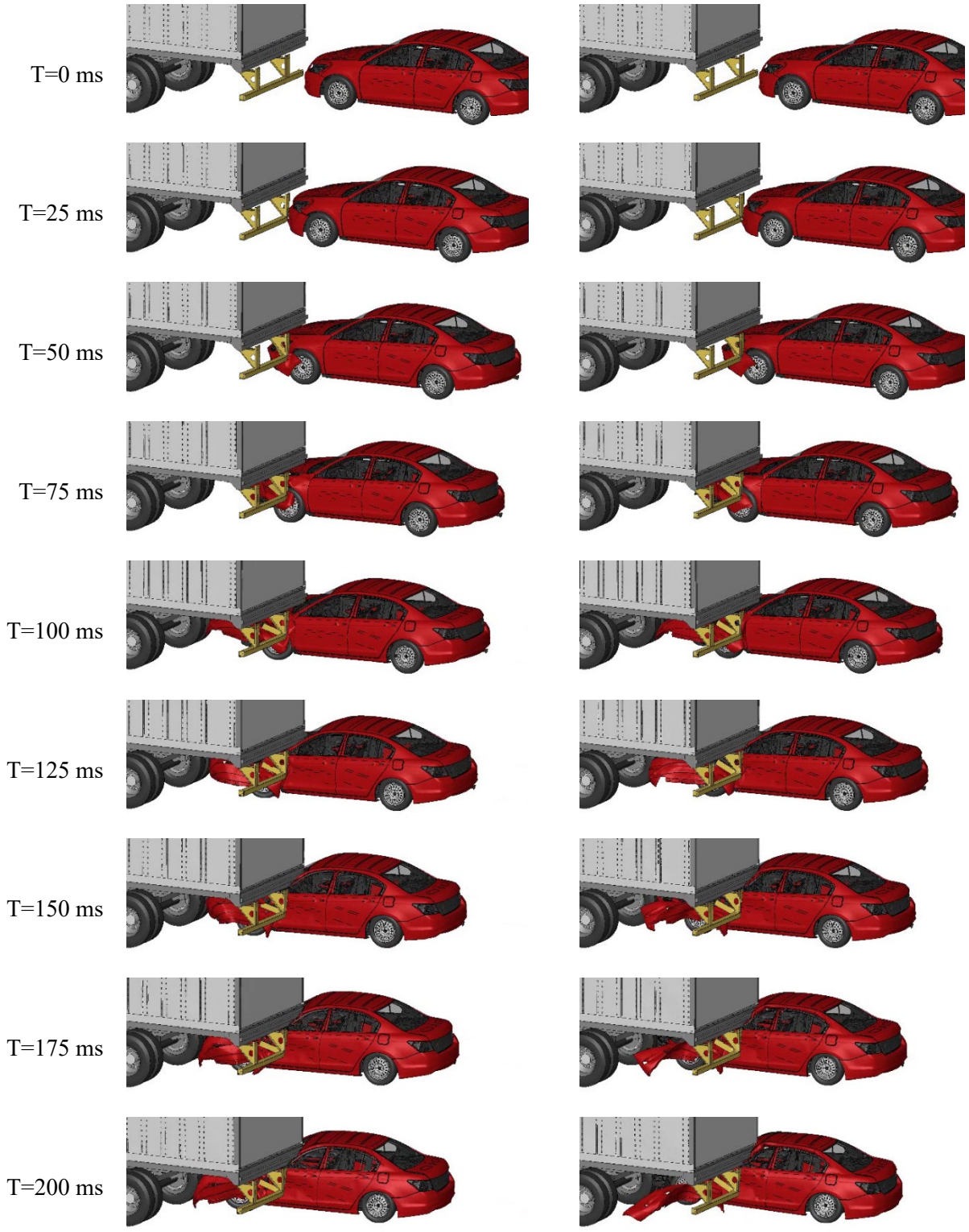

Figure 92. 30 percent overlap 35 mph impact to the Wabash baseline and minimally compliant guards

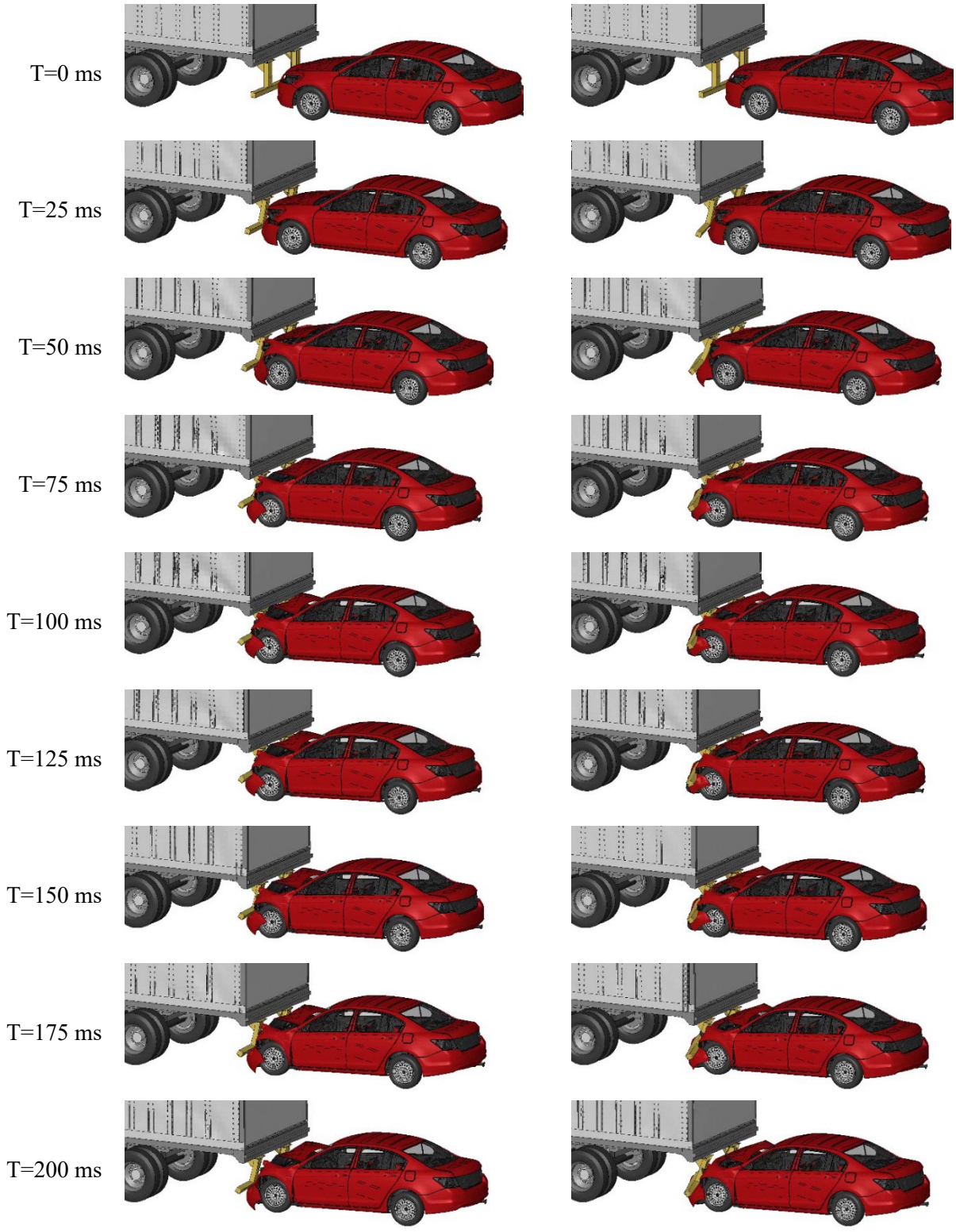

Figure 93. Full overlap 35 mph impact to the Great Dane baseline and minimally compliant guards

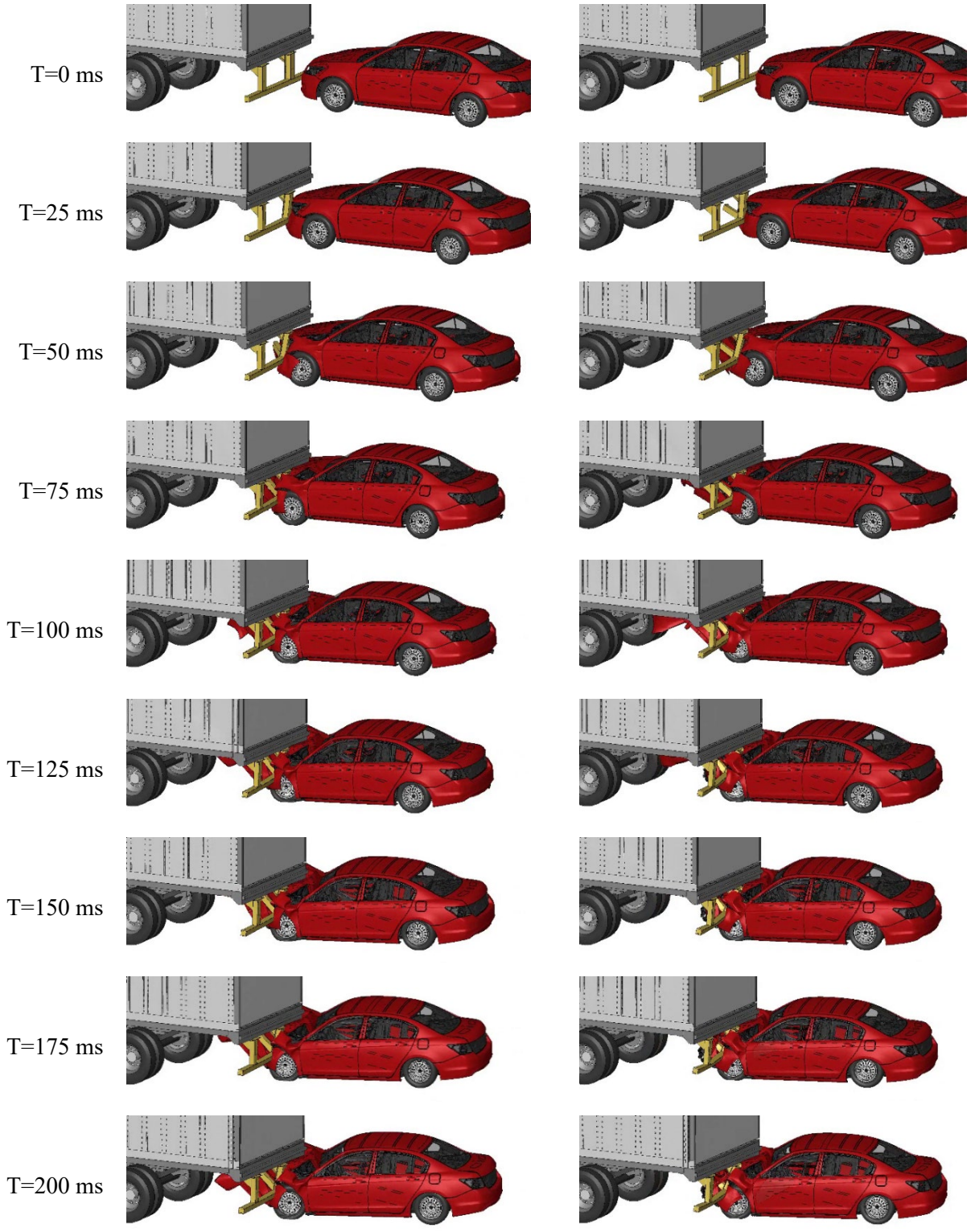

Figure 94. 50 percent overlap 35 mph impact to the Great Dane baseline and minimally compliant guards

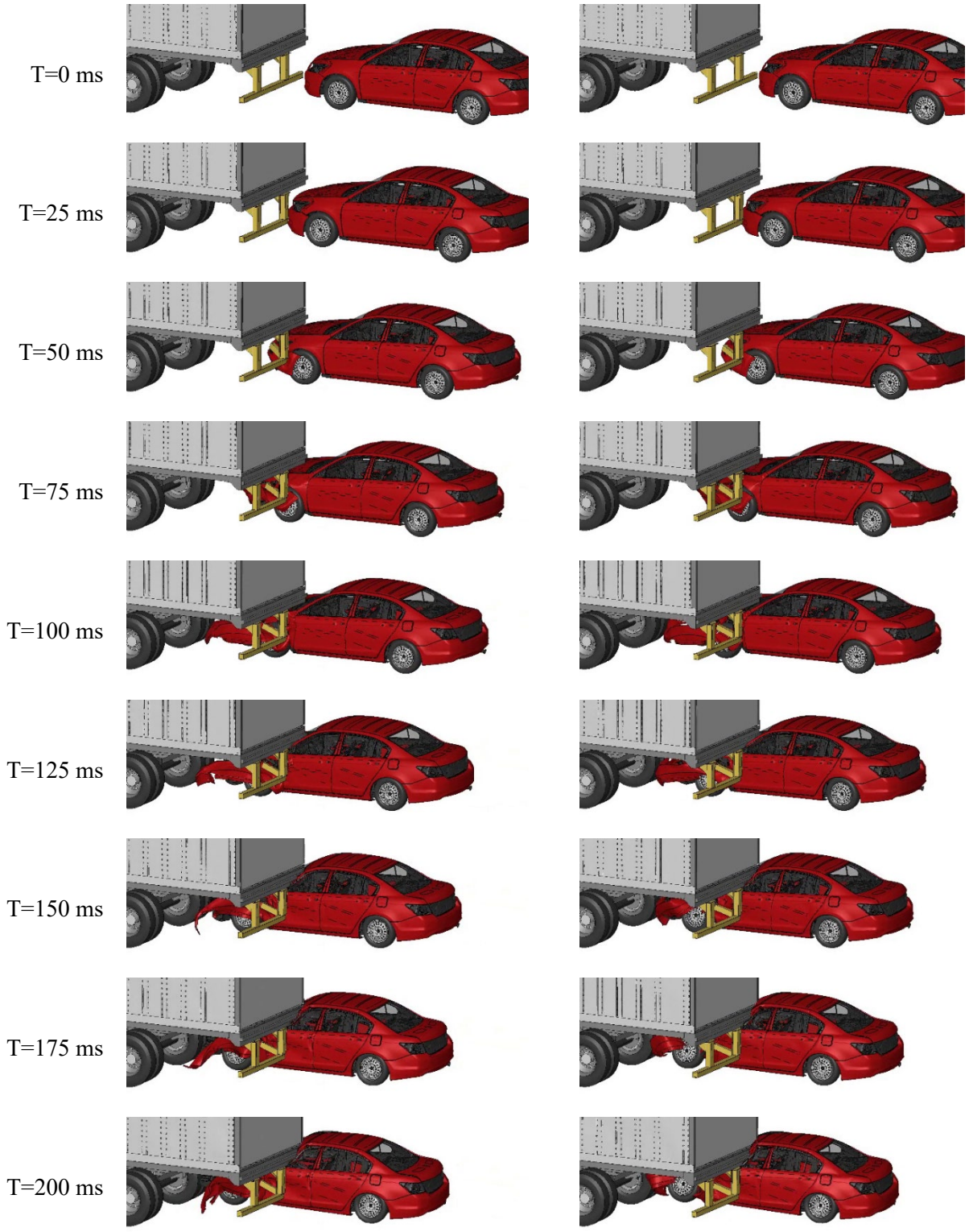

Figure 95. 30 percent overlap 35 mph impact to the Great Dane baseline and minimally compliant guards

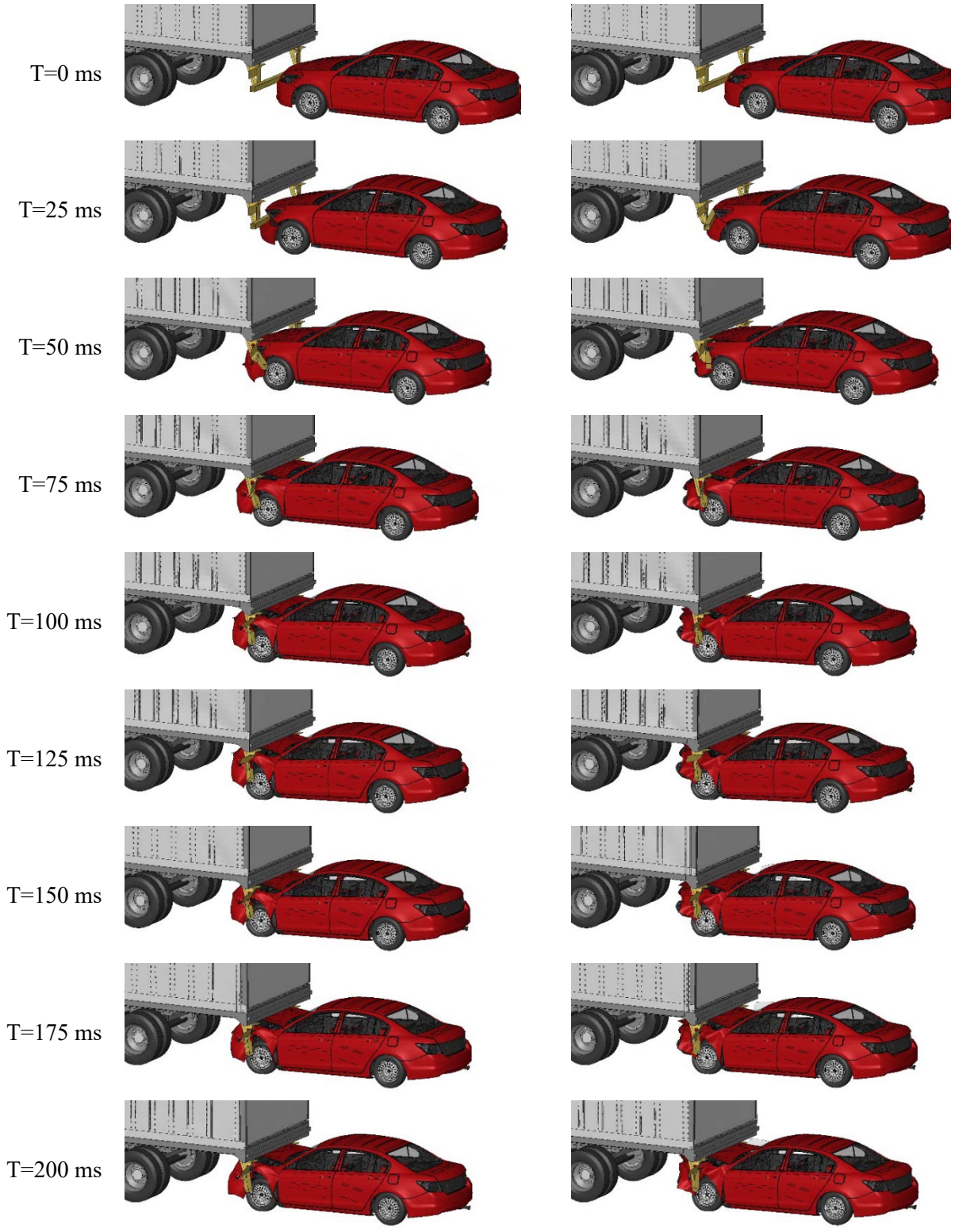

Figure 96. Full overlap 35 mph impact to the Manac baseline and minimally compliant guards

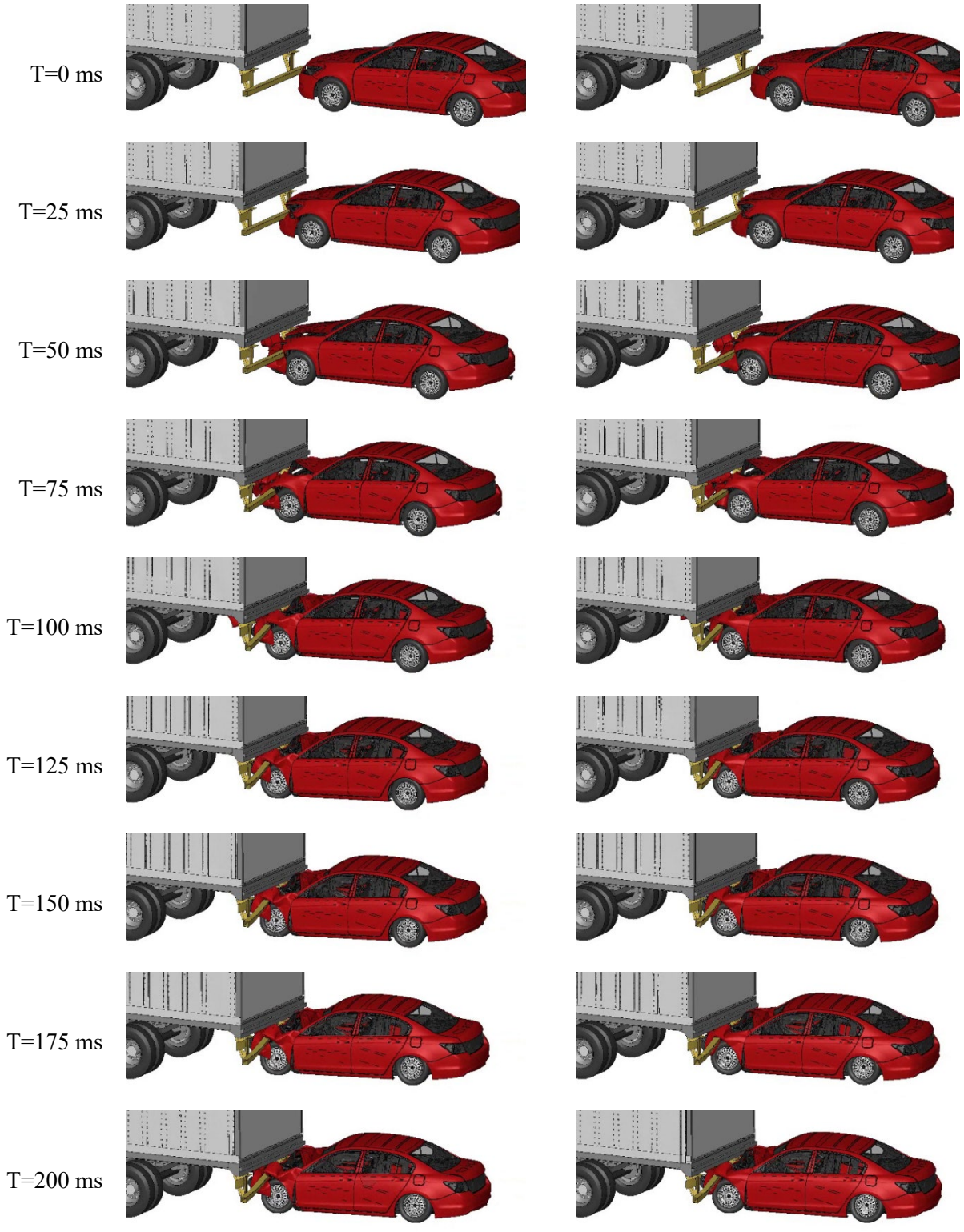

Figure 97. 50 percent overlap 35 mph impact to the Manac baseline and minimally compliant guards

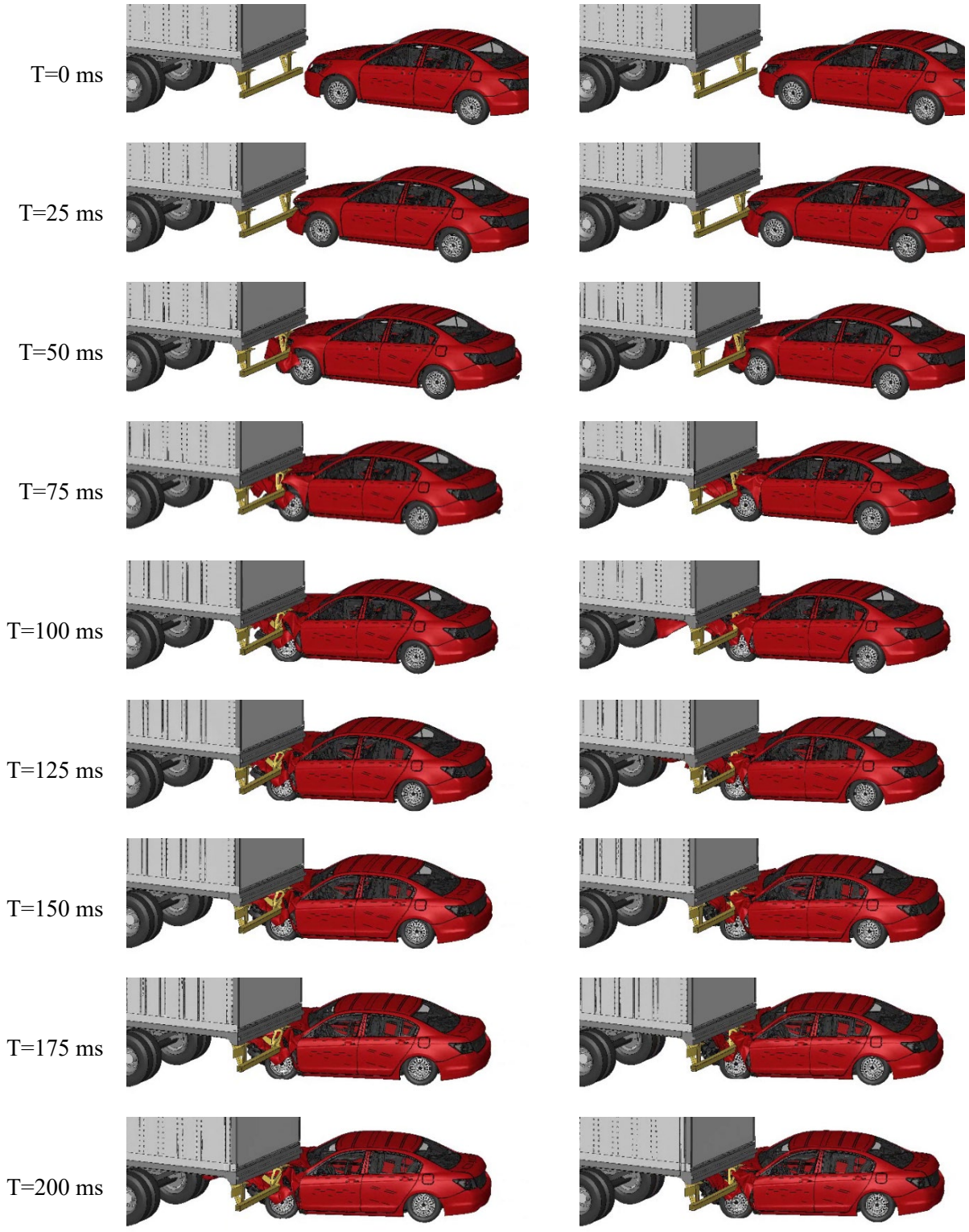

Figure 98. 30 percent overlap 35 mph impact to the Manac baseline and minimally compliant guards

Appendix C: THOR-50M and GHBMC Occupant Injury Metric Response

Head Injury Metrics

The linear head kinematics were strongly correlated between the THOR-50M and GHBMC driver as evidenced in Figure 99 in which all but two simulation results were close to the line of equality. In two simulations (Manac 40 mph 30 percent and 50% overlap), the THOR-50M driver experienced a head strike to the steering wheel, while the GHBMC driver did not. The GHBMC driver experienced consistently higher HIC values than the passenger (105.42 ± 61.98). This trend was more visually pronounced with the THOR-50M model but was not statistically significant. Comparing GHBMC passenger to THOR-50M passenger, the THOR-50M was more apt to experience higher HIC values in matched pair simulations (50.78 ± 93.59). Only 3 simulations resulted in passengers experiencing HIC values above 500 (19% risk AIS or AIS 2+, 5% risk AIS 3+). These were all full-width cases.

The BrIC values ranged from 0.456 to 1.352 in the 40 mph and 45 mph simulations (Figure 100), which covers a wide range of AIS 3+ injury risk (0-89%). Critical values in the calculation of BrIC were ω_{xC} =66.25, ω_{yC} =56.45, and ω_{zC} =42.87. The THOR-50M driver produced statistically significant higher BrIC values than the GHBMC drivers and THOR-50M passengers (0.11 ± 0.13 and 0.09 ± 0.12, respectively). The GHBMC drivers experienced higher BrIC values than the GHBMC passengers (0.09 ± 0.05). The THOR-50M passengers measured higher BrIC values than their GHBMC passenger counterparts (0.11 ± 0.13). Each BrIC comparison was statistically significant. It was noted in the simulations that the THOR-50M head was often forced into more severe coronal rotation compared to the GHBMC, which explains the higher BrIC values.

In summary, as measured by HIC and BrIC, the THOR-50M recorded higher head injury metric values compared to their matched-pair GHBMC counterparts. The drivers were more likely to record higher head injury metric values than the passengers.

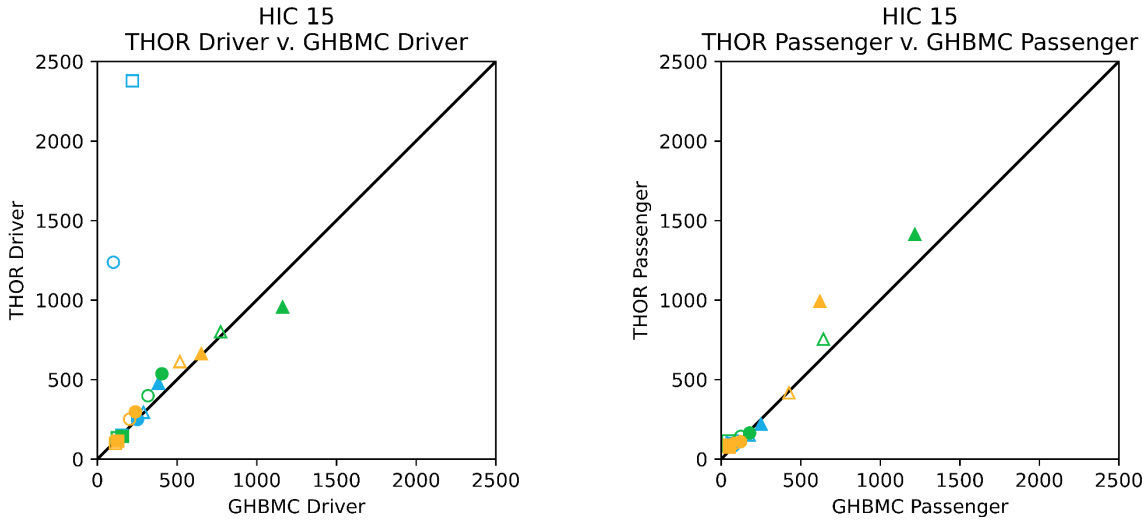

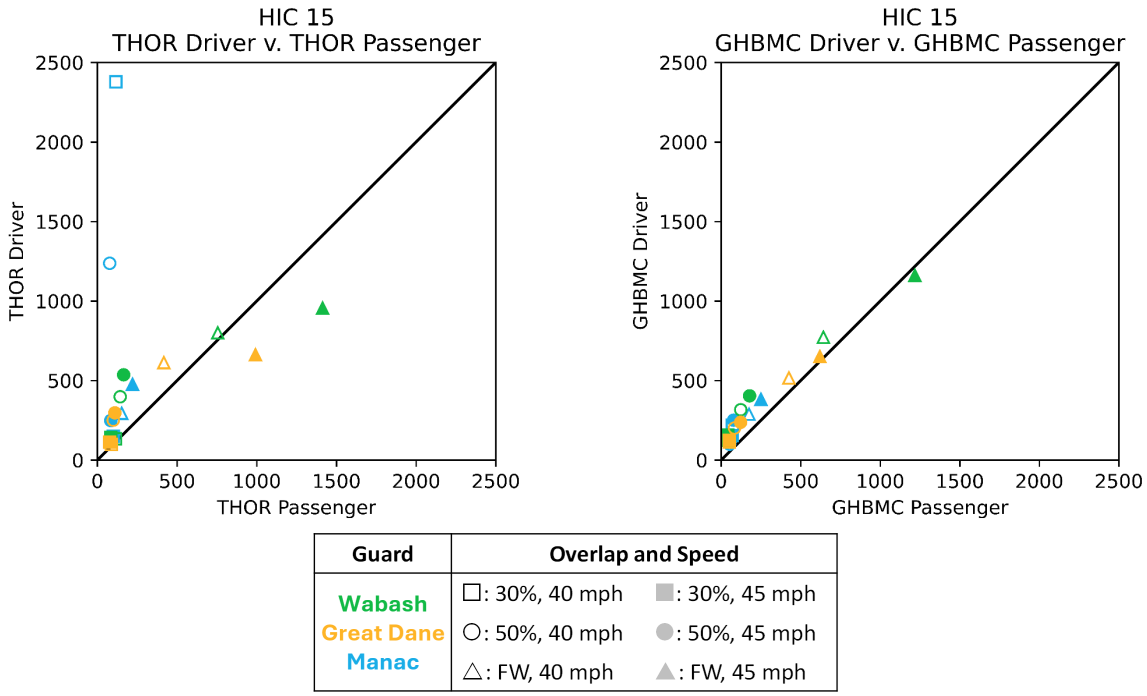

Figure 99. HIC results for the GHBMC and THOR-50M occupants in 40 mph and 45 mph simulations

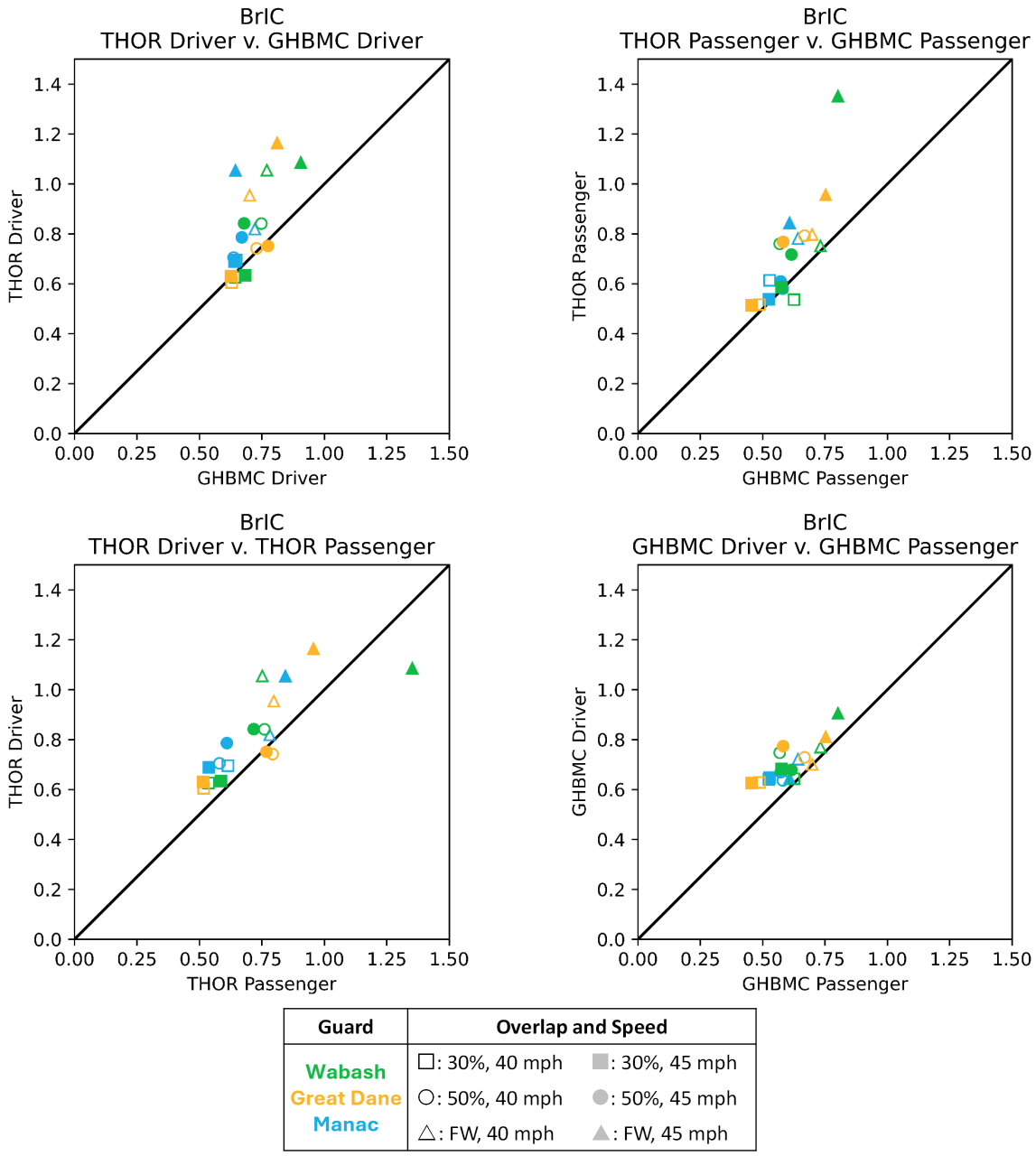

Guard	Overlap and Speed	
Wabash Great Dane Manac	□: 30%, 40 mph	■: 30%, 45 mph
	○: 50%, 40 mph	●: 50%, 45 mph
	△: FW, 40 mph	▲: FW, 45 mph

Figure 100. BrIC results for the GHBMC and THOR-50M occupants in 40 mph and 45 mph simulations

Neck Injury Metrics

The occupant necks primarily were loaded in tension and flexion during the simulations, as expected in primarily frontal crashes with air bags and three-point seat belts. The simulations were truncated shortly after the beginning of rebound of the vehicles, and thus the occupant – seat back//head restraint interactions were not captured.

A strong linear correlation between THOR-50M and GHBMC driver peak neck tension force was observed, with the THOR-50M driver experiencing on average 170 N ± 220 N more tensile force than the GHBMC driver (Figure 101). The THOR-50M passenger vs GHBMC passenger shared a common trend in that the THOR-50M experienced higher neck tension. The THOR-50M passenger on average measured 410 N ± 350 N more tensile force than the GHBMC passenger. Both THOR-50M vs GHBMC comparisons were statistically significant. The THOR-50M driver did not experience statistically significant differences in peak neck tension force compared to the THOR-50M passenger. The higher speed cases produced higher forces for the passenger, while the lower speeds produced higher forces for the driver. The GHBMC driver nearly always saw higher neck tensile forces than the GHBMC passenger (260 N ± 190 N).

The relationship between THOR-50M and GHBMC neck flexion moment was markedly more scattered than the neck tension forces (Figure 102). In all but three cases, the GHBMC driver/passenger experienced higher neck flexion moments than the THOR-50M driver/passenger counterpart. Peak neck flexion moments were 4.50 ± 4.15 Nm and 9.52 ± 5.15 Nm higher in GHBMC drivers and passenger than THOR-50M drivers and passenger, respectively, for matched simulations. The THOR-50M driver experienced 3.87 ± 5.59 Nm higher flexion moment than the THOR-50M passenger, and the GHBMC driver experienced 1.16 ± 0.65 Nm lower flexion moment than the GHBMC passenger. All four flexion moment comparisons were statistically significantly different.

The neck injury criterion (Nij) is calculated by dividing the neck axial force and flexion/extension moments by appropriate critical values before taking the sum of the normalized axial force and bending moments. For axial tension/compression, 4200/4520 N were used for THOR-50M and 3000/3230 N for GHBMC. For flexion/extension, 60.0/79.2 Nm were used for THOR-50M and 54.5/72.0 Nm for GHBMC. The relationship between THOR-50M and GHBMC Nij was strong, but biased. The GHBMC driver experienced on average an Nij 0.19 ± 0.12 higher than the THOR-50M driver, and the GHBMC passenger experienced on average an Nij 0.21 ± 0.11 higher than the THOR-50M passenger. The difference between driver and passenger of the same occupant model was smaller, with the driver tending to experience higher Nij values than the passenger of the same type. The THOR-50M driver on average recorded an Nij 0.08 ± 0.15 higher than the THOR-50M passenger, but this difference was not statistically significant. The GHBMC driver recorded on average 0.07 ± 0.07 higher Nij than the GHBMC passenger, which was statistically significant, albeit a relatively small difference. The risk of AIS 3+ injury to the neck ranged from 2 percent to 75 percent across the simulations.

In summary, the THOR-50M on average recorded higher neck tension force values than the GHBMC, but lower peak neck flexion moments. Once normalized to calculate Nij, the GHBMC predicted higher neck injury metrics than the THOR-50M for both driver and passenger comparisons. The THOR-50M driver versus passenger comparisons showed minimal difference between the two, while the GHBMC driver versus passenger comparisons returned statistically

significant differences in neck injury metric response. The GHBMC driver experienced higher neck tension forces than the passenger, but lower neck flexion moments than the passenger.

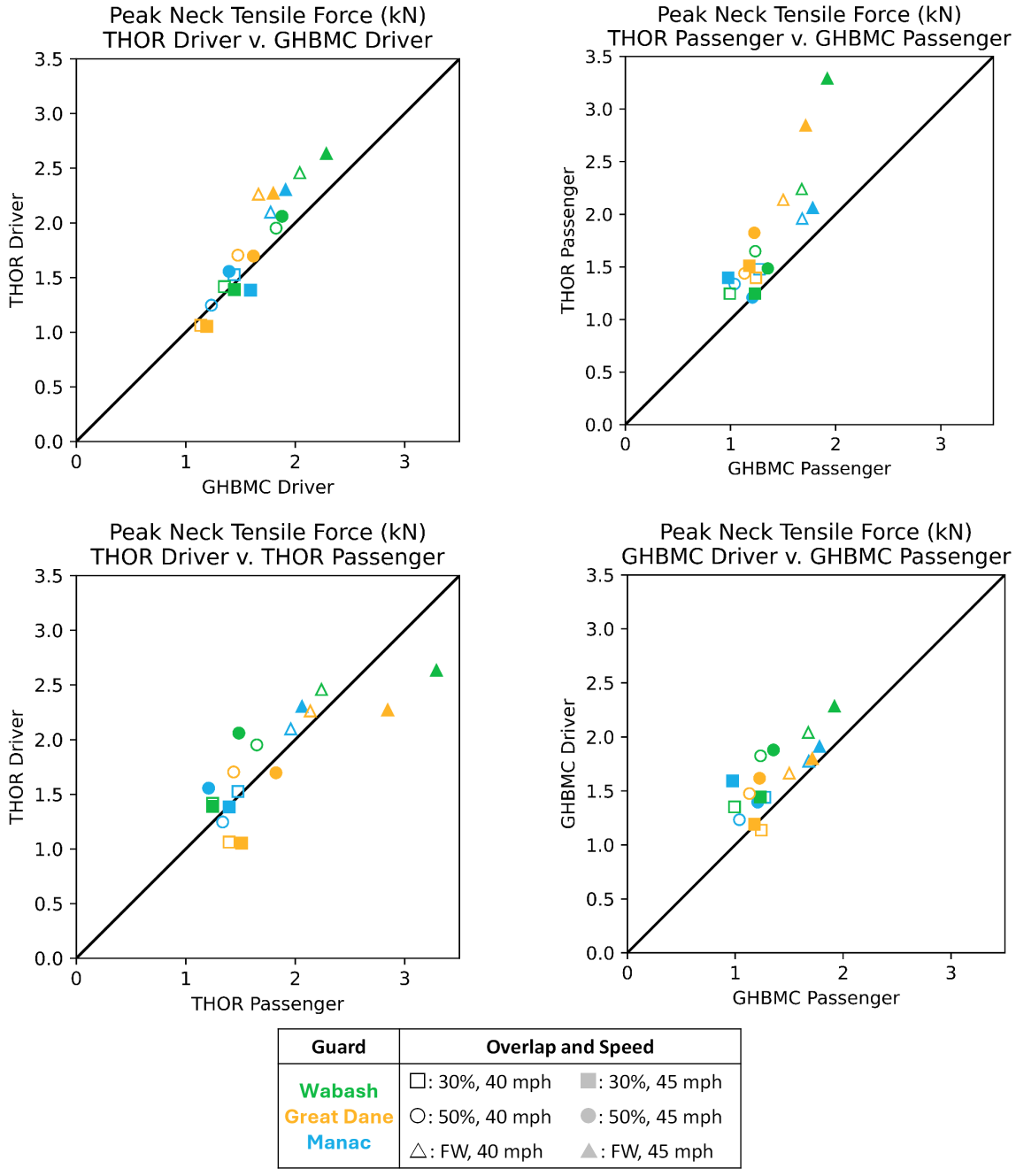

Figure 101. Peak neck tension force for the GHBMC and THOR-50M occupants in 40 mph and 45 mph simulations

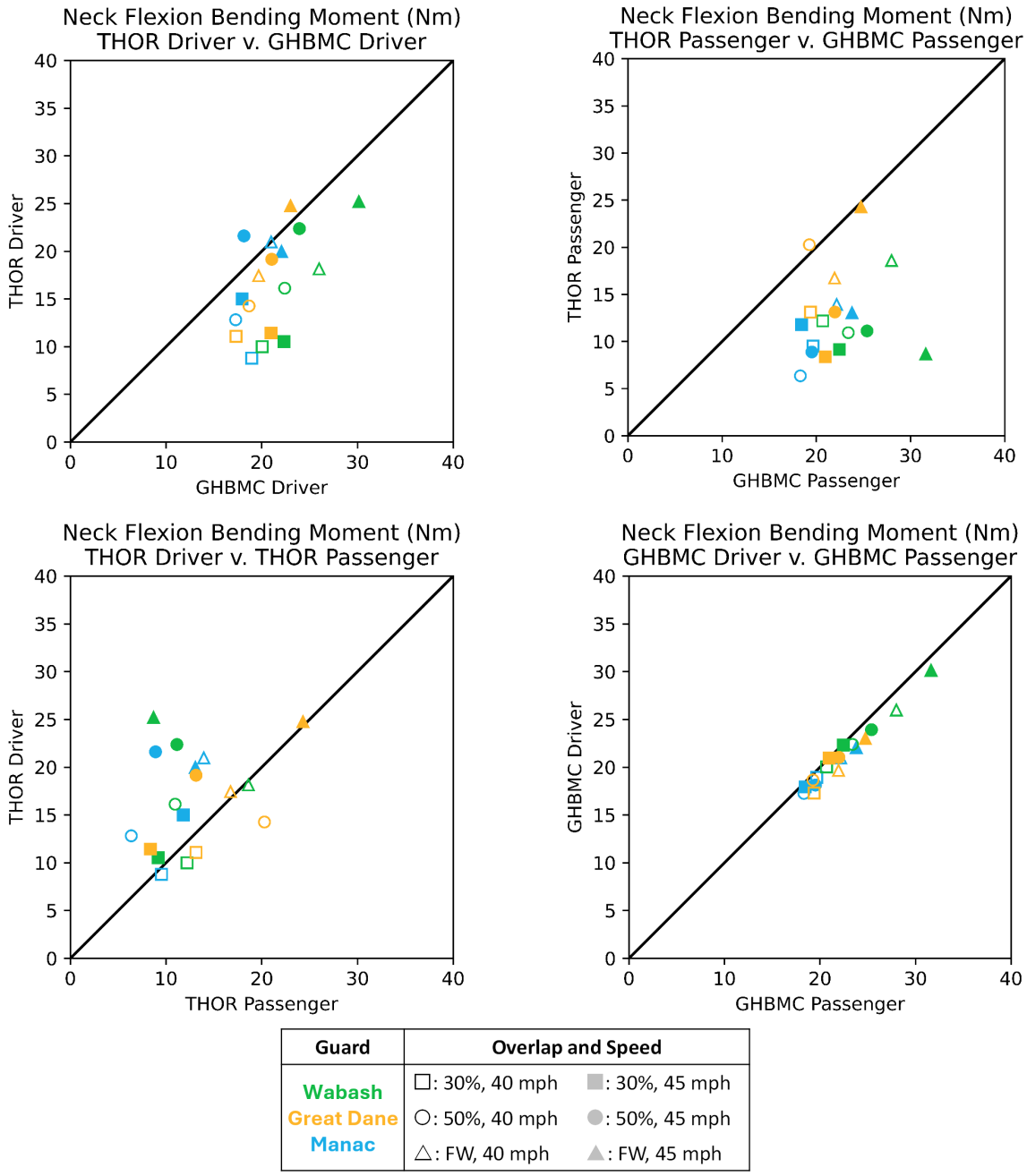

Figure 102. Peak neck flexion moment for the GHBMC and THOR-50M occupants in 40 mph and 45 mph simulations

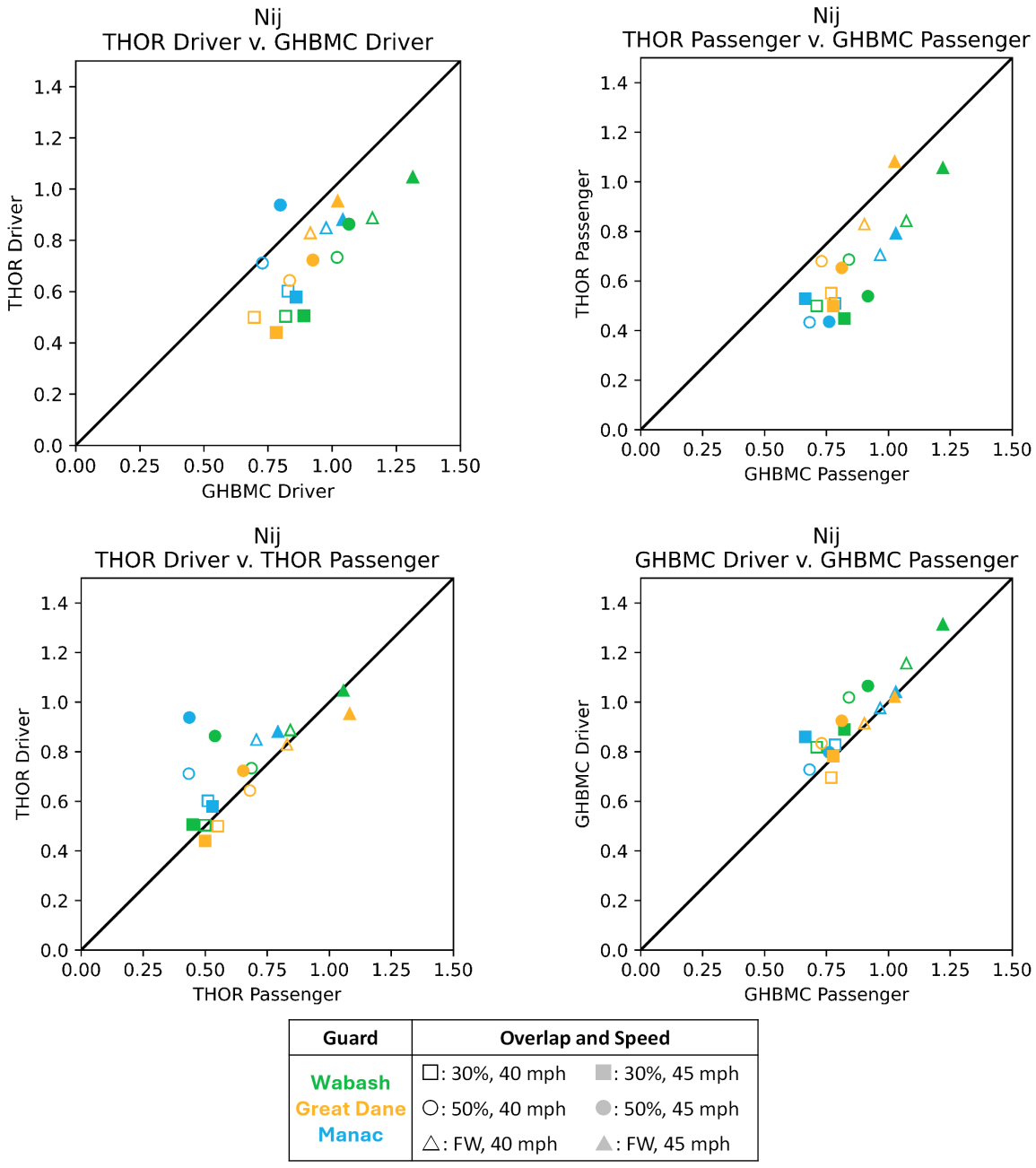

Guard	Overlap and Speed	
Wabash Great Dane Manac	□: 30%, 40 mph	■: 30%, 45 mph
	○: 50%, 40 mph	●: 50%, 45 mph
	△: FW, 40 mph	▲: FW, 45 mph

Figure 103. Peak Nij for the GHBMC and THOR-50M occupants in 40 mph and 45 mph simulations

Thoracoabdominal Injury Metrics

Instrumentation in the THOR-50M and GHBMC differs more in the thorax than any other region of the body. The THOR-50M is equipped with four infrared telescoping rods for assessment of chest compression. These provide time-history compression values in the upper/lower right/lower chest of the THOR-50M. The GHBMC M50-OS is instrumented with the ability to measure antero-posterior and medio-lateral deflection at the chest and abdomen. It also includes several chest bands. The THOR-50M multi-point thoracic injury criterion was calculated and compared to the peak thoracic and abdominal anterior-posterior compression values from GHBMC. Thoracic spine accelerations were measured at T6 in both THOR-50M and GHBMC. The abdominal compression was compared across occupant models using the peak abdominal compression from the lower IR-TRACCs from the THOR-50M and the abdominal AP compression in the GHBMC. Finally, the lumbar spine compression force was extracted from the instrumentation in both the THOR-50M and GHBMC.

While the instrumentation between the GHBMC and THOR-50M for thoracoabdominal compression is different, both occupant surrogates have measurement capability. The THOR-50M uses two IR-TRACCs in the upper thorax, two in the lower thorax, and two in the abdomen, while the GHBMC has a single AP compression measurement in the thorax and abdomen. Comparing the two did not yield statistically significant differences in peak compression between THOR-50M and GHBMC (Figure 104). Nor were statistically significant differences observed between driver and passenger of each occupant type. The strongest correlation was observed between the THOR-50M driver and passenger, but matched-pair comparisons returned an average difference of less than 2 mm on average. The risk of AIS 3+ injury was high across the simulations, ranging from 40 percent to 97 percent.

T6 peak linear accelerations were not statistically significant between THOR-50M and GHBMC when comparing occupants seated in the same position (i.e., driver versus driver, passenger versus passenger). However, when comparing drivers to passengers, for both GHBMC and THOR-50M, the drivers experienced higher peak linear T6 accelerations, though the differences were small (Figure 105). The THOR-50M driver on average experienced 4.60 G ± 2.74 G higher T6 accelerations than the THOR-50M passenger. Similarly, the GHBMC driver experienced 4.44 G ± 3.51G higher T6 accelerations than the passenger.

Abdominal compression was markedly higher in the GHBMC compared to the THOR-50Ms, which is expected based on the difference in the type of model. The GHBMC is significantly more compliant than an ATD in the abdomen. The GHBMC driver on average measured 21.0 mm ± 10.74 mm more abdominal compression than the THOR-50M driver. Between occupants of the same type, the passenger tended to experience higher abdomen compression. The risk of AIS 3+ abdomen compression was never larger than 25 percent for the THOR-50M occupant models.

Lumbar spine kinetics demonstrated disparities between GHBMC and THOR-50M (Figure 107, Figure 108). The THOR-50M driver experienced significantly higher compressive loads than the GHBMC driver (640 N ± 340 N). The THOR-50M passenger trended the same way, experiencing 880 N ± 170 N more compressive force than the GHBMC passenger. Surprisingly, the GHBMC passenger recorded very low peak compressive forces. Instead, the GHBMC passenger experienced mostly tensile forces. In both the THOR-50M and GHBMC occupants, the passengers were subjected to higher tensile lumbar spine loads than the drivers, which is

likely attributable to the difference in air bag interaction. The peak tensile lumbar spine loads between THOR-50M passenger and GHBMC passenger were not statistically significantly different.

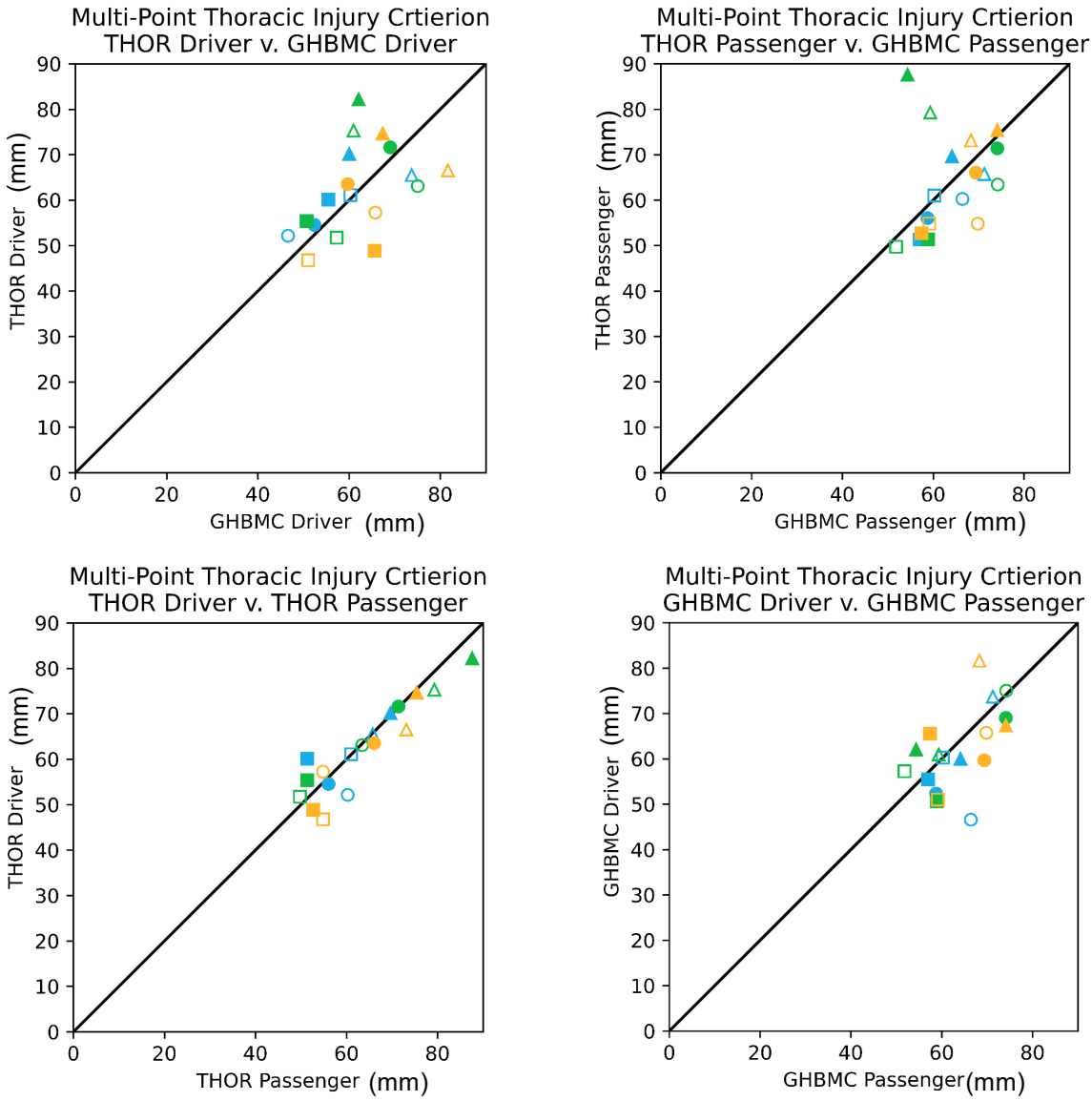

Figure 104. Multi-point thoracic injury criterion and peak thoracoabdominal compression for the THOR-50M and GHBMC occupants in 40 mph and 45 mph simulations

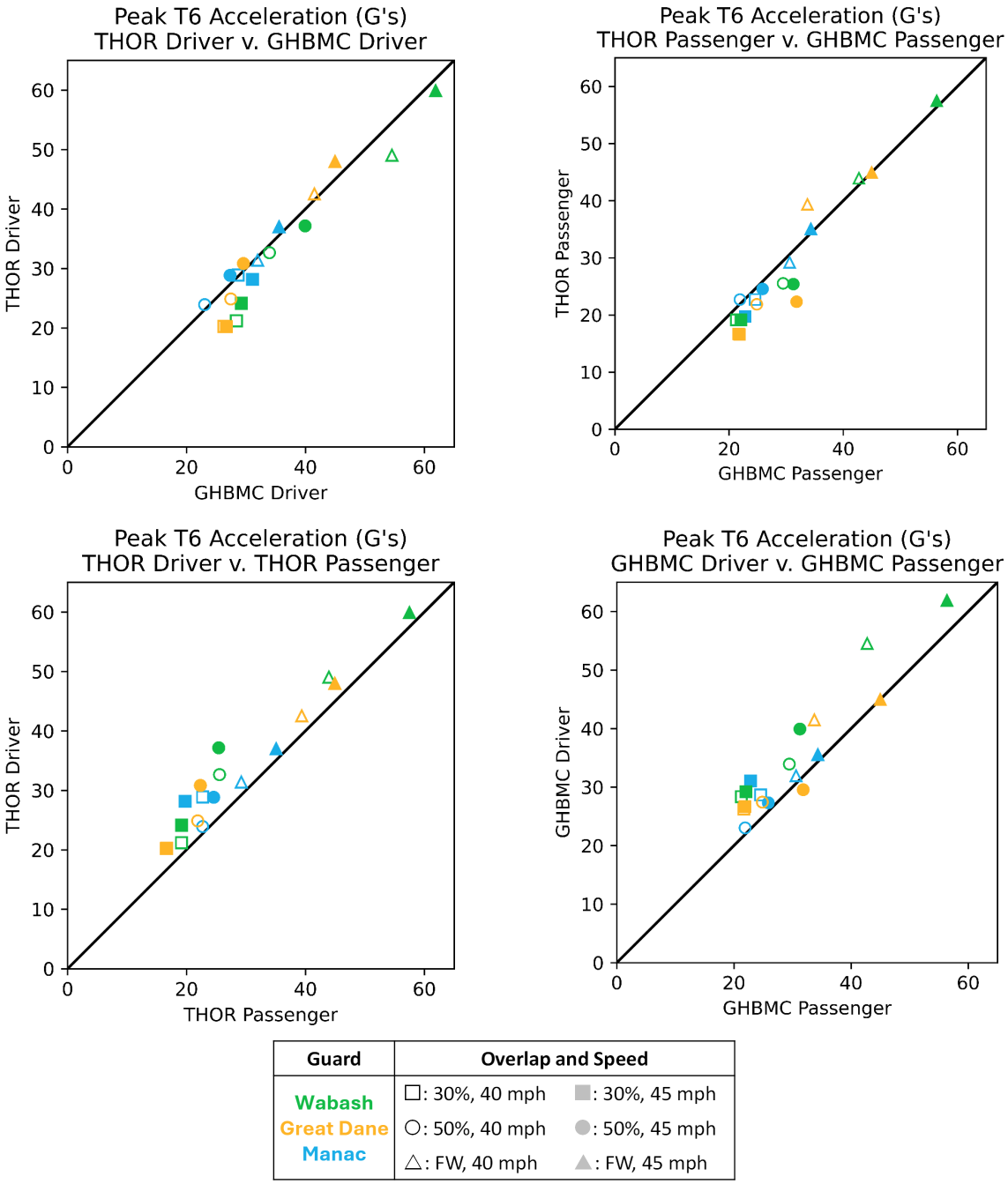

Figure 105. Peak T6 linear acceleration for the GHBMC and THOR-50M occupants in 40 mph and 45 mph simulations

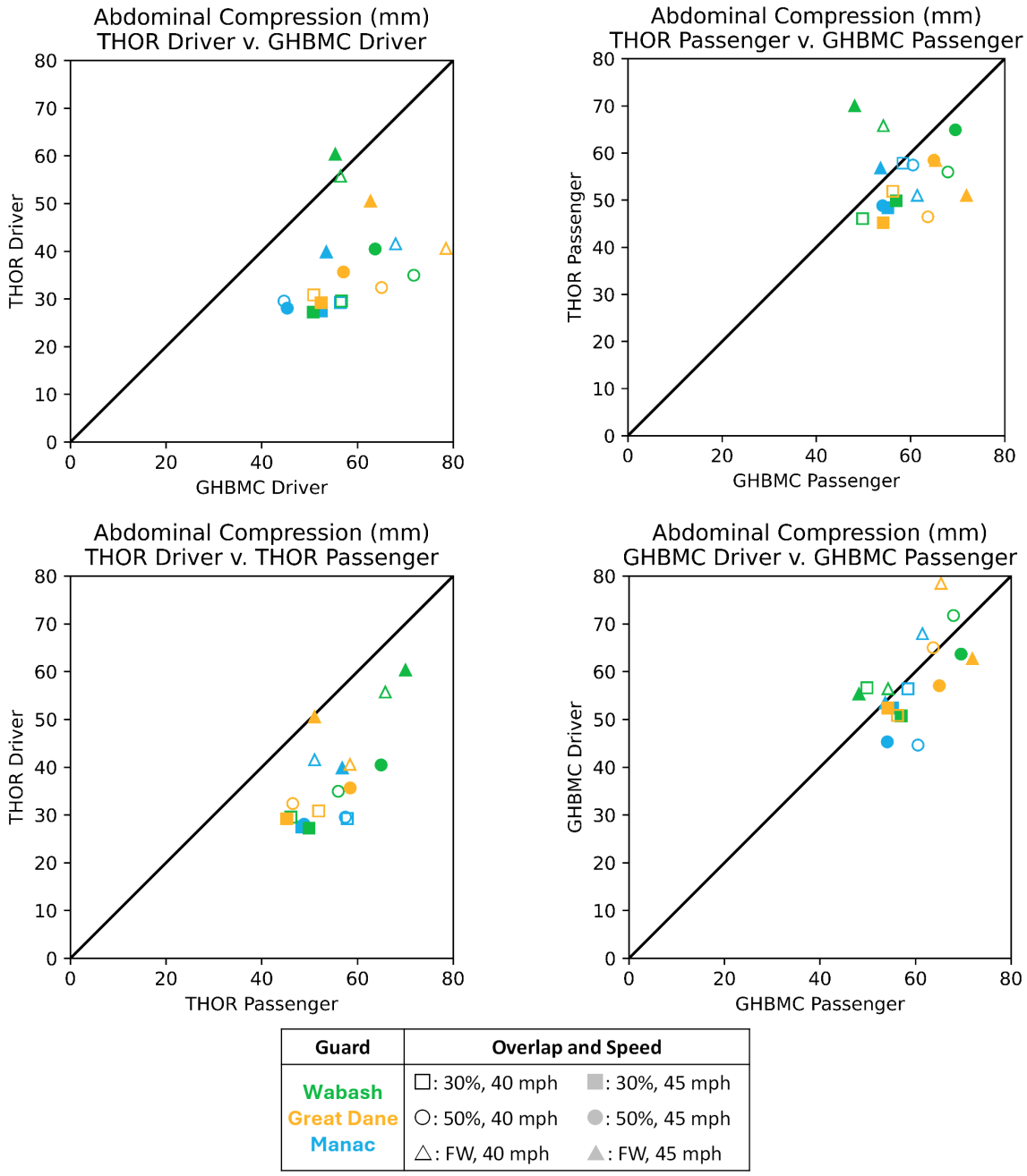

Figure 106. Peak abdominal compression for the GHBMC and THOR-50M occupants in 40 mph and 45 mph simulations

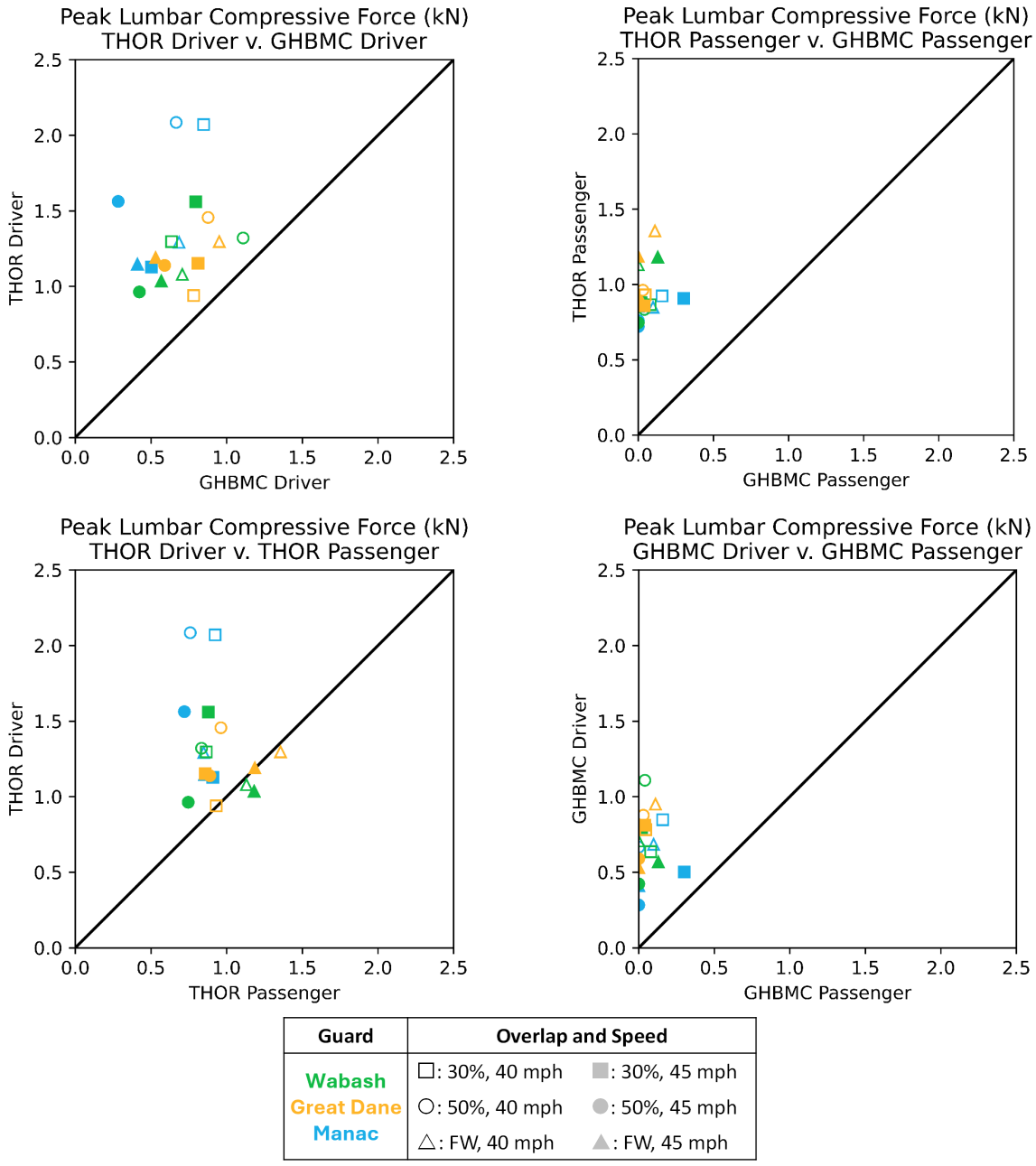

Guard	Overlap and Speed	
Wabash Great Dane Manac	□: 30%, 40 mph	■: 30%, 45 mph
	○: 50%, 40 mph	●: 50%, 45 mph
	△: FW, 40 mph	▲: FW, 45 mph

Figure 107. Peak lumbar spine compression force for the GHBMC and THOR-50M occupants in 40 mph and 45 mph simulations

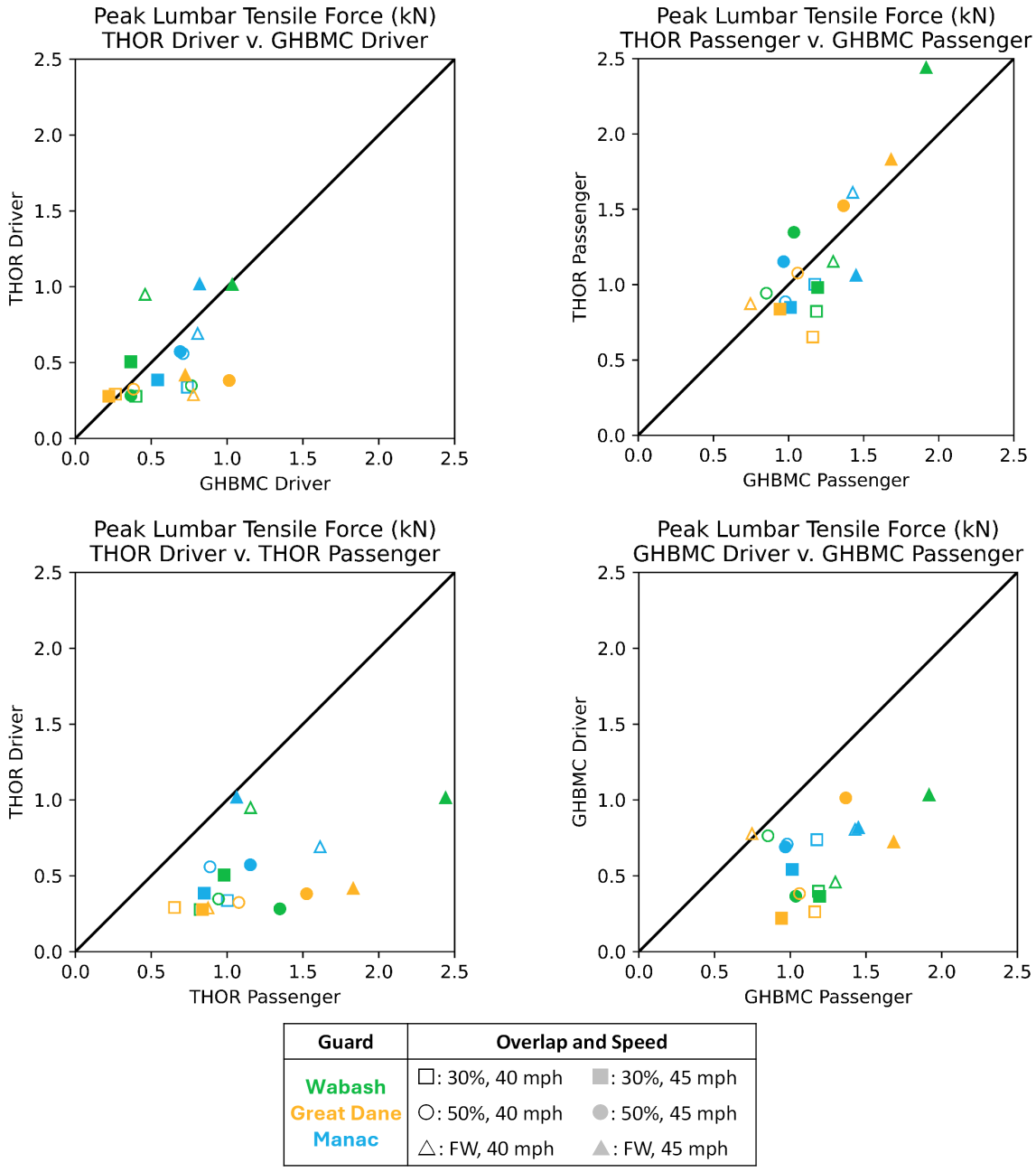

Figure 108. Peak lumbar spine tension force for the GHBMC and THOR-50M occupants in 40 mph and 45 mph simulations

Pelvis and Lower Extremity Injury Metrics

The GHBMC occupants sustained higher peak pelvis linear accelerations compared to THOR-50M occupants (Figure 109). The GHBMC driver on average experienced 5.67 G ± 4.55 G higher pelvis acceleration than the THOR-50M driver. The GHBMC passenger on average experienced 3.66 G ± 2.57 G higher pelvis acceleration than the THOR-50M passenger. The relationship between the two occupant types for pelvis acceleration was strongly linear. The drivers also experienced higher pelvis accelerations than the passengers.

The femur axial force results were mixed. The left femur axial forces (Figure 110) were less different across occupants and positions than the right femur axial forces (Figure 111). For the right femur, the THOR-50M experienced statistically significantly higher forces than the GHBMC occupants seated in the same position. The only statistically significant result for the left femur comparisons was the THOR-50M passenger vs the GHBMC passenger, in which the THOR-50M experiences 1.89 kN ± 0.55 kN higher forces. The Manac 45 mph cases produced the highest femur forces across the occupants. The highest probability of AIS 2+ femur injury across the simulations was 5 percent (6.45 kN).

The results of the analysis of tibia injury metrics were scattered, with some load cells showing strong discrepancies between occupants. The left upper tibia force was higher in the drivers compared to the passengers (Figure 112). The strongest trends for upper tibia force differences were in the right tibia. The GHBMC driver right upper tibia force was consistently higher than the THOR-50M driver and the GHBMC passenger (Figure 113). Peak bending moments were higher in the THOR-50M compared to the GHBMC for both driver and passenger and left and right legs (Figure 116, Figure 117). The Revised tibia index (RTI) was also higher for THOR-50M compared to GHBMC (Figure 118, Figure 119). In many simulations, the knee of the THOR-50M remained high on the dash, which induced a bending moment from the knee bolsters around the upper tibia load cells. The GHBMC knee did not stay as high during the crash, which prevented large bending moments. The highest risk of AIS 2+ injury to the tibia as predicted by upper tibia axial force readings was 17 percent (5.1 kN) in the simulations. The highest risk of AIS 2+ injury to the tibia as predicted by lower tibia axial force was 27 percent (5.91 kN). The highest risk of AIS 2+ injury to the tibia as predicted by peak bending moment was 15 percent (208 Nm). The highest risk of AIS 2+ tibia injury as predicted by RTI was 31 percent (RTI=1.03).

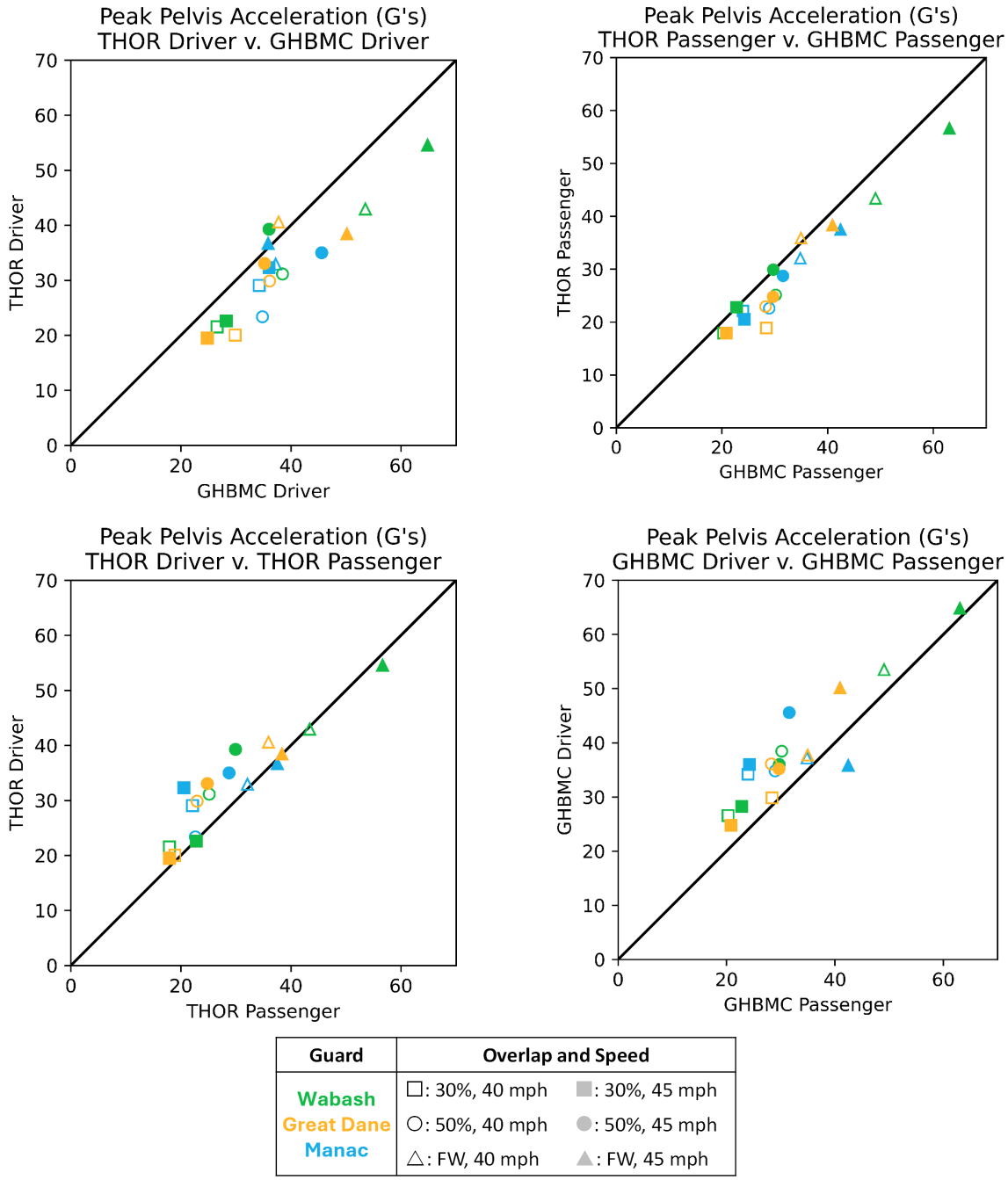

Figure 109. Peak pelvis linear acceleration for the GHBMC and THOR-50M occupants in 40 mph and 45 mph simulations

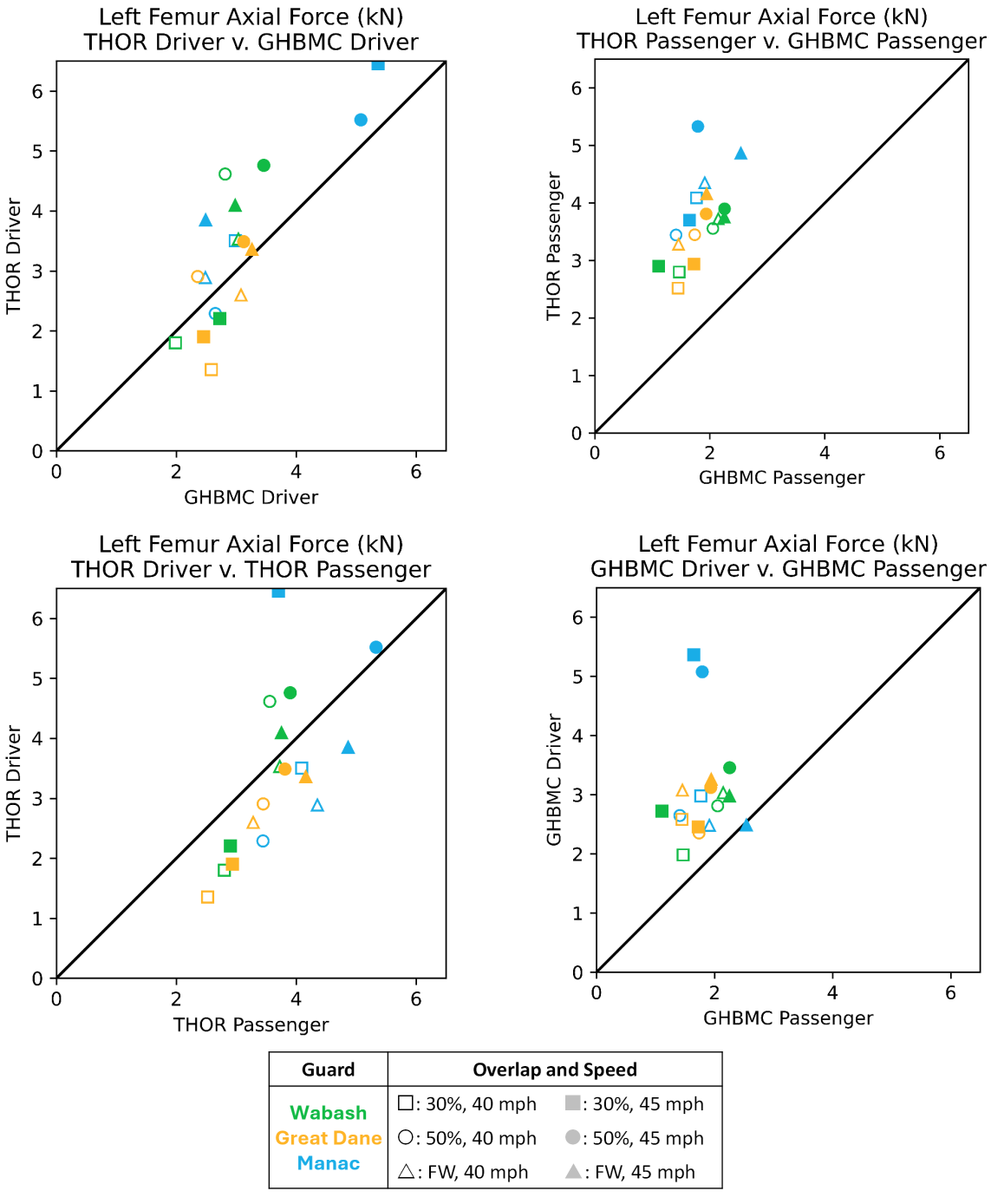

Figure 110. Peak left femur force for the GHBMC and THOR-50M occupants in 40 mph and 45 mph simulations

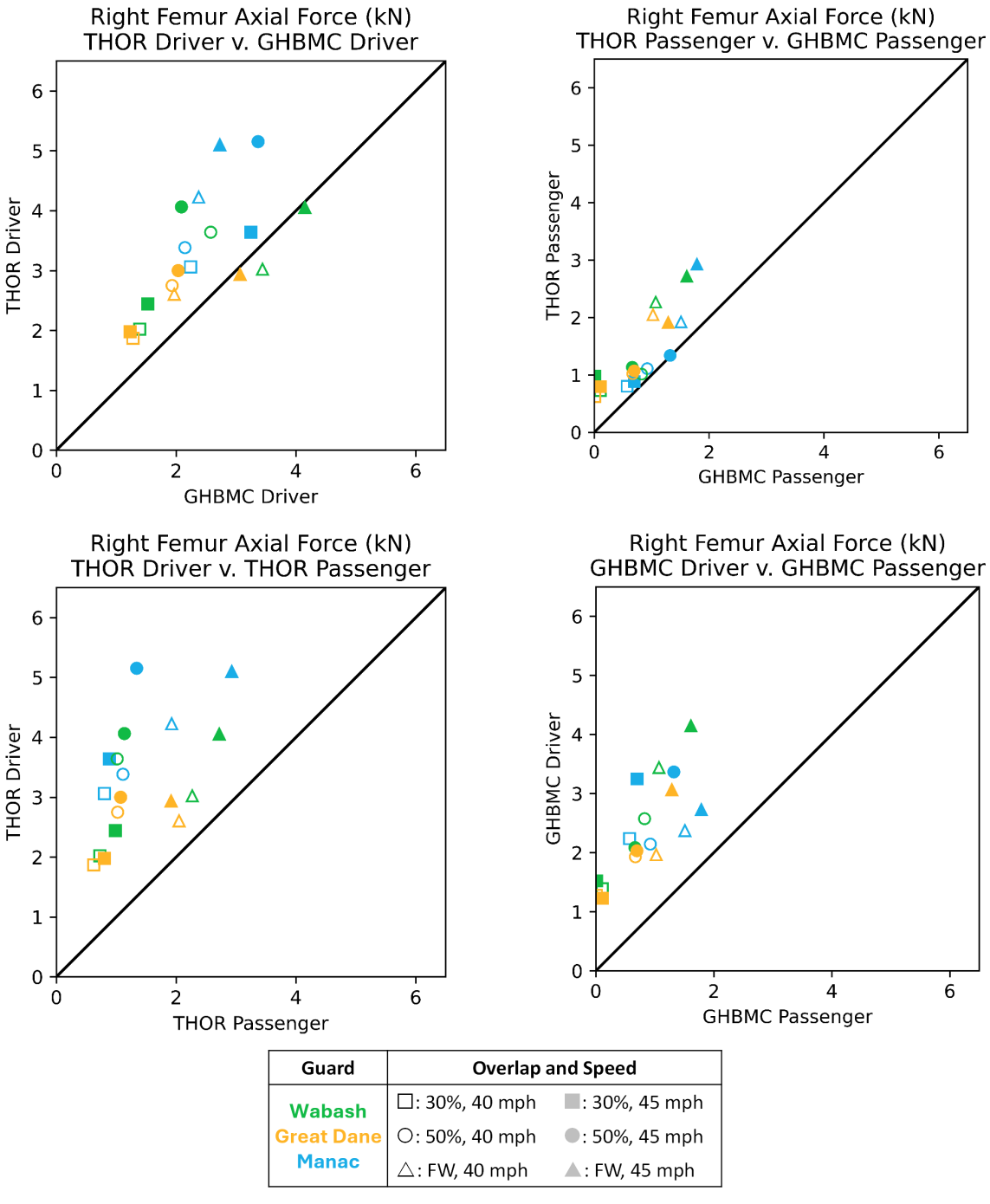

Figure 111. Peak right femur force for the GHBMC and THOR-50M occupants in 40 mph and 45 mph simulations

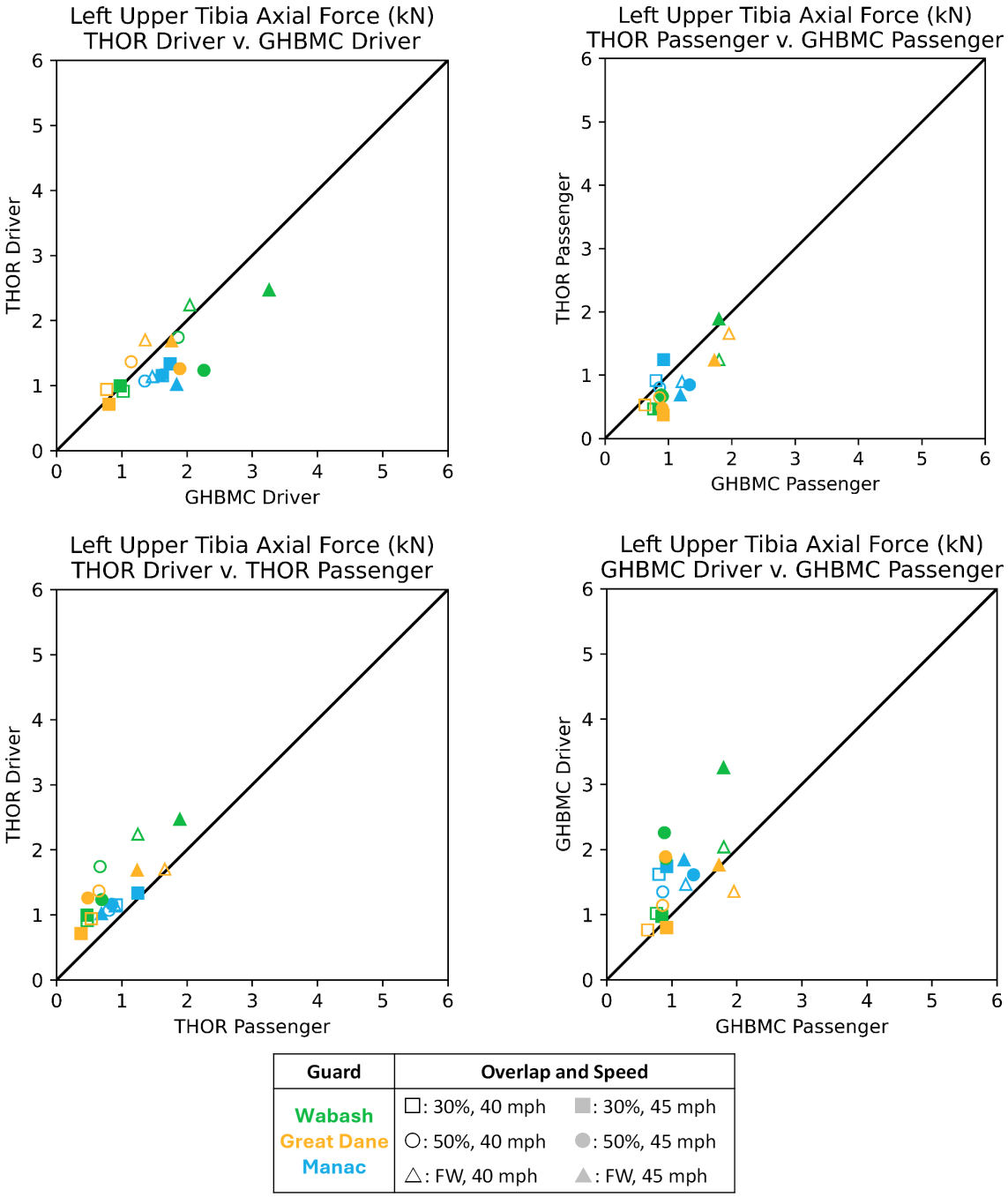

Figure 112. Peak left upper tibia force for the GHBMC and THOR-50M occupants in 40 mph and 45 mph simulations

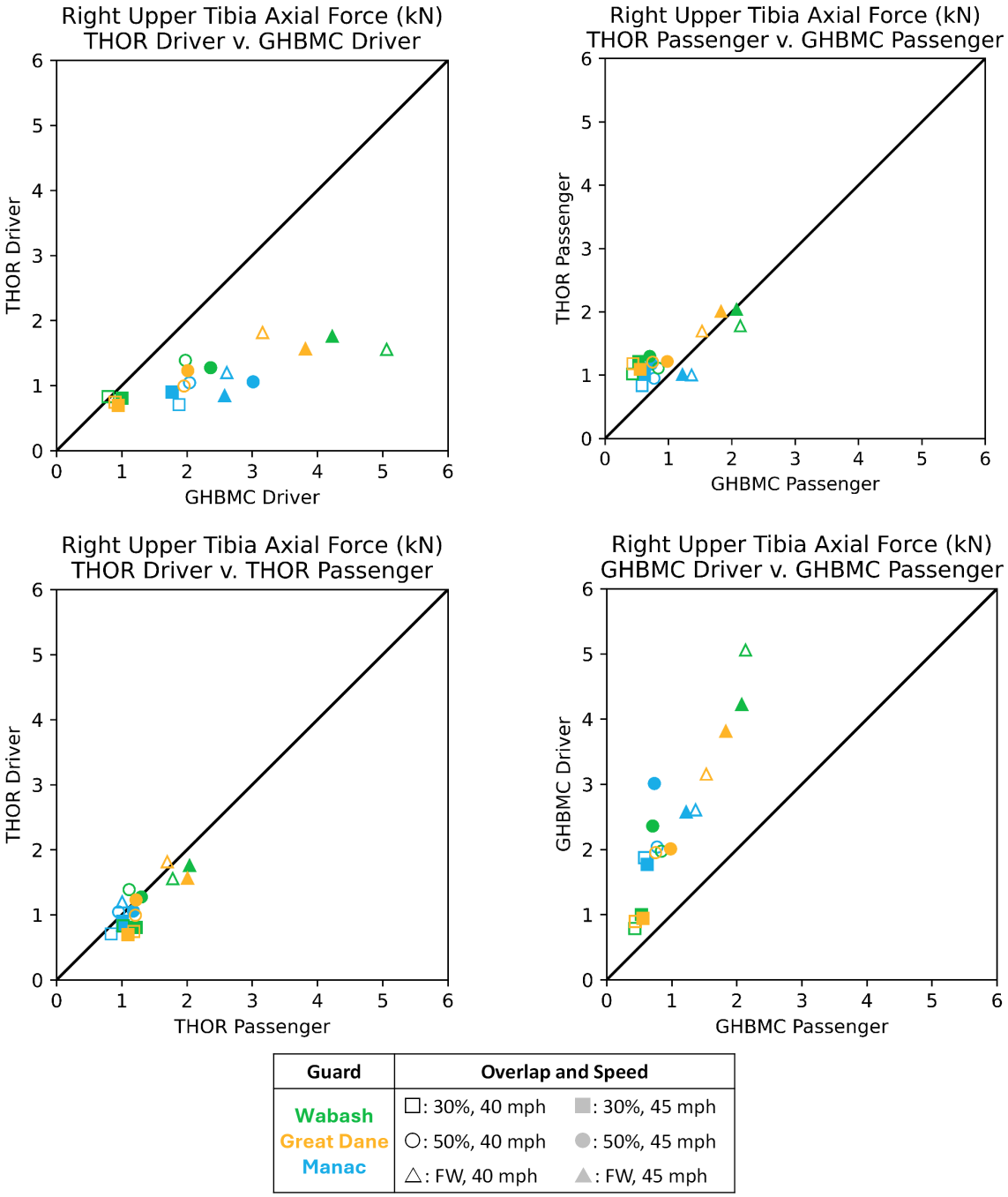

Figure 113. Peak right upper tibia force for the GHBMC and THOR-50M occupants in 40 mph and 45 mph simulations

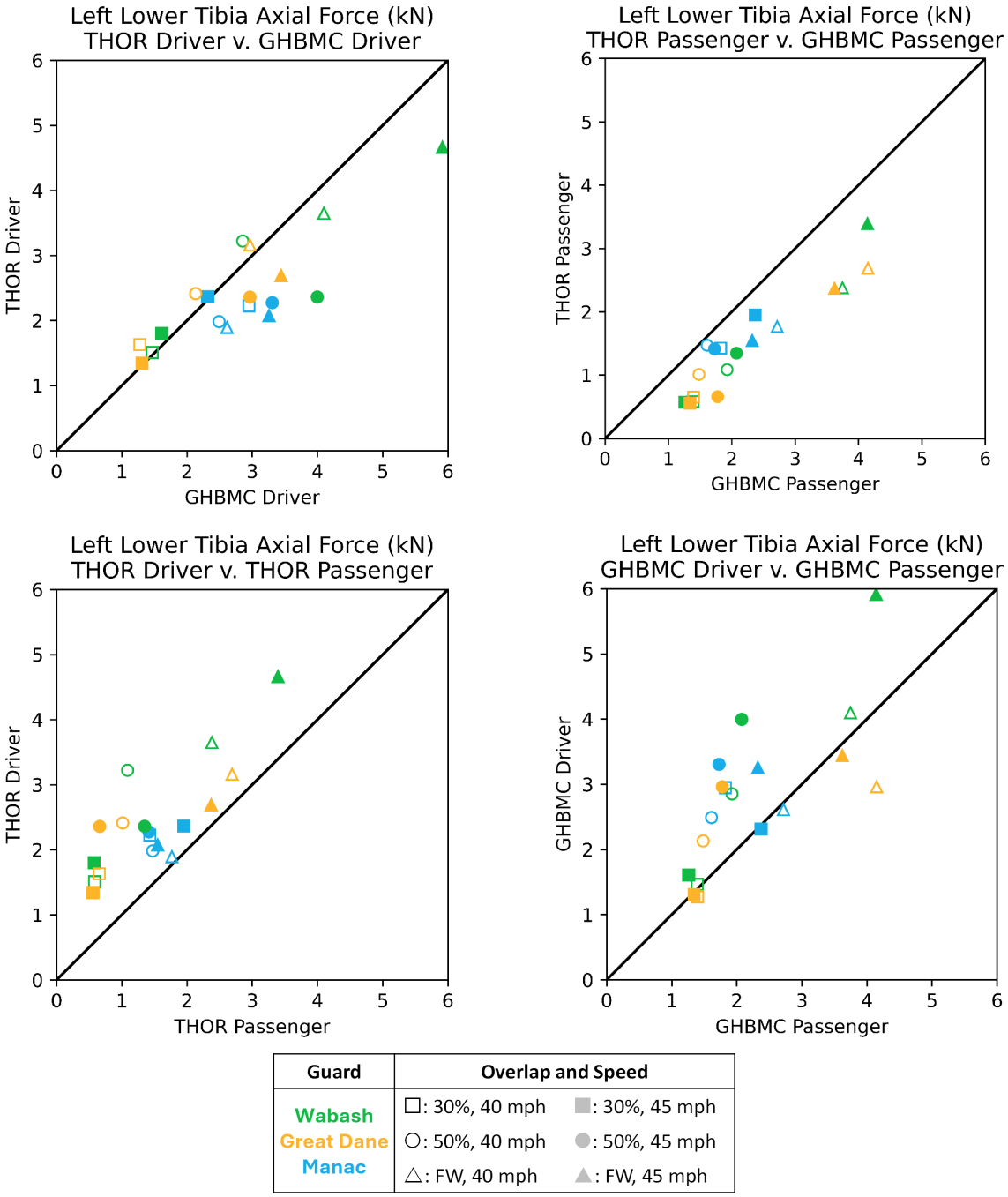

Figure 114. Peak left lower tibia force for the GHBMC and THOR-50M occupants in 40 mph and 45 mph simulations

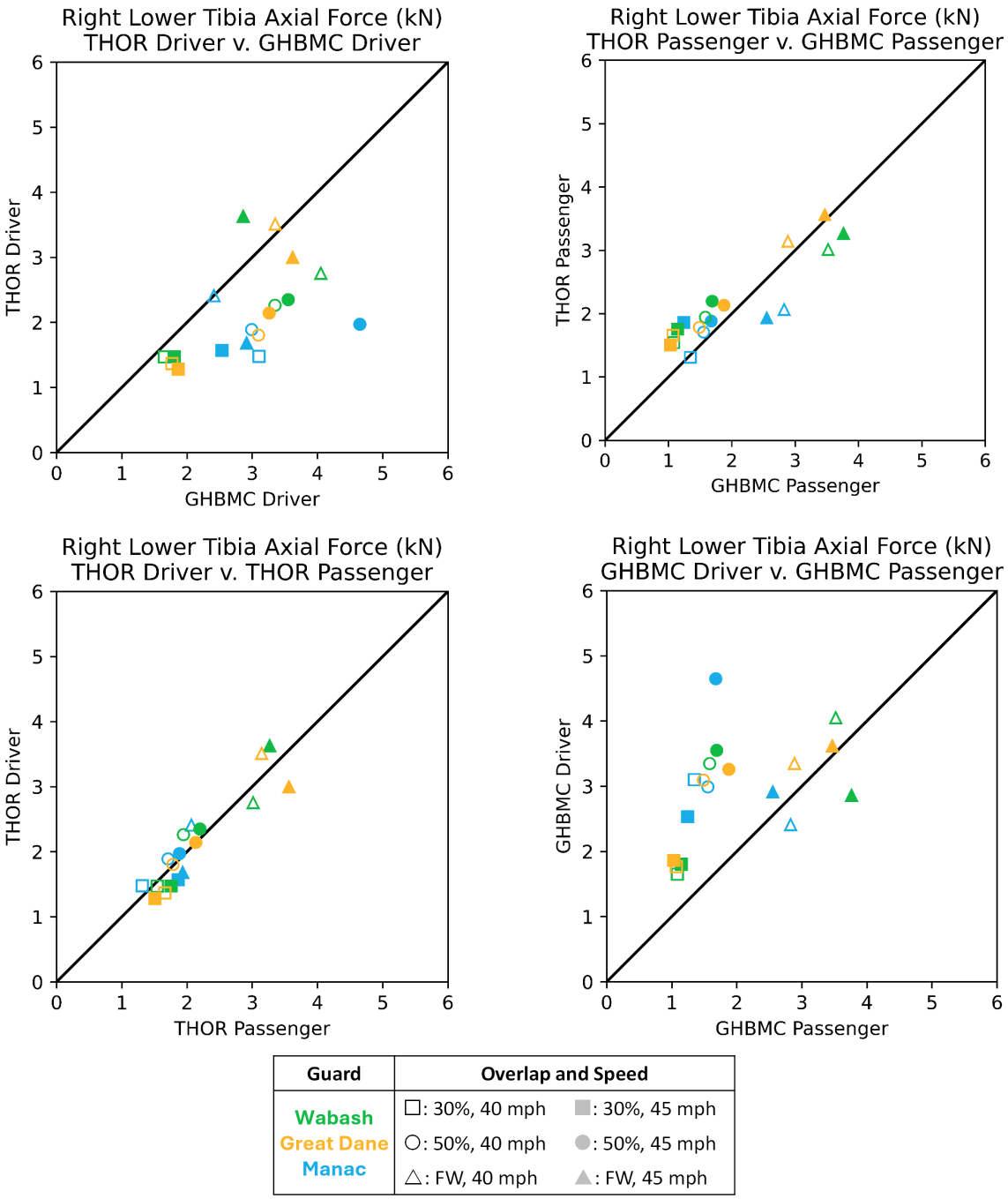

Figure 115. Peak right lower tibia force for the GHBMC and THOR-50M occupants in 40 mph and 45 mph simulations

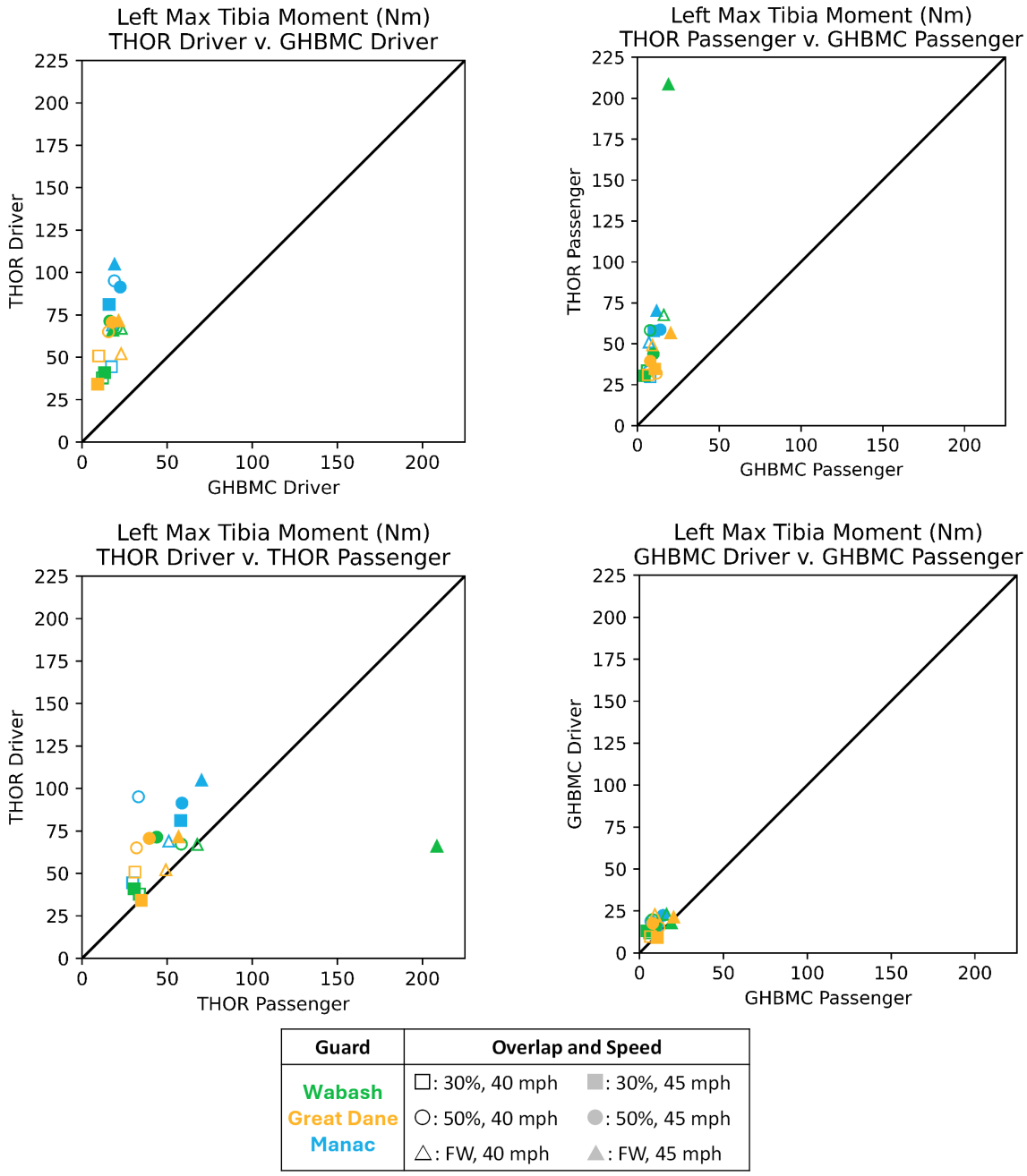

Figure 116. Peak left tibia moment for the GHBMC and THOR-50M occupants in 40 mph and 45 mph simulations

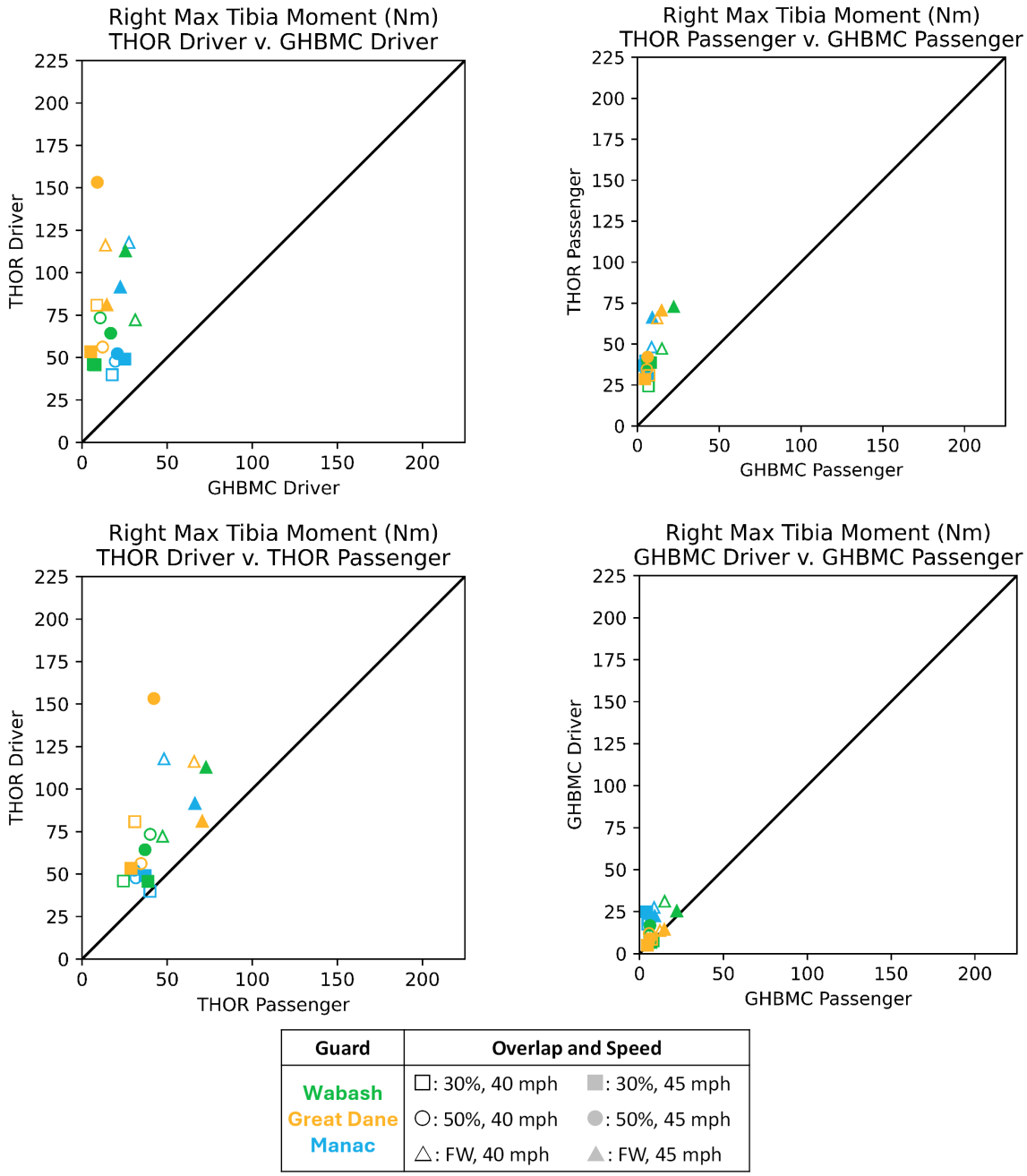

Figure 117. Peak right tibia moment for the GHBMC and THOR-50M occupants in 40 mph and 45 mph simulations

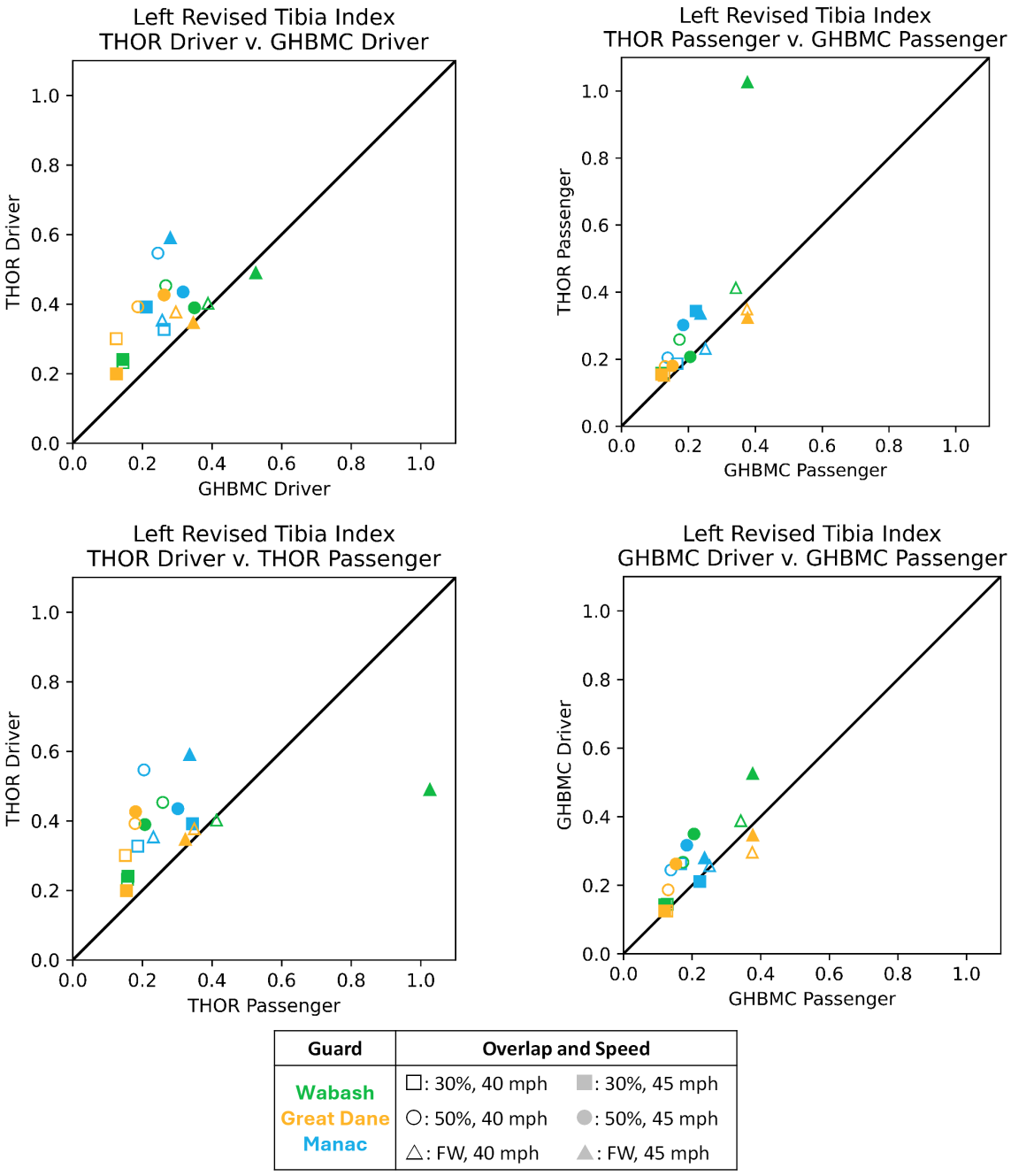

Guard	Overlap and Speed	
Wabash Great Dane Manac	□: 30%, 40 mph	■: 30%, 45 mph
	○: 50%, 40 mph	●: 50%, 45 mph
	△: FW, 40 mph	▲: FW, 45 mph

Figure 118. Left Revised tibia index for the GHBMC and THOR-50M occupants in 40 mph and 45 mph simulations

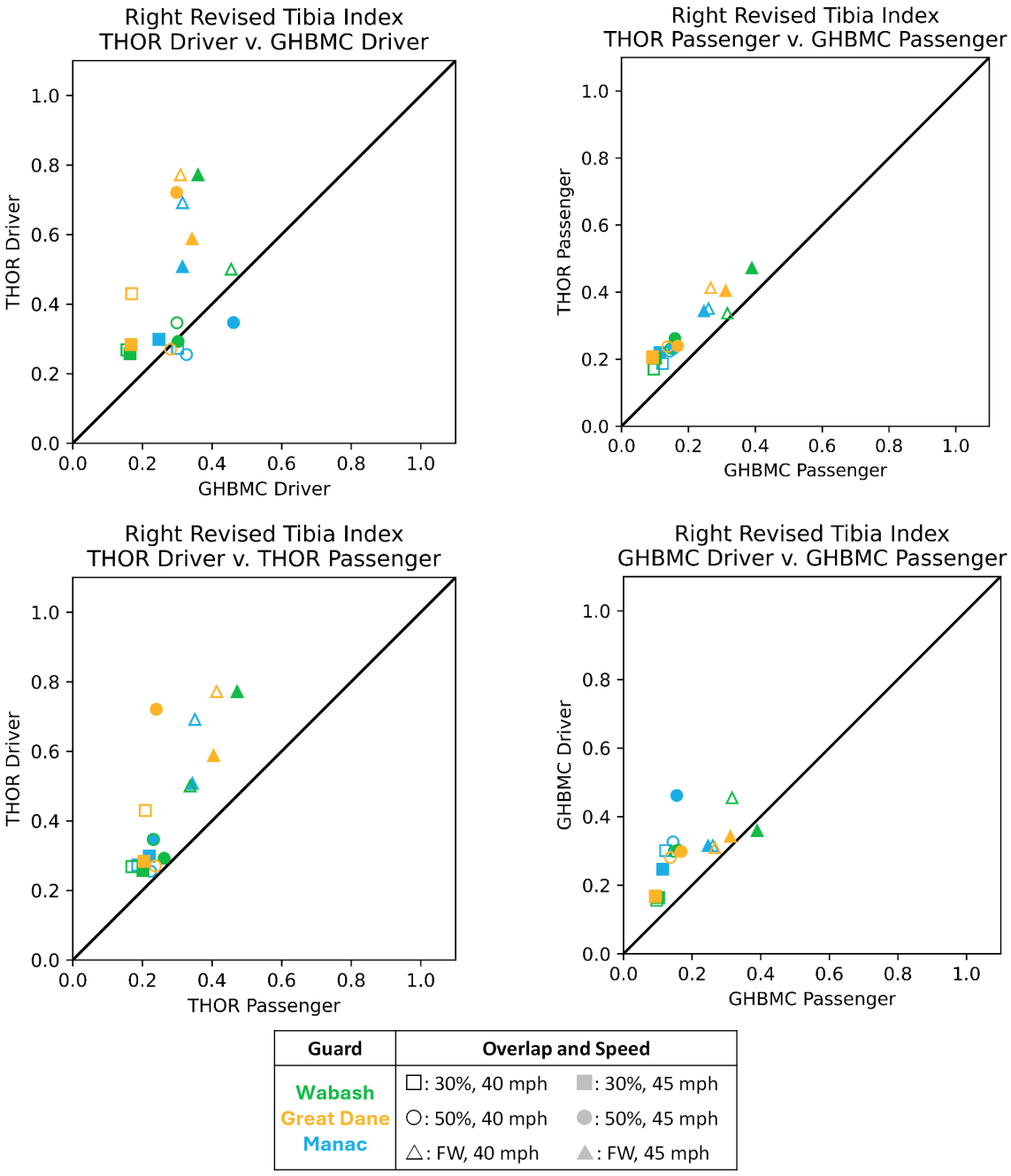

Guard	Overlap and Speed	
Wabash Great Dane Manac	□: 30%, 40 mph	■: 30%, 45 mph
	○: 50%, 40 mph	●: 50%, 45 mph
	△: FW, 40 mph	▲: FW, 45 mph

Figure 119. Right Revised tibia index for the GHBMC and THOR-50M occupants in 40 mph and 45 mph simulations

Occupant Response Summary

Each of the comparisons described above were also quantified using statistical analysis. Both the average and standard deviation of the matched-pair comparisons is provided in Table 23 and 24. As much of the data were not normally distributed, a matched pair t-test was not appropriate. Instead, a Wilcoxon signed-rank test was performed. To account for the comparisons, a Bonferroni correction was employed for each injury metric set (i.e., $\alpha = 0.05/4 = 0.0125$). Bolded entries in Table 23 and 24 represent comparisons that resulted in a statistically significant difference. To help in interpretation of the table, the reader is directed to the "THOR-50M Driver – GHBMC Driver" column and the "HIC 15" row. In this cell, the value is 200.51 ± 544.02 and is not bolded. This means that for each simulation, the GHBMC Driver HIC value was subtracted from its matched simulation THOR-50M Driver HIC value. The average difference was 200.51, indicated the THOR-50M experienced higher HIC values on average. As it is not bolded, that comparison did not meet the criteria for statistical significance.

Table 23. Summary of head, neck, and Thorax injury metric differences in the 40 mph and 45 mph simulations
(Bolded entries represent statistical significance with α=0.0125.)

Injury Metric	THOR-50M Driver - GHBMC Driver	THOR-50M Passenger - GHBMC Passenger	THOR-50M Driver - THOR-50M Passenger	GHBMC Driver - GHBMC Passenger
HIC 15	200.51 ± 544.02	**50.78 ± 93.59**	255.14 ± 579.42	**105.42 ± 61.98**
BrIC	**0.11 ± 0.13**	**0.11 ± 0.13**	**0.09 ± 0.12**	**0.09 ± 0.05**
Upper Neck Tensile Force (kN)	**0.17 ± 0.22**	**0.41 ± 0.35**	0.02 ± 0.33	**0.26 ± 0.19**
Upper Neck Flexion Moment (Nm)	**-4.50 ± 4.15**	**-9.52 ± 5.15**	**3.87 ± 5.59**	**-1.16 ± 0.65**
Nij	**-0.19 ± 0.12**	**-0.21 ± 0.11**	0.08 ± 0.15	**0.07 ± 0.07**
Thoracoabdominal Compression (mm)	0.33 ± 9.73	-0.25 ± 10.87	-1.87 ± 7.63	-1.29 ± 4.19
T6 Peak Linear Acceleration (G's)	-1.82 ± 3.09	-1.98 ± 3.30	**4.60 ± 2.74**	**4.44 ± 3.51**
Abdominal Compression (mm)	**-20.99 ± 10.74**	-4.54 ± 9.41	**-17.83 ± 6.93**	-1.38 ± 7.04
Lumbar Tensile Load (kN)	-0.12 ± 0.26	-0.02 ± 0.26	**-0.67 ± 0.37**	**-0.58 ± 0.28**
Lumbar Compressive Load (kN)	**0.64 ± 0.34**	**0.88 ± 0.17**	**0.38 ± 0.40**	**0.62 ± 0.21**

Table 24. Summary of pelvis and lower extremity injury metric differences in the 40 mph and 45 mph simulations
(Bolded entries represent statistical significance with α=0.0125.)

Injury Metric	THOR-50M Driver - GHBMC Driver	THOR-50M Passenger - GHBMC Passenger	THOR-50M Driver - THOR-50M Passenger	GHBMC Driver - GHBMC Passenger
Pelvis Peak Linear Acceleration (G's)	**-5.67 ± 4.55**	**-3.66 ± 2.57**	**3.61 ± 3.93**	**5.62 ± 4.47**
Left Femur Force (kN)	0.35 ± 0.78	**1.89 ± 0.55**	-0.30 ± 1.01	1.24 ± 0.90
Right Femur Force (kN)	**0.90 ± 0.73**	**0.58 ± 0.36**	**1.87 ± 0.82**	**1.55 ± 0.52**
Left Upper Tibia Force (kN)	-0.26 ± 0.38	**-0.25 ± 0.24**	**0.47 ± 0.27**	**0.47 ± 0.51**
Right Upper Tibia Force (kN)	**-1.20 ± 0.89**	**0.26 ± 0.32**	-0.13 ± 0.21	**1.33 ± 0.68**
Left Lower Tibia Force (kN)	-0.41 ± 0.60	**-0.78 ± 0.35**	**0.93 ± 0.50**	0.56 ± 0.78
Right Lower Tibia Force (kN)	**-0.82 ± 0.75**	0.14 ± 0.43	-0.01 ± 0.27	**0.95 ± 0.89**
Left Tibia Moment (Nm)	**48.40 ± 17.22**	**44.47 ± 36.94**	**10.83 ± 40.15**	**6.89 ± 4.28**
Right Tibia Moment (Nm)	**58.90 ± 30.91**	**35.15 ± 11.51**	**31.53 ± 25.44**	**7.78 ± 7.04**
Left Upper Tibia Index	**0.12 ± 0.09**	**0.10 ± 0.18**	**0.07 ± 0.15**	**0.05 ± 0.06**
Right Upper Tibia Index	**0.14 ± 0.18**	**0.09 ± 0.03**	**0.16 ± 0.13**	**0.11 ± 0.07**

This page is intentionally left blank.

Appendix D: THOR-50M and GHBMC Occupant Data Channels from Dynamic Crash Simulations

Strengthened Wabash 40 mph, 30 Percent Overlap

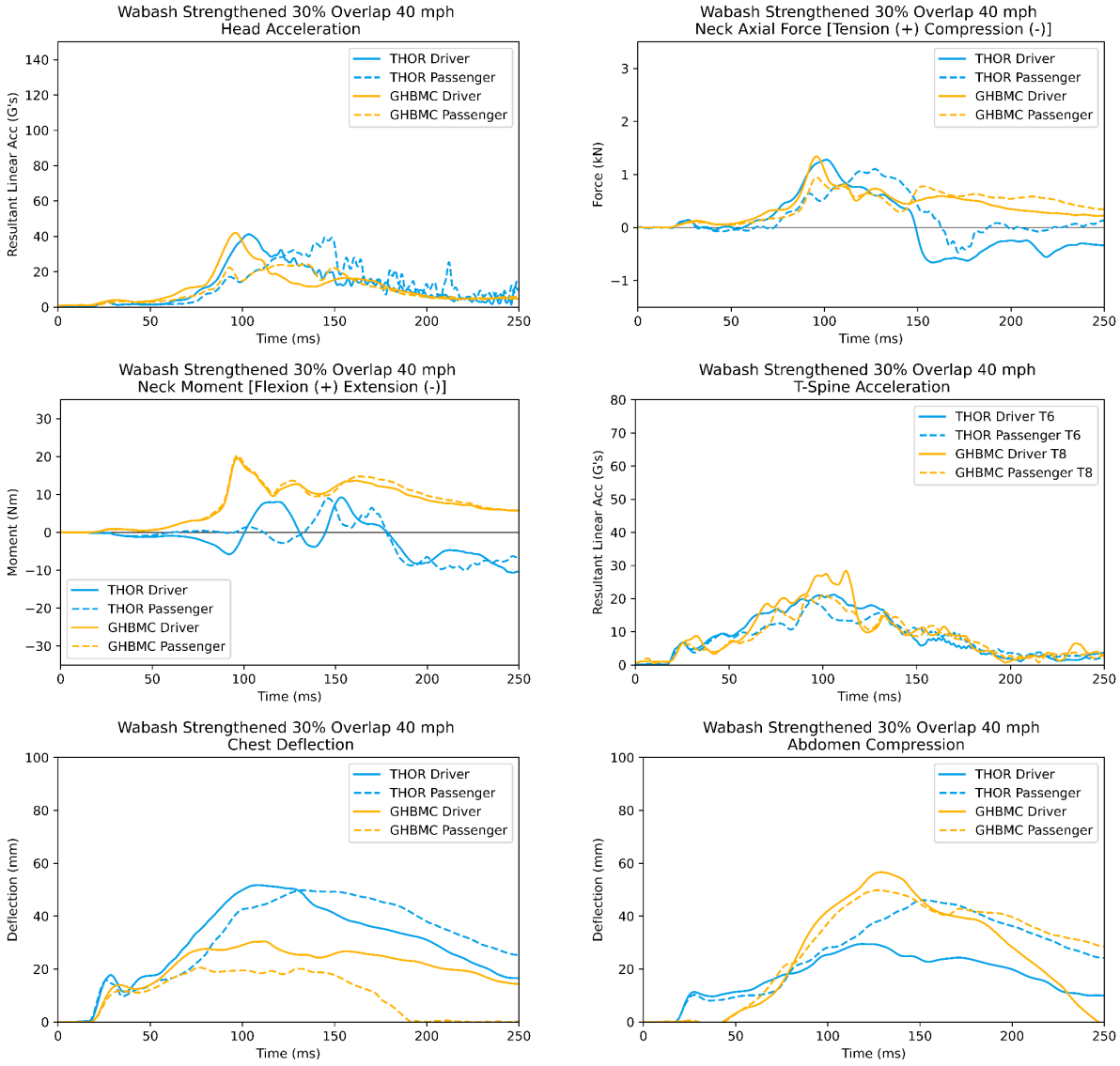

Figure 120. Strengthened Wabash 40 mph, 30 percent overlap THOR-50M and GHBMC upper body data channels

Figure 121. Strengthened Wabash 40 mph, 30 percent overlap THOR-50M and GHBMC lower body data channels

Strengthened Wabash 40 mph, 50 Percent Overlap

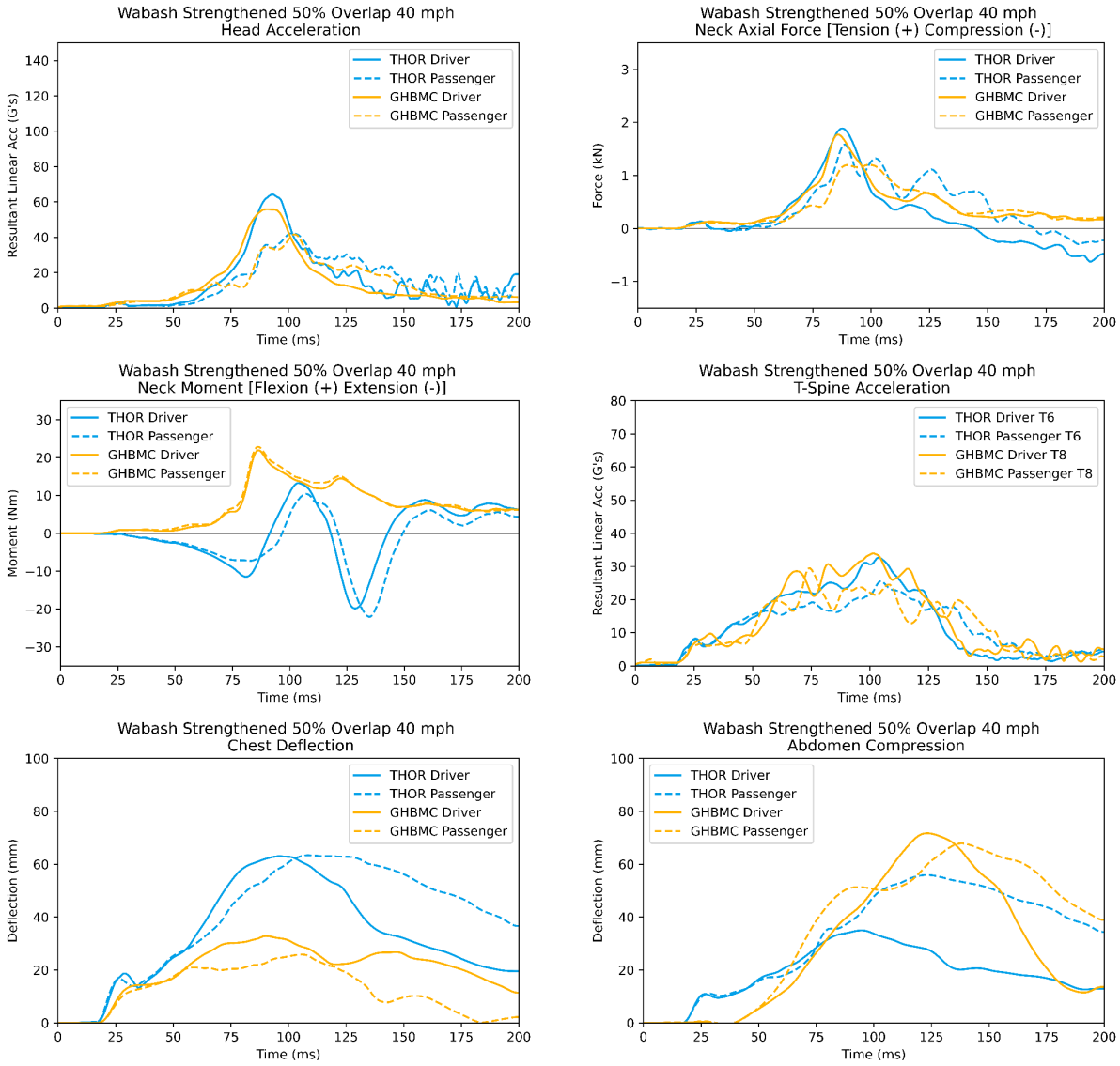

Figure 122. Strengthened Wabash 40 mph, 30 percent overlap THOR-50M and GHBMC upper body data channels

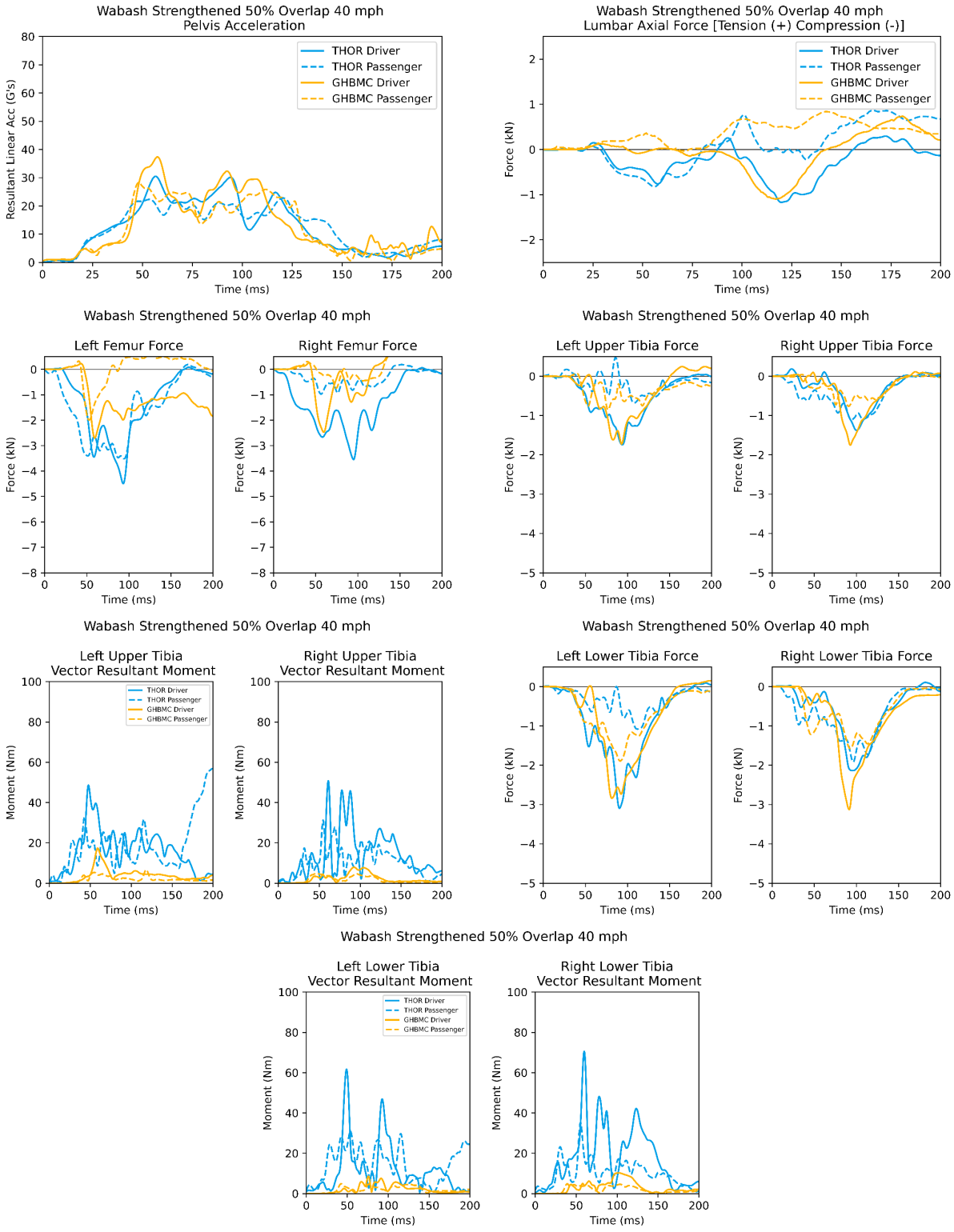

Figure 123. Strengthened Wabash 40 mph, 30 percent overlap THOR-50M and GHBMC lower body data channels

Strengthened Wabash 40 mph, Full Width Overlap

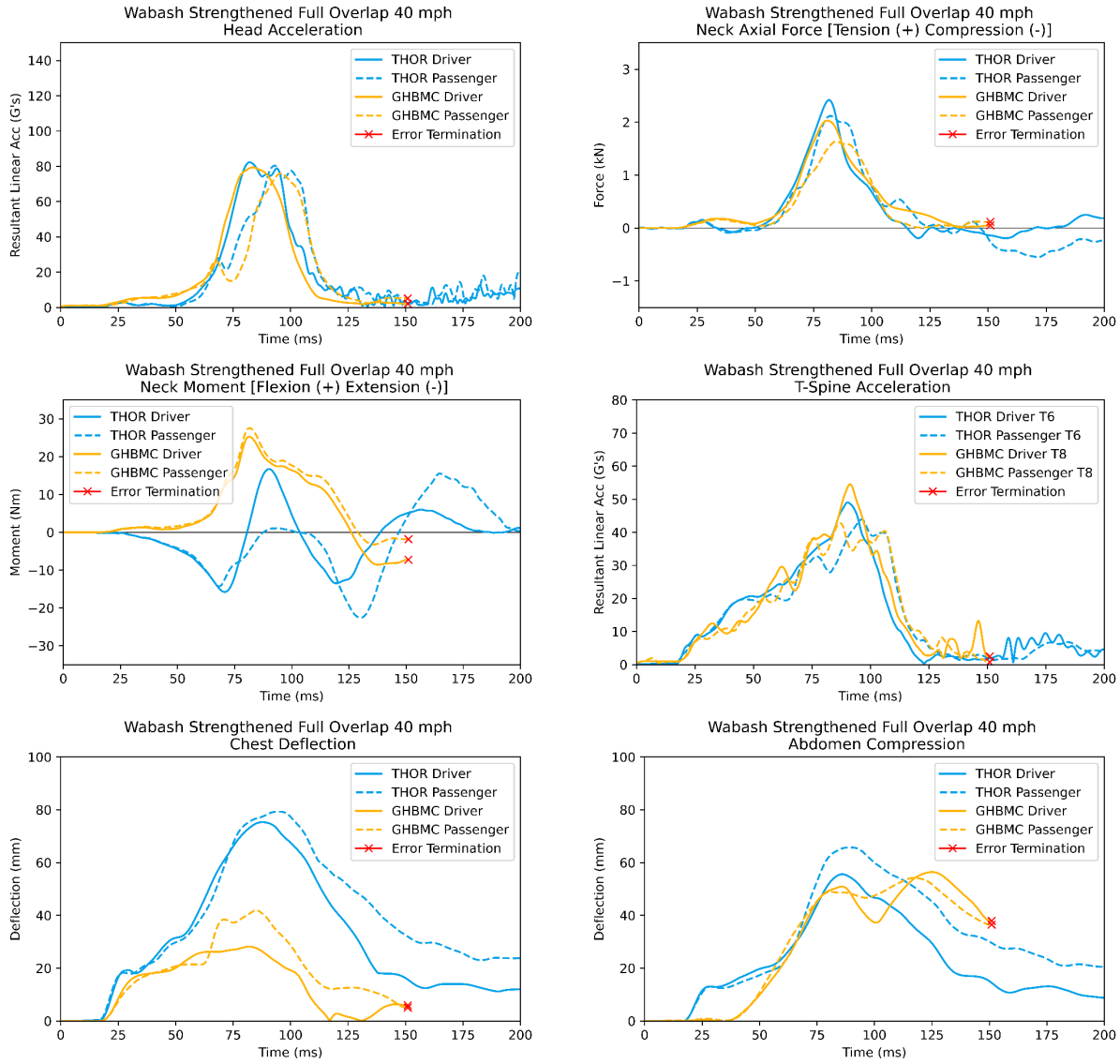

Figure 124. Strengthened Wabash 40 mph, full width overlap THOR-50M and GHBMC upper body data channels

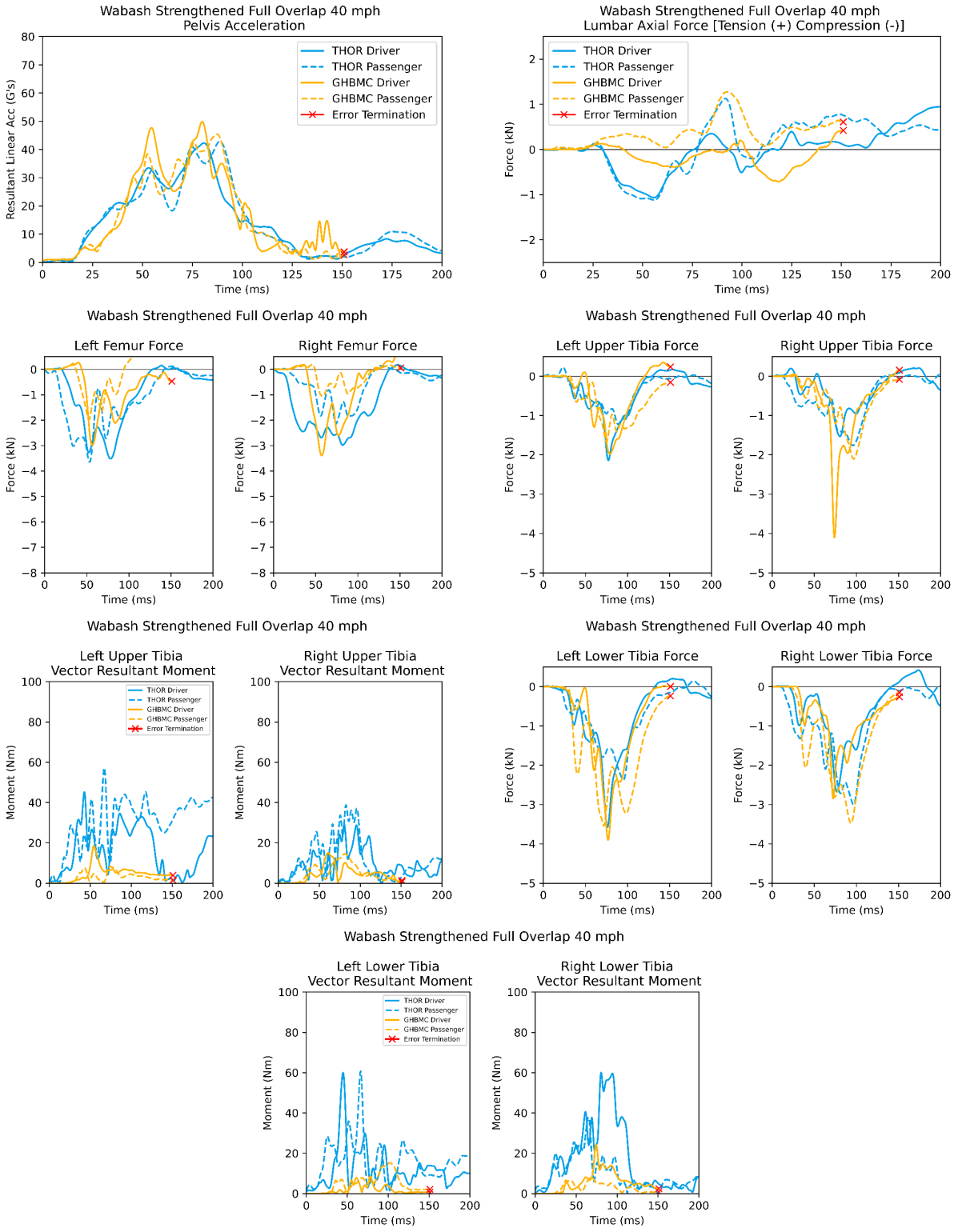

Figure 125. Strengthened Wabash 40 mph, full width overlap THOR-50M and GHBMC lower body data channels

Strengthened Wabash 45 mph, 30 Percent Overlap

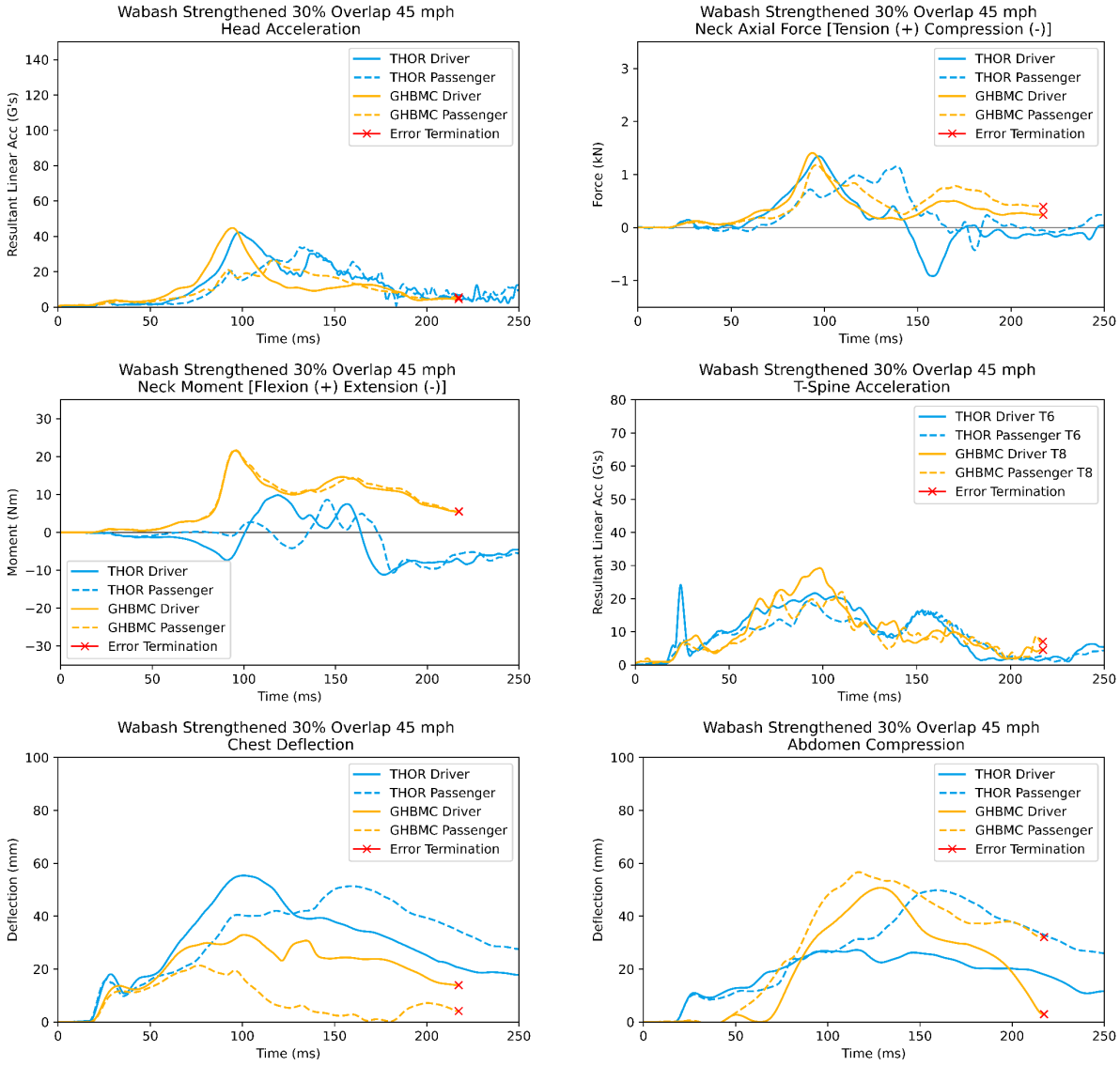

Figure 126. Strengthened Wabash 45 mph, 30 percent overlap THOR-50M and GHBMC upper body data channels

Figure 127. Strengthened Wabash 45 mph, 30 percent overlap THOR-50M and GHBMC lower body data channels

Strengthened Wabash 45 mph, 50 Percent Overlap

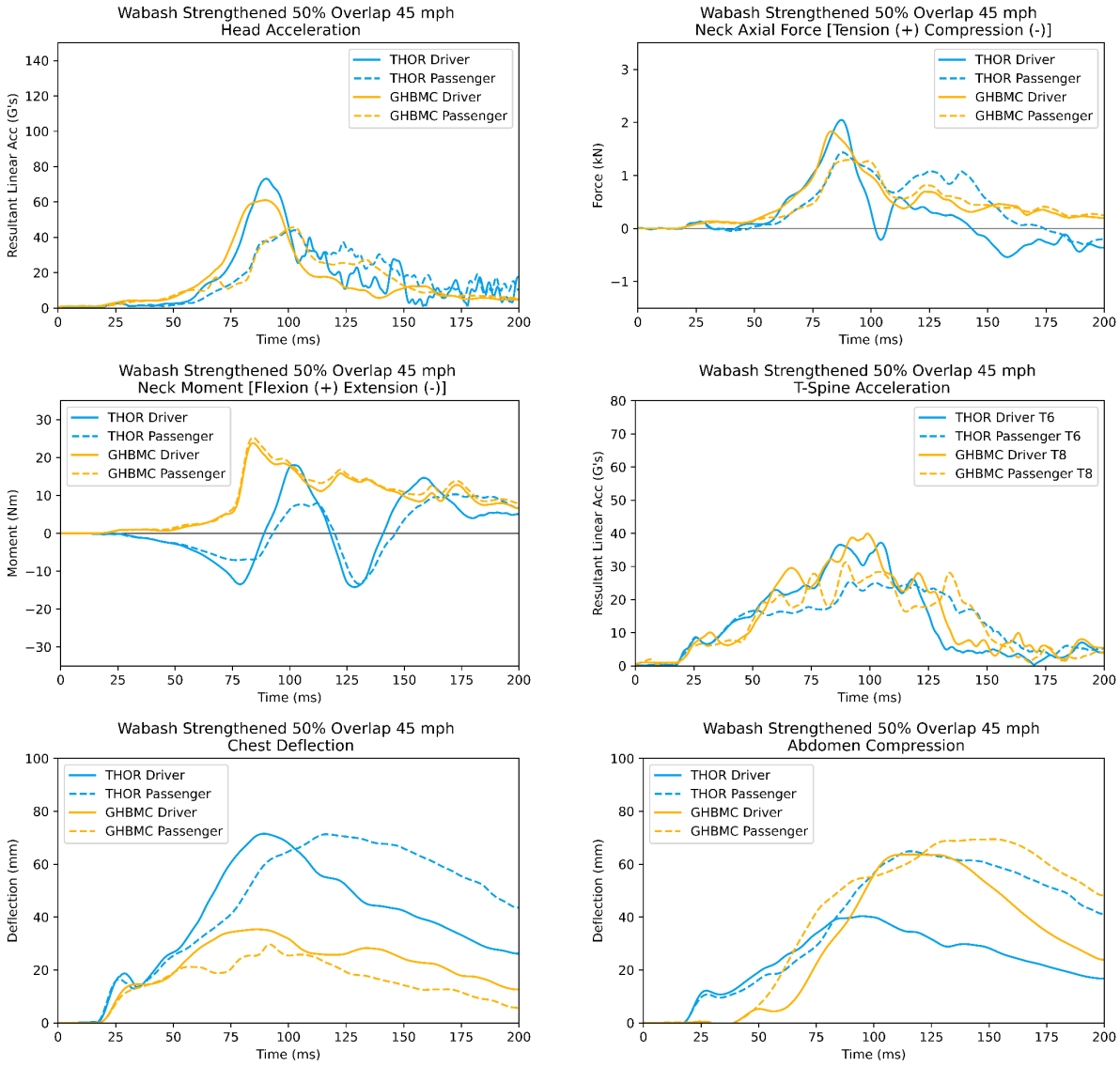

Figure 128. Strengthened Wabash 45 mph, 50 percent overlap THOR-50M and GHBMC upper body data channels

Figure 129. Strengthened Wabash 45 mph, 50 percent overlap THOR-50M and GHBMC lower body data channels

Strengthened Wabash 45 mph, Full Width Overlap

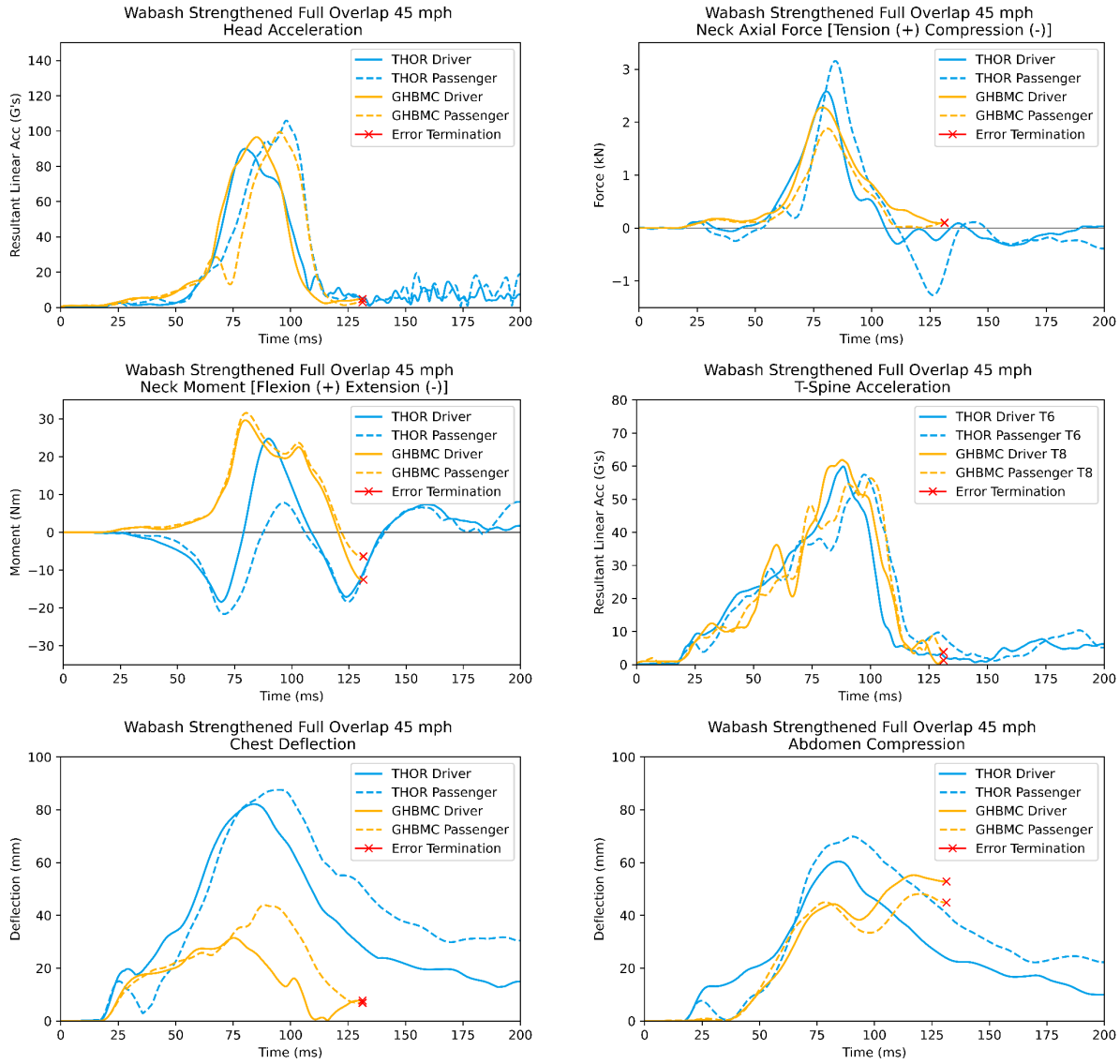

Figure 130. Strengthened Wabash 45 mph, full width overlap THOR-50M and GHBMC upper body data channels

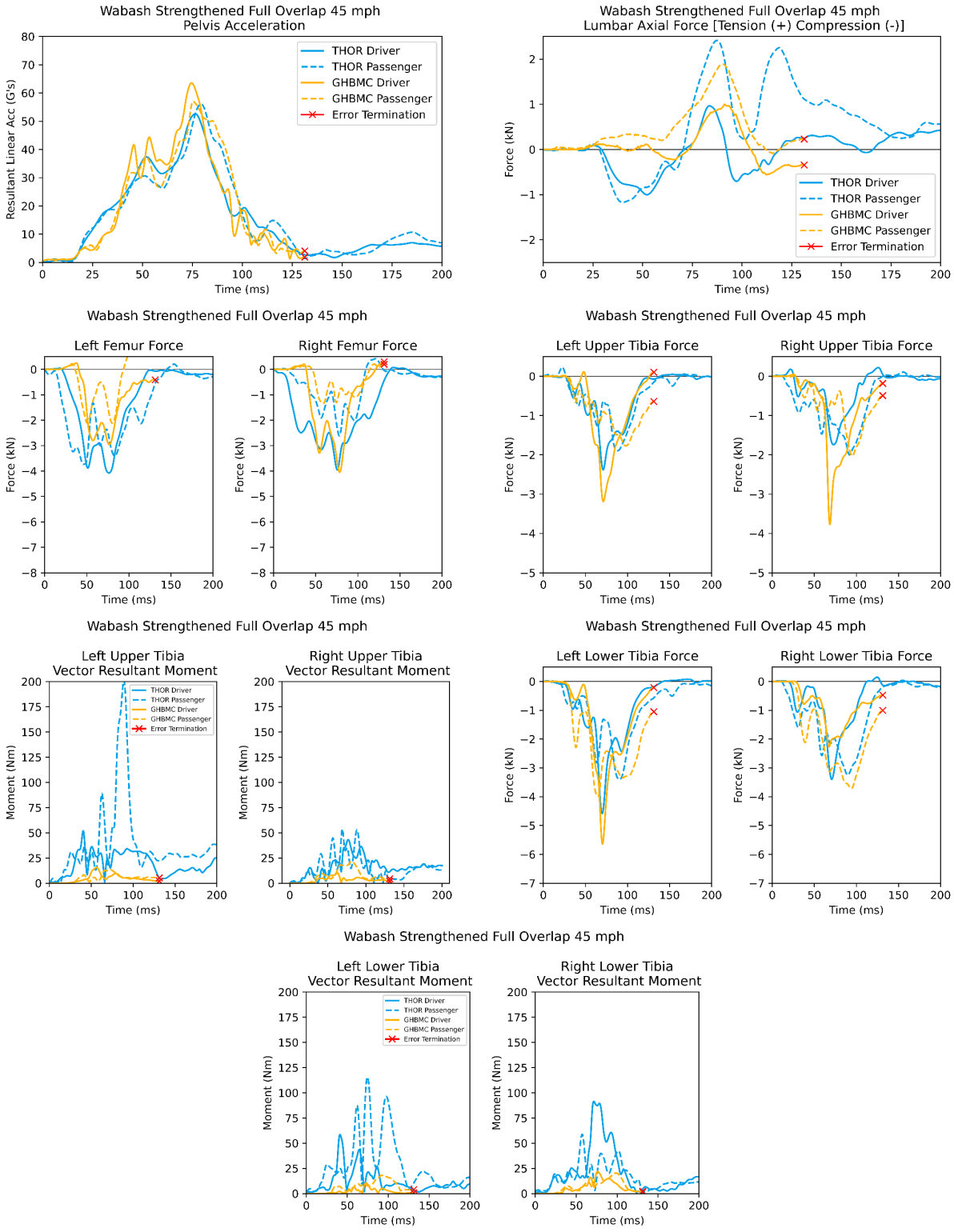

Figure 131. Strengthened Wabash 45 mph, full width overlap THOR-50M and GHBMC lower body data channels

Strengthened Manac 40 mph, 30 Percent Overlap

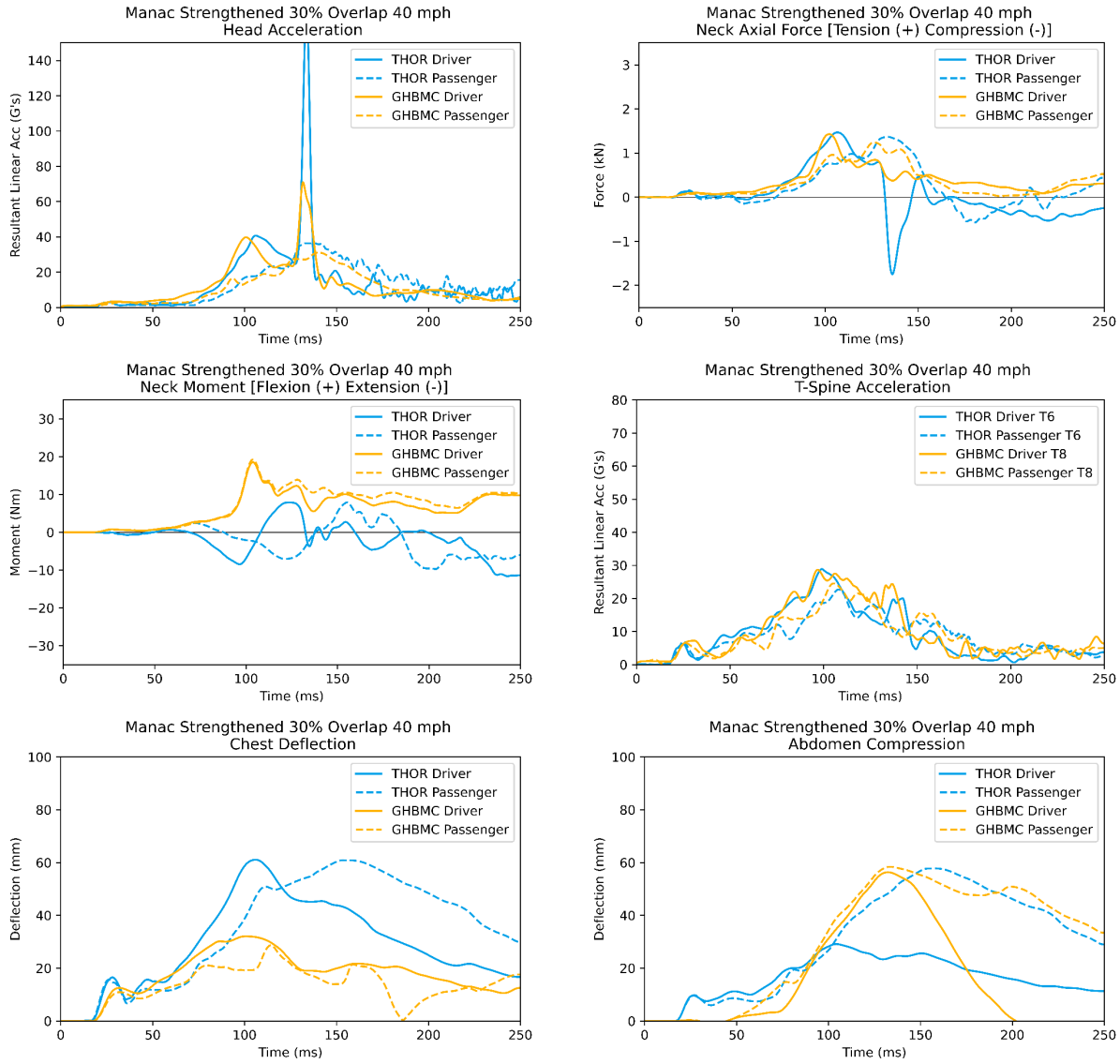

Figure 132. Strengthened Manac 40 mph, 30 percent overlap THOR-50M and GHBMC upper body data channels

Figure 133. Strengthened Manac 40 mph, 30 percent overlap THOR-50M and GHBMC lower body data channels

Strengthened Manac 40 mph, 50 Percent Overlap

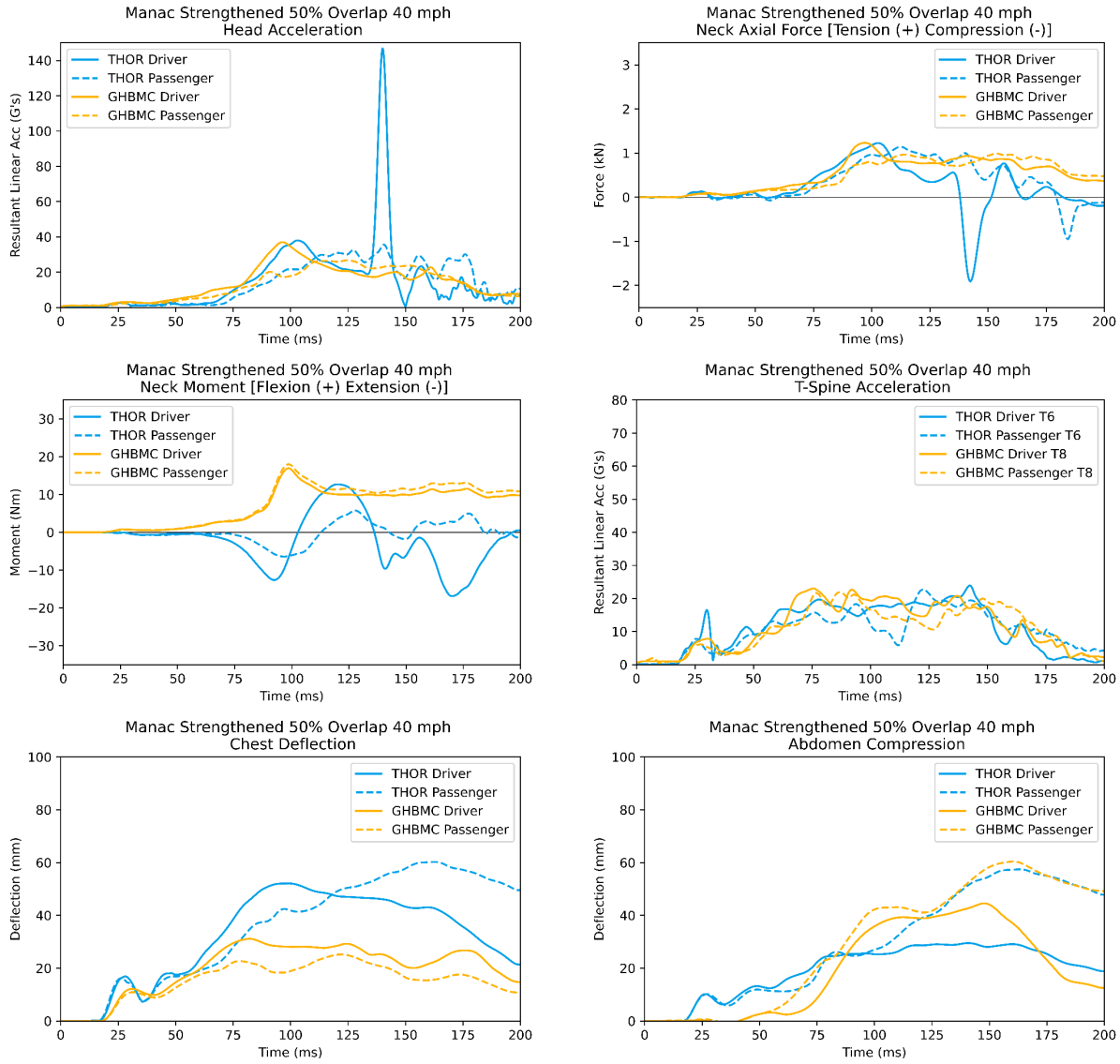

Figure 134. Strengthened Manac 40 mph, 50 percent overlap THOR-50M and GHBMC upper body data channels

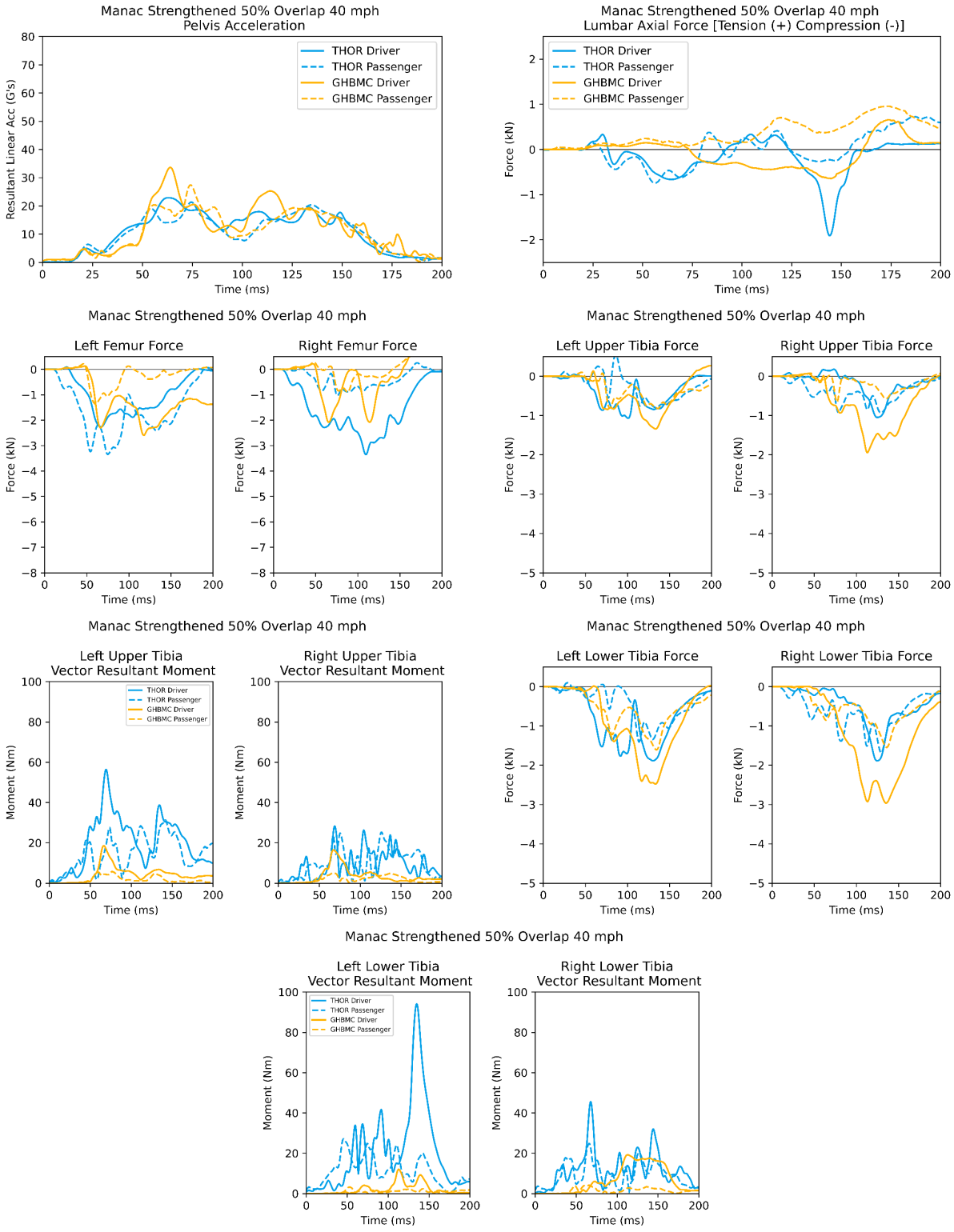

Figure 135. Strengthened Manac 40 mph, 50 percent overlap THOR-50M and GHBMC lower body data channels

Strengthened Manac 40 mph, Full Width Overlap

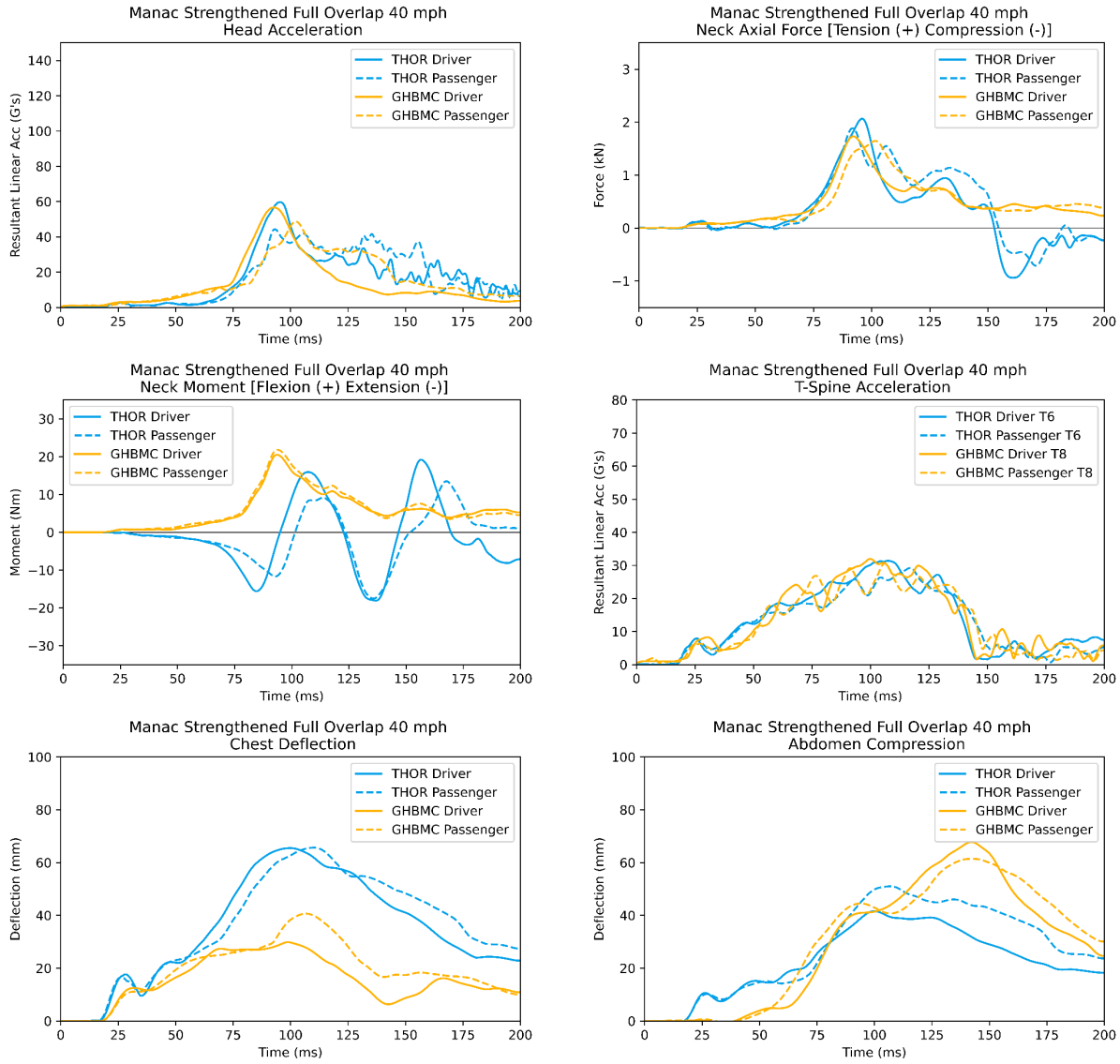

Figure 136. Strengthened Manac 40 mph, full width overlap THOR-50M and GHBMC upper body data channels

Figure 137. Strengthened Manac 40 mph, full width overlap THOR-50M and GHBMC lower body data channels

Strengthened Manac 45 mph, 30 Percent Overlap

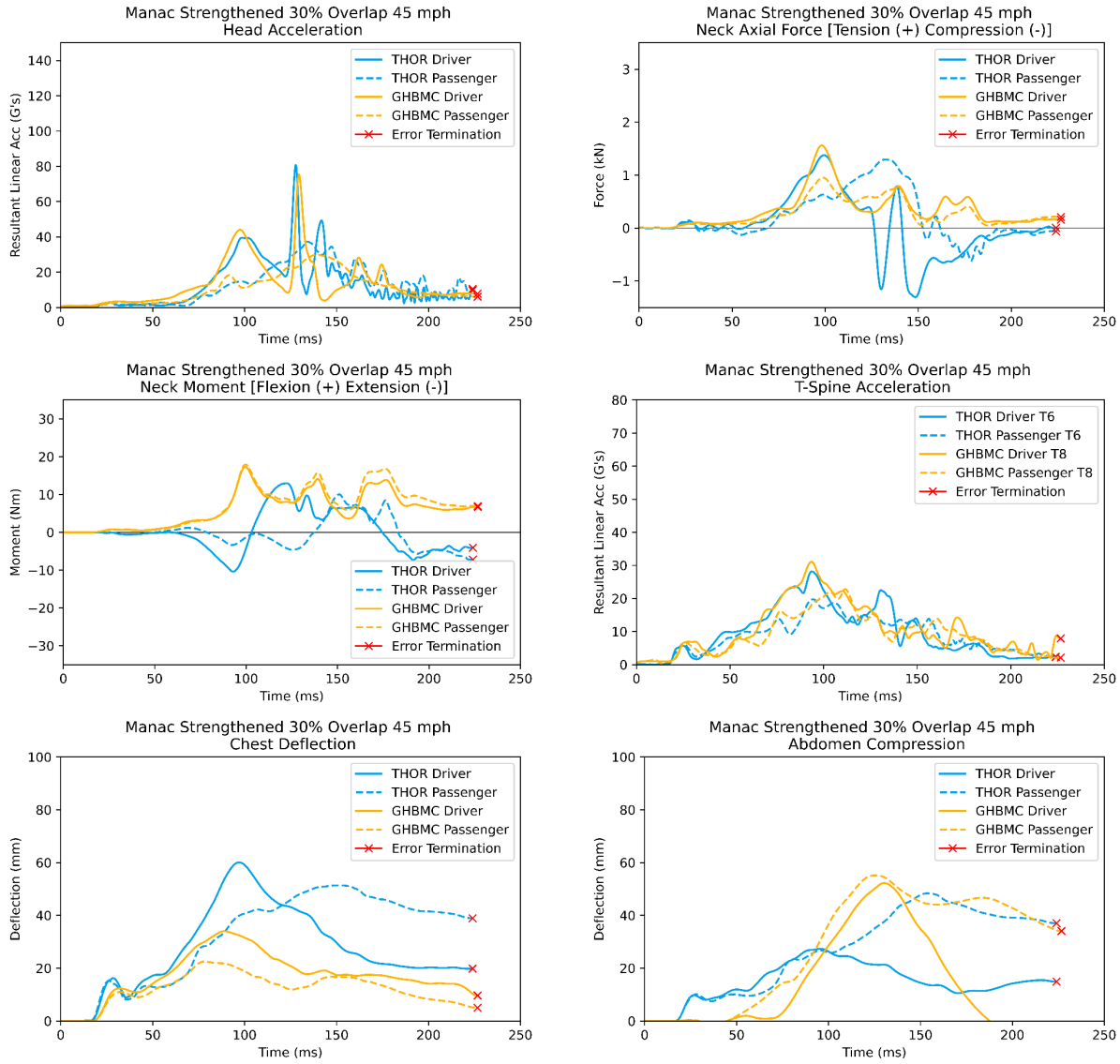

Figure 138. Strengthened Manac 45 mph, 30 percent overlap THOR-50M and GHBMC upper body data channels

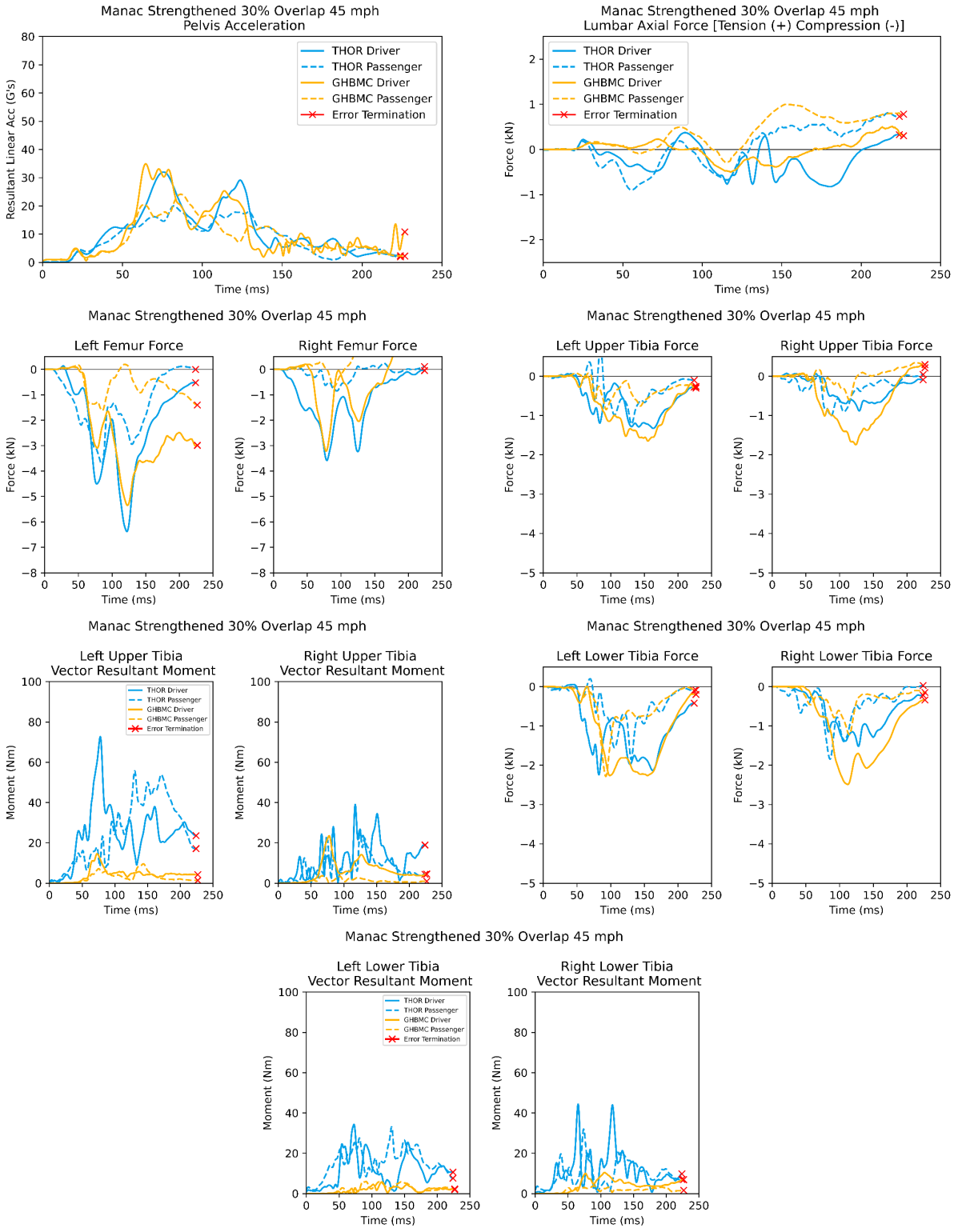

Figure 139. Strengthened Manac 45 mph, 30 percent overlap THOR-50M and GHBMC lower body data channels

Strengthened Manac 45 mph, 50 Percent Overlap

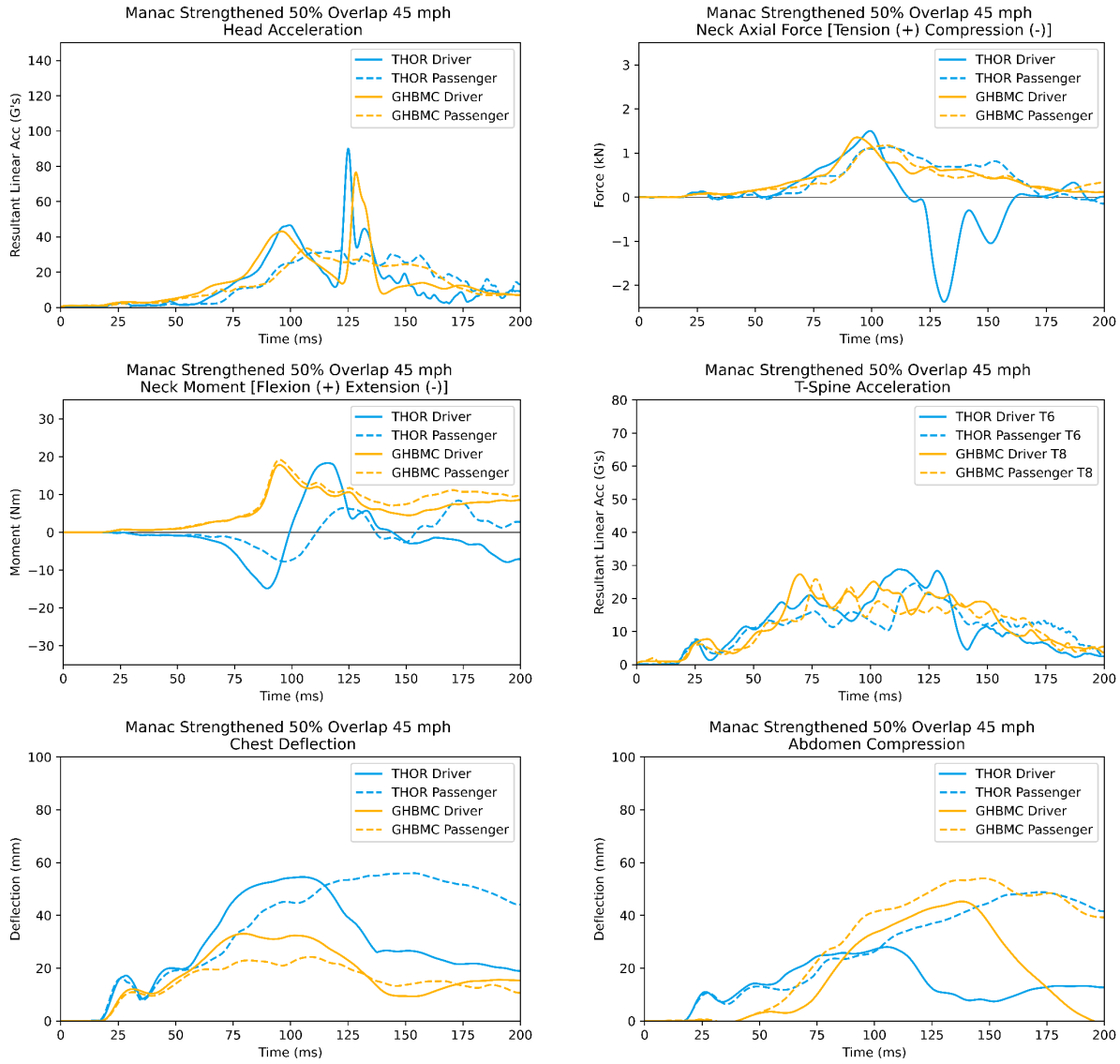

Figure 140. Strengthened Manac 45 mph, 50 percent overlap THOR-50M and GHBMC upper body data channels

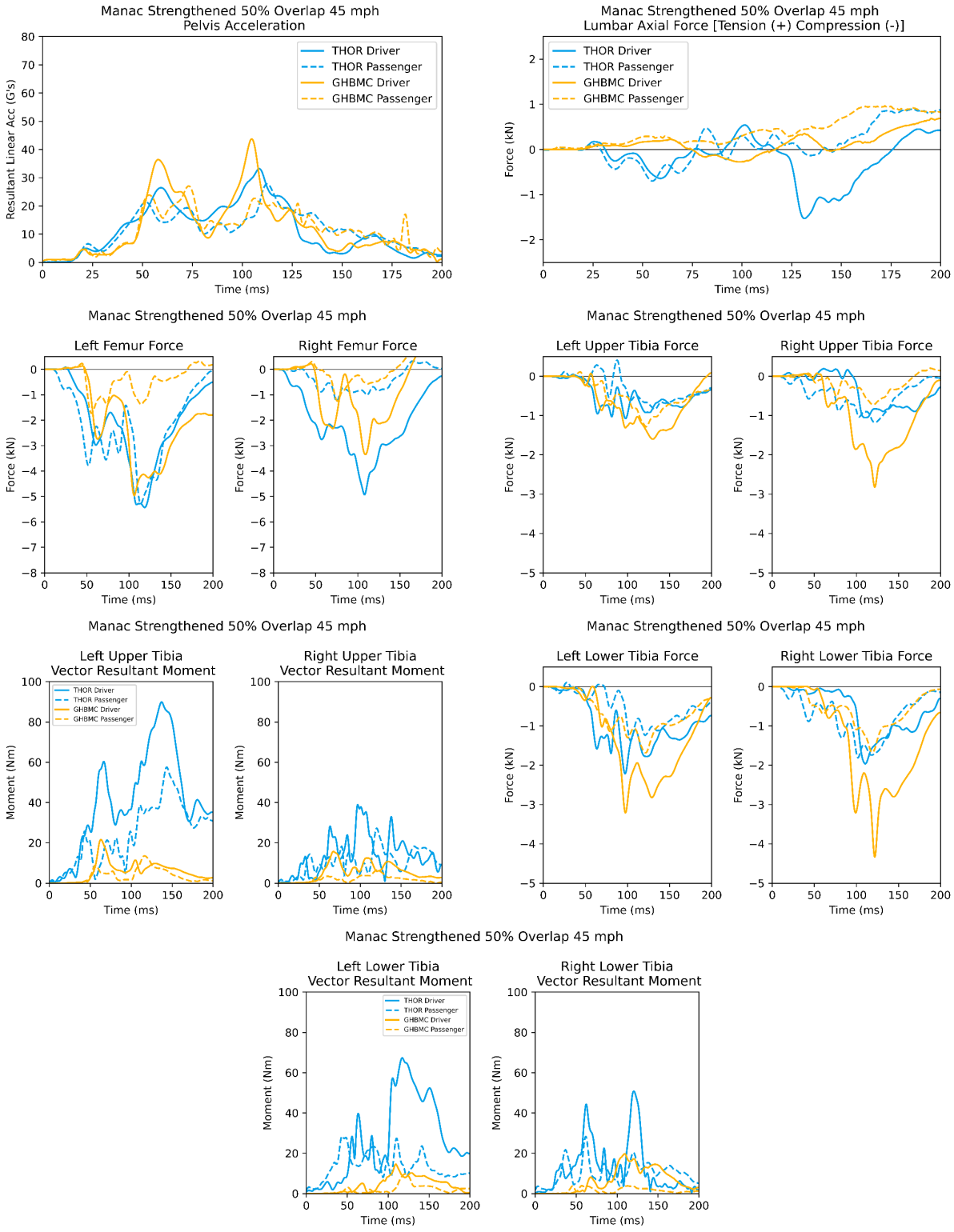

Figure 141. Strengthened Manac 45 mph, 50 percent overlap THOR-50M and GHBMC lower body data channels

Strengthened Manac 45 mph, Full Width Overlap

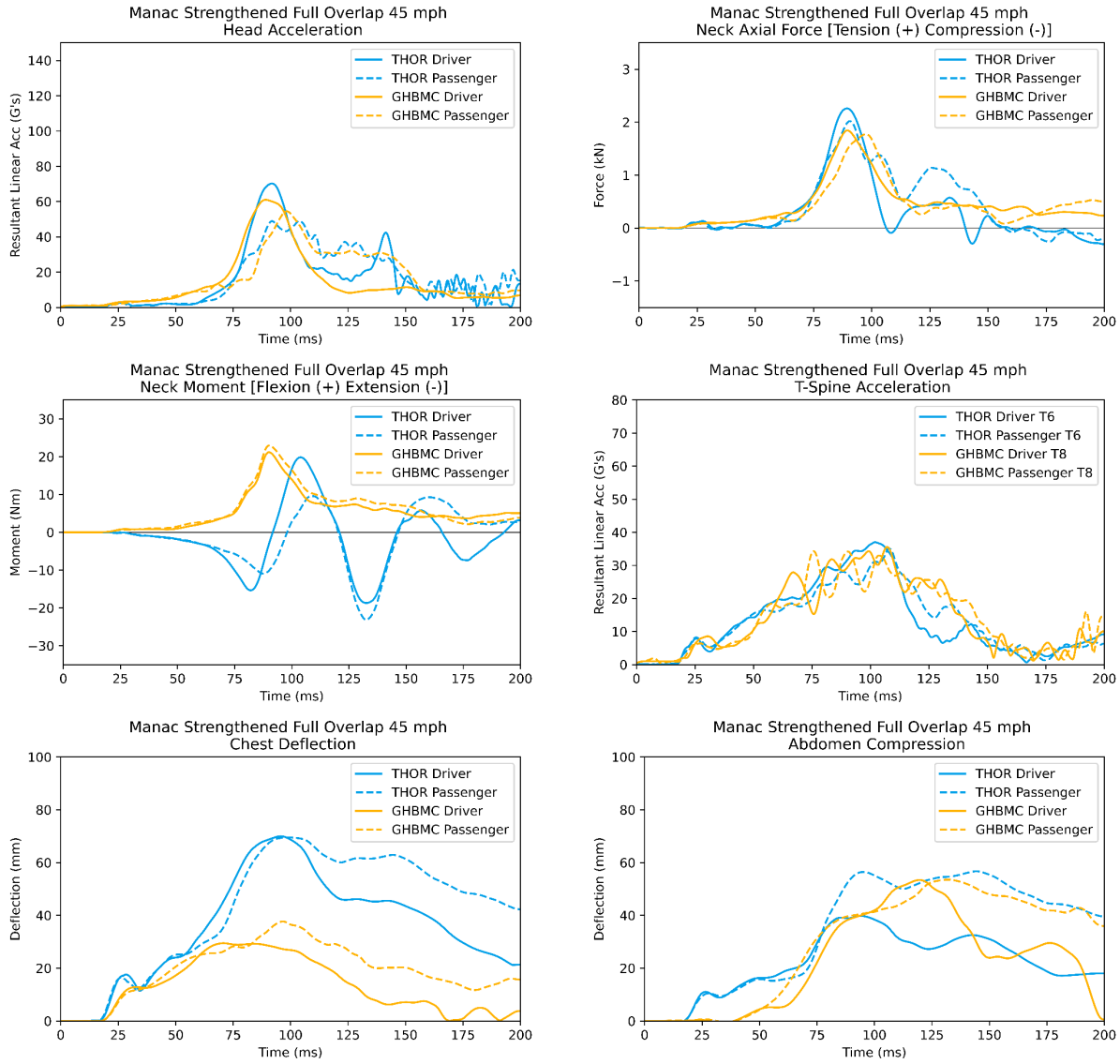

Figure 142. Strengthened Manac 45 mph, full width overlap THOR-50M and GHBMC upper body data channels

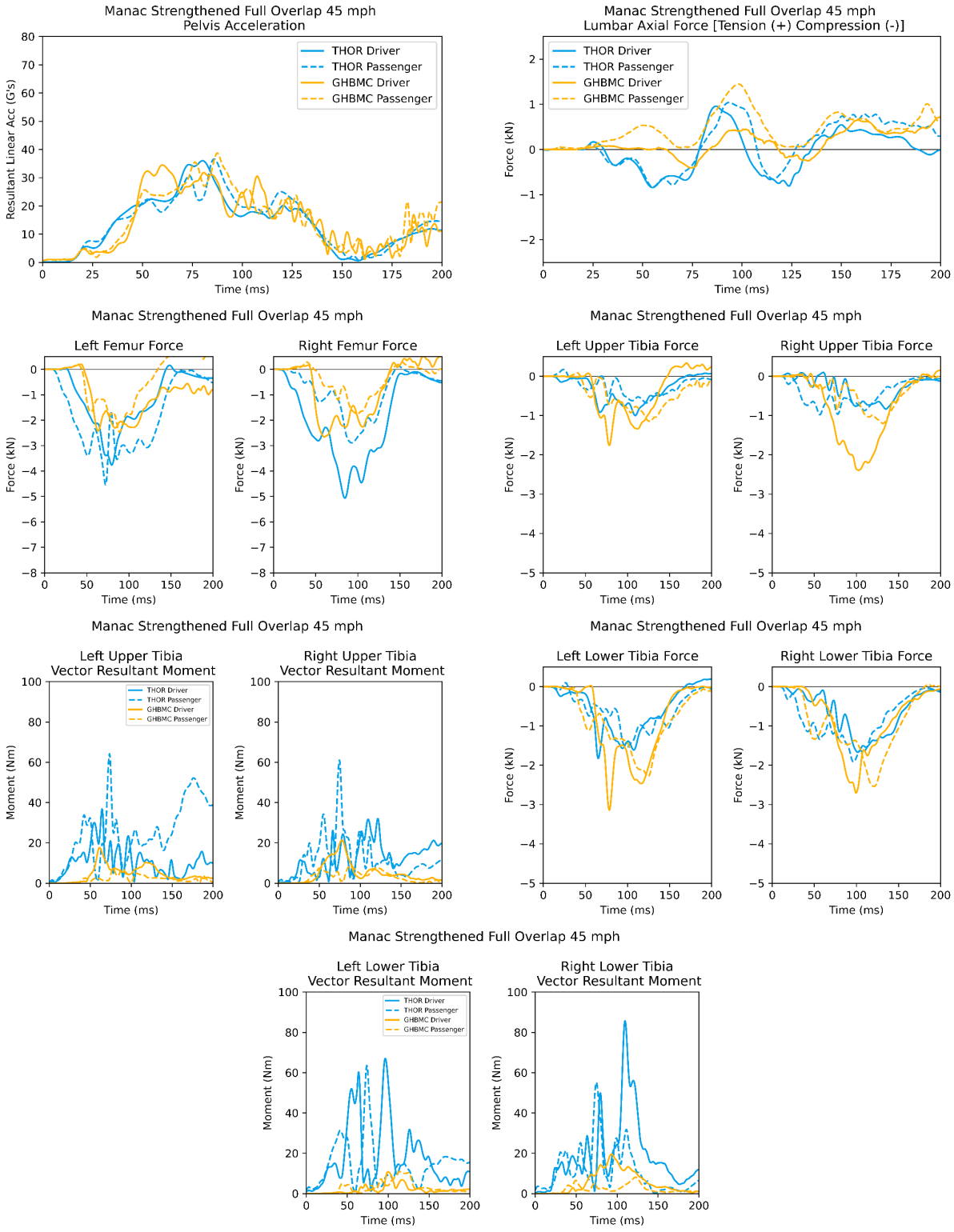

Figure 143. Strengthened Manac 45 mph, full width overlap THOR-50M and GHBMC lower body data channels

Strengthened Great Dane 40 mph, 30 Percent Overlap

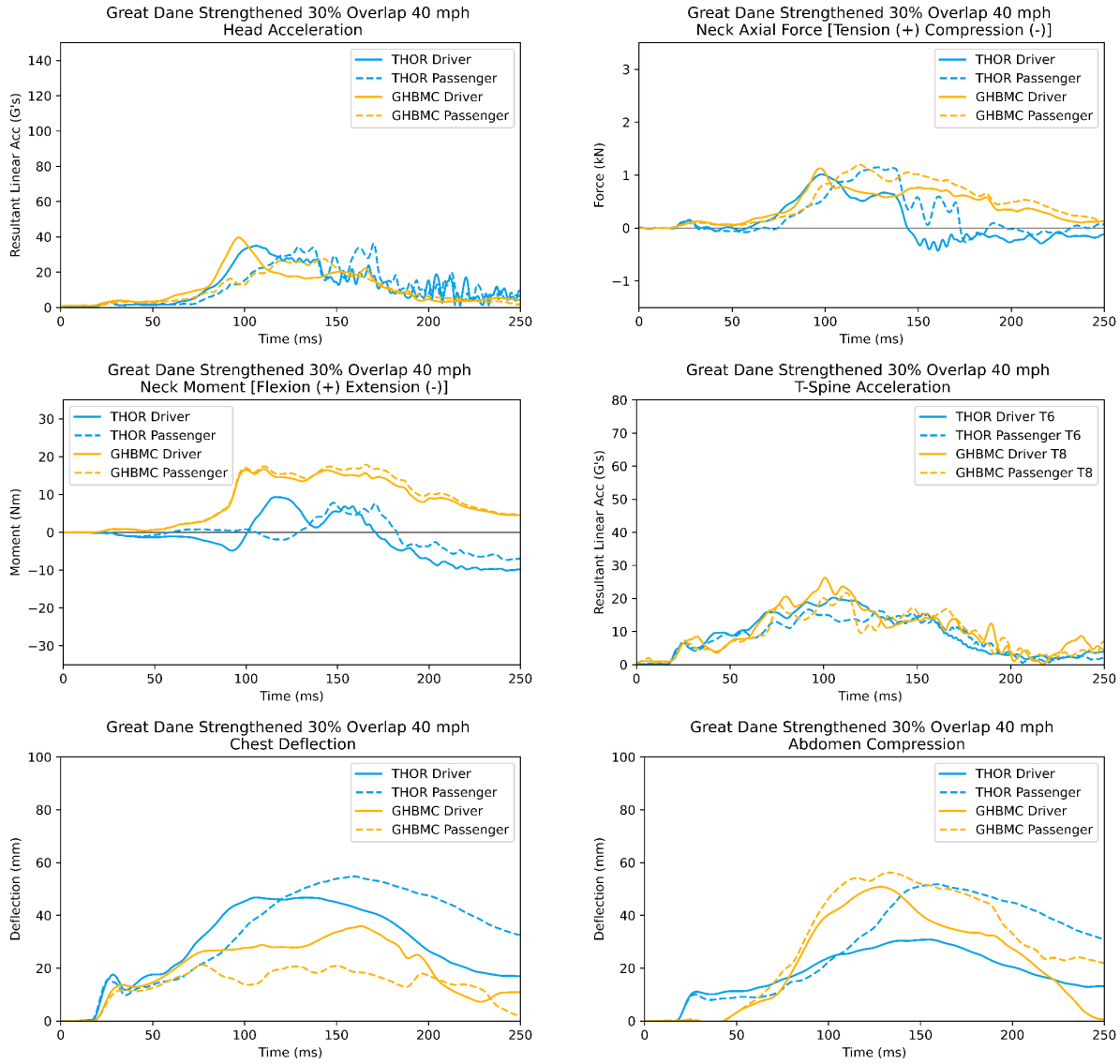

Figure 144. Strengthened Great Dane 40 mph, 30 percent overlap THOR-50M and GHBMC upper body data channels

Figure 145. Strengthened Great Dane 40 mph, 30 percent overlap THOR-50M and GHBMC lower body data channels

Strengthened Great Dane 40 mph, 50 Percent Overlap

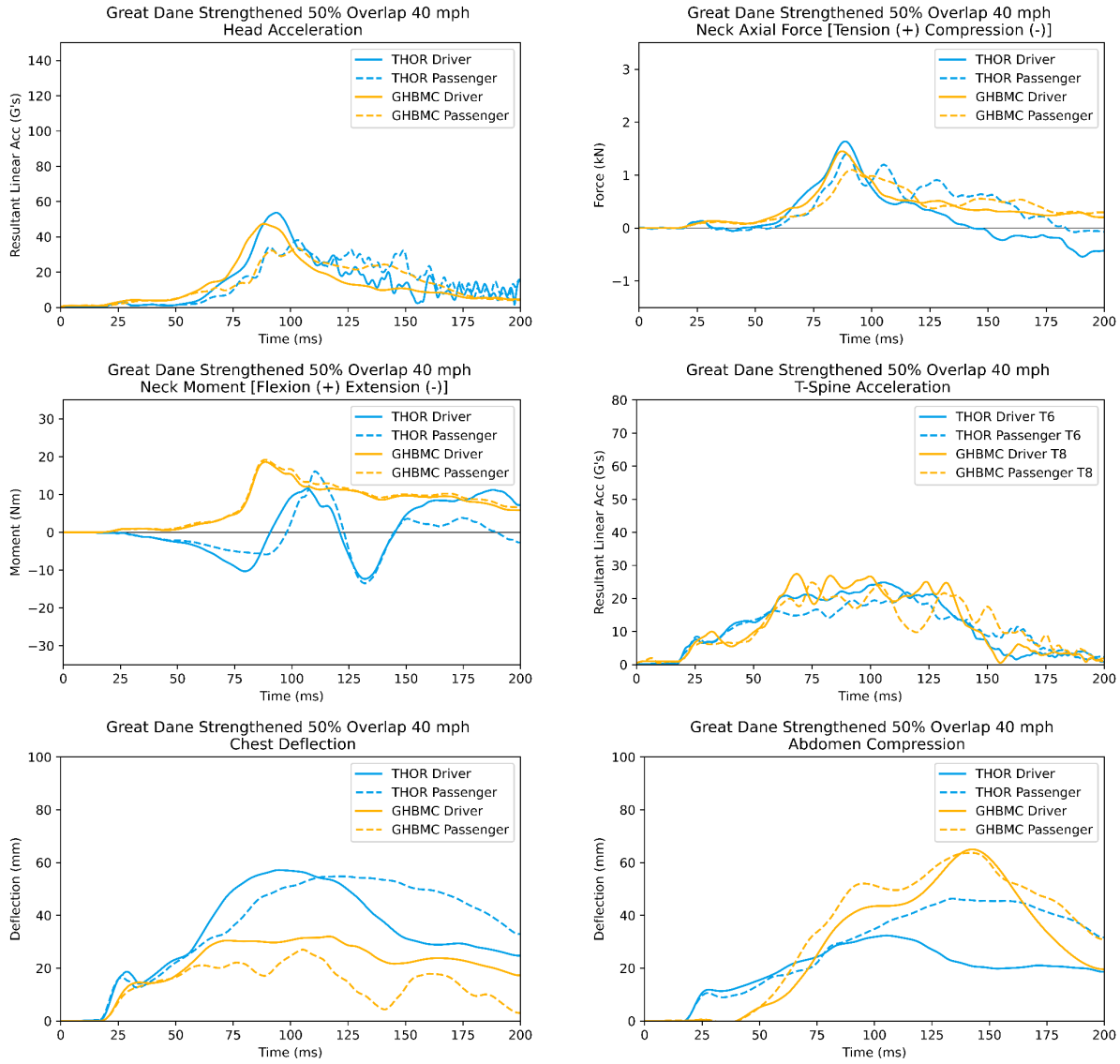

Figure 146. Strengthened Great Dane 40 mph, 50 percent overlap THOR-50M and GHBMC upper body data channels

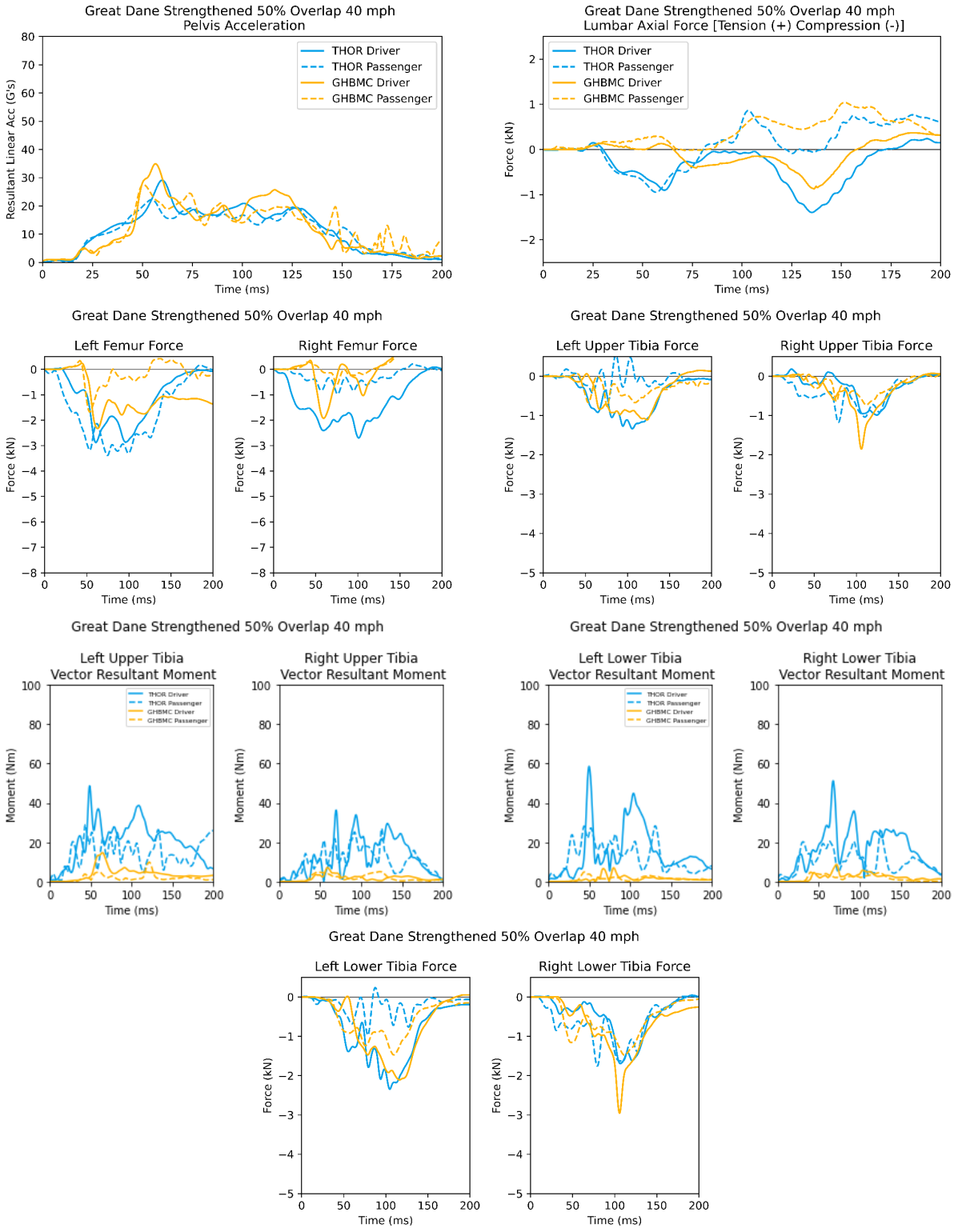

Figure 147. Strengthened Great Dane 40 mph, 50 percent overlap THOR-50M and GHBMC lower body data channels

Strengthened Great Dane 40 mph, Full Width Overlap

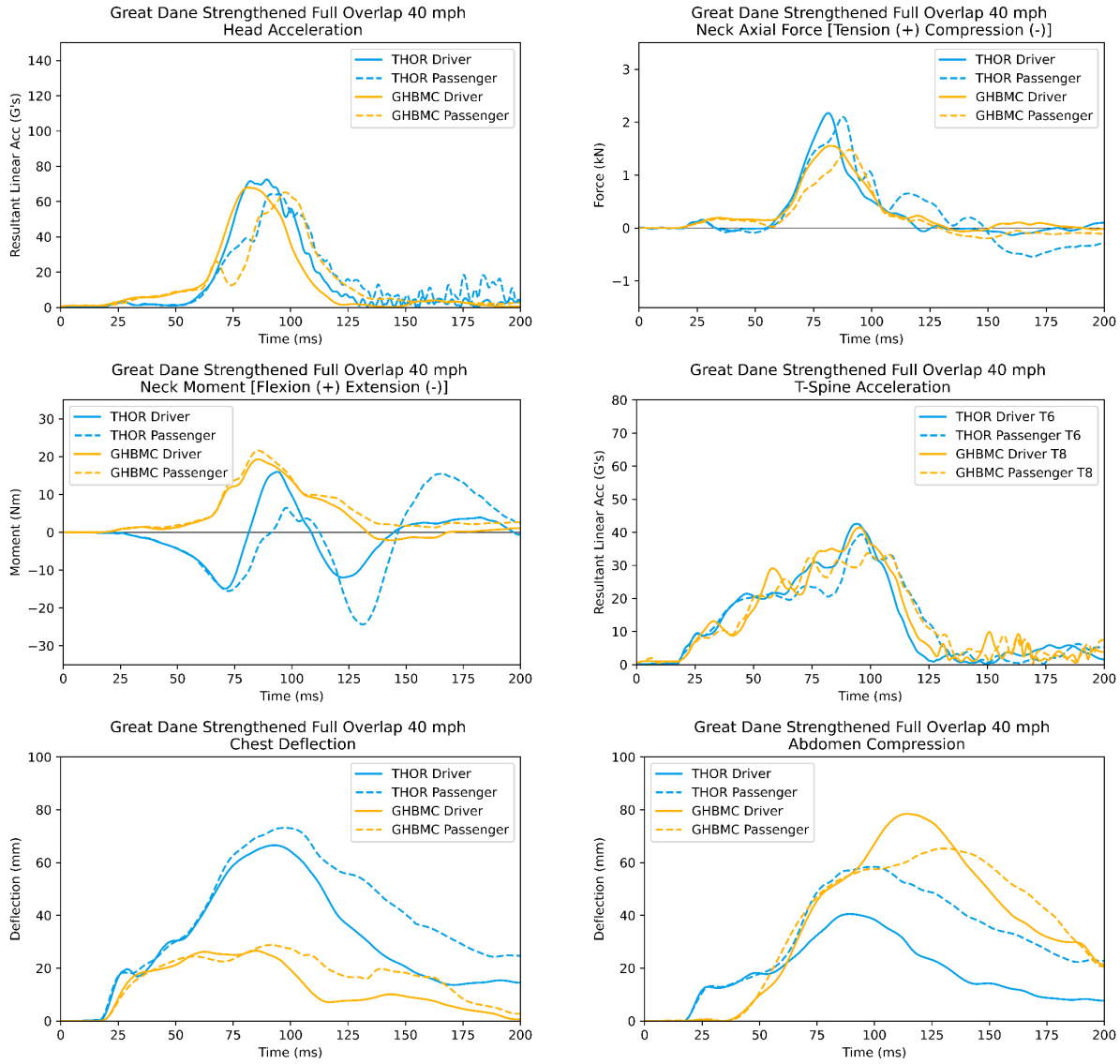

Figure 148. Strengthened Great Dane 40 mph, full width overlap THOR-50M and GHBMC upper body data channels

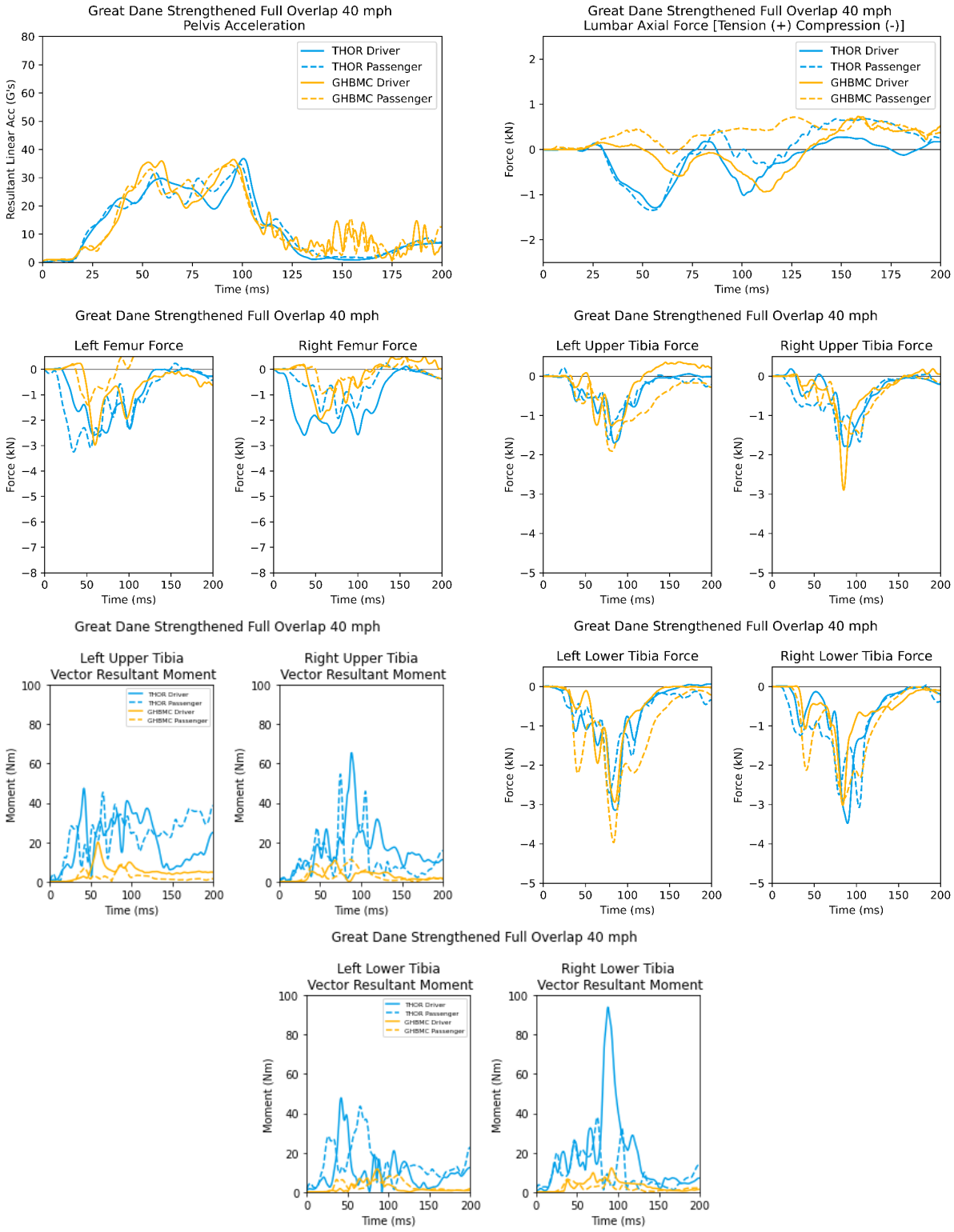

Figure 149. Strengthened Great Dane 40 mph, full width overlap THOR-50M and GHBMC lower body data channels

Strengthened Great Dane 45 mph, 30 Percent Overlap

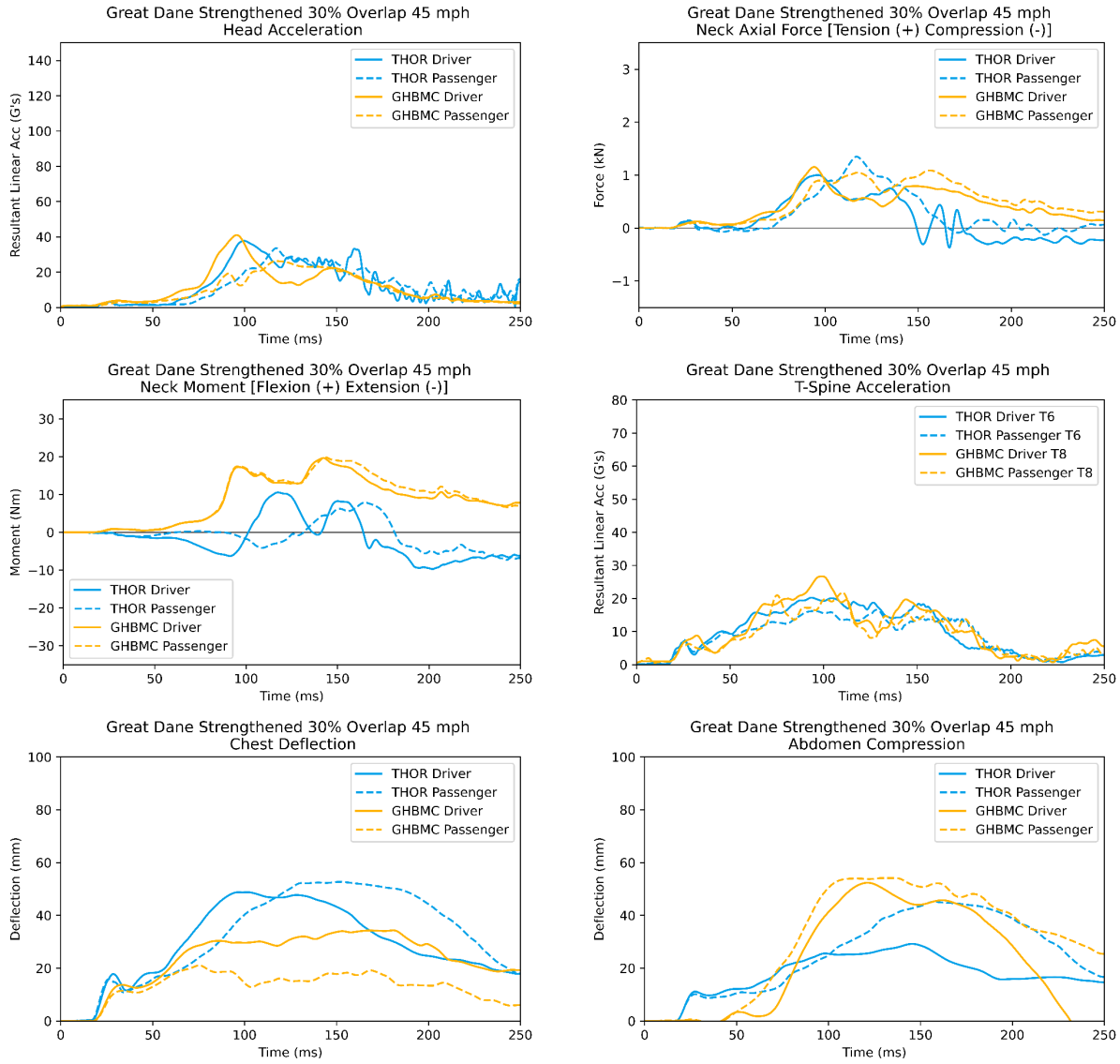

Figure 150. Strengthened Great Dane 45 mph, 30 percent overlap THOR-50M and GHBMC upper body data channels

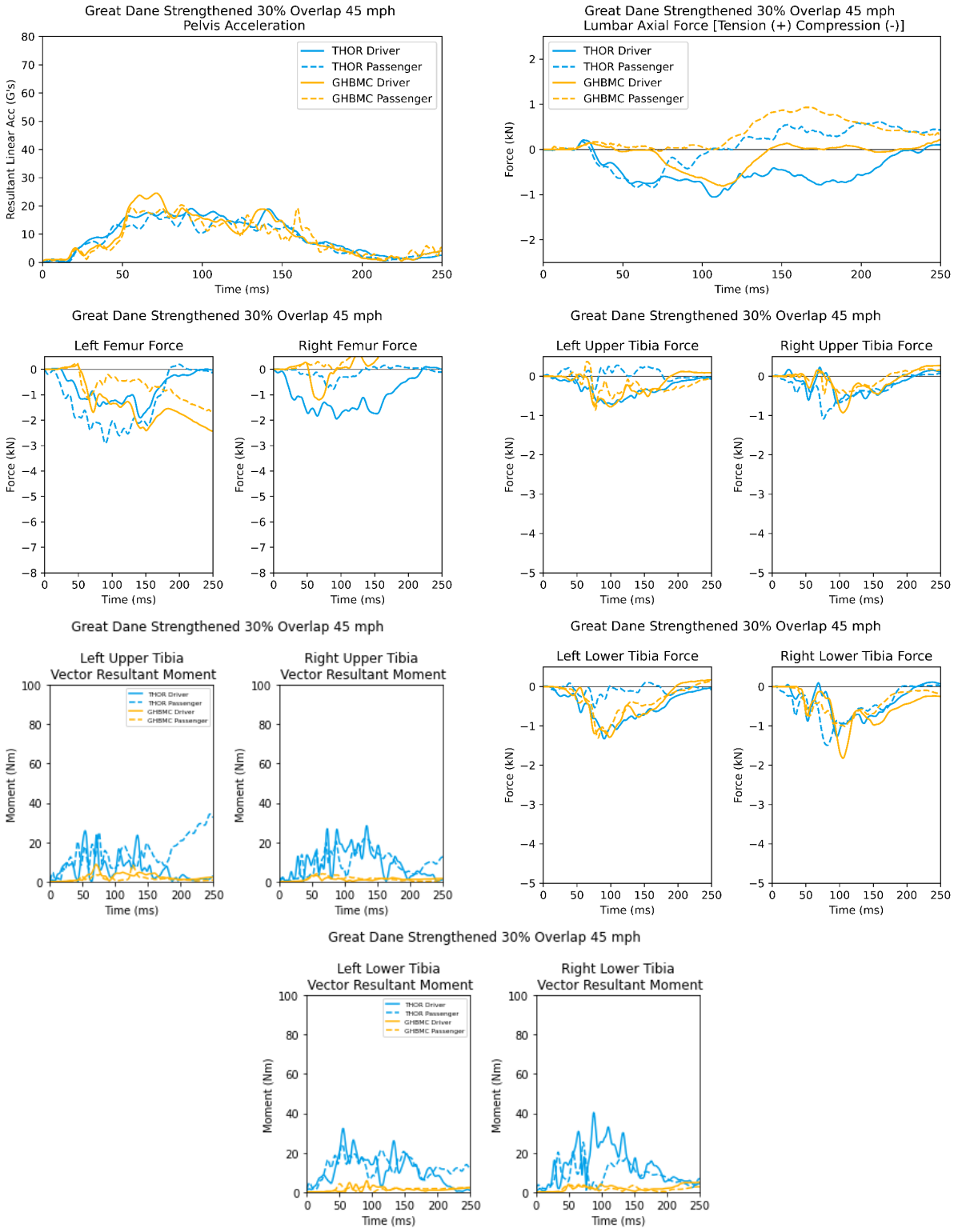

Figure 151. Strengthened Great Dane 45 mph, 30 percent overlap THOR-50M and GHBMC lower body data channels

Strengthened Great Dane 45 mph, 50 Percent Overlap

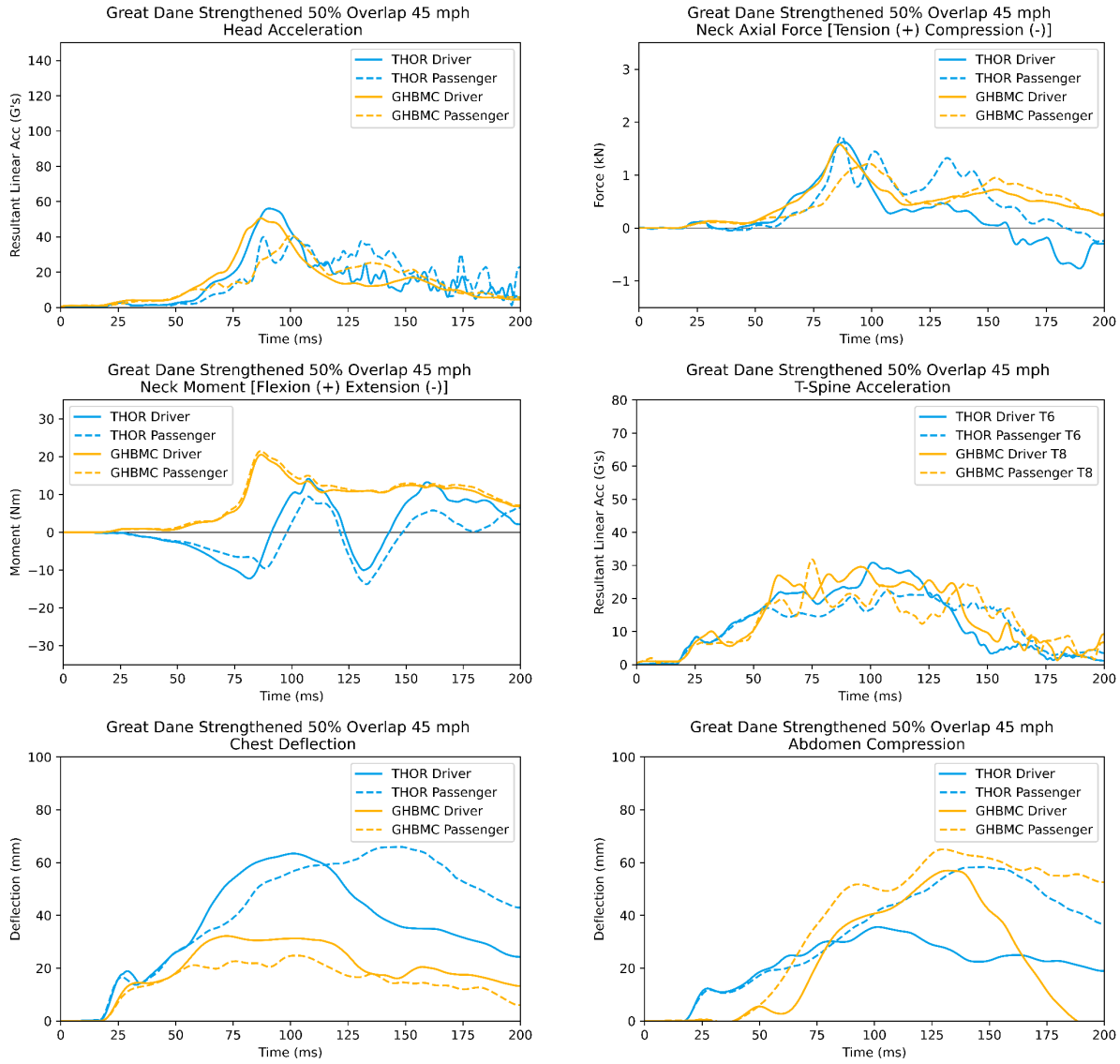

Figure 152. Strengthened Great Dane 45 mph, 50 percent overlap THOR-50M and GHBMC upper body data channels

Figure 153. Strengthened Great Dane 45 mph, 50 percent overlap THOR-50M and GHBMC lower body data channels

Strengthened Great Dane 45 mph, Full Width Overlap

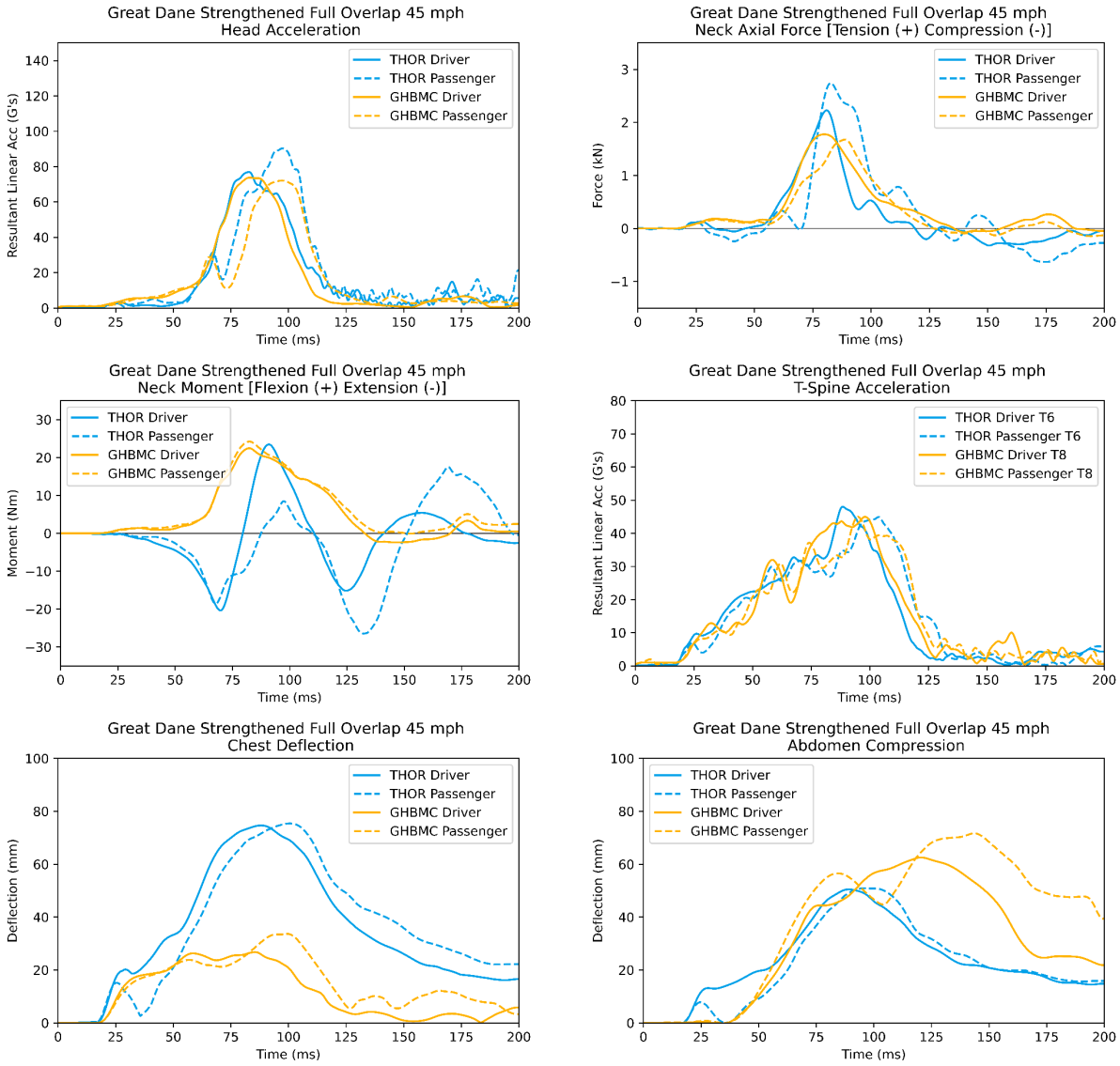

Figure 154. Strengthened Great Dane 45 mph, full width overlap THOR-50M and GHBMC upper body data channels

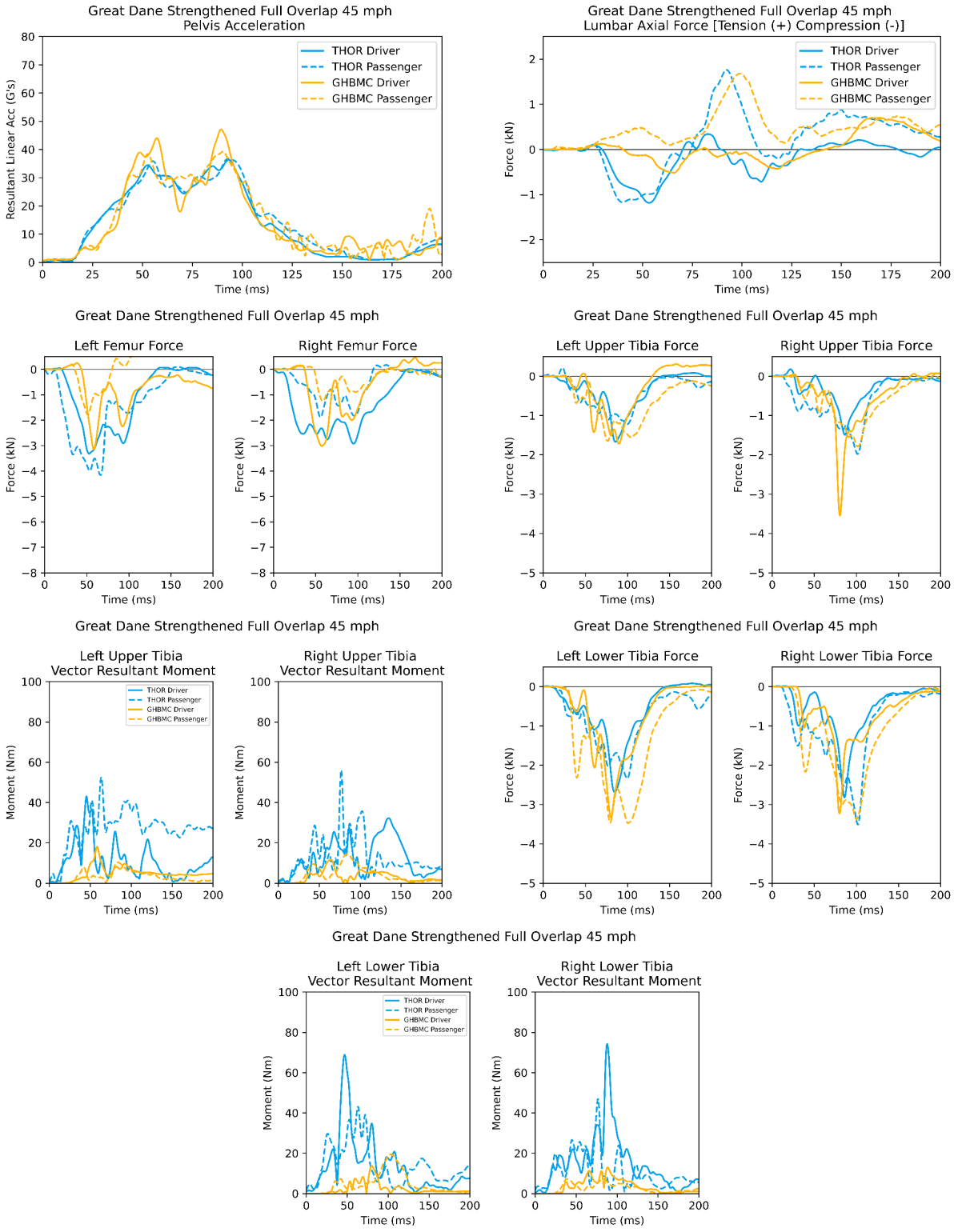

Figure 155. Strengthened Manac 45 mph, full width overlap THOR-50M and GHBMC lower body data channels

DOT HS 813 686
July 2025

U.S. Department
of Transportation

**National Highway
Traffic Safety
Administration**

16552-070125-v4